DEFENCE S&T TECHNICAL BULLETIN

VOL. 18 NUM. 2 YEAR 2025 eISSN 3009-1896

CONTENTS

Ministry of Defence Malaysia

SCIENCE & TECHNOLOGY RESEARCH INSTITUTE FOR DEFENCE (STRIDE)

Published by:

Science & Technology Research Institute for Defence (STRIDE)
Taman Bukit Mewah Fasa 9, 43000 Kajang, Selangor, Malaysia
Email: dinesh.sathyamoorthy@stride.gov.my / mahdi.cheisa@stride.gov.my
Tel.: +603-4012 7040

The Defence S&T Technical Bulletin is published biannually.

eISSN 3009-1896

AIMS AND SCOPE

The Defence S&T Technical Bulletin is the official journal of the Science & Technology Research Institute for Defence (STRIDE). The journal, which is indexed in, among others, Scopus, Index Corpenicus, ProQuest and EBSCO, contains manuscripts on research findings in various fields of defence science & technology. The primary purpose of this journal is to act as a channel for the publication of defence-based research work undertaken by researchers both within and outside the country.

WRITING FOR THE DEFENCE S&T TECHNICAL BULLETIN

Contributions to the journal should be based on original research in areas related to defence science & technology. All contributions should be in English.

PUBLICATION

The editors' decision with regard to publication of any item is final. A manuscript is accepted on the understanding that it is an original piece of work that has not been accepted for publication elsewhere.

PRESENTATION OF MANUSCRIPTS

The format of the manuscript is as follows:

a) Page size A4
b) MS Word format
c) Single space
d) Justified
e) In Times New Roman, 11-point font
f) Should not exceed 15 pages, including references
g) Texts in charts and tables should be in 10-point font.

Please email the manuscript to:

1) Gs. Dr. Dinesh Sathyamoorthy (dinesh.sathyamoorthy@stride.gov.my)
2) Dr. Mahdi bin Che Isa (mahdi.cheisa@stride.gov.my)

The next edition of the journal (Vol. 19, Num. 1) is expected to be published in April 2026. The due date for submissions is 7 January 2026. **It is strongly iterated that authors are solely responsible for taking the necessary steps to ensure that the submitted manuscripts do not contain confidential or sensitive material.**

The template of the manuscript is as follows:

TITLE OF MANUSCRIPT

Name(s) of author(s)

Affiliation(s)

Email:

ABSTRACT

Contents of abstract.

Keywords: *Keyword 1; keyword 2; keyword 3; keyword 4; keyword 5.*

1. TOPIC 1

Paragraph 1.

Paragraph 2.

1.1 Sub Topic 1

Paragraph 1.

Paragraph 2.

2. TOPIC 2

Paragraph 1.

Paragraph 2.

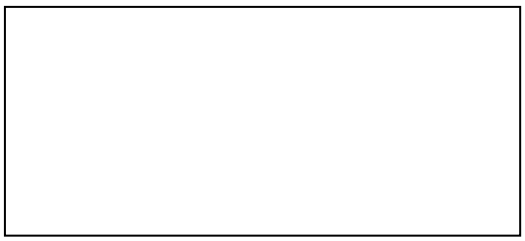

Figure 1: Title of figure.

Table 1: Title of table.

Content	Content	Content
Content	Content	Content
Content	Content	Content
Content	Content	Content

Equation 1 (1)
Equation 2 (2)

REFERENCES

Long lists of notes of bibliographical references are generally not required. The method of citing references in the text is 'name date' style, e.g. 'Hanis (1993) claimed that...', or '…including the lack of interoperability (Bohara *et al.*, 2003)'. End references should be in alphabetical order. The following reference style is to be adhered to:

Books

Serra, J. (1982). *Image Analysis and Mathematical Morphology*. Academic Press, London.

Book Chapters

Goodchild, M.F. & Quattrochi, D.A. (1997). Scale, multiscaling, remote sensing and GIS. *In* Quattrochi, D.A. & Goodchild, M.F. (Eds.), *Scale in Remote Sensing and GIS*. Lewis Publishers, Boca Raton, Florida, pp. 1-11.

Journals / Serials

Jang, B.K. & Chin, R.T. (1990). Analysis of thinning algorithms using mathematical morphology. *IEEE T. Pattern Anal.*, **12**: 541-550.

Online Sources

GTOPO30 (1996). *GTOPO30: Global 30 Arc Second Elevation Data Set*. Available online at: http://edcwww.cr.usgs.gov/landdaac/gtopo30/gtopo30.html (Last access date: 1 June 2009).

Unpublished Materials (e.g. theses, reports and documents)

Wood, J. (1996). *The Geomorphological Characterization of Digital Elevation Models*. PhD Thesis, Department of Geography, University of Leicester, Leicester.

AERODYNAMIC PERFORMANCE OF UNMANNED AERIAL VEHICLE (UAV) PROPELLERS

Adam Gani*, Zainol Abidin Awang Sa & Nurul Najwa Abd Rahman

Science & Technology Research Institute for Defence (STRIDE), Ministry of Defence, Malaysia

*Email: adam.gani@stride.gov.my

ABSTRACT

This paper aims to analyse the aerodynamic performance of propellers, which is essential for advancing unmanned aerial vehicle (UAV) research and optimising their design. The study investigates the aerodynamic performance of four propeller sizes - 12x12, 14x12, 16x12 and 17x12 - manufactured by APC Propeller, to determine the optimal size that maximises thrust while minimising power consumption, thereby enhancing endurance. The objective is to identify the propeller size that achieves the highest thrust with the lowest power consumption, ensuring optimal flight performance. Using a controlled experimental setup, key aerodynamic parameters of thrust, torque and power are measured and analysed at varying rotational speeds. The results confirm that propeller diameter significantly influences aerodynamic performance, with larger diameters generating higher thrust but requiring greater torque and power. These findings provide valuable insights into selecting propellers that optimise aerodynamic performance and improve UAV endurance, contributing to advancements in UAV dynamic systems.

Keywords: *Unmanned aerial vehicles (UAVs); propeller size; aerodynamic performance; thrust and torque; power consumption.*

1. INTRODUCTION

Unmanned aerial vehicles (UAVs) have gained significant importance across various industries due to their ease of operation, high reliability, maintainability, flexibility and advanced performance feedback systems (Zhu *et al*., 2021). Their applications span numerous fields, incuding military reconnaissance and logistics (Mohsan *et al*., 2023), environmental monitoring and post-mining surveillance (Khan *et al*., 2024), as well as infrastructure development (Villarino *et al*., 2025). A critical aspect of UAV performance lies in the design and optimisation of propellers, which are responsible for producing lift and thrust for fundamental forces that govern propulsion efficiency and attitude stability. Regardless of whether a UAV utilises electric motor or internal combustion engine, its operational effectiveness is heavily influenced by the aerodynamic behaviour of its propeller (Etewa *et al*., 2024).

In multi-rotor UAVs, lift is generated by the rotation of multiple propellers, with electronic speed controllers adjusting rotor speed to regulate thrust and manoeuvre the aircraft (Hang *et al*., 2021), whereas in petrol-powered UAVs, where engines typically operate at constant speed, flight control is achieved by varying rotor pitch to modify lift (Ma *et al*., 2017). This underscores the critical role of propeller design and optimisation in UAV performance, particularly as operational demands grow more complex. Recent advancements highlight the importance of aerodynamic optimisation to enhance propulsion efficiency and reliability, including medium-fidelity multidisciplinary optimisation tools balancing aerodynamic efficiency and acoustic performance (Schmähl & Hornung, 2025), multi-objective genetic algorithms for variable-pitch propellers to improve cruising efficiency (Zhang *et al*., 2025), as well as low-speed propeller designs tailored for UAVs operating at low Reynolds numbers that demonstrate significant gains through airfoil customisation and experimental validation (Crona *et al*., 2024). High-fidelity multidisciplinary design optimisation frameworks have also been developed to

achieve optimal aerodynamic and structural characteristics (He *et al*., 2023), while research into coaxial rotor systems has shown high thrust-to-weight ratios, further improving propulsion efficiency (Li *et al*., 2023; Jayakumar *et al*., 2024;), reflecting ongoing efforts to refine propeller technology in line with the evolving demands of UAV applications.

This paper aims to investigates the aerodynamic performance of four UAV propeller sizes - 12x12, 14x12, 16x12 and 17x12 - manufactured by APC Propeller, to determine the optimal size that maximises thrust while minimising power consumption, thereby enhancing endurance. The objective is to identify the propeller size that achieves the highest thrust with the lowest power consumption, ensuring optimal flight performance.

2. METHODOLOGY

2.1 Experimental System Design

The experimental system used for analysing propeller aerodynamic performance is capable of collecting data on propeller speed, individual thrust and propeller torque. It requires manual operation via a remote control to vary the blade's rotational speed. The system consists of two main components: the experimental platform, and the measurement and control system. Figure 1 illustrates the overall system design and the locations of its components.

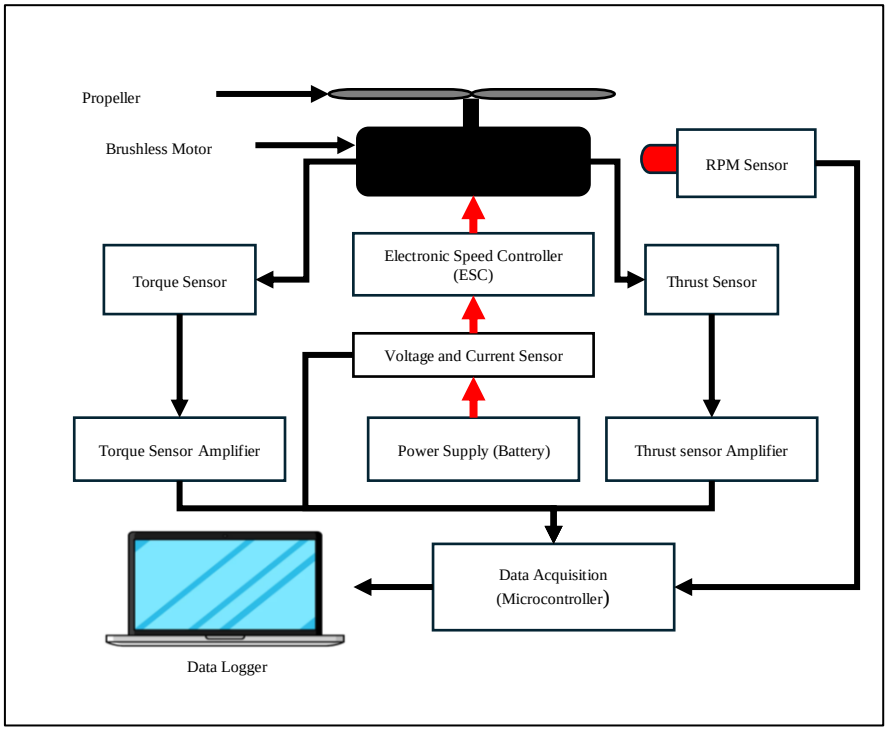

Figure 1: Measurement and control system.

The experimental platform, constructed with a stainless-steel frame, serves as the mounting structure for the propeller under test. It comprises of a brushless motor, force sensor, infrared speed sensor and additional equipment. While the propellers on a multi-rotor UAV are typically arranged vertically, the propeller in this experimental system is positioned horizontally to eliminate ground effect interference.

2.2 Engine Testing System Development

The thrust jig is designed to capture and evaluate the performance of various motor-propeller combinations. It has been specifically engineered to measure critical parameters, including thrust, torque, voltage, current and revolutions per minute (RPM), in order to determine the most efficient motor-propeller configuration. The completed setup of the engine test system is presented in Figures 2 and 3.

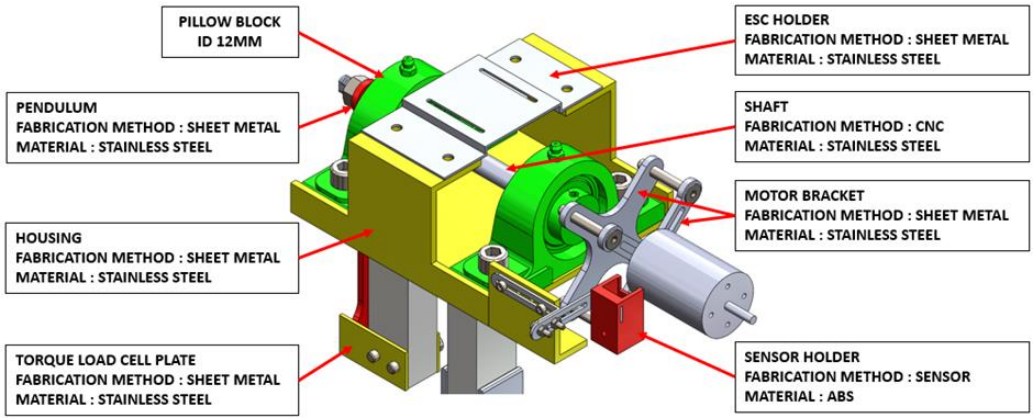

Figure 2: Schematic diagram of the engine test system.

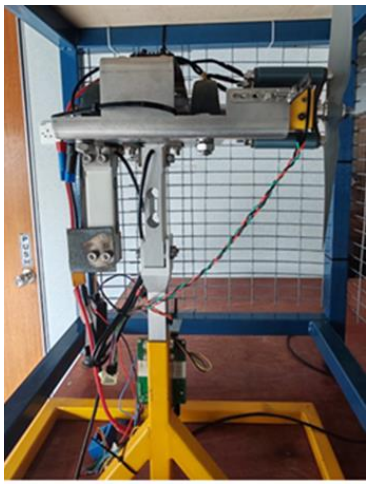

Figure 3: Experimental setup of the engine test system.

The jig assembly comprises several key components, primarily fabricated from stainless steel. The main structural elements include a pillow block with a 12 mm inner diameter for bearing support and a precision-machined shaft for rotary motion transmission. The assembly also incorporates specialised mounting components, such as a torque load cell plate, motor bracket and electronic speed controller (ESC) holder. The sensor holder is 3D-printed to match the sensor design and is easily adjustable for different motor configurations. The integrated design enables accurate force measurement, stable motor mounting and protection of electronic components while maintaining structural integrity throughout the system.

2.3 Motors and Propeller Configurations

A T-Motor AT4130 KV230 brushless motor was used to drive the propellers, facilitating the assessment of aerodynamic performance across four configurations: 12×12, 14×12, 16×12 and 17×12. The propellers have increasing diameter while maintaining a consistent pitch of 12 inches. The specifications of the motor and propellers are provided in Tables 1 and 2 respectively.

Table 1: T-Motor AT4130 KV230 brushless motor specifications.

Characteristics	Data
Model	Long Shaft KV230
Motor Dimensions	Diameter 50 x 79 mm
Lead	Enamelled Wire 100 mm
Shaft Diameter	In: 6 mm Out: 6mm
Idle Current (10V)	1.4 A
Max Power (180s)	2500 W
Weight (incl. cable)	408g
Internal Resistance	60 mΩ
Configuration	12N14P
Rated Voltage (Li-Po)	60A

Table 2: Propeller specifications.

Propeller	Diameter (in)	Pitch (in)
12x12	12	12
14x12	14	12
16x12	16	12
17x12	17	12

3. RESULTS AND DISCUSSION

Figure 4 shows the relationship between thrust and RPM for the four tested propeller sizes (12x12, 14x12, 16x12 and 17x12), demonstrating a clear trend of increasing thrust with higher RPM. Among the tested configurations, the 17x12 propeller consistently delivered the highest thrust, indicating superior performance, particularly at elevated RPMs. The 16x12 propeller closely followed, providing substantial thrust, while the 14x12 propeller offerred moderate performance - outperforming the 12x12 but falling short of the larger sizes. The 12x12 propeller produced the least thrust, underscoring its inefficiency for high-thrust applications but suggesting potential suitability for low-power scenarios.

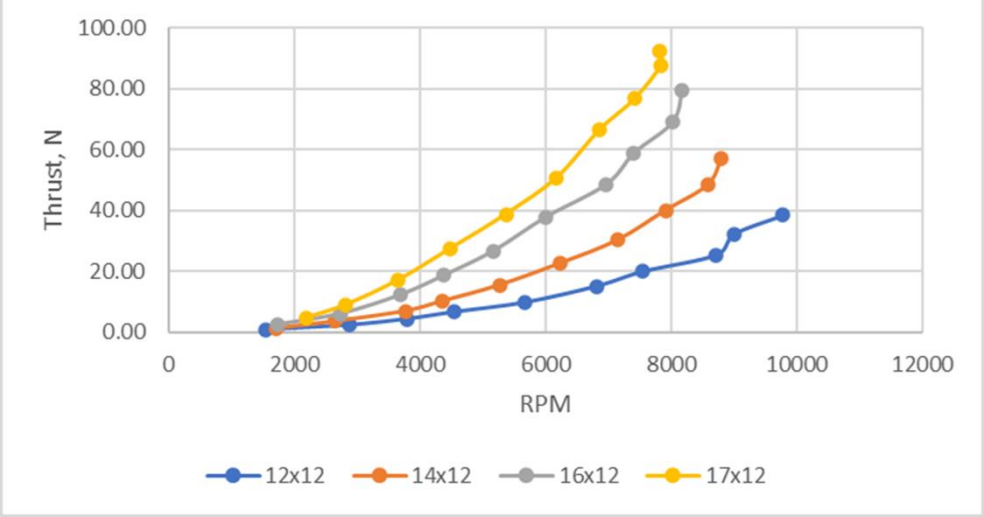

Figure 4: Engine thrust vs RPM for the different propeller sizes.

At lower RPMs, the variations in thrust are less pronounced, but as RPM increases, larger propellers such as the 16x12 and 17x12 exhibited steeper thrust gains, making them more appropriate for high-

power, demanding operations. This analysis highlights the critical impact of propeller selection on system performance, with larger propellers proving more effective for applications requiring maximum thrust output.

Figure 5 presents the increase in torque with higher RPM across all the tested propeller sizes. Among them, the 17x12 propeller exhibited the highest torque output, particularly at elevated RPMs, highlighting its suitability for high-power applications. The 16x12 propeller closely followed, demonstrating significant torque performance, while the 14x12 propeller delivered moderate torque values. The 12x12 propeller generated the lowest torque across all RPM ranges, indicating its limited capacity for high-torque applications.

At lower RPMs, differences in torque among the propellers were less pronounced. However, as RPM increases, the larger propellers (16x12 and 17x12) displayed steeper rise in torque, confirming their efficiency in scenarios requiring substantial power. This analysis underscores the importance of selecting the appropriate propeller configuration based on the torque demands of the application, with larger propellers proving more effective for high-load conditions.

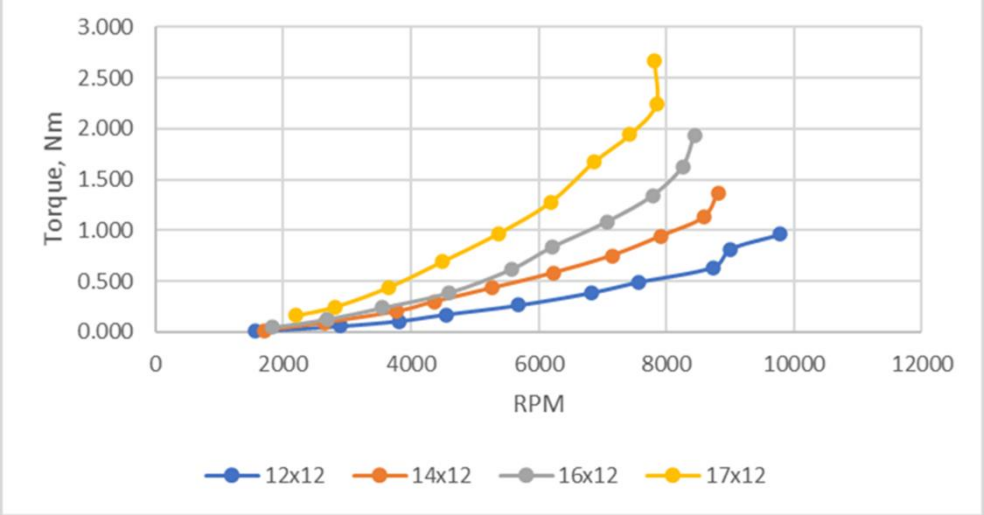

Figure 5: Torque vs RPM for the different propeller sizes.

Figure 6 illustrates a general trend of increasing power with higher RPM across all the propeller sizes. The 17x12 propeller stood out, requiring the highest power as RPM increases, reflecting its ability to generate substantial thrust and torque, but at the cost of higher energy consumption. The 16x12 propeller followed closely, demonstrating significant power requirements, while the 14x12 propeller exhibited moderate power demands. The 12x12 propeller required the least power across all the RPM ranges, highlighting its efficiency for low-power operations.

At higher RPMs, the larger propellers (16x12 and 17x12) displayed steeper increase in power consumption, reinforcing their suitability for high-performance yet energy-intensive applications. This analysis underscores the importance of balancing performance and energy efficiency when selecting a propeller size, with smaller propellers like the 12x12 being better suited for energy-efficient operations, while larger propellers excel in high-power scenarios.

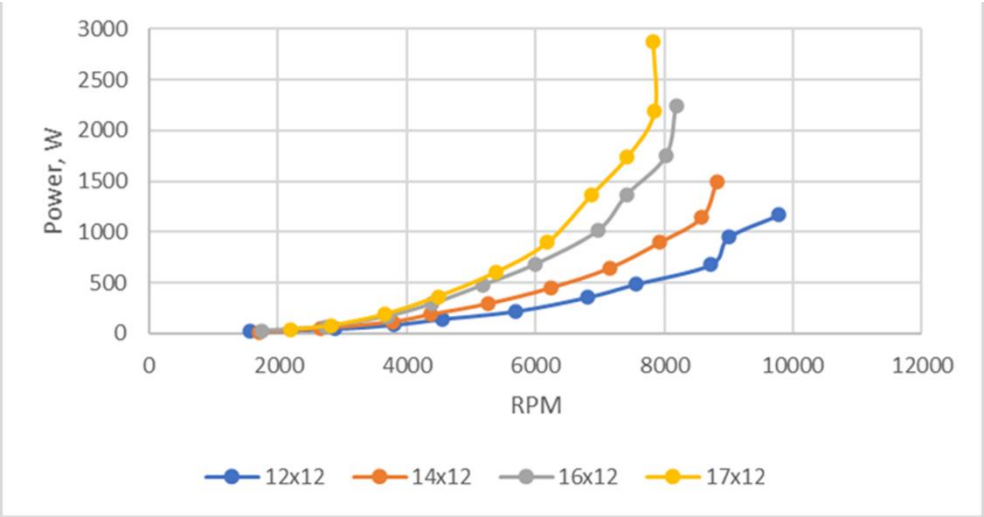

Figure 6: Power vs RPM for the different propeller sizes.

4. CONCLUSION

This study evaluated the aerodynamic performance of four UAV propeller sizes (12x12, 14x12, 16x12, and 17x12), aiming to identify the optimal configuration for maximum thrust and minimal power consumption. The results indicated that the 17x12 propeller consistently provided the highest thrust and torque, making it the most suitable for high-performance applications. However, it also exhibited the highest power consumption, particularly at elevated RPMs, highlighting a trade-off between performance and energy efficiency. The 16x12 propeller demonstrated a balance of high thrust and torque with slightly lower power demands, making it a good alternative for demanding applications where efficiency is still a concern.

The 14x12 propeller offered moderate thrust and torque, with power consumption falling between the larger and smaller sizes, positioning it as a balanced choice for applications requiring both performance and energy efficiency. The 12x12 propeller, while generating the least thrust and torque, was the most power-efficient, making it ideal for low-power operations where efficiency is the priority.

In conclusion, the selection of an optimal propeller size should be based on specific application requirements. For high-performance, power-intensive tasks, the 17x12 or 16x12 propellers are recommended, while the 12x12 propeller is best suited for low-power, efficiency-focused operations. The 14x12 propeller provides a balanced option for moderate performance and energy demands.

REFERENCES

Callister, W.D. & Rethwisch, D.G. (2021). *Materials Science and Engineering: An Introduction*, *10th Ed.* Wiley, New Jersey, US.

Crona, M., Dinger, S., Samuelsson, P., Strömfeldt, H. & Jonsson, I. (2024). Low-speed propeller for UAV applications: From design to experimental evaluation. *34th Congr. Int. Counc. Aeronaut. Sci. (ICAS 2024)*, 9-13 September 2024, Florence, Italy. Chalmers University of Technology, Gothenburg, Sweeden.

Etewa, M., Hassan, A.H., Safwat, E., Abozied, M.A.H., El-Khatib, M.M. & Ramirez-Serrano, A. (2024). Performance estimation of fixed-wing UAV propulsion systems. *Drones*, **8**:424.

Groover, M.P. (2020). *Fundamentals of Modern Manufacturing: Materials, Processes, and Systems*. Wiley, Hoboken, New Jersey, US.

Horowitz, P. & Hill, W. (2015). *The Art of Electronics, 3rd Ed.* Cambridge University Press, Cambridge, UK.

He, P., Koyuncuoglu, H.U., Hu, H., Dhulipalla, A., Hu, H. & Hu, H. (2023). High-fidelity aerodynamic and aerostructural optimization of UAV propellers using the adjoint method. *AIAA Scitech Forum*, 23-27 January 2023, National Harbor, Maryland, US.

Jayakumar, S.S., Subramaniam, I.P., Arputharaj, B.S., Rajendran, S., Rajalakshmi, R., Rajeshkumar, G. & Suresh, S. (2024). Design, control, aerodynamic performances, and structural integrity of a novel coaxial rotor unmanned aerial vehicle. *Sci. Rep.*, **14**:54174.

Khan, A., Gupta, S., & Gupta, S.K. (2024). UAV-enabled disaster management: Applications, open issues, and challenges. *GMSARN Int. J.*, **18**:44–53.

Li, H., Chen, Z. & Jia, H. (2023). Experimental investigation on hover performance of a ducted coaxial-rotor UAV. *Sensors*, **23**: 6413.

Ma, L., M, X., Cheng, L., Du, P. & Liu, Y. (2017). A review of supervised object-based land-cover image classification. *ISPRS J. Photogramm. Remote Sens*., **130:** 277–293.

Mohsan, S.A.H., Othman, N.Q.H., Li, Y., Alsharif, M.H. & Khan, M.A. (2023). Unmanned aerial vehicles: Practical aspects, applications, open challenges, security issues, and future trends. *Intel. Service Robot.*, **16**:109–137.

Schmähl, M. & Hornung, M. (2025). Implementation and validation of an optimization-based propeller design program. *CEAS Aeronaut J*., In press.

Shigley, J.E., Mischke, C.R. & Budynas, R.G. (2020). *Mechanical Engineering Design, 11th Ed.* McGraw-Hill Education, New York, US.

Villarino, A., Valenzuela, H., Antón, N., Domínguez, M. & Méndez Cubillos, X. C. (2025). UAV applications for monitoring and management of civil infrastructures. *Infrastructures*, **10**: 106.

Zhang, Z., Zhang, Y., J., Du, P. & Zhao, J. (2025). Variable pitch propeller: Multi-objective optimization design and performance analysis. *Eng. Proc.*, **80**:36.

Zhu, H., Jiang, Z., Zhao, H., Pei, S., Li, H. & Lan, Y. (2021). Aerodynamic performance of propellers for multirotor unmanned aerial vehicles: Measurement and experiment. *Int. J. Aerosp. Eng.*, **Vol. 2021**: 9538647.

INTEGRATION OF LTE CELLULAR TECHNOLOGY WITH UAV PLATFORMS: A CASE STUDY USING RASPBERRY PI AND TELIT LE910C4-AP MODEM

Omran Alshalabi, Nadhiya Liyana Mohd Kamal*, Zulhilmy Sahwee, Nurhakimah Norhashim & Shahrul Ahmad Shah

Unmanned Aerial System, Avionics Section, Malaysian Institute of Aviation Technology (MIAT), Universiti Kuala Lumpur (UniKL), Malaysia

*Email: nadhiyaliyanamk@unikl.edu.my

ABSTRACT

This paper presents the design and preliminary evaluation of a flexible long-term evolution (LTE) testbed embedded within an unmanned aerial vehicle (UAV) to enable cellular-connected UAV applications. The primary objective of this testbed is to facilitate real-time evaluation of cellular network performance across different altitudes and environments, specifically focusing on metrics, such as reference signal received power (RSRP), received signal strength indicator (RSSI), reference signal received quality (RSRQ) and signal-to-interference-plus-noise ratio (SINR). Utilizing a Raspberry Pi, LTE modem and modular antenna system, the testbed offers a lightweight and adaptable solution for collecting LTE data and maintaining connectivity during UAV flights. Initial testing conducted in a stationary environment validated the system's capability to record cellular parameters consistently, providing a baseline for future aerial testing. The testbed also supports comparative antenna analysis, allowing researchers to determine optimal configurations for varying operational contexts. This LTE testbed is intended to advance research in UAV cellular connectivity by offering a scalable, field-deployable platform for assessing network performance, signal stability and antenna efficacy under real-world conditions.

Keywords: *Unmanned aerial vehicle (UAV); long-term evolution (LTE); cellular connectivity; modular testbed; antenna configuration.*

1. INTRODUCTION

The integration of cellular networks with unmanned aerial vehicles (UAVs) has gained significant attention in recent years due to the expanding scope of UAV applications in fields like surveillance, environmental monitoring, and emergency response. Cellular-connected UAVs offer the advantage of broad coverage, enabling long-range communication and real-time data transmission beyond the limited reach of traditional radio-based ground stations (Mohd Kamal *et al*., 2019). However, achieving reliable connectivity at various altitudes and across diverse environments remains a challenge, given the dynamic nature of aerial communication and the interference susceptibility inherent in cellular networks (Alshalabi *et al*., 2022).

In order to address these challenges, it is essential to evaluate cellular network performance parameters, such as reference signal received power (RSRP), received signal strength indicator (RSSI), reference signal received quality (RSRQ) and signal-to-interference-plus-noise ratio (SINR), in real-world settings. These metrics are critical for determining the quality and stability of cellular connectivity and are influenced by factors such as altitude, interference and antenna configuration. Recent field trials by Brar & Mérida (2024) demonstrated the importance of these parameters in assessing UAV communication reliability in complex urban environments, showing that strong signal levels do not always correlate with high-quality links due to variable interference patterns. Similarly, advancements

in 5G and emerging 6G technologies highlight the importance of enhanced signal estimation and interference mitigation strategies, including SINR-aware connectivity, for ensuring reliable UAV integration into future cellular networks (Chen *et al*., 2023). The ability to systematically analyze these parameters can inform the design of robust UAV communication systems capable of maintaining stable links over cellular networks (Muruganathan *et al*., 2021).

This paper introduces a modular LTE testbed embedded within a UAV, designed to measure cellular network performance and facilitate comparative analysis of different antenna types. The testbed leverages a Raspberry Pi platform equipped with an LTE modem and modular antenna system, enabling researchers to easily switch between different antenna configurations for comparative testing. This setup allows for flexible deployment across various research and operational contexts. By enabling cellular data collection at different altitudes and in multiple environments, this testbed serves as a scalable solution for real-time evaluation of network coverage and signal quality.

The primary objective of this study is to evaluate the LTE testbed's capability to collect and manage key LTE metrics, such as RSRP, RSRQ, RSSI and SINR, for UAV applications. Initial testing, conducted in a stationary setting, demonstrated the system's ability to reliably capture these metrics, providing a solid foundation for future tests in dynamic aerial environments. This paper aims to detail the design and functionality of the testbed, outline the data collection methodology, as well as discuss potential applications in cellular-connected UAV operations. By advancing the understanding of UAV connectivity through cellular networks, this work contributes to the development of more reliable and adaptable communication frameworks for UAVs in diverse fields.

2. RELATED WORK

Research on cellular-connected UAVs has expanded considerably in recent years as UAV applications increasingly rely on reliable, long-range connectivity. Several studies have examined the feasibility and performance of cellular networks in supporting UAV operations, focusing on metrics such as signal strength, latency and interference. Early research efforts utilized universal software radio peripheral (USRP) boards to capture LTE network parameters and assess connectivity at various altitudes. These studies provided valuable insights into signal behavior across different frequencies but were often limited by the weight and power requirements of the equipment, making them less practical for smaller UAV deployments (Izydorczyk *et al*., 2019).

Recent advancements have introduced more efficient alternatives for UAV connectivity. For instance, the integration of software-defined radio (SDR) systems in UAVs offers a flexible solution for managing network parameters like signal strength and latency in real-time. A comprehensive review of SDR deployments in UAV-driven applications demonstrates how SDR can mitigate challenges such as interference and high latency in cellular networks, providing a promising approach for scalable, long-range connectivity (Michailidis *et al*., 2024).

In order to address these constraints, some researchers explored the use of smartphones onboard UAVs as lightweight and cost-effective alternatives for cellular data collection. Smartphones offer built-in LTE connectivity and simplified integration for capturing real-time network performance metrics, such as RSRP and SINR, during flight. Although smartphones present a practical solution for lightweight data collection, they are limited by their non-modular design, which restricts comparative antenna testing and offers less control over specific LTE parameters (Alshalabi *et al*., 2022).

In addition, a recent experimental study assessed LTE network performance by analyzing key parameters such as SINR, latency and signal strength during controlled UAV flights. The researchers highlighted how UAV mobility and altitude affect the consistency of LTE connectivity, with notable fluctuations in delay and throughput observed at varying flight levels. These insights are vital for optimizing UAV deployment strategies in cellular environments, especially in scenarios where stable and responsive communication links are required (Braunfelds *et al*., 2024).

Advancements, such as those in studies by Aalborg University, have implemented cellular modems with diverse antenna types and conducted tests across varied environments. These studies provided a scalable approach to UAV connectivity research by evaluating multiple antenna configurations to assess the effects of altitude and interference on network stability. However, Aalborg University 's approach primarily involved controlling the UAV through direct radio frequency (RF) links while using cellular networks solely for data recording and transmission (Izydorczyk *et al*., 2020a, b).

In contrast, the LTE testbed presented in this paper integrates UAV-Cast Pro to enable the UAV's operation through a cellular modem, allowing it to be controlled directly over the LTE network. This approach introduces a cellular-controlled UAV system that expands beyond traditional RF limitations, facilitating real-time UAV control and data collection over long distances. By embedding this system in a UAV platform, the testbed provides a modular design for comparative antenna testing and can be adapted to varied environments, supporting practical applications in areas requiring robust UAV communication. This novel setup aims to contribute to UAV cellular connectivity research by exploring new dimensions of in-flight LTE network management and control.

3. METHODOLOGY

This section details the steps undertaken to design, set up and operate the LTE-based UAV testbed, focusing on the hardware assembly, software configuration and data collection processes essential for evaluating LTE network performance at different altitudes.

The testbed hardware was selected for its modularity and adaptability, featuring a Raspberry Pi 4 Model B as the central processing unit due to its computational efficiency, compact form and compatibility with a variety of peripheral devices. A Sixfab 3G-4G / LTE Base HAT with Telit LE910C4-AP LTE Modem (Figure 1) was chosen as the LTE interface, connecting to the Raspberry Pi through general-purpose input / output (GPIO) pins and providing dual ports for primary and diversity antennas, as well as a dedicated port for Global Positioning System (GPS) integration. These features enable the system to switch seamlessly between antennas based on signal quality, a crucial factor for UAV applications where connectivity may vary with altitude or environmental interference. The LTE modem was equipped with two antennas to enhance signal stability, with a Global Navigation Satellite System (GNSS) antenna dedicated to GPS functionality (SixFab, 2024). Power for the setup was supplied through a USB-connected power bank or, in aerial deployments, through a universal battery elimination circuit (UBEC) connected to the UAV's main battery, ensuring an uninterrupted power source during flights.

Figure 1: Sixfab 3G-4G / LTE Base HAT and Telit LE910C4-AP LTE modem.

For the software configuration, Raspberry Pi OS was installed and configured to operate headlessly via Secure Shell (SSH) for remote management. In order to facilitate communication between the Raspberry Pi and LTE modem, Minicom was installed as a terminal-based application for managing

serial connections. Following installation, initial tests confirmed connectivity by sending basic AT commands (e.g., “AT”) to the modem (Telit, 2020), with an “OK” response verifying successful communication. Further AT commands were used to retrieve critical LTE metrics, such as RSRP, RSRQ, RSSI and SINR, which collectively provide a comprehensive view of LTE signal quality under various operational conditions. GPS functionality was activated with commands designed to initialize and stream location data in real-time, ensuring accurate spatial data alongside LTE metrics.

Data logging and management were automated through a MySQL database created on the Raspberry Pi, configured to store LTE and GPS data with precise timestamps. A Python script automated the data collection process by periodically sending AT commands to capture and log LTE metrics and GPS coordinates, with data entries stored in the MySQL database every 5 seconds. This script managed dual serial connections for LTE (on ttyUSB2) and GPS (on ttyUSB1), timestamping the collected data and formatting it for database storage.

For real-time monitoring and control during aerial trials, remote access to the Raspberry Pi was established via SSH using Putty from the ground control station (GCS). Given that the UAV and GCS might operate on different LTE networks for the UAV and Wi-Fi for the GCS, secure access was enabled by either Pi Tunnel or Zerotier VPN. This VPN configuration facilitated a secure link, allowing continuous interaction with the Raspberry Pi from the GCS. The Pixhawk flight controller was also integrated into the setup to manage UAV flight parameters, with the Mission Planner software on the GCS providing telemetry and control over the LTE network. In order to support real-time telemetry, UAV-Cast Pro software was installed on the Raspberry Pi, enabling continuous data streaming from the Pixhawk to the GCS over LTE. The UAV-Cast Pro installation was straightforward, initiated with a single command (curl -s http://install.uavmatrix.com | sudo bash), after which the software was ready to interface with the GCS.

The initial stationary testing, conducted in a controlled indoor environment, aimed to validate the system's data collection capabilities and ensure LTE metrics were accurately captured in a consistent and stable setting, without interference from outdoor environmental factors. This phase was essential for proving the testbed's functionality before more complex, altitude-dependent trials. During data collection, the Python script captured LTE parameters and GPS coordinates every 5 s, with the GCS operator remotely monitoring the data stream via UAV-Cast Pro and SSH. All collected data was stored in the MySQL database for subsequent analysis. At the end of each trial, data was exported from the database in CSV format to facilitate analysis in external tools such as MATLAB or Python-based software, where the LTE metrics were further examined across various altitudes.

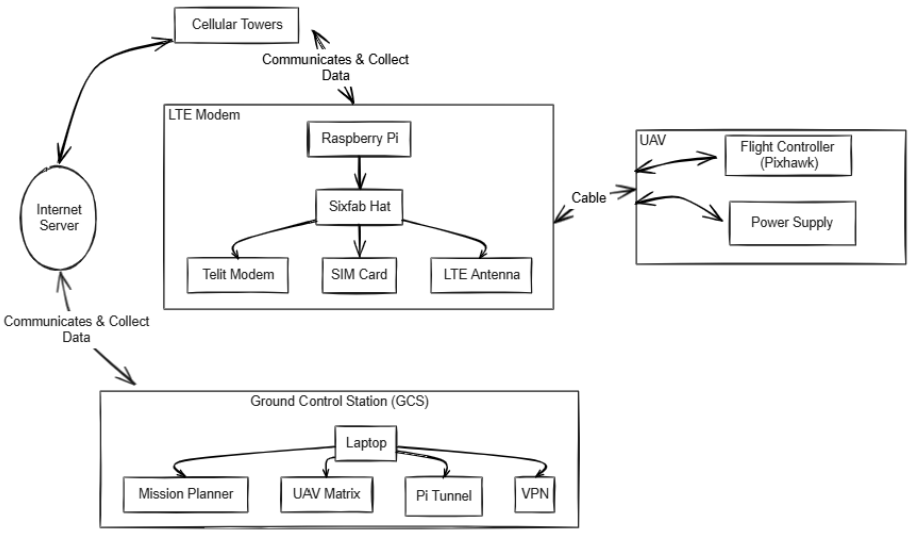

Figure 2: Setup of the initial indoor testing phase.

4. RESULTS AND DISCUSSION

While this paper does not focus on radio propagation effects, the initial testing conducted from a stationary platform effectively demonstrated the testbed's capacity to consistently capture critical LTE network metrics. This highlights the system's ability to manage data logging and ensure connectivity under controlled conditions, providing a baseline for subsequent experiments where altitude and environmental factors will be considered. These metrics RSRP, RSSI, RSRQ and SINR were collected at consistent intervals and recorded alongside GPS coordinates in a structured, timestamped dataset. This preliminary testing phase confirmed the testbed's functional readiness and data accuracy, providing a dependable reference point for future tests that will introduce greater complexity through varying altitudes and environments. Table 1 shows a sample of the data collected during the initial testing phase using the LTE modem.

Table 1: Sample of LTE network metrics collected during initial testing using the LTE modem.

Timestamp	RSRP (dBm)	RSSI (dBm)	RSRQ (dB)	SINR (LINEAR)
15/10/2023 11:41:12	-92	-57	-18	84
15/10/2023 11:42:02	-92	-58	-19	71
15/10/2023 11:43:01	-61	-38	-7	196
15/10/2023 11:44:03	-56	-35	-6	161
15/10/2023 11:45:03	-72	-47	-9	133
15/10/2023 11:46:02	-76	-51	-10	119
15/10/2023 11:47:01	-61	-33	-13	97

The successful recording of consistent LTE metrics underscores the testbed's capability as a reliable tool for UAV connectivity research. By collecting data directly in real-world conditions, the testbed provides a significant advantage over laboratory simulations. Simulations, while useful, often fail to capture practical challenges such as environmental interference, variable signal strength and the effects of obstructions. In contrast, field tests, such as those enabled by this testbed, offer insights that reflect actual conditions, enhancing the relevance and applicability of the findings to UAV applications that require robust, adaptable connectivity.

A particularly notable feature of the testbed is its support for direct antenna comparison in real world settings. By allowing the easy substitution of different LTE antennas, such as off-the-shelf versus standard device antennas, the testbed enables practical assessments of how specific antenna types perform across different scenarios. This is especially valuable for UAV applications where reliable, uninterrupted connectivity is critical, as it provides researchers with data-driven guidance on optimal antenna configurations. In practical terms, this setup allows for empirical comparisons that are more meaningful than theoretical analyses alone, as they consider environmental factors that may impact antenna performance.

The testbed's adaptability and scalability further highlight its potential as a versatile tool for UAV research. Its modular design allows researchers to deploy the system across various altitudes and environmental contexts, opening avenues for testing under conditions that more closely mirror the challenges faced in real UAV operations. This flexibility supports a broad range of research goals, from optimizing connectivity in high-altitude operations to studying the impact of urban environments on LTE signal stability.

While these initial results are promising, they are limited by the stationary nature of the test. Future trials at varied altitudes and in dynamic flight scenarios will be essential to fully assess the testbed's capabilities and limitations. Additional testing under different LTE network configurations or with enhanced GPS accuracy measures could further improve its utility. By expanding the scope of testing, researchers can gain a more comprehensive understanding of the connectivity challenges UAVs face and refine the testbed to support increasingly complex UAV missions.

In summary, this testbed provides a practical, field-deployable solution that advances UAV LTE connectivity research. Its ability to deliver empirical insights on LTE performance across different antennas and environments makes it an effective tool for studying UAV communication in real-world contexts, supporting the development of more robust and adaptable UAV connectivity frameworks.

4. CONCLUSION

In conclusion, this paper presents the design and preliminary evaluation of an LTE-based testbed for UAVs, which aims to advance the development of cellular-connected UAV technologies. The integration of a Raspberry Pi, LTE modem and modular antenna system has provided a flexible, scalable and field-deployable platform capable of collecting critical LTE network metrics, including RSRP, RSSI, RSRQ and SINR. The initial stationary tests have successfully validated the system's ability to capture and log these parameters in real-time, establishing a reliable baseline for future trials under dynamic flight conditions.

Looking forward, the testbed will facilitate further exploration of UAV cellular connectivity across various altitudes and environmental scenarios. The inclusion of antenna analysis within the system will also help identify optimal configurations to enhance signal stability and network performance in different operational contexts. As the field of UAVs continues to evolve, this LTE testbed offers a valuable tool for improving UAV communications, supporting more efficient, reliable and scalable cellular connectivity. Future work will focus on conducting additional flight-based tests and refining the system to meet the challenges of real-world deployment, thereby contributing to the broader goal of integrating UAVs into cellular networks for diverse applications.

5. ACKNOWLEDGEMENT

The authors would like to thank Universiti Kuala Lumpur (UniKL) for its research support. This research work is funded by UniKL under the UniKL Excellent Research Grant Scheme (UERGS) (UER22005).

REFERENCES

Alshalabi, O., Mohd Kamal, N.L., Sahwee, Z., Norhashim, N. & Shah, S.A. (2022). Feasibility of LTE-connected unmanned aerial vehicle. *2022 IEEE Symp. Future Telecomm. Tech. (SOFTT 2022)*, 14-16 November 2022, Johor Baharu, Malaysia, pp. 120–124.

Brar, R.S. & Mérida, W. (2024). Autonomous airborne transportation: Field trials in urban water landscapes. *IEEE Intell. Transp. Syst. Mag.*, **17**: 2–11.

Braunfelds, J., Jakovels, G., Murans, I., Litvinenko, A., Senkans, U., Rumba, R., Onzuls, A., Valters, G., Lidere, E. & Plone, E. (2024). Experimental study on LTE mobile network performance parameters for controlled drone flights. Sensors, **24**: 6615.

Chen, W., Lin, X., Lee, J., Toskala, A., Sun, S., Chiasserini, C. F., & Liu, L. (2023). 5G-advanced towards 6G: past, present, and future. *IEEE J. Sel. A. Commun*, **24**: 1592–1619.

Izydorczyk, T., Berardinelli, G., Mogensen, P., Ginard, M.M., Wigard, J. & Kovacs, I.Z. (2020a). Achieving high UAV uplink throughput by using beamforming on board. *IEEE Access*, **8**: 82528–82538.

Izydorczyk, T., Bucur, M., Tavares, F.M.L., Berardinelli, G. & Mogensen, P. (2018). Experimental evaluation of multi-antenna receivers for UAV communication in live LTE networks. *2018 IEEE Globecom Workshops*, 9-13 December 2018, Abu Dhabi, UAE.

Izydorczyk, T., Ginard, M. M., Svendsen, S., Berardinelli, G. & Mogensen, P. (2020b). Experimental evaluation of beamforming on UAVs in cellular systems. *IEEE 92nd Veh. Technol. Conf. (VTC 2020)*, Victoria, British Columbia, Canada.

Michailidis, E.T., Maliatsos, K. & Vouyioukas, D. (2024). Software-defined radio deployments in UAV-driven applications: A comprehensive review. *IEEE Open J. Veh. Technol.*, **5**: 1545–1586.

Mohd Kamal, N.L., Sahwee, Z., Abdul Hamid, S., Norhashim, N. & Lott, N. (2019). Cellular network and its relevance for unmanned aerial vehicle application in Malaysia. *IOP Conf. Ser. Mat. Sci. Eng.*, **705:** 012009.

Mohd Kamal, N.L., Sahwee, Z., Hamid, SA. & Norhashim, N. (2019). On the reliability of throughput performance in packet-based mobile network under varying load using time-stepped simulation. *7th Int. Conf. Smart Comput. Commun. (ICSCC 2019)*, 28-30 June 2019, Sarawak, Malaysia

Muruganathan, S.D., Lin, X., Määttänen, H.-L., Sedin, J., Zou, Z., Hapsari, W.A. & Yasukawa, S. (2021). An overview of 3GPP release-15 study on enhanced LTE support for connected drones. *IEEE Commun. Stand. Mag.*, **5**: 140-146

Sixfab. (2024). *Getting Started with Base HAT + Telit Modules*. Available at: https://docs.sixfab.com/docs/getting-started-with-base-hat-and-telit-le910c1-module (Last access date: 16 November 2024).

Telit. (2020). *LE910Cx AT Command Reference*. Telit, Sgonico, Italy.

DESIGN OF A BUCK CONVERTER FOR STABLE VOLTAGE OUTPUT IN NANOSATELLITE APPLICATIONS

Yasser Asrul Ahmad*, Tuan Muhammad Aidiel Tuan Kamazon, Anis Hannani Razaman, Norazlina Saidin & Othman Omran Khalifa

Department of Electrical and Computer Engineering, Kulliyyah of Engineering, International Islamic University Malaysia (IIUM), Malaysia

*Email: yasser@iium.edu.my

ABSTRACT

In a nanosatellite or CubeSat operation, the size, weight and power efficiency of the satellite are critical. Traditional linear regulators, being inefficient and prone to excessive heat generation, are unsuitable for these applications. This project designed a buck converter to address these issues by efficiently reducing voltage and minimising power losses. The process included a comprehensive literature review, parameter determination, circuit design, and implementation on a printed circuit board (PCB) using KiCad. This project successfully achieved the design of a buck converter that steps down a +28 V input to a +5 V output and is capable of supplying current of up to 3 A to the load. Simulation results facilitated optimisation, leading to a highly efficient and stable buck converter suitable for CubeSat power regulation, thereby advancing robust power solutions for space missions.

Keywords: *Buck converter; voltage regulation; CubeSat; DC-DC conversion; KiCad.*

1. INTRODUCTION

Satellites operate in harsh conditions where size, weight and power efficiency are critical. Traditional linear regulators are unsuitable due to their inefficiency and heat generation. In satellite power systems, precise voltage regulation is essential for both charging processes and the varied voltages required by the satellite's subsystems. A buck converter, or "step-down" converter, is a type of voltage regulator that reduces the input voltage to a specified lower level. Nanosatellite subsystems, payloads and modules such as star sensors, Global Navigation Satellite Systems (GNSS) modules and transceivers, have varying power demands. A buck converter should maintain a stable +5V output despite these fluctuations. Unstable voltage output can result in malfunctions or system resets, jeopardising mission objectives (Zhang *et al*., 2024).

The fundamental operation of a buck converter involves regulating energy delivered to the load through a switching mechanism. For example, the CubeSat power supply by Page *et al*. (2022) uses a resonant buck converter design with a low-noise circuit to reduce noise coupled through power supply switching. Additionally, the CubeSat electrical power system (EPS) in the source uses a three-level flying capacitor (3L-FCC) architecture for its DC-DC buck converter (Marin *et al*., 2023). This specific design uses a +5V to +3.3V DC-DC conversion system to provide low voltage levels from the battery pack to the satellite's functional blocks. Recent advancements in DC-DC converter technology have significantly enhanced satellite power systems. A comprehensive review highlights the critical role of buck converters in small satellites, emphasising their efficiency in stepping down bus voltages to power low-voltage subsystems (Ravindran & Massoud, 2025).

Circuits known as DC-DC converters are able to change a DC voltage into a different controlled DC voltage level (König & Nagy, 2022). The configuration of the parts that make up a DC-DC converter is referred to as the converter topology. Non-isolated DC-DC converters are often made up of diodes,

transistors, inductors and capacitors. Two different DC-DC converter topologies are used in the electronic power system (EPS) design for CubeSats. For CubeSat EPS applications, the recommended DC-DC converters are buck converter and single-ended primary-inductor converter (SEPIC) (Darbali-Zamora *et al*., 2018). Efficiency, control, load regulation, synchronisation, power consumption with inhibit on, load transient response and turn-on tests are among the tests carried in order to assess potential performance and reliability difficulties with DC-to-DC converter use in space (Barath et al., 2022). An integrated buck converter for usage in satellite EPS with high bus voltage in a two-switch forward converter was proposed by Park *et al*. (2023), where the suggested converter can significantly lower its cost, weight and volume by doing away with the switch and diode and integrating the buck converter into the two-switch forward converter. The proposed converter was verified with +28 V input and +5 V output.

This project focuses on designing a reliable and efficient buck converter for CubeSat power systems, reducing a +28 V input, a standard voltage bus for many modern satellites, to a stable +5 V output at current of 3 A with a 400 kHz switching frequency. The design aims for a voltage ripple below 5% to ensure consistent performance and minimal interference with satellite subsystems. The development processes involve theoretical calculations, simulations using PSPICE from Texas Instruments (TI) to optimise component values and predict behaviour, as well as practical implementation with KiCad for printed circuit board (PCB) design. Rigorous testing will confirm the converter's ability to maintain stable output under varying load conditions, ensuring suitability for critical satellite applications.

2. METHODOLOGY

This section outlines a systematic and thorough approach to achieve the project's dual objectives of designing an efficient buck converter and implementing it on a PCB for CubeSat deployment. Figure 1 shows the block diagram of overall EPS design, while Figure 2 shows the flowchart of designing the buck converter for satellite applications. Designing a buck converter in nanosatellites is crucial for voltage stability because it ensures a steady +5V output from a standard +28V satellite power bus, preventing voltage fluctuations that could disrupt sensitive electronics. The methodology involves a structured process beginning with component sizing to ensure that all parts meet the specific requirements for satellite operations. Following this, a schematic design is created, which outlines the electrical connections and component placements. Simulation and optimisation are then performed using PSPICE from TI to verify the design's functionality and make necessary adjustments. Once the design is validated, it proceeds to circuit implementation on a PCB, utilising KiCad to lay out and produce the physical board. Finally, comprehensive documentation and reporting are conducted to record the design process, test results and performance metrics, ensuring that all steps are meticulously documented, and the design meets the stringent standards required for satellite applications.

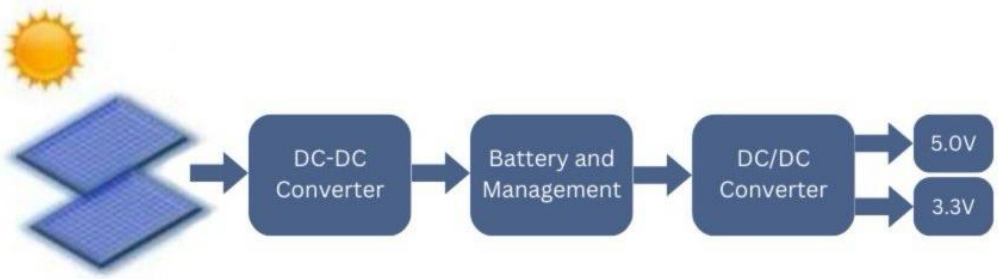

Figure 1: Overall EPS design.

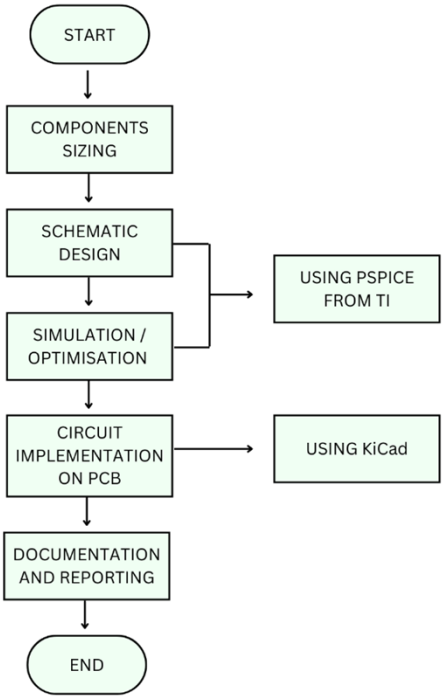

Figure 2: Flowchart for design of the buck converter.

2.1 Design Parameters

The design of a buck converter for CubeSat applications requires careful consideration of several key parameters to ensure reliable operation in the demanding environment of space. The converter is specified to step down an input voltage of +28 V to an output voltage of +5 V, capable of supplying a maximum output current of 3 A. This specification is designed to be versatile, providing stable power to various payloads such as star sensors, GNSS modules, receivers and transceivers in a CubeSat. Since most payloads and subsystems typically operate at +5V, the converter ensures that the current is automatically adjusted based on each subsystem's power consumption. In order to achieve efficient power conversion, and minimise size and weight, the converter operates at a high switching frequency of 400 kHz. This high frequency allows for the use of smaller passive components, which is crucial for the compact and weight-sensitive nature of CubeSat systems. Table 1 shows the parameters of the buck converter design.

Table 1: Design parameters.

Design Parameter	Value
Input voltage, V_{IN}	+28 V
Output voltage, V_{OUT}	+5 V
Maximum output current, I_{OUT}	3 A
Switching frequency, f_{sw}	400 kHz

In this project, an integrated circuit of LMR33630 will be used for the buck converter design. The LMR33630 regulator is a user-friendly, synchronous, step-down DC - DC converter that offers high efficiency for rugged industrial applications. This integrated circuit (IC) supports input voltages up to +36 V, making it suitable for satellite power systems that often experience wide voltage variations. Additionally, the LMR33630's small footprint and integrated features, such as low quiescent current and over-voltage protection, enhance the reliability and compactness of the power supply design,

essential for space-constrained satellite platforms (TI, 2024). These attributes collectively ensure reliable and efficient power conversion critical for satellite operations.

A Raspberry Pi Zero, which requires a +5 V supply voltage and draws around 1.0 - 1.2 A, was chosen as the load for the buck converter design to realistically represent satellite power requirements, necessitating a 3 A output capacity to ensure reliable performance and support additional peripherals. This selection provides a relevant scenario for evaluating the buck converter's effectiveness in meeting the power requirements of satellite subsystems.

2.2 Component Sizing

Component sizing is crucial for ensuring optimal performance, efficiency and reliability when designing the LMR33630 buck converter for satellite applications. These calculations play a vital role in tailoring the buck converter's power stage to meet specific design requirements, optimising performance and ensuring effective power conversion in applications such as CubeSat power systems. All formulas used are based on the LMR33630's datasheet (TI, 2024) and Hauke's buck converter datasheet (Hauke, 2011).

Initially, the switching frequency is required to be selected. Determining the switching frequency value for the LMR33630 buck converter in a satellite application is crucial in providing an optimal balance between component size, efficiency and thermal performance. A 400 kHz frequency allows for the use of smaller inductors and capacitors, reducing the overall weight and volume of the power supply, which is essential in space-constrained satellite systems. In order to set the switching frequency to 400 kHz, an R_T resistor or simply the "timing resistor" with a value of 100 kΩ is chosen, as specified in the converter's datasheet. This resistor is connected to the PG pin of the buck converter LMR33630 IC as shown in Figure 2.

The output voltage of the LMR33630 buck converter is externally adjustable using a resistor divider network. The divider network comprises of R_{FBT} and R_{FBB} and closes the loop between the output voltage and the converter. The converter regulates the output voltage by holding the voltage on the FB pin equal to the internal reference voltage, $V_{REF.}$ The resistance of the divider is a compromise between excessive noise pick-up and excessive loading of the output. Smaller values of resistance reduce noise sensitivity but also reduce the light-load efficiency. The recommended value for R_{FBT} is 100 kΩ because it provides reasonable gain without introducing excessive noise. Once R_{FBT} is selected, Equation 1 is used to select R_{FBB}. V_{REF} is nominally 1 V because modern integrated circuits such as LMR33630 can generate a stable 1 V reference with high precision, which is essential for maintaining a consistent output voltage.

$$R_{FBB} = \frac{R_{FBT}}{\frac{V_{OUT}}{V_{REF}} - 1} = \frac{100\ x\ 10^3}{\frac{5}{1} - 1} = 25\ k\Omega \quad (1)$$

For this project, V_{OUT} is set to 5 V because a subsystem in the satellite which is Raspberry Pi Zero that requires 5 V to operate has been assumed. Therefore, R_{FBB} = 25 kΩ is chosen.

The load resistor value in the circuit of buck converter is determined by the relationship between the output voltage, output current, and Ohm's Law, which states that:

$$R = \frac{V_{OUT}}{I_{OUT}} = \frac{5}{3}\ \Omega \quad (2)$$

Thus, the value of the load resistor in the circuit is $\frac{5}{3}$ Ω. This value ensures that the output current of 3A is maintained when the output voltage is 5V.

The inductance value is critical in controlling the ripple current, with typical designs aiming for a peak-to-peak inductor current ripple of 20-40% of the maximum output current. The optimum value for inductor ripple current is 30% of the maximum load current (Pressman et al., 2009). Therefore, the desired inductor current ripple for this project is 1 A. The selection of inductance for this project is calculated using the following equation:

$$L = \frac{(V_{IN} - V_{OUT})}{(f_{SW} \,.\, K \,.\, I_{OUT})} \cdot \frac{V_{OUT}}{V_{IN}} = \frac{(28-5)}{(400x10^3 \,.\, 0.333 \,.\, 3)} \cdot \frac{5}{28} = 10.3\ \mu H \approx 10\ \mu H \qquad (3)$$

where the constant K is the percentage of desired inductor current ripple, ΔI_L over the maximum load current, I_{OUT}. The value for K is 0.333, which is 30% of the maximum output current. After the calculation has been conducted, an inductance L = 10 µH is found.

Selecting the output capacitor for the LMR33630 buck converter is crucial for stabilising the output voltage and reducing ripples. The output capacitor must have a sufficient capacitance value to smooth out the voltage variations and filter the switching noise. The required capacitance is calculated using the following equation:

$$Cout = \frac{\Delta I_L}{8 \,.\, f_{SW} \,.\, \Delta V_{OUT}} = \frac{1}{8 \,.\, 400\ x\ 10^3 \,.\, 6.5\ x\ 10^{-3}} = 48\ \mu F \qquad (4)$$

where ΔV_{OUT} is the output voltage ripple, ΔI_L is the inductor current ripple and f_{sw} is the switching frequency. A minimal output voltage ripple is crucial for satellite applications to ensure the stability and reliability of sensitive electronic components. Therefore, an output voltage ripple of 6.5 mV is chosen. After the calculation has been conducted, output capacitor, C_{OUT} = 48µF is found.

The selection of input capacitors C_{IN} and C_{HF} for the LMR33630 buck converter in satellite applications is driven by the need to ensure stable operation, filter out high-frequency noise and manage input voltage transients.

- C_{IN} =10 µF

This capacitor serves as the main input capacitor and is responsible for providing the bulk of the charge needed during the switching cycles. A 10 µF capacitor is chosen to smooth out input voltage fluctuations and provide a stable DC input to the converter. It helps in reducing input voltage ripple, ensuring that the input voltage remains steady despite the pulsing nature of the converter's operation (TI, 2024). This is crucial in satellite applications where input voltage stability is critical for reliable performance.

- C_{HF} = 220 nF

This capacitor is typically a high-frequency bypass capacitor placed close to the IC. Its primary function is to filter out high-frequency noise and spikes that can be generated by the switching action of the converter (TI, 2024). A 220 nF capacitor is chosen because it has a low impedance at high frequencies, effectively shunting high-frequency noise away from the power input and preventing it from affecting the performance of the converter and other sensitive satellite electronics.

In the LMR33630 buck converter, the selection of bootstrap capacitor, C_{BOOT} is critical for the efficient operation of the internal high-side MOSFET gate driver. The bootstrap capacitor is connected between the BOOT pin and the SW pin of the LMR33630 IC, and its primary function is to provide the necessary charge to the gate of the high-side MOSFET, enabling it to switch on and off efficiently. A 0.1 µF

capacitor is large enough to hold sufficient charge to keep the gate voltage high, ensuring proper MOSFET operation throughout the switching period.

C_{VCC} stands for the capacitor connected to the V_{CC} pin of the buck converter. The V_{CC} pin typically supplies power to the internal control circuitry of the converter. The selection of the C_{VCC} for LMR33630 buck converter in a satellite application is essential for ensuring stable operation and reliable performance of the converter's internal circuitry. A 1 µF capacitor is large enough to filter out any noise and voltage fluctuations, ensuring a smooth and stable V_{CC} voltage, which is critical for the consistent operation of the internal logic and gate drivers.

Table 2 shows all the calculated component values to meet the desired design.

Table 2: Component Values

$C_{IN} + C_{HF}$	C_{VCC}	C_{BOOT}	L	R_T	R_{FBT}	R_{FBB}	C_{OUT}	R_{LOAD}
$10\ \mu F + 220\ nF$	$1\ \mu F$	$100\ nF$	$10\ \mu H$	$100\ k\Omega$	$100\ k\Omega$	$25\ k\Omega$	$47\ \mu F$	$5/3\ \Omega$

2.3 Schematic Design

Once all the parameters and components in the buck converter circuit have been carefully calculated, a detailed design process is initiated to implement the converter. Using the PSPICE, the components are arranged carefully because it is crucial for optimal performance and efficiency. Figure 3 shows the schematic design of the buck converter.

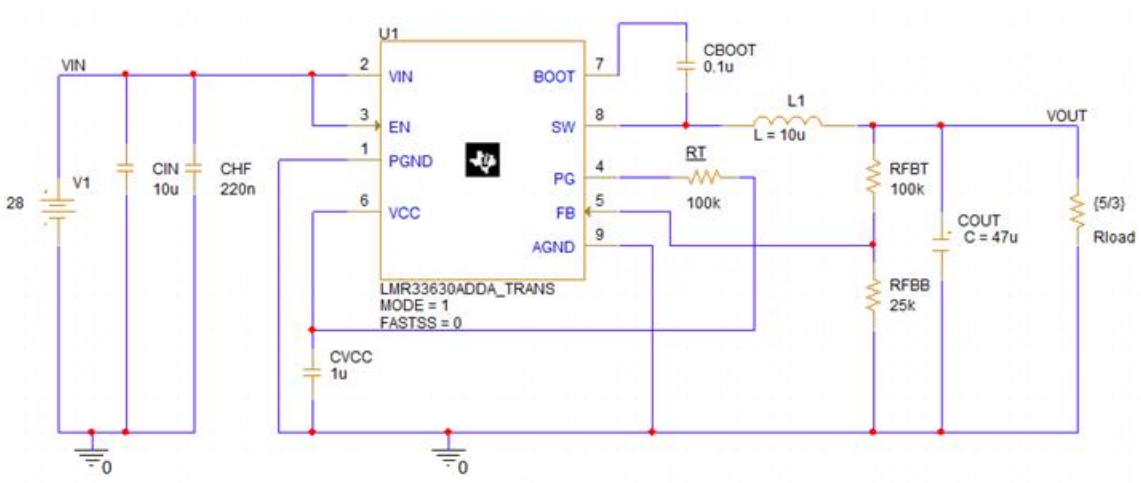

Figure 3: Schematic design of buck converter.

The circuit design for the LMR33630 buck converter tailored for satellite applications involves carefully considered component placement and positioning to achieve the desired conversion from a +28 V input to a +5 V output at 3 A. The input voltage (V_{IN}) is stabilised with a 10 µF ceramic capacitor (C_{IN}) and a 220 nF high-frequency capacitor (C_{HF}) to filter out any noise. The LMR33630 IC (U1) is centrally placed, with its V_{IN} pin (pin 2) connected to the input voltage. The enable pin (EN, pin 3) is tied to V_{IN}, ensuring the converter is always active. A 1 µF capacitor (C_{VCC}) is placed between the V_{CC} pin (pin 6) and ground to stabilise the internal supply voltage. The switching node (SW, pin 8) connects to a 10 µH inductor (L1), which then connects to the output voltage (V_{OUT}). The feedback network consists of resistors R_{FBT} (100 kΩ) and R_{FBB} (25 kΩ), which set the output voltage. A 47 µF output capacitor (COUT) ensures smooth output. The boot capacitor (C_{BOOT}, 0.1µF) is connected between the

BOOT pin (pin 7) and SW pin to drive the high-side FET. Additionally, a resistor (R_T, 100 kΩ) is connected to the R_T pin (pin 4) to set the switching frequency to 400 kHz. Proper grounding and short, direct connections are maintained to minimize noise and ensure stability, which is crucial for the high-reliability requirements of satellite applications (Kőnig *et al*., 2021).

2.4 Simulation and Optimisation

After completing the design of the circuit, the buck converter is simulated using PSPICE. The simulation is to analyse the performance of the buck converter under various operating conditions without the need for physical prototypes. In this designing a buck converter for satellite applications, we will analyse the desired design specifications such as input voltage, output voltage and output current performance. Besides that, we will do a performance comparison under different loads between the basic buck converter design and the actual design of this project which is LMR33630 buck converter. Both circuits will be placed on the same schematic page to conduct the performance comparison.

2.5 Circuit Implementation on PCB

The circuit implementation on PCB for the buck converter involves several meticulous steps to ensure reliability and performance in satellite applications. Initially, the design is created using KiCad, an open-source PCB design tool that allows for detailed schematic capture and PCB layout. The process starts with importing the verified circuit design from PSPICE for TI simulations, followed by component selection tailored to meet the specific electrical and thermal requirements. Key components such as capacitors and the inductor are placed close to the IC to reduce the loop area of high-current paths, minimising EMI and ensuring stable operation. Appropriate routing of power and signal traces, and the use of proper grounding techniques are critical to minimise noise and enhance the overall performance of the buck converter. Once the PCB design is complete, it undergoes a series of reviews and simulations such as electrical rule check (ERC) and design rule check (DRC) within KiCad to verify the integrity of the design before moving to the fabrication and assembly stages (Shaheen & Mohamed, 2022).

3. RESULTS & DISCUSSION

In this section, we present the results obtained from the design, simulation and implementation of the buck converter. The primary focus of this project is to create an efficient and stable buck converter capable of stepping down +28 V input voltage to +5 V of output voltage while maintaining a high level of efficiency. In order to achieve this, various design parameters such as switching frequency, duty cycle as well as inductor and capacitor values are carefully selected and optimised. The buck converter is tested under different load conditions, and the output voltage is measured and recorded. The results demonstrate that the converter performs within the expected parameters, achieving the objectives of design specifications. This section provides a thorough evaluation of the converter's performance, highlighting its reliability and potential for satellite applications.

3.1 Performance Analysis

Performance analysis for a buck converter involves evaluating its behaviour under various conditions such as startup and steady state conditions to ensure optimal operation. Together, these analyses ensure the converter meets design specifications, performs reliably under varying conditions, and maintains stability across its operational range.

3.1.1 Input Voltage

The input voltage simulation graphs for the buck converter during startup and steady-state conditions, depicted in Figure 4, demonstrate a consistent 28V input. This constant voltage ensures that the converter operates within its specified range, maintaining efficient performance and stable power delivery to the satellite's electronic systems. The stability of the input voltage, with no significant fluctuations or noise, is critical for reliable satellite operation, indicating that the buck converter's power regulation mechanism functions effectively, providing a dependable and steady supply voltage both during startup and steady-state operations.

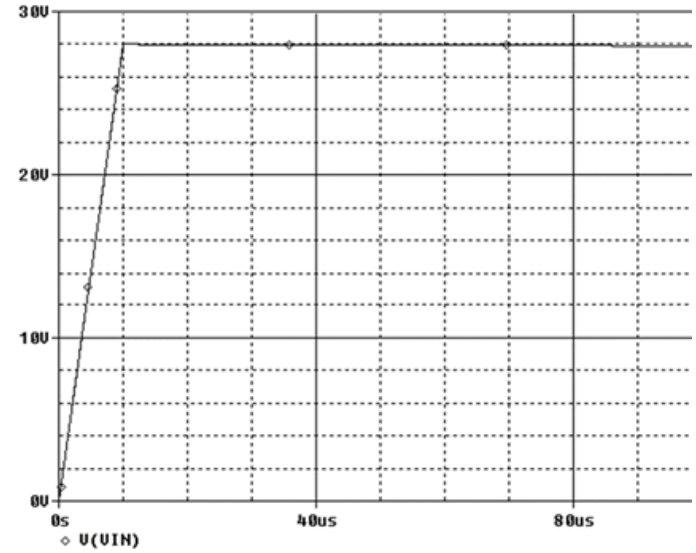

(a)

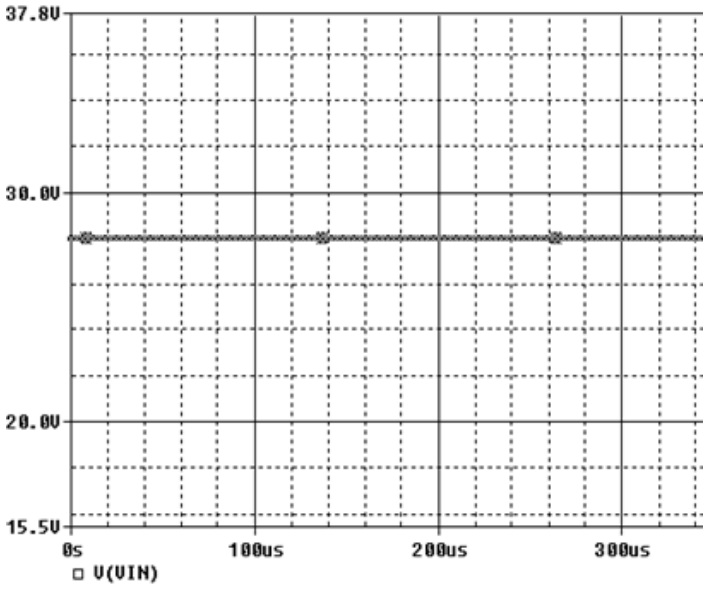

(b)

Figure 4: (a) V_{IN} startup condition. (b) V_{IN} steady state condition.

3.1.2 Output Voltage

The output voltage simulation graphs for the buck converter during startup and steady-state conditions, shown in Figure 5, illustrate the converter's performance and stability. During startup, the output voltage begins at 0 V, experiences a brief oscillation within the first 0.5 ms, and then rises linearly to stabilize near 5 V by around 4 ms, indicating effective regulation and minimal overshoot. In steady-state condition, the output voltage initially dips to about 4.4 V but quickly stabilises at 5 V, maintaining a consistent output. This stable output voltage, essential for reliable satellite operation, demonstrates the LMR33630's effective voltage regulation and steady performance under varying conditions.

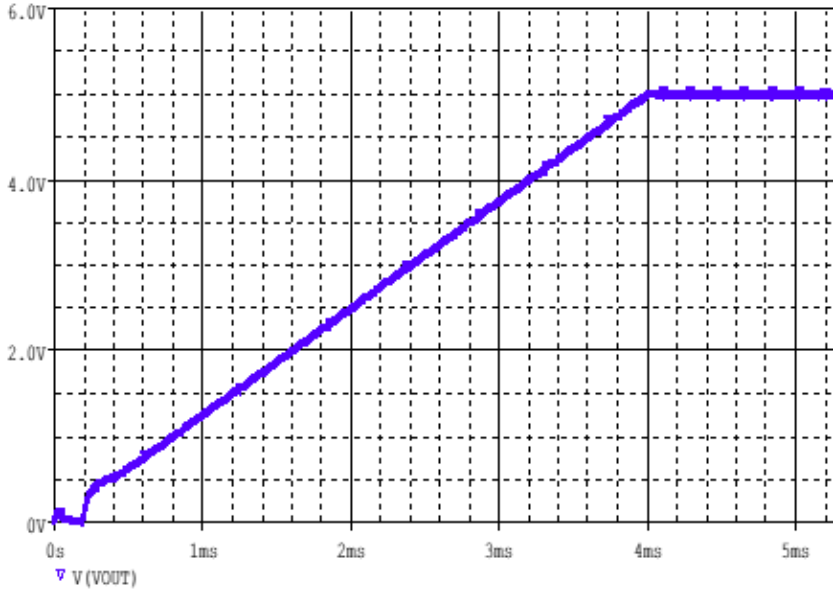

(a)

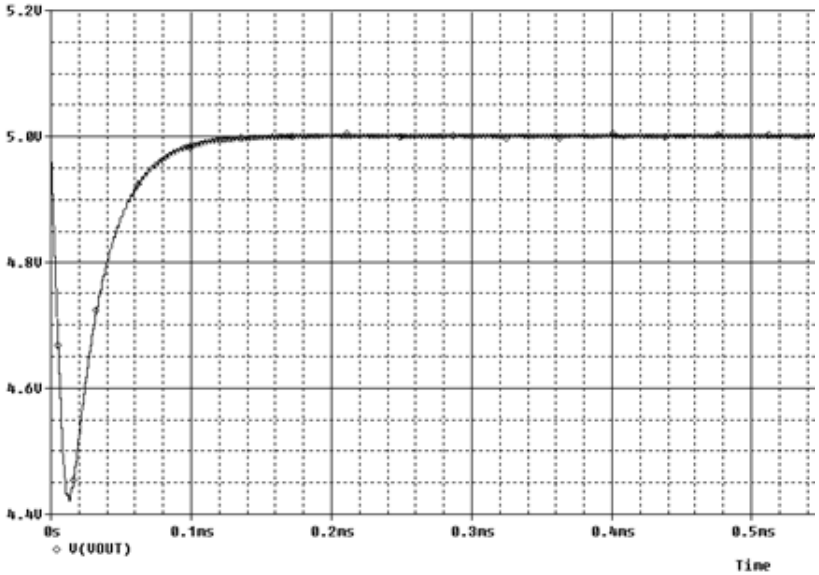

(b)

Figure 5: (a) *VOUT* startup condition. (b) *VOUT* steady state condition.

3.1.3 Output Current

The output current simulation graphs for the buck converter during startup and steady-state conditions, shown in Figure 6, demonstrate the converter's ability to provide consistent and reliable current to the load. During startup, the current begins at 0 A, exhibits brief oscillations in the first 0.5 ms, and then rises steadily to stabilise at 3 A by around 4 ms, indicating a controlled ramp-up. In steady-state conditions, the current initially dips to about 2.65 A but quickly stabilises at approximately 3 A, confirming effective regulation and consistency. This stable current delivery, essential for reliable satellite operation, highlights the LMR33630's ability to manage load requirements and maintain steady performance under varying conditions.

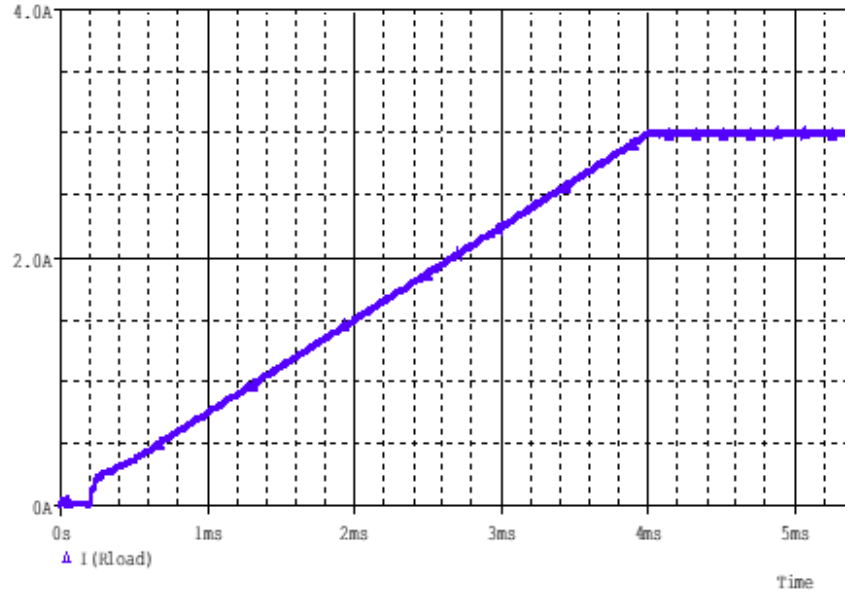

(a)

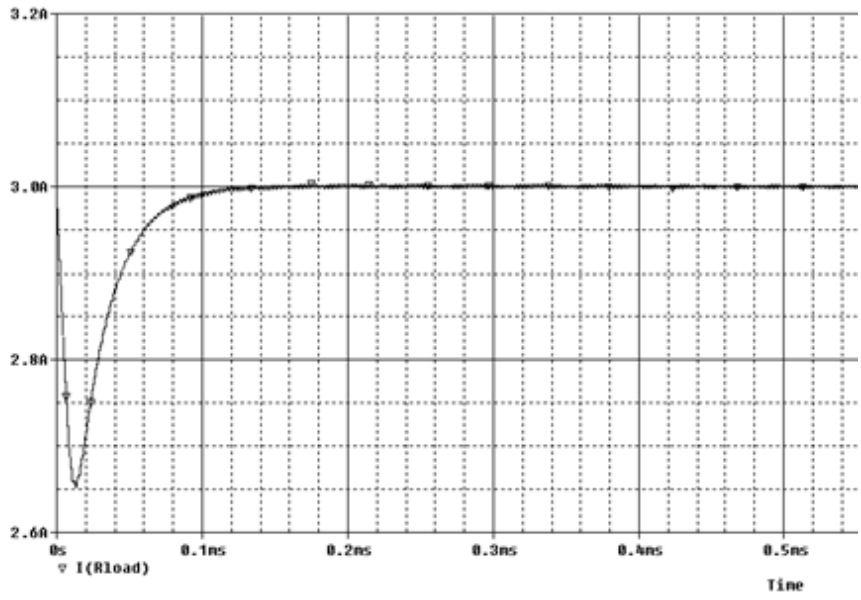

(b)

Figure 6: (a) *IOUT* startup condition. (b) *IOUT* steady state condition.

3.1.4 Inductor Current Ripple

In a buck converter, inductor current ripple is the oscillating component of the current flowing through the inductor due to switching action, superimposed on the average current, which equals the output current in steady-state operation. For satellite applications, inductor current ripple is typically maintained within 20 to 40% of the average current, translating to a range of 0.6 to 1.2 A for an average current of 3 A. Figure 7 shows the inductor current oscillating between approximately 2.5 and 3.5A, resulting in a peak-to-peak ripple of about 1.0 A, which falls within the acceptable range. This indicates that the designed LMR33630 buck converter is efficient and suitable for satellite applications. The steady-state ripple is influenced by factors such as switching frequency, input voltage, output voltage, and inductance value, ensuring the converter's stability and efficiency.

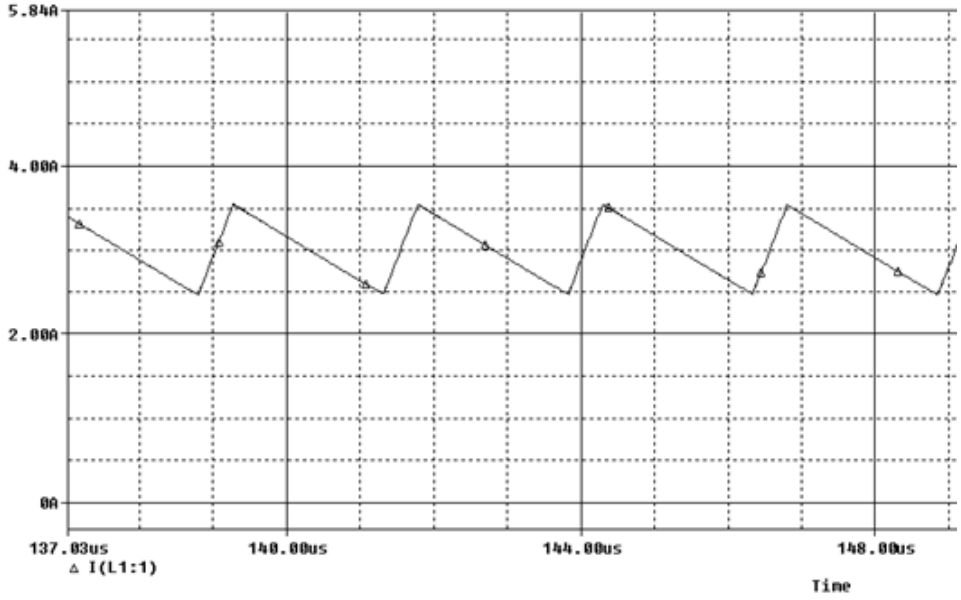

Figure 7: Indicator current ripple waveform.

3.1.5 Output Voltage Ripple

The output voltage ripple in a buck converter is a critical parameter for ensuring stable operation of sensitive electronic equipment in satellite applications. In order to meet the stringent requirements, the ripple should be less than 5% of the output voltage, or 50 mV peak-to-peak for a 5 V output. Figure 8 shows the output voltage ripple of the buck converter in steady-state, oscillating between approximately 4.9963 and 5.0032 V, resulting in peak-to-peak ripple of about 6.9 mV, which is well within the acceptable range. This minimal ripple, achieved through effective filtering, highlights the LMR33630's ability to maintain stable and consistent voltage levels, ensuring reliable performance of onboard systems in satellite applications and demonstrating its suitability for high-precision power regulation in demanding aerospace environments.

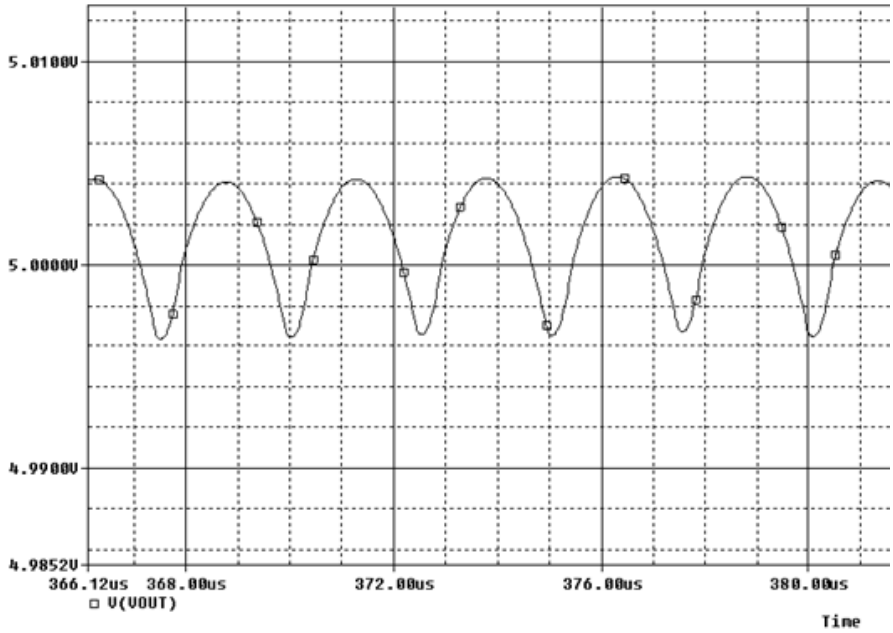

Figure 8: Output voltage ripple waveform.

3.2 Performance Comparison

Testing a buck converter under different load conditions is crucial to assess its performance and reliability, particularly for satellite applications where stable power delivery is essential. By varying load resistance and measuring key parameters, such as output voltage, the converter's load regulation and efficiency can be evaluated. This sub-section presents the performance comparison under different load resistances (1, 2, 3 and 4 Ω) of the designed LMR33630 buck converter with a basic or theoretical buck converter that shares the same design specifications.

As shown in Figure 9 and Table 3, it is observed that the output voltage for the basic buck converter has different values under different loads. Meanwhile, the output voltage value for the LMR33630 buck converter is kept constant under different loads except for 1 Ω load resistance. This indicates that the basic buck converter lacks robust regulation and stability, making it less suitable for satellite applications where consistent performance is essential. On the other hand, the LMR33630 buck converter maintains stable output voltage across various loads, demonstrating superior load regulation. This consistent output ensures reliable operation of satellite systems and instruments, which is crucial for mission success. The LMR33630's stable performance under varying loads makes it a more dependable choice for the precise and reliable power requirements of satellite applications.

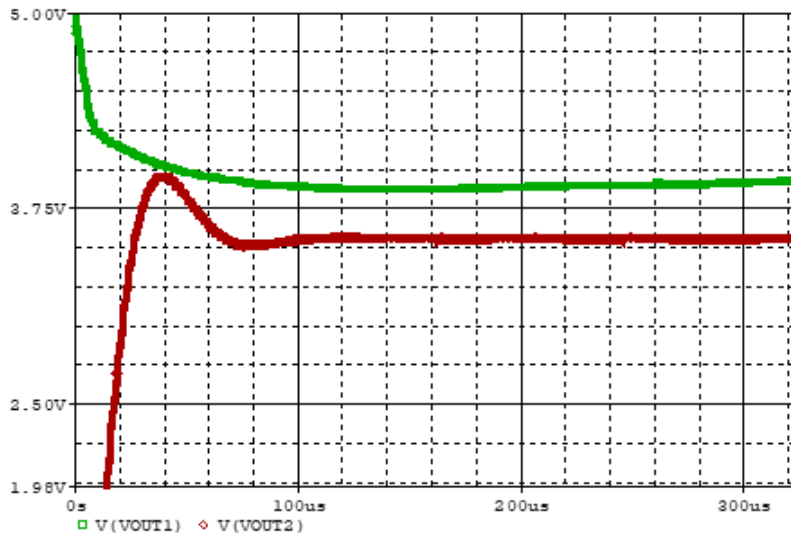
5.00V
3.75V
2.50V
1.98V
0s
100us
200us
300us
V(VOUT1)
V(VOUT2)

(a)

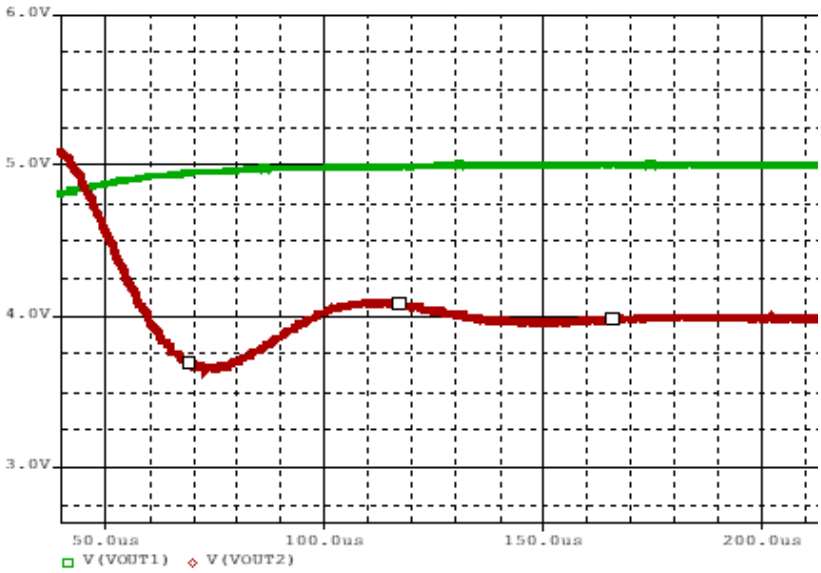
6.0V
5.0V
4.0V
3.0V
50.0us
100.0us
150.0us
200.0us
V(VOUT1)
V(VOUT2)

(b)

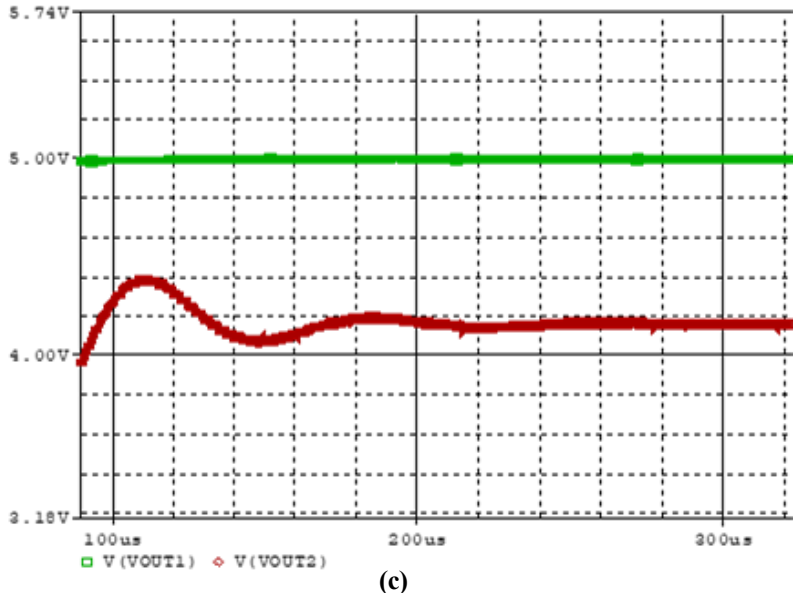
5.74V
5.00V
4.00V
3.18V
100us
200us
300us
V(VOUT1)
V(VOUT2)

(c)

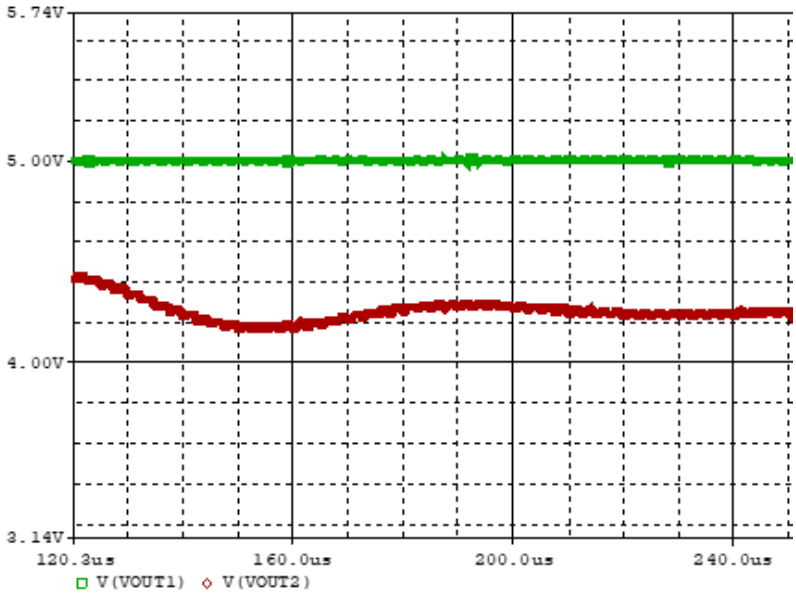

(d)

Figure 9: Performance comparison under different load resistances of (a) 1 Ω, (b) 2 Ω, (c) 3 Ω and (d) 4 Ω.

Table 3: Performance comparison for the LMR33630 and basic buck converters.

Load Resistance (Ω)	**Output Voltages (V)**	
	V_{out} LMR33630 Buck Converter (Green)	V_{out} Basic Buck Converter (Red)
1	3.94	3.56
2	5.00	3.98
3	5.00	4.16
4	5.00	4.25

In contrast, both the basic and LMR33630 buck converters are unable to achieve an output voltage of 5 V under 1 Ω load due to current limiting and thermal protection mechanisms. With output voltage of 5 V and load resistance of 1 Ohm, the current drawn would be 5 A, which exceeds the specified output current capacity of 3 A. This excessive current demand triggers the converters' overcurrent protection, reducing the output voltage to protect the device from damage.

3.3 PCB Layout Design

After completing the design and simulation of the buck converter in PSPICE, the schematic is imported into KiCad to implement it on a PCB. Defining the board outline and size based on the project requirements involves determining the physical dimensions and shape of the PCB to accommodate all the necessary components and fit within the constraints of the overall device design. Using the KiCad software, the board's perimeter was drawn using the ***Edge.Cuts*** layer, ensuring that it meets all mechanical and spatial constraints. In this project, the board dimensions for the buck converter are specified as 43.4340 mm in width and 27.6860 mm in height. Properly defining the board outline and size helps to optimise the layout process, ensuring efficient use of space and adherence to design specifications, which ultimately contributes to the functionality and manufacturability of the final product.

Next, the components on the PCB are placed with precision, beginning with the central IC to serve as the core of the layout. Essential components such as capacitors, inductors, and resistors are positioned near the IC to keep the connections as short as possible as shown in Figure 10.

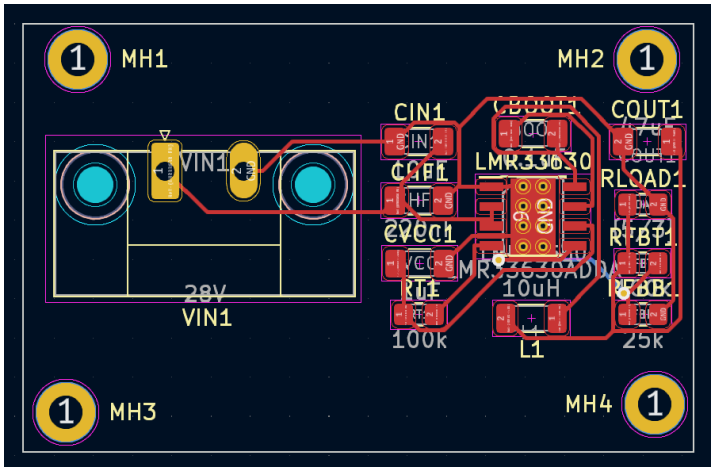

Figure 10: Placement of components on the PCB.

Four mounting holes (MH1, MH2, MH3 and MH4) are used to provide secure attachment points for the PCB, aiding in mechanical stability. The layout also shows clear distinction between the power and ground planes, which helps in reducing ground loop issues and maintaining signal integrity. This strategic placement helps to minimise the length of the electrical traces, which is crucial for reducing resistance and inductance that can cause inefficiencies and noise in the circuit. By organising the components in this manner, we can ensure better performance and reliability of the buck converter, leading to more stable and efficient power conversion.

After placing the components on the PCB, the electrical connections are carefully routed to ensure precision and optimal signal integrity. Figure 10 also shows the complete electrical connections route of the buck converter circuit on the PCB. In order to minimise resistance and heat buildup, wide traces are prioritised for high-current paths, ensuring efficient current flow. To prevent interference and maintain signal integrity, signal traces are kept separate from noisy areas, such as the switching node. Additionally, ground planes are implemented to provide a low impedance return path and enhance overall stability. In order to facilitate heat dissipation from critical components such as the integrated circuit and minimise electromagnetic interference, thermal vias are placed to maintain optimal operating temperatures (not visible in Figure 10). Thermal vias are typically small holes in a PCB that are plated with copper and used to dissipate heat from components to the board's copper layers or to heat sinks. They would appear as small, circular holes in the copper layers of the PCB once it is fabricated. This meticulous routing and grounding strategy is essential for achieving reliable and efficient buck converter design.

PCB error validation is a critical step in the design process, involving electrical rule checks (ERC) and design rule checks (DRC) to ensure the final layout is free from potential issues. The ERC process focuses on the electrical integrity of the circuit, checking for issues such as unconnected nets, short circuits, and incorrect component values or connections. Meanwhile, the DRC process examines the layout for physical issues, such as spacing violations, trace width problems and component placement errors, ensuring that the design adheres to the manufacturing constraints and standards.

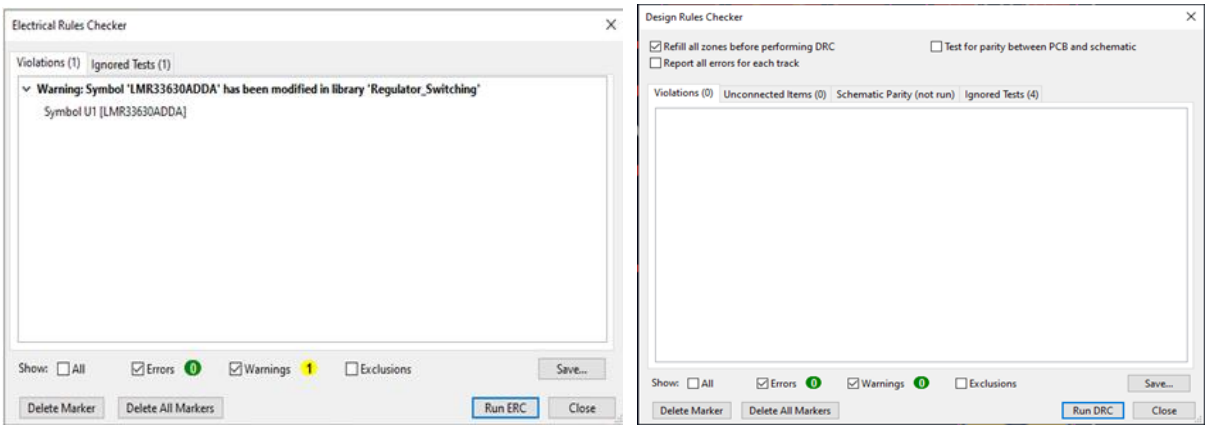

(a) **(b)**

Figure 11: Results of (a) ERC and (b) DRC.

ERC validates the electrical connections and component values, confirming that there are no unconnected nets or short circuits. Figure 11(a) shows no errors in ERC, with a minor warning due to the lack of a compatible SPICE model for the LMR33630, which does not affect the PCB implementation. DRC assesses the physical layout aspects such as component spacing, trace widths and placement. Figure 11(b) indicates no DRC violations, confirming that the PCB meets manufacturing standards and is free of schematic parity issues. The absence of errors or warnings implies that the design is robust and ready for fabrication, ensuring reliable and manufacturable PCB. Comprehensive validation through ERC and DRC is essential to guarantee a functional and dependable final product.

3.4 The 3D PCB View Result

The 3D view feature in KiCad is crucial for PCB design as it provides a realistic visual representation of the final product, allowing designers to inspect the layout in three dimensions. This helps in verifying component placements, ensuring there are no mechanical conflicts or misalignments, and checking the overall aesthetics of the board.

The 3D view of the LMR33630 buck converter on the PCB (Figure 12) offers a realistic visualisation of the component layout, ensuring neat placement, clear labels, and optimal positioning of capacitors and the inductor for minimising noise and improving efficiency. It also highlights mechanical aspects such as mounting holes and ensuring proper component clearance and fit within the enclosure, which is crucial for early issue identification and reducing costly revisions.

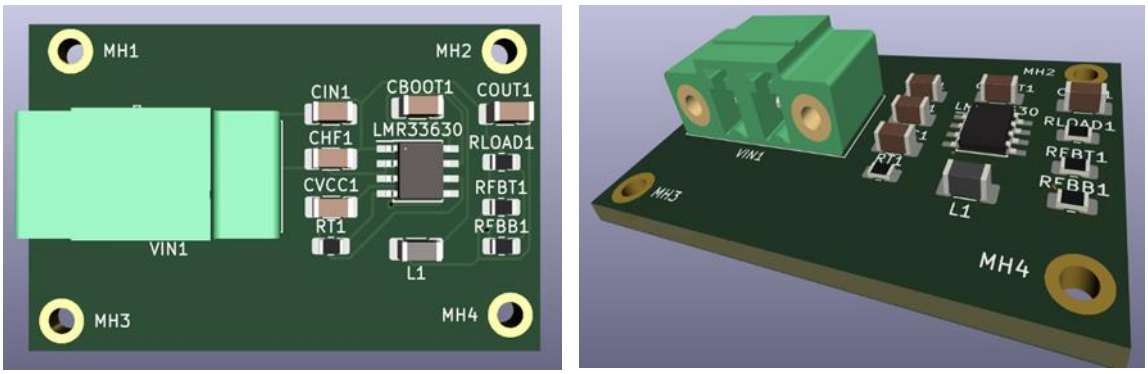

(a) **(b)**

Figure 12: The 3D view feature of PCB design: (a) Top view (b) 3D view.

4. CONCLUSION

In conclusion, this project embarked on the challenging task of designing and implementing a buck converter tailored for satellite applications, with particular emphasis on CubeSats. The critical role of power conditioning in regulating voltage for satellite subsystems and the need for efficient, compact solutions in the harsh conditions of outer space set the foundation for this study. The project successfully addressed the inefficiency associated with traditional linear regulators, introducing the buck converter as a viable alternative to meet the size, weight and power efficiency constraints crucial for satellite operations. The primary objective of designing a buck converter capable of efficiently converting input voltage to a specified output voltage, notably +5 V for CubeSats, was met through a systematic approach. The project unfolded through a comprehensive methodology, encompassing component sizing in the buck converter, a more advanced design of the buck converter using an IC with simulation, and the final implementation on a PCB using KiCad. The integration of theoretical knowledge, simulation tools and practical design considerations ensured a well-rounded project outcome. By achieving the objectives and successfully navigating the outlined methodology, this project contributes to advancing the field of power conditioning for satellite systems, enhancing their overall performance and extending mission life in the demanding conditions of space.

ACKNOWLEDGMENT

This project was funded by the Fundamental Research Grant (FRGS), Ministry Project ID: FRGS/1/2024/TK07/UIAM/02/1 through the International Islamic University Malaysia (IIUM) registered as FRGS24-347-0956.

REFERENCES

Bharath, R., Chiranjeevi, Dhanush, G.V., Karthik S. & Prarthana, J.V. (2022). Design of Buck DC-DC converter space application. *Int. J. Res. Appl. Sci. Eng. Technol.,* **10**: 1790–1794.

Darbali-Zamora, R., Cobo-Yepes, N. & Ortiz-Rivera, E. I. (2018). Design considerations based on the effects of varying temperature conditions on the efficiency of size constrained electronic power supplies for CubeSat applications. *17th IEEE Intersoc. Conf. Therm. Thermomech. Phenom. Electron. Syst. (ITherm 2018),* 29 May - 1 June 2018, San Diego, California, US, pp. 778–787.

Hauke, B. (2011). *Basic Calculation of a Buck Converter's Power Stage. Texas Instruments.* Available online at: https://www.ti.com/lit/pdf/slva477 (Last access date: 1 November 2024).

König, T. & Nagy, L. (2022). Conducted emission measurement of interleaved DC-DC buck converters. *2022 ESA Workshop Aerosp. EMC,* 23-25 May 2022, Held online, pp. 1–5.

Marin, J., Gak, J., Cortes, A., Calarco, N., Oliva, A., Lindstrom, E., Miguez, M., Falcon, A., Osterman, N. & Rojas, C. A. (2023). Integrated Three-Level Flying Capacitor DC-DC Buck Converter for CubeSat Applications. *2023 Arg. Conf. Electron. (CAE 2023),* 9-10 March 2023, Cordoba, Argentina, pp. 90–95.

Page, C. L., Hess, H. & Cahoy, K. (2022). A CubeSat power supply implementing a zero voltage switching resonant buck converter design with low electronic & radio frequency noise. *IEEE Int. Symp. Ind. Electron. 2022 (ISIE 2022),* 1-3 June 2022, Anchorage, Alaska, US, pp. 921–926.

Park, J.-E., Han, J.-K., Choi, S.-H. & Moon, G.-W. (2023). Two-switch forward converter with an integrated buck converter for high bus voltage in satellites. *IEEE Trans. Power Electron.,* **38**: 2041–2051.

Pressman, A. I., Billings, K. & Morey, T. (2009). *Switching Power Supply Design (3rd Ed.)*. McGraw-Hill, New York, US.

Ravindran, R. & Massoud, A. M. (2025). State-of-the-art DC-DC converters for satellite applications: A comprehensive review. *Aerospace,* **12**: 97.

Shaheen, M.A. & Mohamed, A. M. (2022). Modelling and power management of a CubeSat electrical power system. *Int. Undergrad. Res. Conf. ,* 18 December 2022, Kuala Lumpur, Malaysia, pp. 1–12.

TI (Texas Instruments). (2024). *LMR33630 Simple Switcher 3.8-V to 36-V, 3-A Synchronous Step-down Voltage Converter. Texas Instruments*. Available online at: https://www.ti.com/product/LMR33630 (Last access date: 20 November 2024)

Zhang, Y., Si, J., Wang, X.-T., Li, J. & Zhao, H. (2024). Stability analysis of buck converter based on passivity-based stability criterion. *Appl. Sci.,* **14**: 1755

ESTABLISHMENT OF REFERENCE POINTS FOR EVALUATION OF GNSS RECEIVER ACCURACY

Dinesh Sathyamoorthy*, Amirah Sakinah Mohd Rozlan, Maizurina Kifli, Abdul Azim Anuar Veera & Muhammad Hamizan Wafiy Ahmad Rashidi

Science & Technology Research Institute for Defence (STRIDE), Malaysia

*Email: dinesh.sathyamoorthy@stride.gov.my

ABSTRACT

The accuracy of Global Navigation Satellite System (GNSS) receivers is crucial for applications requiring precise positioning, including navigation, disaster management and environmental monitoring. This study establishes four reference points at STRIDE's Main Complex in Kajang, Selangor using a Trimble DA2 GNSS receiver with Trimble Catalyst precise point positioning (PPP) service. These reference points serve as benchmarks to evaluate the positional accuracy of three types of handheld GNSS receivers: single frequency Global Positioning System (GPS), single frequency multi-GNSS and dual-frequency multi-GNSS. Positional errors are assessed through field evaluations and GNSS simulations, revealing significant differences between simulated and real world conditions. The findings underscore the limitations of GNSS simulations in replicating environmental factors such atmospheric effects and multipath reflections, highlighting the critical need for field evaluations. This comprehensive approach provides actionable insights for selecting and deploying GNSS receivers across various practical applications.

Keywords: *Global Navigation Satellites System (GNSS) receiver accuracy; field evaluation; reference point; GNSS simulation; positional error.*

1. INTRODUCTION

The accuracy of Global Navigation Satellite System (GNSS) receivers is vital for a wide range of applications where precise positioning and reliable navigation are indispensable. GNSS technologies underpin activities such as guiding autonomous vehicles, optimising logistical operations and supporting disaster management efforts. They are equally critical in environmental monitoring, resource management and synchronising telecommunications networks. Therefore, evaluating the accuracy of GNSS receivers is essential to ensure their reliability and to confirm that they meet the precision requirements of these diverse and significant applications. Such evaluations enhance operational efficiency and support informed decision-making across numerous fields (Kaplan & Hegarty, 2017; Jackson *et al*., 2018; Janos & Kuras, 2021; Stopar *et al*., 2024).

Our previous works have explored the performance evaluation of GNSS receivers through GNSS simulation (Dinesh *et al*., 2012a, 2023; Dinesh, 2021), highlighting its benefits, such as controlled environments, repeatability and the ability to test a variety of scenarios, including those that may be challenging or costly to replicate in the field (Arul Elango & Sudha, 2016; Bi & Yuan, 2021; Emerick, 2022; Luccio, 2024). However, simulation cannot fully replicate real world conditions, including atmospheric effects, multipath reflections and other unpredictable factors that influence GNSS performance. While simulation provides a robust foundation for controlled evaluations, field testing remains indispensable for verifying receiver performance under practical operating conditions (Dinesh *et al*., 2012b; Cristodaro *et al*., 2018; Luccio, 2024).

Recognising these limitations, this study establishes reference points at STRIDE's Main Complex in Kajang, Selangor to enable field evaluations of GNSS receiver accuracy under real world conditions, bridging the gap between GNSS simulation and practical assessments. By integrating both simulation and field evaluations, this study presents a comprehensive framework for assessing GNSS receiver performance, addressing critical challenges faced in diverse operational environments.

2. ESTABLISHMENT OF REFERENCE POINTS

The establishment of reliable reference points is crucial for evaluating GNSS receiver accuracy under real world conditions. For this study, reference points are determined using a Trimble DA2 GNSS receiver paired with the Trimble Catalyst precise point positioning (PPP) service (Trimble, 2023). This setup ensures high-precision positioning, enabling the reference points to serve as robust benchmarks for GNSS receiver evaluation. The following criteria were observed when selecting the locations of the reference points:

- **Unobstructed Sky View:** Each location is chosen to ensure consistent and uninterrupted satellite signal reception, minimising the impact of line-of-sight (LOS) obstructions and multipath interference from nearby structures such as buildings, trees and terrain features.
- **High Positional Accuracy:** The positioning of each reference point is designed to achieve horizontal accuracy of no more than 0.02 m. This level of precision ensures reliability for subsequent GNSS receiver assessments while balancing practical feasibility in real world environments.
- **Absence of Radio Frequency Interference (RFI):** The selected locations are assessed to eliminate significant sources of RFI, such as cellular towers, power lines and electronic equipment, which could degrade GNSS signal quality. A Spectran HF-60105 spectrum analyser (Aaronia, 2015) is used to monitor candidate sites for potential interference, ensuring the chosen locations are free from significant disruptions.

Four reference points are selected as follows (Figure 1). These reference points provide a reliable basis for evaluating the positional accuracy of GNSS receivers in practical applications.

- Point A: Behind the Badminton Hall - 2.96661238 °N, 101.8107545 °E
- Point B: Besides the Futsal Court - 2.96684604 °N, 101.8107124 °E
- Point C: Open area in the gardener's field - 2.96729429 °N, 101.8100419 °E
- Point D: In front of Block B - 2.96858205 °N, 101.8098648 °E

Figure 1: Locations of the reference points.

3. GNSS RECEIVER EVALUATION

3.1 Methodology

The accuracies of three handheld GNSS receivers are assessed by comparing their recorded positions against the established reference points. The receivers evaluated are:

- A single frequency Global Positioning System (GPS) receiver: Garmin GPSMAP 78s (Garmin, 2011) (Receiver A)
- A single frequency multi-GNSS receiver: Trimble TDC600 (Trimble, 2022) (Receiver B)
- A dual-frequency multi-GNSS receiver: Garmin GPSMAP 66sr (Garmin, 2021) (Receiver C)

For each receiver, positional data is collected at the reference points, with three readings recorded to account for variability. The average of these readings is calculated to determine a representative positional value. The positional error for each receiver is then computed as the difference between the averaged value and the known position of the reference point.

In order to complement the field evaluations, GNSS simulation is conducted based on the procedure described by Dinesh (2021). Simulation allows the receivers to be tested in a controlled environment, free from real world factors such as atmospheric effects, multipath reflections and RFI. This provides a baseline for comparing the performance of receivers under idealised conditions.

The analysis focuses on comparing the positional errors observed in the field with those obtained from GNSS simulation, highlighting performance variations across different environments. This dual approach of field and simulation-based evaluations provides a comprehensive assessment of GNSS receiver accuracy and reliability, accounting for both controlled and real world conditions.

3.2 Results & Discussion

Table 1 summarises the positional errors recorded during field evaluation and GNSS simulation for each receiver. The field results reflect real world influences such as atmospheric effects and multipath interference, while the simulation results provide a controlled baseline. Comparing these datasets highlights discrepancies caused by environmental factors and underscores the benefits of multi-GNSS and dual-frequency capabilities. The findings emphasise the limitations of simulations alone and the necessity of field evaluations for comprehensive accuracy assessment.

Table 1: Recorded positional errors for field evaluation and GNSS simulation.

Receiver	Reading	Positional Error (m)	
		Field Evaluation	GNSS Simulation
Receiver A	Reading 1	2.46	1.97
	Reading 2	2.52	2.40
	Reading 3	2.67	2.17
	Reading 4	2.58	2.02
Receiver B	Reading 1	1.67	1.63
	Reading 2	1.24	1.29
	Reading 3	1.14	1.05
	Reading 4	1.69	0.96
Receiver C (Single Frequency)	Reading 1	1.34	1.56
	Reading 2	1.30	1.42
	Reading 3	1.72	1.23
	Reading 4	1.19	1.07
Receiver D (Dual-Frequency)*	Reading 1	0.41	-
	Reading 2	0.80	-
	Reading 3	0.47	-
	Reading 4	0.82	-

*The GNSS simulator only supports single frequency transmission.

Receiver A, which operates exclusively on GPS signals, demonstrated higher positional errors as compared to Receivers B and C, which utilise multi-GNSS capabilities. This suggests that reliance on GPS alone limits positional accuracy, particularly in environments where the availability or geometry of GPS satellites may be suboptimal. The results highlight the benefits of multi-GNSS receivers, which can leverage signals from multiple satellite constellations to improve positioning reliability and accuracy. Furthermore, Receiver A is an older model with lower receiver sensitivity and higher receiver noise, which further contributes to its increased positional errors.

Receiver C, capable of operating in both single- and dual-frequency modes, showed significantly lower positional errors when using the dual-frequency mode. This result underscores the advantage of dual-frequency operation, which reduces the impact of ionospheric delays and multipath reflections, as well as enhances positioning accuracy especially in challenging environments. The dual-frequency capability allows for more precise measurements, making Receiver C a more robust choice for applications requiring high accuracy.

Across all evaluated GNSS receivers, positional errors recorded during field evaluations were consistently higher than those observed during GNSS simulations. This discrepancy highlights the influence of real world factors including atmospheric effects, multipath reflections and RFI, which are absent in controlled simulation environments. These findings emphasise the importance of field evaluations to fully understand receiver performance under practical operating conditions and validate simulation-based assessments.

While this study successfully established reference points and evaluated GNSS receiver accuracy under real world conditions, several limitations should be acknowledged. Firstly, the evaluation was conducted at a single site, STRIDE's Main Complex in Kajang, which may limit the generalisability of the findings to other environments with varying terrain and urban structures. Secondly, the study focused on three types of handheld GNSS receivers, which while representative, do not encompass the full range of GNSS technologies available in the market. Additionally, the GNSS simulation setup, while valuable for controlled testing, was limited to single frequency transmission, restricting a comprehensive comparison with dual-frequency receivers.

Future work could expand the scope by incorporating evaluations across diverse geographic locations, including urban canyons and densely forested areas, to better understand environmental impacts on GNSS accuracy. Moreover, testing a broader array of GNSS receivers, including emerging low-cost and high-precision models, could provide deeper insights into the evolving capabilities of GNSS technologies. Enhancing simulation tools to support dual-frequency and multi-constellation setups would also improve the robustness of performance comparisons. These steps would further refine our understanding of GNSS receiver accuracy and support the development of best practices for their deployment in varied applications.

4. CONCLUSION

The establishment of reference points for GNSS receiver evaluation is crucial for ensuring accurate and reliable positioning in various applications. By creating well defined reference points in real world settings, this study bridges the gap between GNSS simulations and field evaluations, providing a robust framework for assessing receiver performance. Both approaches have their advantages and limitations; while GNSS simulations offer controlled environments that facilitate repeatability and the testing of diverse conditions, they cannot fully replicate the complexities of real world scenarios such as atmospheric effects and multipath reflections. Conversely, field evaluations provide essential insights into actual performance but may be influenced by unpredictable environmental factors. Therefore, integrating both field evaluations and GNSS simulations is essential for comprehensive assessment of GNSS receiver accuracy, ensuring that users can make informed decisions based on thorough understanding of performance across different conditions.

REFERENCES

Aaronia (2015). *Handheld Spectrum Analyzer Spectran V4*. Aaronia AG, Strickscheid, Germany.

Aeroflex (2010). *Avionics GPSG-1000 GPS / Galileo Portable Positional Simulator*. Aeroflex Inc., Plainview, New York.

Arul Elango, G. & Sudha, G.F. (2016). Design of complete software GPS signal simulator with low complexity and precise multipath channel model. *J. Electr. Syst., Inform. Tech.*, **3**: 161-180.

Bi. Y. & Yuan, J. (2021). A portable GPS signal simulator design based on ZYNQ. *2nd Int. Symp. Comp. Eng. Intell. Comm. (ISCEIC 2021)*, 6-8 August 2021, Nanjing, China.

Cristodaro, C., Ruotsalainen, L. & Dovis, F. (2018). Benefits and limitations of the record and replay approach for GNSS receiver performance assessment in harsh scenarios. *Sensors*, **18**: 2189.

Dinesh, S., Mohd Faudzi., M., Rafidah, M., Nor Irza Shakhira, B., Siti Robiah, A., Shalini, S., Aliah, I., Lim, B.T., Zainal Fitry, M.A., Mohd. Rizal, A.K., & Mohd Hasrol, H.M.Y. (2012a). Evaluation of the effect of varying Global Positioning System (GPS) signal power levels on GPS accuracy. *Defence S&T Tech. Bull.*, **5**: 57-71.

Dinesh, S., Mohd Faudzi., M. & Zainal Fitry, M.A. (2012b). Evaluation of the effect of radio frequency interference (RFI) on Global Positioning System (GPS) signals: Comparison of field evaluations and GPS simulation. *J. Defence Secur.*, **5**: 71-86.

Dinesh, S. (2021). Evaluation of accuracy of Global Positioning System (GPS) receivers. *Defence S&T Tech. Bull.*, **14**: 211-216.

Dinesh, S., Hafizah, M.Y., Ahmad Firdaus, A.K. Mohd Zuryn, M.D. & Maizurina, K. (2023). Evaluation of multi-GNSS performance via GNSS simulation. *Defence S&T Tech. Bull.*, **16**: 13-23.

Garmin (2011). *GPSmap 78 Series Owner's Manual*. Garmin International Inc., Olathe, Kansas.

Garmin (2021). *GPSMAP 66 Owner's Manual*. Garmin International Inc., Olathe, Kansas.

Jackson, J., Saborio, R., Ghazanfar, S.A & Gebre-Egziabher, D. (2018). *Evaluation of Low-Cost, Centimeter-Level Accuracy OEM GNSS Receivers*. Minnesota Department of Transportation, Minnesota, US.

Janos, D. & Kuras, P. (2021). Evaluation of low-cost GNSS receiver under demanding conditions in RTK network mode. *Sensors*, **21**: 5552.

Kaplan, E.D. & Hegarty, C.J. (2017). *Understanding GPS: Principles and Applications*. Artech House, Norwood, Massachusetts.

Luccio, M. (2024). *Simulating New GNSS Signals and Threats*. Available online at: https://www.gpsworld.com/simulating-new-gnss-signals-and-threats (Last access date: 25 January 2025).

Stopar, B., Sterle, O., Pavlovčič-Prešeren, P. & Hamza, V. (2024). Observations and positioning quality of low-cost GNSS receivers: a review. *GNSS Sol.*, **28**: 149.

Trimble (2022). *Trimble TDC600 Handheld*. Trimble, Colorado, US.

Trimble (2023). *Trimble DA2*. Trimble Inc., Westminster, Colorado, US.

Trimble (2024). *Trimble Catalyst*. Trimble Inc., Westminster, Colorado, US.

DESIGN AND OPTIMISATION OF MILITARY VEHICLE CHASSIS: A REVIEW

Fadzli Ibrahim*, Ezza Nur Adzlilliya Azali, Sangiitha Tamilarasu, Shamsul Akmar Ab Aziz & Nor Azlan Sarjo

Automotive and Mechanical Technology Division, Science and Technology Research Institute for Defence (STRIDE), Ministry of Defence, Malaysia

*E-mail: fadzli.ibrahim@stride.gov.my

ABSTRACT

The design and optimisation of military vehicle chassis play a pivotal role in ensuring operational efficiency, durability and adaptability to harsh terrains and combat scenarios. This paper presents a comprehensive review of military chassis design and optimisation, encompassing an evaluation of commonly used chassis architectures, which are ladder frame, monocoque, space frame and modular systems, as well as the role of advanced material technologies, including high-strength steels, aluminium alloys, composites, smart materials and advanced coatings. Recent advancements in simulation tools, virtual prototyping and additive manufacturing are also discussed, with emphasis on their impact in accelerating development cycles, reducing costs and enhancing structural performance. By drawing these aspects together, the paper identifies key challenges, emerging opportunities and future directions for developing robust, lightweight and modular chassis systems that meet the evolving demands of modern military operations.

Keywords: *Military vehicle chassis; design; material selection; simulation and virtual prototyping; additive manufacturing.*

1. INTRODUCTION

An automotive chassis serves as the fundamental structural backbone that supports and integrates all essential components, including the engine, driveline, suspension, braking and steering assemblies (Knouff *et al.*, 2012; Shiva *et al.*, 2020; Cicek *et al.*, 2021). It is primarily responsible for maintaining the vehicle's structural integrity under both static and dynamic conditions, ensuring safe operation across a range of demanding environments. Its role in absorbing and dampening forces generated between the road and vehicle ensures continuous contact and contributes significantly to vehicle handling and safety (Belloni *et al*., 2024). Additionally, the chassis also plays a key role in maintaining vehicle alignment and geometry under varying operational stresses, directly contributing to the overall mobility, stability and survivability of the vehicle during missions (Gandhi & Thompson, 2018; Pandya *et al*., 2022). Its load-bearing capability and structural layout also influence vehicle modularity and the integration of protection systems such as armour plating, making the chassis indispensable to mission readiness and operational performance (Deulgaonkar, 2020). A well-designed chassis ensures sufficient torsional and bending stiffness, which are crucial for handling stability, ride comfort and load distribution. Typically fabricated from materials such as steel, aluminium and composites, the chassis offers a balance of durability, lightweight construction and structural flexibility. Ultimately, the chassis serves as the core structural platform, critically shaping a vehicle's performance, safety and functional integration (Shrivastava *et al.*, 2019).

In military applications, the chassis must meet a range of demanding requirements that far exceed those of conventional passenger vehicles. The requirements vary considerably depending on operational roles, whether for combat, transport, logistics or reconnaissance, each presenting unique mechanical and structural challenges. These vehicles must perform reliably under extreme and unpredictable conditions, which often involve high-intensity operations, rough terrains, variable climates and combat

zones that subject the chassis to constant vibrations, high-impact dynamic loads, severe combat impact and sustained mechanical stress (Kumar *et al*., 2020; Arimadla *et al*., 2022b). Moreover, military chassis must integrate complex auxiliary systems, such as advanced communication devices, armour plating, suspension for weapon platforms and modular equipment bays, which add to the structural complexity and necessitate robust design considerations (Smith *et al*., 2021). The modularity and adaptability of the chassis design are crucial for ensuring that vehicles can be reconfigured quickly to meet mission-specific requirements, enhancing operational versatility and logistical efficiency (Lee *et al*., 2023). As such, the design, development and optimisation of military vehicle chassis represent a critical engineering domain that must adhere to stringent performance, reliability and safety standards, requiring multidisciplinary approaches with a strong emphasis on maintainability and survivability to meet the rigorous demands of military operations (Kumar *et al*., 2020).

Multiple factors influence the selection of an appropriate chassis design for military vehicles to ensure optimum performance, reliability and safety in diverse operational conditions. Design priorities often include payload capacity, mobility, adaptability and protection, influenced by vehicle's operational role, tactical requirements and compliance with military standards and specifications. For instance, payload requirement in particular is a key consideration where chassis designs must be tailored to accommodate specific weight and volume demands while ensuring axle configurations support for high-load operations (Arimadla *et al.*, 2022a). Mobility is also another critical consideration, with the chassis design influencing the vehicle's ability to traverse challenging terrains. The integration of appropriate suspension systems and axle configurations within the chassis framework enhances off-road capabilities and ride comfort. Optimising these components ensures that the vehicle maintains stability and control across various terrains, which is essential for mission success (Mohsen *et al*., 2018). Adherence to strict military standards such as MIL-STD 810G is also essential to ensure that the chassis can withstand harsh operational environments without failure (Rahman & Abdullah, 2021). Additionally, chassis design must also account for modularity and field reconfigurability, while balancing cost constraints and technological readiness particularly when adopting advanced materials and manufacturing techniques into the design and development process (Patel & Bhargava, 2022).

This review aims to provide insights into developing innovative and robust chassis systems that align with modern defence strategies. It critically evaluates different chassis configurations, material choices and optimisation strategies, as well as identify key performance trade-offs and engineering constraints. Furthermore, it addresses existing knowledge gaps in the integration of lightweight materials and advanced manufacturing techniques. As the operational environment grows more complex and demanding, this review underscores the necessity of an interdisciplinary approach to chassis optimisation. By adopting such perspective, this paper seeks to establish a comprehensive foundation for future research and development of innovative and robust chassis systems that align with modern defence strategies, ultimately contributing to the creation of more agile, resilient and mission-ready military vehicle.

2. TYPES OF VEHICLE CHASSIS

Various chassis types have been developed across civilian and military domains, each tailored to specific operational roles, tactical requirements and performance standards, while providing distinct structural characteristics, advantages and limitations. This review focuses on four configurations are the most widely used in military wheeled vehicle applications, which are ladder frame, monocoque, space frame and modular. Understanding the distinctions among these chassis types is essential for selecting the most suitable configuration based on factors such as load-bearing capacity, ease of manufacturing, adaptability and terrain compatibility (El-Sayed *et al*., 2020; Ravi Kumar *et al*., 2020; Yang *et al*., 2023). The following sections provide a comparative analysis of these chassis' types, highlighting their applicability in different vehicle contexts, with particular focus on their relevance to modern military applications.

2.1 Ladder Frame Chassis

The ladder chassis is one of the most reliable frame designs. Its straightforward construction consists of two parallel longitudinal rails, which serve as the primary support for the vehicle's load. These rails are joined by cross-members, enhancing overall structural rigidity and evenly distributing stress across the frame. This design is particularly advantageous for vehicles requiring high strength and durability (Francis *et al.*, 2014; Gurjar *et al.*, 2019; Ashok & Elayaraja, 2020). It is widely used in heavy-duty vehicles, including military applications, due to its robustness and high load-carrying capacity. However, it exhibits limited resistance to torsion and warping (Patel *et al*., 2013; Mahmoodi-k *et al.*, 2014; Mishra, 2020).

Figure 1: Ladder frame chassis.
(Source: Ren *et al.*, 2005)

2.2 Monocoque Chassis

The monocoque chassis, also known as a unibody construction, integrates the structural framework and vehicle body into a single unit. This design enhances ride comfort and handling while offering greater stability due to a lower floor panel, which lowers the vehicle's centre of gravity (Muthyala, 2019). Engineered for safety, the monocoque chassis is designed to deform in a controlled pattern during impacts, effectively absorbing energy to protect occupants. Its seamless construction provides a lightweight yet strong framework, making it ideal for applications such as armoured personnel carriers and light tactical vehicles (Ren *et al.*, 2005; Widiyanto *et al.*, 2021).

Figure 2: Monocoque chassis frame.
(Source: Ren *et al.*, 2005)

2.3 Space Frame Chassis

The space frame chassis features a three-dimensional skeletal framework composed of interconnected tubes or beams. This design maximises rigidity while minimising weight by strategically using triangular structures. The forces within each strut are either tensile or compressive to avoid bending,

which allows the components to remain lightweight and thin. Space frames offer an exceptional strength-to-weight ratio, making them ideal for advanced applications, including specialised combat and military vehicles. The body panels attached to the frame serve little to no structural function, further contributing to its lightweight and efficient design (Thota *et al.*, 2011; Mishra, 2020).

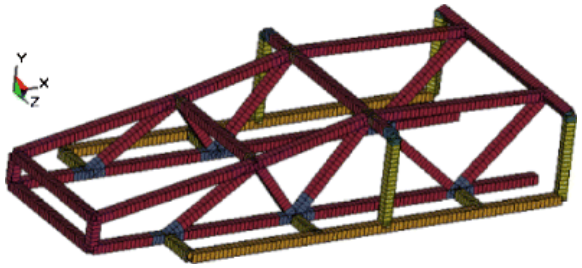

Figure 3: Space frame chassis.
(Source: Thota *et al.*, 2011)

2.4 Modular Chassis

A modular chassis frame for a heavy vehicle is a frame that is made up of separate parts that can be assembled to create the vehicle's main structure. The chassis is the frame or main structure of a vehicle, and for heavy vehicles, it can also refer to the entire vehicle without the body. The modular chassis system is designed for versatility, allowing it to adapt to various vehicle configurations. It enables rapid customisation and seamless integration of mission-specific equipment, making it ideal for diverse operational requirements. This design enhances flexibility, simplifies maintenance and improves overall efficiency, making it a preferred choice for vehicles requiring adaptability and streamlined upkeep (Hartmann *et al.*, 2021).

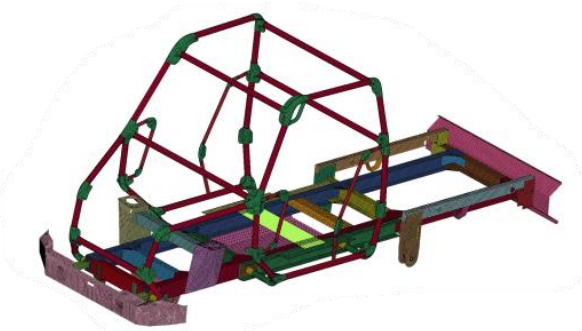

Figure 4: Modular chassis frame.
(Source: Hartmann *et al.*, 2021)

2.5 Comparative Evaluation and Operational Trade-offs

In summary, chassis design significantly influences the structural performance and operational capability of military vehicles. Ladder chassis offers robust load-bearing capacity and structural durability, making them ideal for heavy-duty military transport applications. However, its limited torsional rigidity, high weight and reduced manoeuvrability constrain its suitability for agile operations. In contrast, monocoque chassis provides improved ride comfort, enhanced safety through energy absorption and weight savings, which are characteristics that are beneficial to light tactical or armoured vehicles. Nonetheless, its high manufacturing cost, limited adaptability to modular equipment and complex maintenance requirements reduces its field flexibility. Space frame chassis provides an exceptional strength-to-weight ratio and high rigidity, supporting high-speed manoeuvring and fuel efficiency in specialised combat vehicles. Despite these advantages, its limited payload capacity and complex fabrication make it less practical for large-scale or logistically intensive deployments. Meanwhile, modular chassis stands out for its high versatility, enabling rapid integration of mission-specific components and facilitating streamlined maintenance. Although potentially less rigid and more

costly to produce, it is particularly well-suited for multi-role military platforms requiring operational flexibility and rapid field reconfiguration. As such, each chassis type presents a distinct set of trade-offs, and their application must align with specific mission profiles, environmental conditions and performance requirements. Table 1 provides a comparison of the chassis types in terms of advantages, limitations and applicability.

Table 1: Comparison of chassis type.

Chassis Type	Advantages	Limitations	Applicability
Ladder chassis	High strength and durability; straightforward construction; excellent load-carrying capacity	Limited torsional rigidity; heavyweight increases fuel consumption; less suited for dynamic handling	Ideal for heavy-duty military trucks requiring robustness and high payload capacity
Monocoque chassis	Lightweight and rigid; enhanced ride comfort and handling; energy absorption during impact improves safety	Expensive manufacturing; limited adaptability for modular systems; challenging maintenance	Suitable for armoured personnel carriers and light tactical vehicles requiring lightweight yet strong construction
Space frame chassis	Exceptional strength-to-weight ratio; lightweight components reduce fuel consumption; highly rigid	Complex and costly fabrication; requires precise assembly; limited load carrying-capacity for heavy vehicles	Ideal for specialised combat vehicles and high-performance military applications where agility and weight are critical
Modular chassis	High versatility and adaptability; simplifies integration of mission-specific equipment; streamlines maintenance and repair	May lack the structural rigidity of fixed designs; potentially higher manufacturing costs	Perfect for vehicles with diverse operational requirements such as multi-role military vehicles needing rapid customisation

3. MATERIAL SELECTION FOR MILITARY VEHICLE CHASSIS

Military vehicles should be capable of enduring extreme operational conditions while remaining sufficiently lightweight to ensure manoeuvrability and strategic deploy ability (Tan *et al*., 2021). This necessitates the integration of advanced materials and components, such as steel, aluminium alloys and composite structures, without compromising mechanical robustness or increasing logistical complexity. Recent advancements in materials science have significantly influenced chassis engineering by enabling the development of lightweight yet robust structural frameworks. Innovations in new formulations of steel, advanced aluminium alloys, fibre-reinforced polymer composites and smart materials have introduced new opportunities to reduce vehicle weight while preserving or even enhancing structural performance and crashworthiness (Guo *et al*., 2024).

3.1 Steel

Steel has been a predominant material for vehicle chassis construction due to its accessibility, affordability and ease of fabrication. Its widespread use is attributed to its ability to provide the strength and rigidity necessary to support the body, engine and mechanical components under varying static and dynamic loading conditions. Various types of steel, including and medium carbon steel, are commonly utilised, each offering distinct mechanical properties such as ultimate strength, yield strength, Poisson's ratio and modulus of elasticity (Khan *et al*., 2022).

High strength steel (HSS) has emerged as a preferred material for ladder chassis designs due to its superior mechanical characteristics when compared to traditional steel grades, suggesting its suitability for high-load-bearing structures (Aathira *et al*., 2021). The incorporation of HSS in chassis construction

ensures enhanced performance in terms of strength-to-weight ratio, making it a suitable choice for applications that require high structural integrity and reduced weight. The material properties are shown in Table 2.

Table 2: Material properties of different types of steel.
(Source: Aathira *et al.*, 2021)

Material	Ultimate Tensile Strength (Mpa)	Yield Strength (Mpa)	Poisson's Ratio	Modulus of Elasticity (GPa)	Modulus of Rigidity (GPa)
Low carbon steel	440	370	0.29	205	80
Medium carbon steel	565	310	0.29	200	80
High strength steel (HSS)	2000	1400	0.3	210	75

Advanced high-strength steels (AHSS), including dual-phase (DP) and transformation-induced plasticity (TRIP) steels, have gained prominence in modern chassis manufacturing. A comprehensive review of AHSS highlights their complex microstructures, which contribute to their high strength and formability, making them ideal for automotive applications where both safety and efficiency are paramount (Perka *et al.*, 2022). Additionally, AHSS alloys also demonstrate superior strength as compared to traditional steels, allowing for weight reduction in vehicle components. However, the complex microstructures of AHSS should be thoroughly understood in order to optimise their properties for use in automotive applications (Stoudt, 2016).

3.2 Aluminium Alloy

Aluminium alloy has emerged as a prominent material for vehicle chassis construction due to its exceptional properties, including low density, high strength and corrosion resistance. An aluminium alloy chassis provides the optimal balance of rigidity and lightweight characteristics, essential for absorbing movements and vibrations from the engine, suspension and axles while enhancing vehicle performance and fuel efficiency. The use of aluminium alloy in chassis construction significantly improves power-to-weight ratio by reducing vehicle weight, hence leading to improved fuel efficiency and handling (Chen, 2023). It also offers excellent strength-to-weight ratio, which is crucial for enhancing the load-bearing capacity of heavy vehicles without significantly increasing their weight (Agarwal & Mthembu, 2022).

Despite its higher cost and the additional challenges in fabrication as compared to steel, its inherent corrosion resistance further ensures the longevity and durability of the chassis under various environmental conditions (Hägele *et al.*, 2011). This reduces environmental impact during the vehicle's use phase, making it a sustainable choice for chassis manufacturing. When alloyed, aluminium exhibits increased yield strength while maintaining adequate stiffness, making it suitable for heavy-duty applications such as military vehicles and commercial trucks. Aluminium alloys generally have elastic modulus of around 70 GPa (Skejić *et al.*, 2021), which is roughly one-third that of most steel and steel alloys. It also has superior stress distribution characteristics, making it a viable alternative to traditional steel in heavy vehicle chassis design (Vannan, 2022). In automotive engineering, vehicles constructed with aluminium alloys often utilise space frames made from extruded profiles to maintain rigidity (Shiva *et al.*, 2020).

3.3 Composites

Composite materials, such as carbon fibre-reinforced plastics (CFRP) and glass fibre-reinforced plastics (GFRP), have become increasingly significant in automotive engineering due to their ability to combine the desirable properties of separate materials into a single, enhanced structure. First used in the 1953 Chevrolet Corvette's fibreglass body, composites now play a key role in creating lighter, more efficient and environmentally friendly vehicles while improving structural integrity (Pruez *et al*., 2013). The use of composites in vehicles has gained traction due to their exceptional material properties. The application of CFRP in automotive chassis design has been extensively studied, highlighting its potential to significantly reduce vehicle weight while maintaining or enhancing structural performance. CFRP offers a superior strength-to-weight ratio, high stiffness, as well as excellent fatigue and impact resistance, making it an ideal material for automotive components, including chassis structures (England *et al.*, 2010; Othman *et al.*, 2018; Bhattacharya *et al.*, 2024).

Advancements in composite manufacturing techniques, such as the development of carbon fibre-reinforced thermoplastics (CFRTP), have further enhanced the feasibility of using composites in automotive applications. CFRTP's applications for automotive manufacturing allow for lightweight vehicle design, reduced cycle times and improved recyclability, which address some of the challenges associated with traditional thermoset-based composites (Wan & Takahashi, 2021). In addition to their structural benefits, composites contribute to environmental sustainability through reduced weight, leading to improved fuel efficiency and lower CO_2 emissions. The integration of composite materials in automotive chassis design exemplifies the industry's shift towards materials that offer both performance benefits and environmental sustainability. However, challenges such as high material costs and production complexities currently limit their widespread adoption in mass-market vehicles (Spasenović & Blagojević, 2021).

3.4 Smart Materials

Advancements in material science have significantly influenced structural engineering, notably within the military vehicle industry. Smart materials, known for their self-adaptability, self-sensing, shape-memory and multifunctional capabilities, have emerged as a transformative innovation. Originally studied in the Naval Ordnance Laboratory with nickel-titanium alloys, these materials have been widely adopted in aerospace, mechanical and biomedical engineering (Cai *et al*., 2003). In the military vehicle industry, smart materials offer substantial advantages by enhancing vehicle performance, durability and adaptability (Barbarino *et al*., 2014; Reddy *et al*., 2024).

The integration of smart materials into military vehicle chassis systems enables self-monitoring and self-repairing systems, improving vehicle longevity and reducing maintenance requirements. For instance, the use of piezoelectric materials in sensor systems allows for real-time health monitoring of the chassis, facilitating proactive maintenance and enhancing safety (Reddy *et al*., 2024). Apart from that, the application of aluminium-propylene composites in vehicle chassis frames offers significant weight reduction while providing superior strength to endure high loads as it exhibits low deformation and optimised stress distribution, making them highly suitable for military vehicle applications (Saravanan *et al*., 2021). Additionally, smart materials can be tailored to optimise load distribution, vibration damping and structural rigidity, ensuring better operational efficiency under dynamic and extreme conditions. As advancements in material science continue, smart materials are poised to play a pivotal role in the next generation of lightweight durable, and high-performing military vehicles (Tiwari *et al*., 2021).

3.5 Advanced Coatings

Advanced coatings have emerged as a vital innovation for enhancing the durability and operational efficiency of heavy vehicle chassis, particularly in military applications. These coatings not only

significantly improve corrosion resistance, protecting the chassis from harsh environmental conditions such as high humidity, salt spray and abrasive terrains, but also extend the service life of vehicles operating under extreme conditions. For military vehicles, where exposure to extreme weather and rugged terrains is frequent, advanced coatings such as self-healing coatings and nano-coatings offer unique advantages. These coatings can autonomously repair minor damages and enhance the tensile strength of structural components while maintaining lightweight properties essential for mobility (Aljibori *et al*., 2023).

Additionally, thermal barrier coatings (TBC) provide insulation and protects critical vehicle systems from high-temperature stresses ensuring the integrity of components (Joseva *et al*., 2023). Beyond their protective properties, advanced coatings contribute to improved mechanical performance by enhancing the tensile strength and impact resistance of chassis components while maintaining lightweight properties essential for mobility (Xu *et al*., 2022). Moreover, their environmental benefits, such as reduced maintenance requirements and longer operational lifespans, contribute to lower lifecycle costs and reduced carbon footprint. As a result, advanced coatings have become indispensable for ensuring the performance, safety and sustainability of heavy military vehicles (Aljibori *et al*., 2023).

3.6 Comparative Assessment and Material Trade-offs

In brief, the selection of materials in military vehicle design critically influences performance, survivability and lifecycle cost. High-strength steel offers high durability, crash resistance and cost-effectiveness due to its established fabrication processes, making it a preferred material for applications requiring structural toughness and ballistic protection. However, its heavy weight limits fuel efficiency and reduces payload capacity, which can hinder mobility in tactical operations. Aluminium alloy provides a favourable strength-to-weight ratio and are corrosion-resistant, making it ideal for improving manoeuvrability and operational range in lighter military platforms. However, its high cost, fabrication complexity and reduced stiffness pose challenges for high-load structural components for heavy military vehicles. In comparison, composite materials offer superior strength-to-weight ratios and low thermal expansion, making it suitable for high-performance vehicles where weight reduction is paramount. Nevertheless, its high manufacturing cost, difficult repairability and limited recyclability restrict widespread use in standard military fleets. Smart materials introduce advanced capabilities such as real-time monitoring, self-healing and adaptive responses to environmental stimuli, enhancing system longevity and situational awareness. Despite its advantages, high development costs and limited scalability confine it largely to research and prototype stages. Lastly, advanced coatings contribute to corrosion resistance, reduced maintenance and thermal protection, and are increasingly employed to extend component lifespan. Although its application requires specialised processes and incurs high initial costs, its long-term benefits align with the demands of sustained military deployments. Ultimately, the optimal material choice depends on the specific operational role, cost constraints and performance requirements of the vehicle system. Table 3 provides a summary of the comparison of materials used for chassis development in terms of advantages, challenges and economic viability.

Table 3: Types of material used for chassis development and its comparison.

Material	Advantages	Challenges	Economic Viability
High Strength Steel	High durability; crash resistant; cost-effective; established fabrication process	Heavier; limited fuel efficiency and payload capacity	High
Aluminium Alloy	Lightweight; high strength; corrosion resistant; improved power to weight ratio	Higher cost; complex fabrication process; low stiffness	Moderate
Composites	Super strength-to-weight ratio; low thermal expansion	High manufacturing cost; complex repair process; limited recyclability	Low to moderate

Smart Materials	Self-adaptive; self-healing properties; enable real time monitoring; improves longevity	High development cost; limited large-scale application; ongoing R&D phase	Low to moderate
Advanced Coatings	Corrosion resistant; reduced maintenance; self-healing and thermal barrier coatings	High initial cost; application requires specialised process	High

4. RECENT ADVANCEMENTS IN CHASSIS DESIGN AND OPTIMISATION

Emerging engineering technologies such as virtual prototyping, finite element analysis (FEA) and additive manufacturing are reshaping the design and development process of chassis systems by facilitating faster iterations, reducing costs and enhancing design precision (Zhou *et al*., 2024). These technologies have enabled iterative testing, design validation and performance optimisation early in the development cycle, thereby accelerating innovation and supporting the integration of next-generation materials.

4.1 Simulation and Virtual Prototyping

Vehicle chassis design faces challenges such as weight reduction for fuel efficiency and payload capacity while maintaining strength to prevent structural failure. Ensuring strength and stiffness is crucial for stability and performance, requiring precise stress and deformation analysis (Bhoyate & Patel, 2020; Muzammil *et al*., 2023). Fatigue resistance is vital due to repeated loading cycles, particularly in commercial applications (Desai & Lingannavar, 2018). Minimising vibrations and resonance are essential for passenger comfort and structural integrity, which underscores the importance of conducting comprehensive dynamic behaviour analyses to ensure optimal chassis performance under varying operational conditions (Ibrahim & Aziz, 2023; Ibrahim *et al*., 2024). Material selection should balance strength, weight, durability and cost-effectiveness, all within budget and time constraints (Shiva *et al.*, 2020). FEA aids optimisation by simulating chassis behaviour under various loads and identifying stress points, deformation and potential failures. Tools such as CATIA and ANSYS enable detailed modelling and performance evaluation under diverse conditions, addressing resonance and dynamic loads for safer and more efficient designs (Agrawal & Razik, 2015; Yasar & Bircan, 2015; Yinghao, 2023; Liu *et al*., 2025).

Overall, simulation and virtual prototyping technologies in the development of chassis design will enable faster development times, reduced costs and enhanced design optimisation. These tools allow for the creation of virtual prototypes early in the design process, facilitating comprehensive analyses of vehicle performance, mobility and protection capabilities without the need for physical prototypes. This approach helps in identifying key design components, assessing risks and optimising structural integrity, including for ballistic resistance, ultimately leading to more efficient and effective military vehicle designs (Letherwood & Gunter, 2001; Ghazaly, 2014; Ibrahim *et al*., 2023; Vido *et al*., 2024).

4.2 Additive Manufacturing

Additive manufacturing, commonly known as 3D printing, offers key benefits for military vehicle chassis design, including rapid prototyping and on-site part production, thereby reducing manufacturing costs, maintenance time and logistics dependencies. The flexibility of 3D printing allows for high customisation, enabling the production of parts tailored to specific operational requirements (Love *et al*., 2016; Kumaresan *et al.*, 2021). This adaptability is essential for manufacturing low-volume and complex parts such as military vehicle chassis without the need for extensive retooling (Atzeni & Salmi, 2012; Ngo *et al*., 2018). Additionally, additive manufacturing reduces material waste as components

are built layer by layer using only the necessary material. This approach not only conserves resources but also lowers manufacturing costs (Baumers *et al*., 2011; Rahmani *et al*., 2025).

Additive manufacturing also facilitates the creation of intricate, optimised designs that are challenging to achieve with conventional manufacturing methods. This capability allows for the development of components with improved functionality and performance. For instance, the integration of complex internal structures can enhance the strength-to-weight ratio of chassis components, contributing to overall vehicle efficiency (Sarzyński *et al*., 2024). The process starts with CAD design and slicing the model into layers, followed by material deposition using methods such as stereolithography (SLA), fused deposition modelling (FDM), laminated object manufacturing (LOM), powder-based or selective laser sintering (SLS) (Hossain *et al*., 2023). The materials include polymers for lightweight parts, advanced metal alloys for strength, and composites for reduced weight and durability. While 3D printing for military chassis remains in the research phase, it shows promise for producing complex, mission-critical components, though large-scale integration is still evolving (Sarzyński *et al*., 2024).

5. CONCLUSION

The design and optimisation of military heavy-wheeled vehicle chassis are integral to ensuring operational success and long-term performance in demanding military environments. This review reveals that advancements in materials and technologies have significantly enhanced the strength, agility, and durability of chassis systems while addressing critical requirements such as survivability, mobility and maintainability. The integration of high-strength materials including advanced steels and composites has reduced chassis weight while improving strength and fatigue resistance, enabling vehicles to handle heavier payloads and navigate diverse terrains.

Technological innovations such as virtual prototyping, FEA and additive manufacturing have streamlined the design and production process, facilitating rapid prototyping and precise structural optimisation. These advancements not only reduce development time and costs, but also enhance the adaptability of chassis designs for multi-role applications. Modular systems further extend the operational versatility of military vehicles, allowing customisation for specific missions while simplifying maintenance and repair.

Looking forward, the successful development of next-generation military vehicle chassis will require ongoing collaboration among researchers, engineers and defence organisations. Investments in cutting-edge materials, smart technologies and sustainable manufacturing methods will be crucial to meeting the challenges of modern warfare. By leveraging these advancements, future chassis systems can ensure superior performance, resilience and operational readiness in increasingly complex and unpredictable combat scenarios.

REFERENCES

Aathira, K.U., Keerthi, V.C., Arjun, S., Kiran, S.J. & Ramesh, S. (2021). High specific strength steel as an alternative material for heavy vehicle chassis – an explicit analysis. *IOP Conf. Ser. Mater. Sci. Eng.*, **1114**: 012064.

Agarwal, A., & Mthembu, L. (2022). Structural analysis and optimization of heavy vehicle chassis using aluminium P100/6061 Al and Al GA 7-230 MMC. *Processes*, **10**: 320.

Agrawal, M.S. & Razik, M. (2015). Finite element analysis of truck chassis frame. *Int. Res. J. Eng. Tech.*, **2**: 1949-1956.

Aljibori, H.S., Alamiery, A. & Kadhum, A.A.H. (2023). Advances in corrosion protection coatings: A comprehensive review. *Int. J. Corros. Scale Inhib.*, **12**: 1476-1520.

Arimadla, S., Anil, P, Jhansi, P., Vivek, M. & Susheel, P. (2022a). Design and static analysis of heavy vehicle chassis with different alloy materials at different optimum load conditions. *Int. Res. J. Eng. Tech.*, **9**: 1203.

Arimadla, S., Kulkarni, A. & Yadav, S. (2022b). Dynamic analysis of military vehicle suspension systems under combat conditions. *J. Defence Tech.*, **18**: 225–235.
Ashok, K. & Elayaraja, D. (2020). Dynamic analysis and design optimization of ladder chassis. *Int. J. Recent Tech. Sci.*, **4**: 10-21.
Atzeni, E. & Salmi, A. (2012). Economics of additive manufacturing for end-usable metal parts. *Int. J. Adv. Manuf. Tech.*, **62**: 1147–1155.
Bhattacharya, S., Shohel, S.M., Kumar, D., Ashish, P., Teja, C. & Gupta, A. (2024). Optimization of ladder frame chassis using CFRP using finite element analysis. *AIP Conf. Proc.*, **2962**: 020023.
Barbarino, S., Flores, E.S., Ajaj, R.M., Dayyani, I. & Friswell, M. I. (2014). A review on shape memory alloys with applications to morphing aircraft. *Smart Mater. Struct.*, **23**: 063001.
Baumers, M. (2012). *Economic Aspects of Additive Manufacturing: Benefits, Costs and Energy Consumption*. PhD Thesis, Loughborough University, UK.
Bhoyate, S.T. & Patel, A.Z. (2020). Weight optimization and FEA analysis of truck chassis. *Int. Res. J. Eng. Tech.*, **7**: 813-822.
Belloni, M., Vignati, M. & Sabbioni, E. (2024). Analysing the effect of chassis torsional flexibility on the rollover threshold of a multi-purpose agricultural vehicle. *Vehicles*, **6**: 415-432.
Cai, C.S., Wu, W., Chen, S. & Voyiadjis, G.Z. (2003). *Applications of Smart Materials in Structural Engineering*. Project Report, Department of Civil Eng., Louisiana State University, Louisiana.
Chen, J. (2023). Research on aluminum alloy materials and application technology for automotive lightweighting. *Acad. J. Mater. Chem.*, **4**: 1-7.
Cicek, B.C., Acar, B. & İder, S.K. (2021). Dynamic analysis and design optimisation of a heavy military vehicle. *Int. J. Heavy Veh. Syst.*, **28**: 309-328.
Desai, V.U. & Lingannavar, R.G. (2018). Weight optimization and fatigue life estimation of heavy vehicle chassis under service loading conditions. *Int. Res. J. Eng. Tech.*, **5**: 722-728.
Deulgaonkar, V.R. (2020). Analysis of auxiliary structure mounted on 8×8 military vehicle chassis for off-road logistics. *Int. J. Veh. Struct. Syst.*, **12**: 123–130.
El-Sayed, M., Abd El-Hamid, A. & Shaaban, E. (2020). Comparative assessment of military vehicle chassis architectures: Ladder frame vs. monocoque vs. space frame. *Int. J. Auto. Mech. Eng.*, **17**: 7747–7762.
England, J.C., Hadavinia, H., Marchant, D.R. & Aboutorabi, A. (2010). Design of automotive metal and composite chassis structures. *Recent Pat. Mech. Eng.*, **3**: 211-225.
Francis, V., Rai, R.K., Singh, A.K., Singh, P.K. & Yadav, H. (2014). Structural analysis of ladder chassis frame for jeep using Ansys. *Int. J. Mod. Eng. Res.*, **4**: 41-47.
Gandhi, R. & Thompson, R. (2018). Analysis and design of off-road vehicle chassis systems: Structural considerations and integration. *Int. J. Auto. Eng. Tech.*, **7**: 85–92.
Ghazaly, N.M. (2014). Applications of finite element stress analysis of heavy truck chassis: survey and recent development. *J. Mech. Des. Vib.*, **2**: 69-73.
Guo, H., Zhou, X. & Liu, Z. (2024). Advanced lightweight structural materials for automobiles: Properties, manipulation and perspective. *Sci. Adv. Mater.*, **16**: 563-580.
Gurjar, M., Deshmukh, S., Goswami, S., Mathankar, V. & Shrivastava, S. (2019). Design and durability analysis of ladder chassis frame. *SSRN Electr. J.*, **10.2139**: 3368110
Hägele, N. & Sonsino, C. M. (2011). Structural durability of forged automotive aluminium chassis components submitted to spectrum loading and salt-corrosion by the example of a tension strut. *Procedia Eng.*, **10**: 330-339.
Hartmann, C., Welm, M., Schreyer, S., Hartmann, C. & Volk, W. (2021). A modular car body for sustainable, cost-effective, and versatile vehicle development. *Technologies*, **9**: 13.
Hossain, K.R., Shishir, M.M.A., Rashid, S., Ahmed, M.H., Basher, A., Risad, R.H. & Paul, A.C. (2023). Application of 3D printing technology in the military. *J. Chem. Lett.*, **4**: 103-116.
Hu, X. & Feng, Z. (2021). *Advanced High-Strength Steel-Basics and Applications in the Automotive Industry*. Oak Ridge National Laboratory (ORNL), US.
Ibrahim, A.M., Ali, A.M. & Kamel, H. (2023). Design optimization and production of a small-scale semi-trailer chassis for testing. *J. Eng. Appl. Sci.*, **70**: 35.
Ibrahim, F. & Aziz, S.A.A. (2023). Study on human comfort of military vehicles in Malaysian tropical environment. *Defence S&T Tech. Bull.*, **16**: 62–68.

Ibrahim, F., Azali, E.N.A. & Aziz, S.A.A. (2024). Comparison on human vibration exposure between wheeled and tracked armoured vehicles in Malaysian tropical environment. *Defence S&T Tech. Bull.*, **17**: 134–141.

Joseva, J., Smart, D.R., Raja, C. & Ramachandran, M. (2023). Recent developments in the field of thermal barrier coatings solutions for structural repair. *J. Appl. Chem. Phys.*, **2**: 31-39.

Khan, W., Tufail, M. & Chandio, A. D. (2022). Characterization of microstructure, phase composition, and mechanical behavior of ballistic steels. *Materials*. **15**: 2204.

Knouff, B. J., Abumeri, G. & Abdi, F. (2012). Chassis weight reduction in military vehicles and the advantages of utilizing high-performance computing. *SAMPE Int. Symp. Exhib. Emerg. Opportun.: Mater. Process Solut.*, 21-24 May 2012, Baltimore Convention Center, Baltimore, Maryland, US.

Kumar, R., Singh, B., & Sharma, D. (2020). Design and analysis of military vehicle chassis for rugged terrains. *Int. J. Veh. Struct. Syst.*, **12**: 101–108.

Kumaresan, R., Samykano, M., Kadirgama, K., Ramasamy, D., Keng, N.W. & Pandey, A.K. (2021). 3D printing technology for thermal Application: a brief review. *J. Adv. Res. Fluid Mech. Therm. Sci.*, **83**: 84-97.

Letherwood, M.D. & Gunter, D.D. (2001). Ground vehicle modeling and simulation of military vehicles using high performance computing. *Parallel Comput.*, **27**: 109-140.

Lee, J. H., Park, S. & Cho, M. (2023). Modular design approach for enhancing adaptability in tactical military vehicles. *J. Mil. Eng*, **29**: 45–57.

Liu, Y., Liu, C., Gao, X. & Tan, J. (2025). Multiphysics finite element analysis and optimization of load-bearing frame for pure electric SUVs. *Symmetry*, **17**: 1143.

Love, L., Nycz, A., Noakes, M., Post, B., Roschli, A. & Babu, S. (2016). *Development and Demonstration of Large-Scale Metal Additive Manufacturing for Military Vehicle Applications (Final Report)*. Oak Ridge National Laboratory (ORNL), US.

Mahmoodi-k, M., Davoodabadi, I., Višnjić, V. & Afkar, A. (2014). Stress and dynamic analysis of optimized trailer chassis. *Tech. Gaz.*, **21**: 599-608.

Mishra, Y. (2020). Design & analysis of ladder frame chassis. *Int. Res. J. Eng. Tech.*, **7**: 3695-3704.

Mohsen, M., Kamel, H., Sharaf, A. M. & El-Demerdash, S. M. (2018). Optimal design of passive suspension system of a 6×6 multi-wheeled all-terrain vehicle using genetic algorithm. *Int. J. Heavy Veh. Syst.*, **25**: 508-533.

Muthyala, M. (2019). *Design and Crash Analysis of Ladder Chassis*. Master's Degree Thesis, Department of Mechanical Engineering, Blekinge Institute of Technology, Sweden.

Muzammil, S.H., Hussain. M., Khalid, M.U. & Amin, A. (2023). Structural optimization of truck ladder chassis using Finite Element Method. *Int. J. Eng. Appl. Sci. Tech.*, **8**: 64-69.

Ngo, T.D., Kashani, A., Imbalzano, G., Nguyen, K.T. & Hui, D. (2018). Additive manufacturing (3D printing): A review of materials, methods, applications and challenges. *Compos. Part B: Eng.*, **143**: 172-196.

Othman, R., Ismail, N.I., Pahmi, M.A.A.H., Basri, M.H.M., Sharudin, H. & Hemdi, A.R. (2018). Application of carbon fiber reinforced plastics in automotive industry: A review. *J. Mech. Manuf.*, **1**: 144-154.

Pandya, P., Patel, V. & Patel, R. (2022). Structural design and analysis of vehicle chassis for military application under static and dynamic loading. *J. Mech. Eng. Sci.*, **16**: 1005–1018.

Patel, H., Panchal, K.C. & Jadav, C.S. (2013). Structural analysis of truck chassis frame and design optimization for weight reduction. *Int. J. Eng. Adv. Tech.*, **2**: 665-668.

Patel, R. & Bhargava, R. (2022). Modular design strategies for adaptive military vehicles: Challenges and innovations. *Defence Tech.*, **18**: 1642–1655.

Ren, P.H., Wei, Z.L. & Wang, Q.Y. (2005). Finite element analysis of HFC6100KY bus chassis frame. *J. HeFei*, **8**: 34-45.

Perka, A.K., John, M., Kuruveri, U.B. & Menezes, P.L. (2022). Advanced high-strength steels for automotive applications: Arc and laser welding process, properties, and challenges. *Metals.* **12**: 1051.

Pruez, J.C., Shoukry, S.N., Williams, G.W. & Shoukry, M.S. (2013). *Lightweight Composite Materials for Heavy Duty Vehicles*. West Virginia University, West Virginia, United States.

Rahman, M.A. & Abdullah, M. (2021). Assessment of military vehicle chassis under multi-axial loading conditions based on MIL-STD standards. *Defence Tech. Rev.* **11**: 314–322.
Rahmani, R., Bashiri, B., Lopes, S.I., Hussain, A., Maurya, H.S. & Vilu, R. (2025). Sustainable additive manufacturing: an overview on life cycle impacts and cost efficiency of laser powder bed fusion. *J. Manuf. Mater. Proc.*, **9**: 18.
Ravi Kumar, L., Vasanth Krishnan, A., Yashwant, K., Aravindan, B. & Prabhakaran, R. (2020). Design and analysis of all terrain vehicle chassis using finite element analysis. *AIP Conf. Proc.*, **2283**: 020093.
Reddy, P.S., Sreenivasulu, M., Nandyala, K. & Esanakula, J.R. (2024). Smart materials revolutionizing automotive technology: Applications, challenges, and future directions. *Int. J. Eng. Trends Tech.*, **72**: 353–363.
Saravanan, K., Kumar, S. & Vetrivel, S. (2021). Investigation on smart materials for light duty goods vehicle chassis frame using FEA. *IOP Conf. Ser. Mater. Sci. Eng.*, **1123**: 012021.
Sarzyński, B., Śnieżek, L. & Grzelak, K. (2024). Metal additive manufacturing (MAM) applications in production of vehicle parts and components: a review. *Metals*, **14**: 195.
Shiva, P.U., Babu, A.R., Sairaju, B., Amirishetty, S. & Deepak, D. (2020). Automotive chassis design material selection for road and race vehicles. *J. Mech. Eng. Res. Dev.*, **43**: 274-282.
Shrivastava, S., Tiwari, R. & Sharma, S. (2019). Design and analysis of heavy commercial vehicle chassis through material optimization. *Int. J. Eng. Trends Tech.*, **67**: 33-36.
Skejić, D., Dokšanović, T., Čudina, I. & Mazzolani, F.M. (2021). The basis for reliability-based mechanical properties of structural aluminium alloys. *Appl. Sci.*, **11**: 4485.
Smith, D. L., Nguyen, H. & Carter, B. (2021). Integration of mission-critical systems on modular vehicle platforms. *J. Defence Mobil. Syst.* **7**: 89–99.
Spasenović, J. & Blagojević, I. (2021). Composite materials in automotive industry - a review. *Industrija*, **49**: 57-68.
Stoudt, M.R. (2016). Shaping, forming and modeling of advanced high strength steel. *JOM*, **68**: 1830-1831.
Thota, J., O'Toole, B.J. & Trabia, M.B. (2011). Optimization of shock response within a military vehicle space frame. *Struct. Multidiscip. Optim.*, **44**: 847-861.
Tiwari, N.D., Gogoi, A., Hazra, B. & Wang, Q. (2021). A shape memory alloy-tuned mass damper inerter system for passive control of linked-SDOF structural systems under seismic excitation. *J. Sound Vib.*, **494**: 115893.
Vannan, P. (2022). Analysis of aluminium alloy made chassis for heavy duty vehicle with comparative static strength analysis. *Int. J. Creat. Res. Thoughts*, **10**: 287-292.
Vido, M., Neto, O.G.C., Lourenço, S.R., Amorim, M. & Rodrigues, M.J.F. (2024). Computer-aided design and additive manufacturing for automotive prototypes: a review. *Appl. Sci.*, **14**: 7155.
Wan, Y. & Takahashi, J. (2021). Development of carbon fiber-reinforced thermoplastics for mass-produced automotive applications in Japan. *J. Compos. Sci.*, **5**: 86.
Widiyanto, I., Sutimin, S., Laksono, F.B. & Prabowo, A.R. (2021). Structural assessment of monocoque frame construction using finite element analysis: A study case on a designed vehicle chassis referring to Ford GT40. *Procedia Struct. Integr.*, **33**: 27-34.
Xu, R.G., Chen, Z., Chen, P. & Peng, G. (2022). Mechanical properties of advanced multifunctional coatings. *Coatings*, **12**: 599.
Yang, A., Zang, Y., Xu, L., Li, L. & Tan, D. (2023). A systematic review and future development of automotive chassis control technology. *Appl. Sci.*, **13**.
Yasar, A. & Bircan, D.A. (2015). Design, analysis and optimization of heavy vehicle chassis using finite element analysis. *Int. J. Sci. Tech. Res.*, **1**: 1-9.
Yinghao, J. (2023). Finite element analysis and optimization of medium truck frame based on ANSYS. *J. Eng. Res. Rep.*, **24**: 13-22.
Zhou, L., Miller, J., Vezza, J., Mayster, M., Raffay, M., Justice, Q., Al Tamimi, Z., Hansotte, G., Sunkara, L.D. & Bernat, J. (2024). Additive manufacturing: a comprehensive review. *Sensors*, **24**: 2668.

INFLUENCE OF STRAKE LINE DESIGN ON UNDERWATER HULL PERFORMANCE OF ASSAULT BOATS

Lenisha Ravie Chandren[1,], Mohd Moesli Muhammad[1,*], Mohd Subhi Din Yati[1,], Abdul Rauf Abdul Manap[1,], Azmahani Sulaiman[1,], Nik Hassanuddin Nik Yusoff[1,], Mohd Hambali Anuar[1], Muhammad Izzamir Firdaus Idris[2], Mohammad Syafiq Mohammad Rafi[3], Muhammad Azrain Mohammad[4] & Mahdi Che Isa[4]

[1]Maritime Technology Division (BTM)
[2] Rocket & Missile Research Centre (RAMREC) Technology Division
[3]Robotics and Artificial Technology Intelligence Technology Division (ROBOAI)
[4]Headquarters

Science & Technology Research Institute for Defence (STRIDE), Malaysia

[*]Corresponding author: moesli.muhammad@stride.gov.my

ABSTRACT

This study evaluates the influence of strake line design on the performance of aluminium assault boats. Ten boats were tested under simulated operational conditions, each loaded with 12 personnel, equipped with a 60 hp outboard motor (OBM) and carrying a 40 L fuel tank. The research focused on three critical performance parameters: speed, manoeuvrability and emergency stopping efficiency. The boats were configured with two distinct strake designs, which are Boats B1 to B5 with six strake lines (three per side), and Boats B6 to B10 with eight strake lines (four per side), featuring a combination of one V-shaped and multiple U-shaped per side. Performance tests were conducted in calm and coastal waters. The speed tests revealed that the boats with eight strake lines achieved up to 9% higher speeds in calm conditions and maintained better performance in coastal waters, with Boat B6 recording the highest speed of 21.05 kn. The manoeuvrability tests showed a 30% reduction in turning time for boats with optimised strake placement with Boat B4 completing a 360° turn in just 11.03 s. Boats equipped with eight strake lines demonstrated enhanced emergency stopping efficiency. Boat B8 recorded the shortest stopping time of 4.50 s as compared to 7.34 s for the boats with six strake lines. Additionally, the boats with eight strake lines demonstrated superior control, stability and reduced resistance in rougher sea conditions, confirming the role of strake geometry in mitigating wave-induced drag. The findings emphasise the critical role of strake configuration in enhancing hydrodynamic lift, reducing drag, as well as improving safety and handling under full-load tactical operations. This study offers practical insights for naval architects and defence applications supporting design optimisation for high-speed crafts intended for diverse operational environments.

Keywords: *Assault boats; strake lines; manoeuvrability; emergency stopping efficiency; speed trail.*

1. INTRODUCTION

Assault boats are specialised watercrafts designed for high-speed tactical operations in both military and rescue scenarios. These boats are built to perform critical missions of transporting personnel, equipment and supplies swiftly and efficiently in demanding environments. Their compact size, agility and ability to operate in shallow waters make them indispensable for missions such as amphibious assaults, riverine patrols and emergency evacuations. The performance of an assault boat hinges on various design factors, with the hull configuration playing a central role in ensuring optimal speed, manoeuvring and stability. In the realm of naval engineering, the design of assault boats plays a critical role in ensuring the success and safety of military operations. Particularly, the influence of strake line design on bottom hull performance is a crucial factor that can significantly impact a boat's speed,

manoeuvrability and emergency stopping efficiency capabilities (Drimer *et al.*, 2016; Hakmon & Drimer, 2020; Zhou *et al*., 2021).

Strakes are horizontal profiles attached to the hull surface that significantly enhance vessel performance by reducing spray displacement and providing lift at the forward section of the hull (Sadiq *et al*., 2022) (Figure 1). This lift improves stability at higher speeds and enhances the vessel's manoeuvrability, particularly in reducing the tactical diameter during turns. These properties are crucial for planning hulls, which are often used in vessels that require precise control and responsiveness in high-speed situations. The impact of strakes is further highlighted during emergency manoeuvres such as an emergency stop, where rapid speed reduction is essential. By increasing lift and contributing to more controlled deceleration, strakes improve the hull's stability during high-speed operations as well as allow for more predictable and efficient stops (Shumylo *et al*., 2023). These attributes are vital in preventing accidents during critical operations and ensuring operational safety (Maljković *et al.* 2024). While strakes are well-documented in their contribution to the hydrodynamic performance of small waterplane area twin hull (SWATH) vessels (Vernengo & Brizzolara, 2017), their specific effects on hard chine planning hulls such as those used in assault boats, remain unexplored.

Figure 1: Strake lines running along the underwater hull of a boat. (Source: Boats, 2024)

Numerical studies have emphasised the importance of understanding the hydrodynamics of heavily loaded hard-chine hulls especially during emergency situations or special operations where the ability to quickly alter speed or execute sharp manoeuvres is crucial. The presence of strakes contributes not only to maintaining speed and stability but also to improving the vessel's overall handling in both routine and high-pressure scenarios. Therefore, the ability to predict the effect of strake design on critical performance parameters such as achievable speeds, manoeuvring efficiency and deceleration is vital for ensuring the success and safety of operations (Wheeler *et al.*, 2021).

Speed, manoeuvrability and emergency stopping efficiency are critical parameters in tactical operations involving assault boats. The ability to transport personnel and equipment swiftly can determine mission success, while precise manoeuvring allows navigation through complex waterways and evasive action in high-pressure environments. The efficiency of emergency stopping, which refers to the boat’s capacity to decelerate rapidly and come to a controlled halt, is paramount during emergency response scenarios. Previous numerical studies have highlighted the importance of understanding the hydrodynamic behaviour of heavily loaded hard-chine hulls during such demanding situations. When configured correctly, strakes have been shown to enhance vessel handling by maintaining speed, improving turning performance and providing greater stability during rapid deceleration. These benefits underline the need for a predictive understanding of strake line design and its effect on performance particularly for operations where precision and safety are non-negotiable (Loffler *et al.*, 2023).

This study investigates the performance of aluminium assault boats fitted with strake lines along their underwater hulls, with the aim of assessing their impact under both calm and rough water conditions. The evaluation focuses on three key performance metrics: speed, manoeuvrability and emergency stopping efficiency. The findings support the hypothesis that the inclusion of strakes lines contributes to increased speed, improved handling during manoeuvres and more effective emergency stopping efficiency. These results substantiate the potential of strake line configurations to enhance the operational capability and safety of high-performance maritime boats.

2. METHODOLOGY

The methodology for this study involves evaluating the influence of strake line design on the performance of assault boats through structured experimental tests. The tests focused on three critical performance metrics: speed, manoeuvring and emergency stopping efficiency. Each test was conducted under controlled conditions and the boats' specifications, test setups and procedures were standardised for consistency.

2.1 Test Specification & Condition

2.1.1 Boat Specification

The boats used in this study were constructed from marine-grade aluminium alloy, chosen for its high strength-to-weight ratio and excellent resistance to corrosion. Each boat featured a Vee-bottom hull design, optimised for stability and smooth navigation in both calm and rough waters. A total of ten boats, labelled B1 through B10 were used as the sample of research and each was equipped with a 60 hp outboard motor (OBM). The dimensions of the boats are provided in Table 1.

Table 1: Dimension of the boats used in this study.

Feature	Specification
Length	5 m
Beam	2 m
Empty Weight	320 kg (without OBM)
Full Load Weight	1,300 kg (including fuel and personnel)
Fuel Capacity	40 L
Capacity	12 persons (2 crew + 10 personnel)

The boats were configured with different strake line arrangements: Boats B1 to B5 were fitted with three strake lines on each side (port and starboard) resulting in a total of six strake lines, while Boats B6 to B10 were equipped with four strake lines on each side (port and starboard), giving a total of eight strake lines. The configuration of the boats is presented in Table 2.

Table 2: Configuration of the boat samples.

No.	Research Sample (Boat No.)	Characteristics of the Research Samples
1.	B1	Fitted with three strake lines on each side (port and starboard) resulting in a total of six strake lines
2.	B2	
3.	B3	
4.	B4	
5.	B5	
6.	B6	Fitted with four strake lines on each side (port and starboard) resulting in a total of eight strake lines
7.	B7	
8.	B8	
9.	B9	
10.	B10	

The strake lines attached to the underwater hull are configured in a V-shape and securely welded onto the bottom hull surface. These V-shape strakes also known as V-strakes are formed at an angle of approximately 45°. As shown in Figure 2, in addition to the V-shaped strakes, U-shaped strakes which feature a rectangular cross-sectional profile are also incorporated into the design which contribute to the boat's hydrodynamic performance. These U-strakes are strategically positioned to enhance water flow disruption, reduce drag and improve stability. They are symmetrically installed on both the port and starboard sides of the boat, ensuring uniform hydrodynamic benefits. Positioned longitudinally along the entire length of the underwater hull, the strake lines are precisely aligned to optimise the water flow around the hull, thereby enhancing the boat's overall performance. This configuration aims to improve stability, especially at higher speeds, increase manoeuvrability in complex conditions, as well as boost overall operational efficiency by reducing resistance and maintaining better control (Rahmaji *et al.*, 2022).

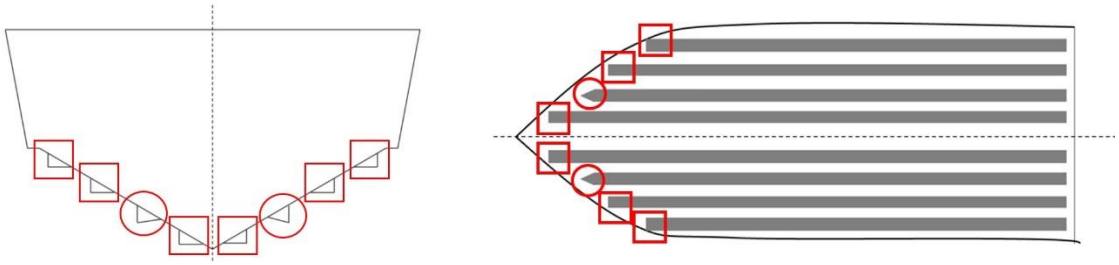

(a) **(b**

Figure 2: Strake lines on the bottom hull. (a) Front view: Displays the symmetrical arrangement of V-shaped and U-shaped strake lines on both port and starboard sides (b) Bottom view: Longitudinal alignment of strake lines. U-shaped strakes are indicated with red squares and V-shaped strakes are indicated with red circles.

2.1.2 Full Load Configuration

The boats were tested under a full-load scenario, simulating real-world operational conditions. This configuration included two crew members, ten fully equipped personnel, a 40 L fuel tank and operational equipment. The total load ensured that the boat's performance metrics reflected practical usage scenarios such as military or rescue missions.

2.1.3 Equipment

For this study, precision equipment was utilised to ensure accurate and reliable data collection under varied operational conditions. A Garmin GPSMAP 65s handheld GNSS receiver was employed to measure the boat's speed during trials. This advanced GNSS receiver is renowned for its high sensitivity and ability to provide accurate readings even in challenging environments such as coastal areas with wave interference. It uses multi-band technology and a wide range of satellite support, ensuring consistent performance and minimal errors (Garmin, 2020).

A digital stopwatch was used for timing tests including emergency stopping efficiency time and manoeuvrings trials. This device ensured precise time measurement with a resolution accurate to fractions of a second, which is essential for evaluating performance metrics that demand a high level of precision.

2.1.4 Test Conditions

The performance evaluation of the assault boats was conducted in two distinct environmental conditions: calm waters (rivers) and coastal waters, to simulate a range of operational scenarios. These conditions were selected to rigorously assess the boats' hydrodynamic performance and stability under varying circumstances.

The calm water environment offered controlled conditions, making it ideal for obtaining baseline measurements. These conditions allowed for isolating the effects of the strake line designs on key performance metrics, including speed, manoeuvring and emergency stopping efficiency. The absence of external disruptions such as waves ensured a consistent hydrodynamic response, enabling precise and repeatable data collection

Coastal testing introduced moderate environmental challenges, including wave-induced resistance and wind to mimic realistic operational scenarios encountered during military or rescue missions. The test encompassed sea states ranging from Sea States 1 to 2. Sea State 1 is characterised by a smooth surface with small, infrequent wavelets, while Sea State 2 features short but pronounced waves of up to 0.5 m in height (Corigliano *et al*., 2024). These conditions assessed the boats' ability to maintain stability, control and efficiency in dynamic environments. The presence of waves offered valuable insights into the boats' responses to drag and turbulence, emphasising the impact of the strake line design on operational performance.

In calm waters, the boats exhibited predictable hydrodynamic behaviour, achieving higher speeds and smoother turns, facilitating a clear analysis of the effects of the strake lines. In contrast, the coastal environment revealed the advantages of optimised strake designs, as the boats demonstrated enhanced stability and control, effectively countering additional resistance from waves. These observations underscored the comprehensive insights gained from testing under contrasting conditions.

2.2 Speed Tests

The speed tests were conducted to measure the maximum and minimum velocities achievable by the boats under full-load conditions. Using the GNSS receiver, the boats were operated at 100% RPM across both calm water and coastal conditions. Speed data was recorded at regular intervals to ensure consistency and accuracy.

2.3 Manoeuvring Tests

The manoeuvring tests evaluated the boat's ability to execute tight turns while maintaining stability and control. Each boat was tested under full-load conditions, making full 360-degree turns to both port and starboard at 100% RPM. The time taken to complete the turn and the radius of the turn were recorded for analysis. The turning performance depended heavily on the strake design. The tests were conducted under calm conditions typically on a river.

2.4 Emergency Stopping Efficiency

The emergency stopping efficiency was designed to simulate real-life scenarios where a boat might need to halt abruptly to avoid collisions or respond to unexpected obstacles. During this trial, the boat was operated at 100% RPM representing maximum speed and then transitioned to an idle state immediately upon receiving the signal to stop. Key performance metrics included the stopping distance (measured in boat lengths) and the time taken from the moment the signal was given until the boat became stationary. The standard criteria required the stopping distance to be under eight boat lengths and the stopping time to be less than 15 s (IMO, 2002). The tests were carried out in calm waters to ensure controlled and consistent conditions.

3. RESULTS

The speed test results (Figure 3) demonstrate clear variations in performance across differing environmental conditions. Under calm water (river) conditions, average boat speeds ranged between 18 and 21 kn whereas under coastal (sea) conditions the range decreased to 15 to 19 kn indicating a measurable decline in performance in more turbulent environments. Boats B1 to B5, which were outfitted with six strake lines, achieved speeds of 18 to 20 kn in calm waters and 15 to 18 kn in coastal waters. In comparison, Boats B6 to B10, fitted with eight strake lines, exhibited enhanced performance, recording 19 to 21 kn in calm conditions and 17 to 19 kn in coastal conditions. The average reduction in speed from calm to coastal conditions was approximately 2.5 kn for the boats with six strake lines, while the boats equipped with eight strake lines experienced a smaller reduction of approximately 1.5 kn. These findings suggest that increasing the number of strake lines contributes to greater hydrodynamic efficiency and improved performance stability in rougher sea conditions.

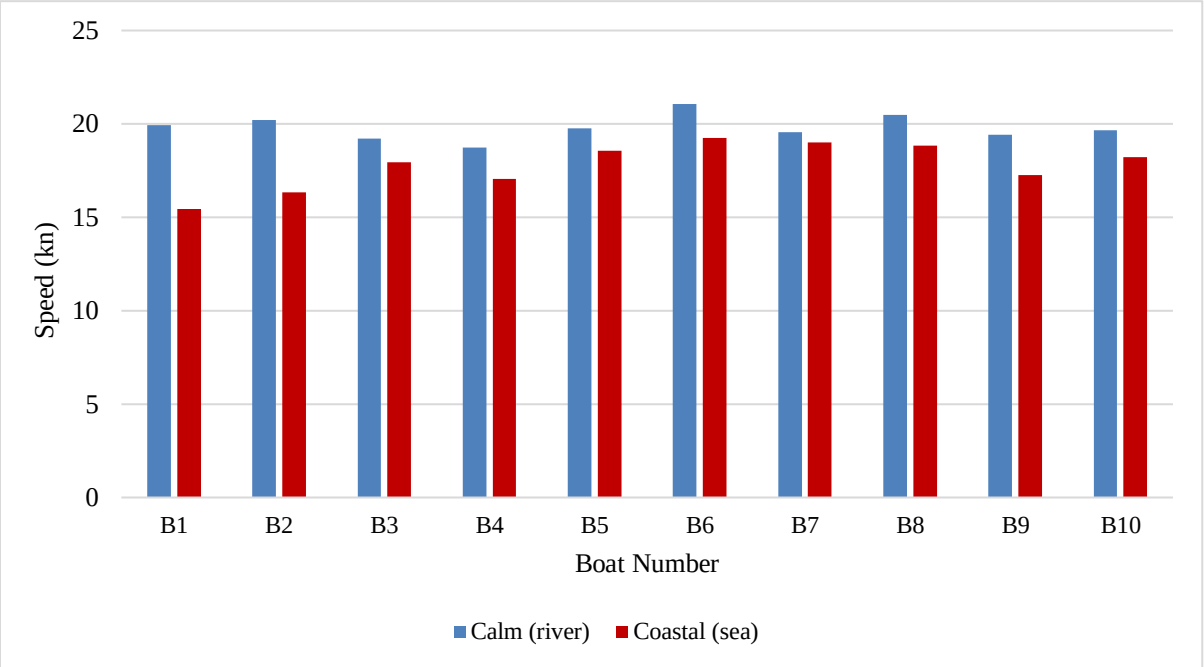

Figure 3: Comparison of average speeds under calm (river) and coastal (sea) conditions.

The manoeuvring test results in Figure 4 revealed distinct differences in turning performance between the boats equipped with six and eight strake lines. Under calm water conditions, the boats were evaluated based on the time taken to complete 360° turns to both port and starboard directions. Boats B1 to B5, fitted with six strake lines, demonstrated generally shorter turning times particularly evident in Boat B4, which achieved the lowest average manoeuvring time of 11.03 s (port) and 11.49 s (starboard). In contrast, Boats B6 to B10, equipped with eight strake lines, showed slightly increased turning durations with Boat B10 recording the highest times of 18.25 s (port) and 17.59 s (starboard). Notably, for both strake configurations the turning times for port and starboard directions remained relatively consistent for each boat indicating symmetrical handling characteristics. This suggests that strake line configuration influences overall turning efficiency but does not significantly affect directional turning balance.

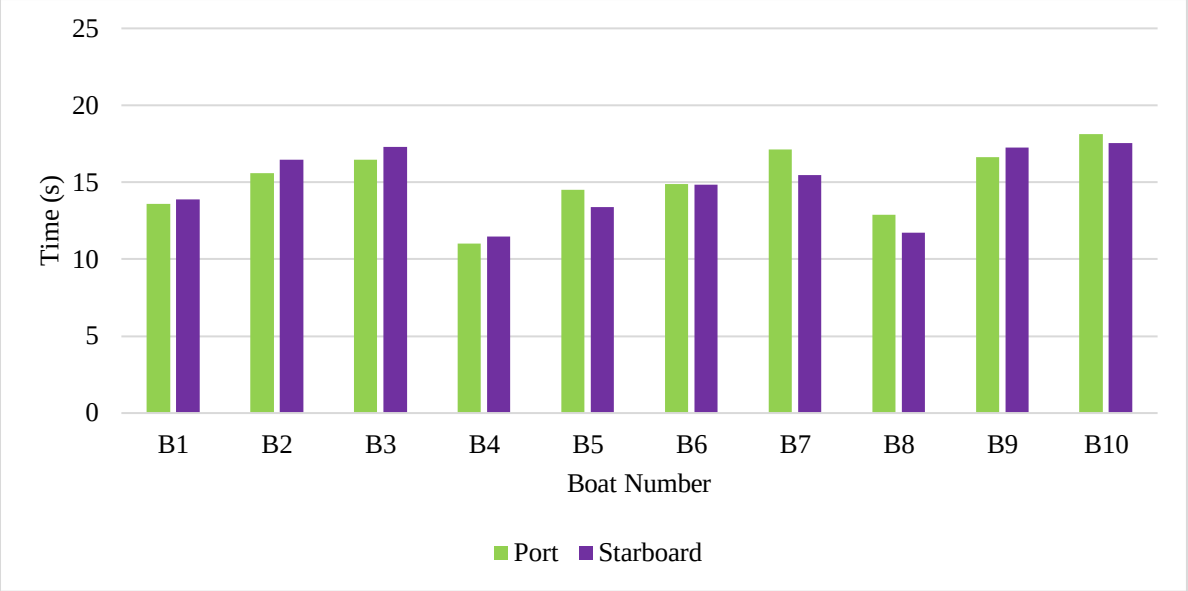

Figure 4: Comparison of turning times for port and starboard directions.

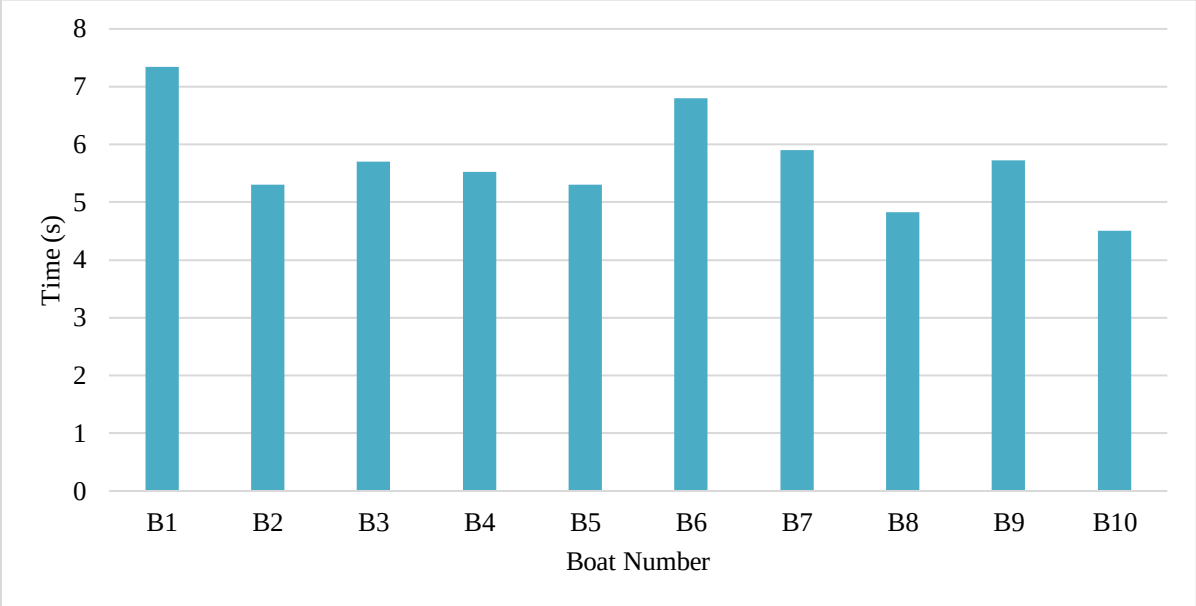

Figure 5: Comparison of emergency stopping times for the boats.

Table 3 presents the summary of the performance metrics for each boat, including the results of the average speeds under both calm and sea conditions, turning speeds (both port and starboard) and emergency stopping times. The table summarises the key performance indicators for each boat as well as the averages for each group.

Table 3: Summary of performance metrics for each boat.

Stake Lines	Boat No.	Average Speed (kn)		Turning Speed (s)		Emergency Stopping Time (s)
		Calm	Sea	Port	Starboard	
6 Lines	B1	19.93	15.43	13.60	13.90	7.34
	B2	20.20	16.33	15.60	16.45	6.10
	B3	19.20	17.95	16.48	17.30	5.70
	B4	18.75	17.06	11.03	11.49	5.52
	B5	19.75	18.56	14.52	13.39	6.00

	Average	19.566	17.066	14.246	14.506	5.832
8 Lines	B6	21.05	19.25	14.90	14.83	6.20
	B7	19.55	19.00	17.13	15.46	5.90
	B8	20.48	18.85	12.89	11.73	4.83
	B9	19.43	17.25	16.63	17.24	5.73
	B10	19.65	18.23	18.14	17.56	4.50
	Average	20.032	18.516	15.938	15.364	5.482

4. DISCUSSION

This study examined the performance of boats equipped with different strake line configurations under varying operational conditions focusing on speed, manoeuvrability and emergency stopping efficiency. The two configurations evaluated, which are six and eight strake lines, demonstrated distinct hydrodynamic behaviours that influenced each aspect of boat performance.

In the speed tests, conducted under both calm and coastal conditions, the boats with eight strake lines consistently outperformed those with six. This performance advantage is primarily attributed to the increased ability of the additional strakes to streamline water flow along the hull surface, reducing turbulence and drag while enhancing hydrodynamic lift (Miller *et al.,* 2023). As a result, Boats B6 to B10 recorded higher speeds, with some exceeding 20 kn in calm conditions. These improvements are closely linked to the placement, geometry and alignment of the strakes, which together contribute to optimised flow distribution and reduced resistance across the hull (Assi *et al.,* 2018).

When operating in coastal conditions, wave action introduced additional drag resulting in overall reduction in speed across all boats. However, the effect was smaller for the boats with eight strake lines, which retained a higher average speed than their six-strake counterparts. For example, Boat B6 maintained average speed of 19.25 kn despite varying wave directions demonstrating that an optimised strake layout can effectively mitigate resistance from head seas and maintain directional stability. In contrast, boats such as B1 equipped with six strake lines recorded average speeds below 16 kn. Nevertheless, all the boats met the minimum operational speed requirement under full load as prescribed by ISO (2015). These findings align with previous research highlighting the influence of wave direction on propulsion efficiency, where following seas may enhance speed while head seas increase resistance (Ting *et al.,* 2012; Chang *et al.,* 2020).

In addition to speed, manoeuvrability was assessed through 360° turning tests in calm waters. Here, the boats with six strake lines displayed superior agility by completing the turning manoeuvres in shorter durations. This outcome may be attributed to the reduced hydrodynamic resistance associated with a lower number of strakes, which allows for faster angular motion. Although the eight-strake design enhances straight-line stability and directional control, it introduces additional wetted surface area, which can impede quick manoeuvres by increasing drag during turning (Matveev & Bari, 2016; Jeong *et al.*, 2019; Pratama *et al.,* 2023). The turning performance discrepancy was most evident for Boats B9 and B10, both of which recorded the longest times in the manoeuvring trials. Nevertheless, port and starboard turning times were largely consistent across all the boats, indicating symmetrical handling and balanced hull response. This trade-off between agility and stability underscores the importance of tailoring strake configurations to specific operational demands. In scenarios where rapid directional changes are critical, such as in rescue operations or confined navigational spaces, a reduced strake layout may be preferable. On the other hand, applications that prioritise course stability in open or turbulent waters may benefit from the added control provided by the eight-strake configuration (Ting *et al.*, 2012; Budiyanto *et. al.,* 2021; Ghadimi *et al.,* 2025).

Further differences between the two designs emerged the during emergency stopping tests, which were also conducted in calm water conditions. The boats with eight strake lines exhibited noticeably shorter stopping distances, reflecting greater hydrodynamic braking efficiency. The enhanced deceleration is likely due to the increased drag produced by the additional strakes, which disrupt flow more

significantly and create resistance when propulsion is cut. The resulting vortices and increased wetted surface area help dissipate momentum rapidly and contribute to a more controlled stop. This effect is further supported by the lateral stability offered by the additional strakes, which reduces drift and improves stopping precision (Hossen & Rahman, 2012).

In contrast, the boats with six strake lines showed longer stopping durations, suggesting lower resistance during deceleration. Although they remained within acceptable operational limits the difference in performance reinforces the role of strake geometry in supporting not only speed and manoeuvrability but also safety-critical responses. These results mirror the findings from speed tests where the hydrodynamic benefits of additional strakes consistently translated into performance gains across different conditions (Utama *et. al.*, 2021: Leal, 2023).

Taken together, the results highlight the importance of strake design in influencing multiple dimensions of boat performance. Boats equipped with eight strake lines exhibited superior speed, stability and stopping efficiency making them well-suited for high-speed transit and operations in variable environmental conditions. Meanwhile, the six-strake configuration though slightly limited in top-end performance offered advantages in agility and turning responsiveness. These findings reaffirm earlier conclusions in the literature (Faltinsen, 2005; Mousaviraad *et. al.*, 2015; Yusfianda *et al.*, 2023), emphasising the role of optimised strake placement and geometry in enhancing hydrodynamic performance. Ultimately, the selection of strake configuration should be based on the intended operational profile of the boat, balancing the trade-offs between speed, control and manoeuvrability.

5. CONCLUSION

This study successfully demonstrated the significant influence of strake line configuration on the hydrodynamic performance of assault boats under calm and coastal conditions. The findings confirmed that the boats equipped with six strake lines consistently outperformed those with eight strake lines in terms of speed and manoeuvrability particularly in calm water conditions. However, the boats with eight strake lines demonstrated superior performance in emergency stopping efficiency, offering enhanced stability and braking control in operational scenarios.

The optimised strake design, featuring one V-shaped and multiple U-shaped strakes on each side, contributed to enhanced water flow management, drag reduction and lift generation, aligning with previous hydrodynamic studies. Emergency stopping performance further validated the role of additional strakes in improving deceleration control, likely due to increased drag and water displacement surface area.

Ultimately, the selection of strake line configuration should be aligned with the intended operational profile of the vessel. While six-strake configurations may be adequate for operations in calmer waters requiring tighter turning ability, the eight-strake configuration offers clear advantages for high-speed navigation, improved stopping and superior performance in rougher sea states.

ACKNOWLEDGEMENT

The authors would like to thank the officers and staff from the various laboratories in the Science & Technology Research Institute for Defence (STRIDE), Ministry of Defence, Malaysia for their technical support during the boat tests.

REFERENCES

Assi, G.R.S., Meneghini, J.R., Aranha, J.A.P., Bearman, P.W. & Casaprima, E. (2018). Performance of two- and three-start helical strakes in suppressing vortex-induced vibration of a low mass ratio flexible cylinder. *J. Fluids Struct.*, **22**: 819–827.

Boats (2024). *Boat hull types; what hull shape is best?*.Available online at: https://uk.boats.com/boat-buyers-guide/boat-hull-types/ (Last access date: 23 February 2025).

Budiyanto, M.A., Prawira, N.Y. & Dwiputra, H. (2021). Lift-to-drag ratio of the application of hydrofoil with variation mounted position on high-speed patrol vessel. *CFD Letters*, **13**: 1-9.

Chang, Z., Deng, C., Zhang, J., Feng, Z. & Zheng, Z. (2020). Propulsion performance analysis of wave-powered boats. *Int. J. Eng. Technol. Innov*., **10**:121-129.

Corigliano, P., Frisone, F., Chianese, C., Altosole, M., Piscopo, V. & Scamardella, A. (2024). Fatigue overview of ship structures under induced wave loads. *J. Mar. Sci. Eng*., **12**: 1-36.

Drimer, N., Moshkovich, Y. & Neuberg, O. (2016). A design method for planning hulls, considering hydro-elasticity and nonlinear dynamic structural response. *Ships Offshore Struct.*, **12**: 971 - 979.

Faltinsen, O.M. (2005). *Hydrodynamics of high-speed marine vehicles*. Cambridge University.

Garmin. (2020). *GPSMAP® 65/65s Owner's Manual*. Garmin Ltd, USA.

Ghadimi, P., Sajedi, S. & Ghadimi, A. (2025). Impact of aft deformation with wedge and step on performance and stability of high-speed hard chine monohulls via experimental and numerical assessments. *Phys. Fluids*, **37**: 025165.

Hakmon, R. & Drimer, N. (2020). Verifying a new hydro-elastic design method for planning boats by full-scale sea trials. *Ships Offshore Struct.* **16**:747–761.

Hossen, M.A. & Rahman, M. A. (2012). Storm resistant boat designing based on the geometry and movement of water strider. *J. Mech. Eng.*, **42**: 12-18.

IMO (International Maritime Organisation) (2002). *Guidelines for Marine Evacuation Systems*. Int. Marit. Organ., London, United Kingdom.

ISO (International Standard Orgaisation) (2020). *Small Craft – Hull Construction and Scantlings*. (International Organization for Standardization, Geneza, Switzerland.

ISO (International Standard Orgaisation) (2015). *Small Craft – Determination of Maximum Speed and Power Rating*. International Organization for Standardization, Geneza, Switzerland.

Jeong, Y., Park, M., Kim, J. & Song, S. (2019). Wave force characteristics of large-sized offshore wind support structures to sea levels and wave conditions. *Appl. Sci*., **9**:1855.

Leal, R.L. (2023). Effect of speed and hull length on the hydrodynamic performance of a semi-planing hull of a shallow-draft watercraft. *J. Mar. Sci. Eng*., **11**:2328.

Löffler, R.J.G., Roliński, T., Kitahata, H., Koyano, Y. & Górecki, J. (2023). New types of complex motion of a simple camphor boat. *Chem. Phys*., **25**: 7794–7804.

Maljković, M., Pavić, I., Meštrović, T. & Perković, M. (2024). Ship maneuvering in shallow and narrow waters: predictive methods and model development review. *J. Mar. Sci. Eng*., **12**: 1-22.

Matveev, K. & Bari, G. (2016). Effect of deadrise angles on hydrodynamic performance of a stepped hull. *J. Eng. Marit. Environ*, **230**: 616-622.

Miller, L.M., Njaka, T., Brizzolara, S. & Curtin, T. (2023). Drag reduction and power optimization due to an innovative, toroidal hull form of an AUV. IOP *Mater. Sci. Eng.*, **1288**: 012039.

Mousaviraad, M., Wang, Z. & Stern, F. (2015). Urans studies of hydrodynamic performance and slamming loads on high-speed planing hulls in calm water and waves for deep and shallow conditions. *Appl. Ocean Res*., **51**: 222-240.

Pratama, A.S., Prabowo, A.R., Tuswan, T., Adiputra, R., Muhayat, N., Cao, B., Hadi, S. & Yaningsih, I. (2023). Fast patrol boat hull design concepts on hydrodynamic performances and survivability evaluation. *J. Appl. Eng. Sci*. **21**: 501–531.

Rahmaji, T., Prabowo, A. R., Tuswan, T., Muttaqie, T., Muhayat, N., & Baek, S.-J. (2022). Design of fast patrol boat for improving resistance, stability, and seakeeping performance. *Des.*, **6**: 105.

Sadiq, M. T., Shariati, M., Khorami, M. & Toghroli, A. (2022). Novel geometries of serrated helical strakes to suppress vortex-induced vibrations and reduce drag. *J. Wind Eng. Ind. Aerodyn.*, **202**: 104206.

Shumylo, O., Yarovenko, V., Malaksiano, M. & Melnyk, O. (2023). Comprehensive assessment of hull geometry influence of a modernized ship on maneuvering performance and propulsion system parameters. *Sci. J. Marit. Res.*, **37**: 314–325.

Ting, C., Babanin, A., Chalikov, D. & Hsu, T. (2012). Dependence of drag coefficient on the directional spreading of ocean waves. *J. Geophys. Res. Atmos*., **117**:11.

Utama, I.K.A.P., Sutiyo, I.K., Suastika, A., Sulistiyono, A., Hasanudin, Y.A., Hermawan, Y.A. & Aryawan, W.D. (2021). Resistance analysis of rescue boat in calm water condition. *5th Int. Conf. Marine Technol.*, December 3-4, 2020, Surabaya, Indonesia,

Vernengo, G. & Brizzolara, S. (2017). Numerical investigation on the hydrodynamic performance of fast SWATHs with optimum canted struts arrangements. *Appl. Ocean Res.*, **63**: 76–89.

Wheeler, M., Matveev, K. & Xing, T. (2021). Numerical study of hydrodynamics of heavily loaded hard-chine hulls in calm water. *J. Mar. Sci. Eng*., **9**: 184 -190.

Yusfianda, A.R., Prabowo, A.R., Do, Q.T., Adiputra, R., Putranto, T. & Bae, D.M. (2023). Investigation of environmental factors on the resistance characteristic: Study case of the designed patrol boat hull. *IOP Conf. Ser.: Earth Environ. Sci*., **1278**: 012013

Zhou, Z., Zhang, X. & Liu, Y. (2021). Novel geometries of serrated helical strakes to suppress vortex-induced vibration of a circular cylinder. *Ocean Eng.*, **234**: 109254.

IMPACT OF DESIGN VARIATIONS ON THE HYDRODYNAMIC PERFORMANCE OF UNDERWATER TOWING VEHICLES FOR UNDERWATER SURVEY APPLICATION: A CFD-BASED APPROACH

Mohammad Syafiq Mohammad Rafi[1*], Nor Nazifah Muhammad Saidi[2], Mohd Moesli Muhammad[2], Abdul Rauf Abdul Manap[2], Mohd Hambali Anuar[2], Nur Afande Ali Hussain[2], Muhammad Izzamir Firdaus Idris[3], Muhammad Azrain Mohammad[4], Muhammad Ramdhan Mohd Suhaili[5], Aizul Fazli Suhaimi[1], Muhammad Nur Annuar Mohd Yunos[1], Mohd Azim Md Burhanuddin[4], Ezza Nur Adzlilliya Azali[4], Rosdi Yaacob[2] & Mohd Hafiz Mohd Noor[1]

[1]Robotics and Artificial Intelligence Technology Division (ROBOAI)
[2]Maritime Technology Division (MARTECH)
[3]Rocket & Missile Research Centre (RAMREC)
[4]Automotive and Mechanical Technology Division (AUTOMECH)
[5]Electronic and Communication Technology Division (BTEK)
Science & Technology Research Institute for Defence (STRIDE), Malaysia

[*]Corresponding author: syafiq.rafi@stride.gov.my

ABSTRACT

This study explores the hydrodynamic performance of three different underwater towing vehicle designs (Models 1, 2 and 3) for underwater survey applications, focusing on the impact of varying angles of attack on the vehicle's performance. Computational fluid dynamics (CFD) simulations were conducted at four angles of attack (0°, 5°, 10° and 15°) to evaluate key performance parameters, including drag force, lift force, lift-to-drag (L/D) ratio, stability and manoeuvrability. The results show that Model 3 consistently outperformed the other two models, especially at higher angles of attack, showing the highest lift-to-drag ratio and optimised drag performance for high-resistance underwater tasks. Static pressure contours also revealed that Model 3 experiences more uniform pressure distribution, contributing to its superior stability. In contrast, Model 1 demonstrated superior performance at low angles of attack with moderate lift and drag resistance. Model 2, while showing improvement at higher angles, lagged in overall efficiency and requires further optimisation. Steady-state CFD analysis was employed to derive the hydrodynamic coefficients and assess the impact of different towing conditions on each model's stability and efficiency. The findings suggest that Model 3 is the most efficient design for underwater towing, with each model offering distinct advantages based on operational requirements.

Keywords: *Hydrodynamic performance; underwater towing vehicle; computational fluid dynamics (CFD) simulations; angle of attack; stability.*

1. INTRODUCTION

Underwater towing vehicles play a critical role in various underwater survey applications, ranging from environmental monitoring to exploration and resource extraction. The main advantage of underwater towing vehicles lies in their ability to support specialised applications such as detailed seabed mapping, marine biodiversity assessment and underwater infrastructure inspections. The towing concept increases the duration of operation by reducing energy demand through hydrodynamic passivity, relying on external forces for movement. This improves energy efficiency, extends range and increases endurance, making the towing vehicle suitable for long missions in remote underwater environments, effectively meeting the needs of modern exploration and surveying. These vehicles are typically designed to operate efficiently under challenging hydrodynamic conditions, where minimising drag while maintaining stability and sufficient lift are essential. The hydrodynamic performance of these

vehicles significantly impacts their energy efficiency, operational range and overall functionality in underwater environments (Hong *et al*., 2023; Li *et al*., 2024).

Design optimisation of underwater towing vehicles presents unique challenges due to the complex interaction between the vehicle's geometry and the surrounding fluid dynamics. Factors such as shape, surface roughness and flow conditions directly influence the drag and lift forces acting on the vehicle, which in turn affect its operational performance (Liu *et al*., 2020), with recent studies further exploring these dynamics. For instance, Li *et al*. (2024) conducted a hydrodynamic analysis and drag-reduction design of an unmanned underwater vehicle using computational fluid dynamics (CFD), highlighting significant improvements in drag reduction through geometric modifications. Although significant advancements in CFD have provided researchers with powerful tools to analyse and predict hydrodynamic behaviour, there remains a lack of comprehensive studies comparing the performance of different design configurations under consistent conditions (Shirazi *et al*., 2019).

Stability in underwater towing vehicles is primarily achieved through the optimisation of lift force, as propulsion is externally provided by a mother ship, reducing the need to focus on drag minimisation (Zhou *et al*., 2020). Lift force, generated by the interaction of hydrodynamic surfaces with water, is critical for maintaining equilibrium and resisting destabilising factors such as roll, pitch and yaw. The lift-to-drag ratio (L/D) is a key aerodynamic and hydrodynamic performance metric that compares the lift generated by an object to the drag it experiences. By optimising fins and control surfaces, underwater towing vehicles can remain stable even in turbulent conditions, ensuring precise performance during towing operations (Park *et al*., 2023). This focus on lift force as a cornerstone of stability underscores its importance in underwater towing vehicle design, enabling efficient and reliable underwater functionality (Liu *et al.*, 2023).

CFD is a simulation tool used to analyse fluid flow and its interaction with surfaces by creating a digital model and dividing it into smaller elements (Stryczniewicz & Drężek, 2019). It numerically solves the fundamental equations of fluid motion, such as the Navier–Stokes equations, to predict how fluids behave under various conditions. This method allows engineers to study complex flow behaviours, such as pressure distribution, turbulence and flow separation, without the need for extensive physical experiments (Ferziger & Peric, 2020). CFD has become widely used in marine, aerospace and mechanical engineering due to its ability to provide accurate and cost-effective insights into fluid behaviour. Furthermore, this research underscores the potential of CFD simulations as a reliable method for performance evaluation and design optimisation (Phillips *et al.*, 2010; Dantas *et al.*, 2013).

This study employs CFD to analyse the hydrodynamic performance of underwater towing vehicles, with particular emphasis on drag and lift forces. Using ANSYS CFD simulations, three distinct vehicle designs are evaluated to determine their associated drag and lift forces, along with their respective coefficients, in order to assess the impact of design variations. The results are expected to contribute to the broader field of underwater vehicle design by providing practical insights for enhancing energy efficiency and stability. By demonstrating the influence of design modifications, the study supports the development of more effective and efficient towing vehicles suitable for a wide range of underwater survey applications.

2. METHODOLOGY

2.1 Vehicle Geometry and Design

This study evaluates three underwater towing vehicle designs for survey operations using ANSYS CFD simulations at Universiti Teknologi Petronas. The designs were finalised based on their distinct hydrodynamic characteristics to improve efficiency and performance under various towing conditions, as presented in Figure 1. Model 1, inspired by the G-882 towing fish, adopts its streamlined geometry to minimise drag and support stability, making it effective for shallow-water operations. Model 2 is based on the NACA 0012 aerofoil profile, which balances lift and drag forces for stability and precise

control. Optimised for operations at 50 m in depth, it includes fins and wings to enhance hydrodynamic efficiency and manoeuvrability (Yang *et al*., 2021; Zhou *et al*., 2023). Model 3 employs a torpedo-shaped design using Myring's equations, featuring specific dimensions and tip angles to reduce drag and ensure stability, making it ideal for towing operations requiring low resistance (Myring, 1976; Stryczniewicz & Drężek, 2019). These designs reflect established principles of underwater towing efficiency and stability to improve performance in diverse aquatic environments.

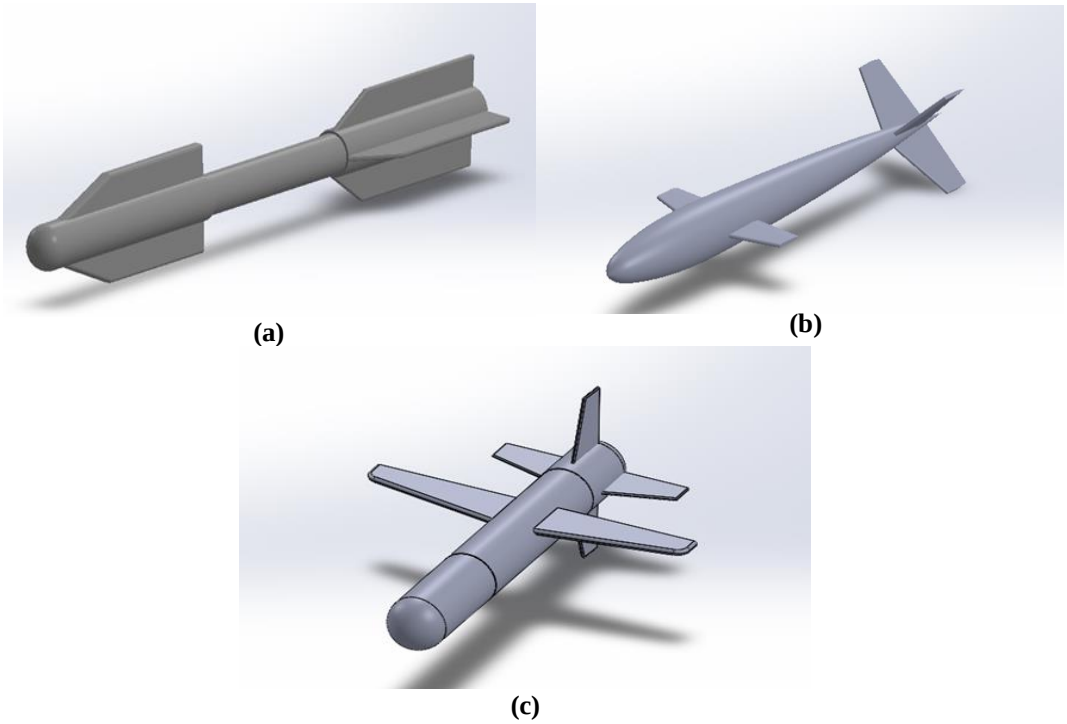

(a) **(b)**

(c)

Figure 1: The three underwater towing vehicle designs evaluated in this study: (a) Model 1 (b) Model 2 (c) Model 3.

2.2 Governing Equations

The ANSYS Fluent CFD software is commonly used for hydrodynamic coefficient estimation of underwater vehicles due to its accuracy and reliability (Stryczniewicz & Drężek, 2019). The underactuated underwater vehicle is designed to be fully immersed in water when in operation. The Navier–Stokes (NS) equations are adopted as the governing equations in this work to simulate the flow fields around the underwater vehicle model:

$$\rho\left(\frac{\partial v_i}{\partial t} + v_j \cdot \frac{\partial v_i}{\partial x_j}\right) = -\frac{\partial p}{\partial x_i} + \mu \cdot \frac{\partial^2 v_i}{\partial x_i \partial x_j} + f_i \quad (1)$$

where:

- ρ is the density of fluid
- v is the velocity
- t is the time
- x is the position
- p is the pressure
- μ is the dynamic viscosity
- f_i is the external force

The total pressure P_t is:

$$P_t = P_s + P_d \tag{2}$$

where:

P_t is the total pressure
P_s is the static pressure
P_d is the dynamic pressure

The total drag force includes the friction force caused by surface shear stress in the boundary layer and the pressure force generated by the pressure difference exerted on the torpedo body. Therefore, the total drag coefficient (C_d) and lift coefficient (C_L) are as follows:

$$C_d = C_{df} + C_{dp} = \frac{F_{df}}{\frac{1}{2}\rho V^2 . A_f} + \frac{F_{dp}}{\frac{1}{2}\rho V^2 . A_f} \tag{3}$$

$$C_L = \frac{F_L}{\frac{1}{2}\rho V^2 . A_f} \tag{4}$$

where

C_{df} is the coefficient of skin friction drag
C_{dp} is the coefficient of pressure drag
F_{df} is the friction drag force that is caused by the roughness of the surfaces of the glider
F_{dp} is the pressure drag force
A_f is the submerged surface area of a torpedo body
F_l is the lift force
C_l is the lift coefficient

2.3 Boundary Conditions

The fluid domain related to the boundary conditions is shown in Figure 2. In order to obtain the correct results, three specified boundary conditions of different sizes shown in Figure 3 are applied for this CFD simulation. In this study, the domain dimensions were designed to be sufficiently large to prevent backflow at high drift angles (Sakaki & Sadeghian Kerdabadi, 2020). The prescription of the boundary conditions for the fluid around the underwater towing vehicle's body is shown in Table 1. It specifies the type and value of each boundary, including velocity inlet, pressure outlet and wall conditions for various surfaces of the fluid domain.

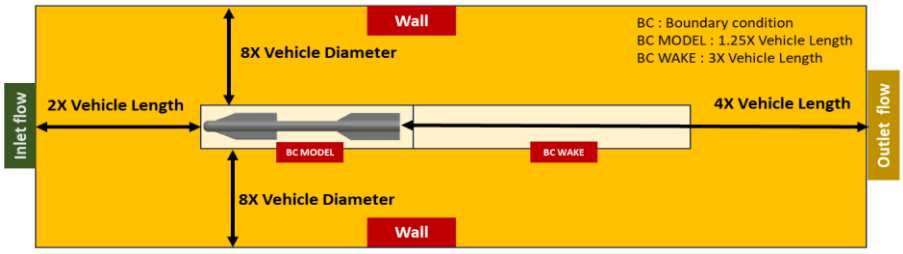

Figure 2: Details of boundary conditions for the fluid domain for straight line simulation.

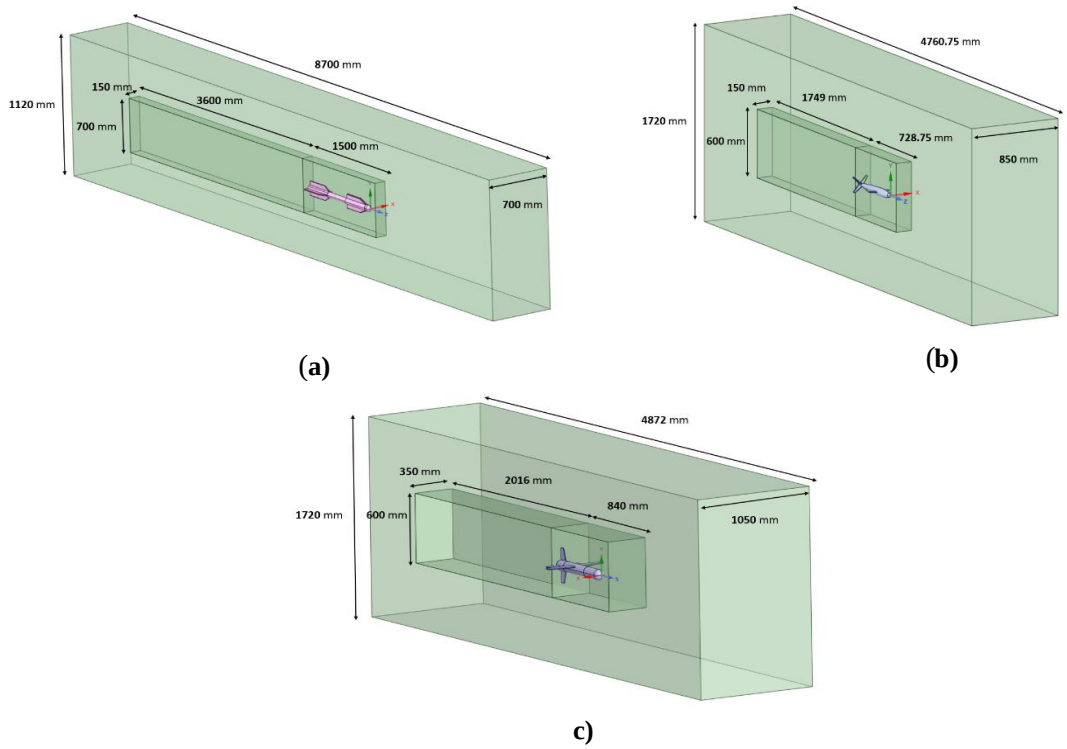

Figure 3: Boundary condition sizings for: (a) Model 1 (b) Model 2 (c) Model 3.

Table 1: Boundary condition parameters.

Boundary	Boundary Type
Inlet	Velocity_Inlet
Outlet	Pressure_Outlet
Top	Wall
Side	Symmetry
Bottom	Wall
Model	Wall

The velocity inlet is 2.05 m/s (4 knots), which is the speed of the fluid entering the simulation domain. The pressure outlet is set to 0-gauge pressure, indicating that the fluid exits the domain at atmospheric pressure, ensuring realistic flow behaviour. The parameters of the fluid (seawater) selected in the simulations are temperature = 15 ℃, density = 998.2 kg/m³ and fluid viscosity = 0.017894 mPa·s.

2.4 Mesh Generation

The mesh generation process is essential for precise and stable CFD simulations. Structured or unstructured meshes are employed based on the complexity of the underwater vehicle models. A fine mesh is implemented near the surfaces to capture flow characteristics at the fluid-solid interface, while a coarser mesh is utilised in far-field regions with lower flow gradients (Figure 4) (Sakaki & Sadeghian Kerdabadi, 2020). Three-dimensional tetrahedral elements are employed for complex geometries. Mesh

quality is assessed using metrics such as aspect ratio, skewness and orthogonality (Knupp, 2001), with poor-quality elements refined to avoid errors (Yildiz, 2023). The meshing setup parameters used in this study are summarised in Table 2. A mesh independence study ensures that the results are unaffected by further refinement, achieving a balance between computational efficiency and accurate hydrodynamic analysis.

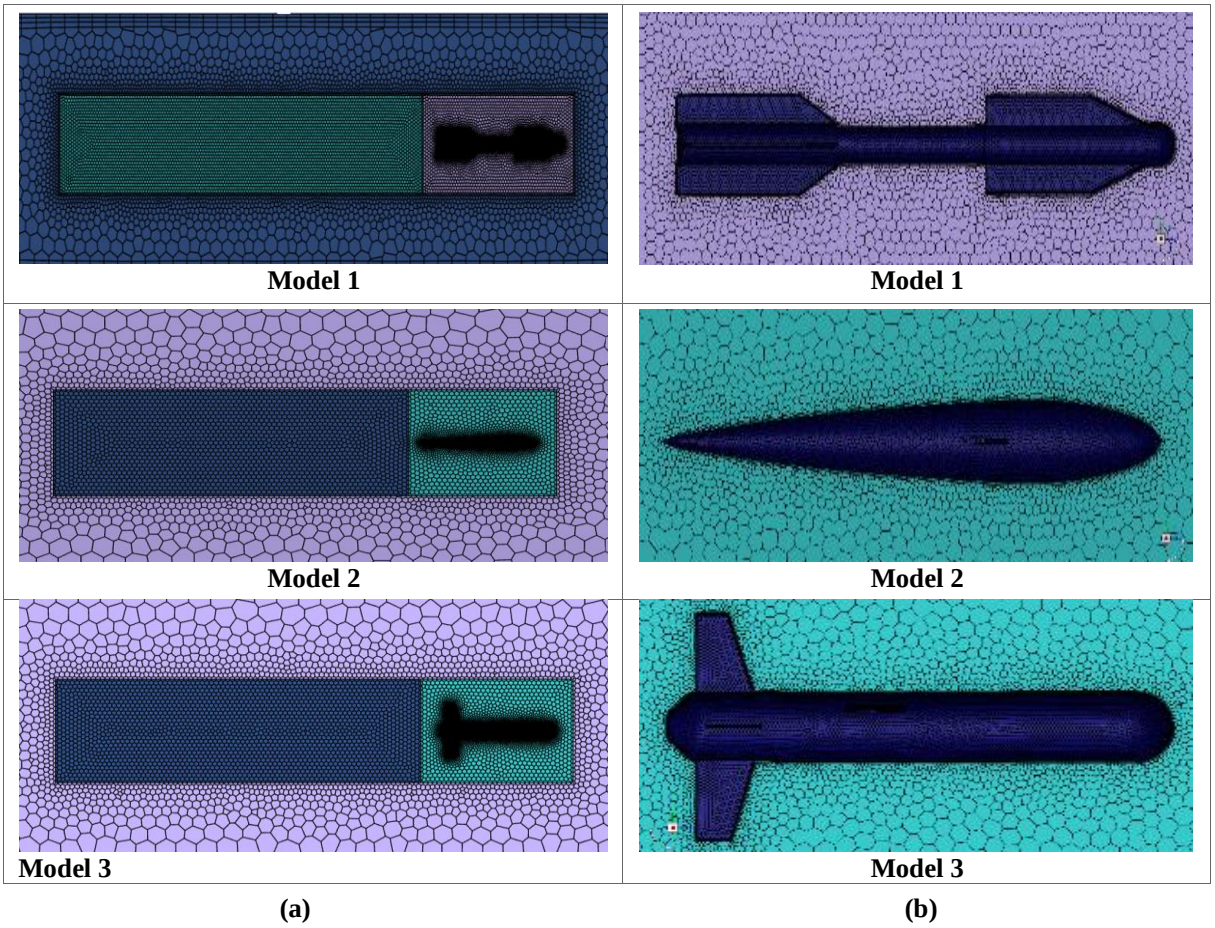

Figure 4: (a) Overall meshing for the three different models. (b) Meshing around the underwater towing vehicle models.

Table 2: Meshing setup for simulation.

Boundary Properties	Share Topology
Mesh Growth Rate	1.2
Mesh Curvature Angle	16°
No Boundary Layer	3
Mesh Type	Polyhedra
Turbulence Model	K-epsilon (2 eqn) Realisable
Fluid Material	Water-Liquid
Turbulence Intensity	5%

2.5 Simulation Parameters

Key simulation parameters are selected to replicate realistic operational conditions for the underwater towing vehicles during straight-line drift tests. The towing speed is set at 2.05 m/s (approximately 4 knots), representing a typical survey speed for such applications. In order to investigate the impact of orientation on hydrodynamic performance, simulations are conducted at varying angles of attack: 0°, 5°, 10° and 15°. These angles are chosen to cover a range of scenarios, from neutral alignment to more aggressive orientations relative to the flow direction. This range allows for a comprehensive analysis of the drag and lift characteristics under different operational conditions. These parameters are consistent across all three vehicle models to ensure a fair and systematic comparison of their hydrodynamic performance. The combination of steady towing speed and varying angles of attack provides insights into the vehicles' stability, manoeuvrability and energy efficiency during survey operations (Divsalar *et al.*, 2020).

3. RESULTS & DISCUSSION

3.1 Drag Coefficient & Drag Force

Drag coefficient (C_d) and drag force (F_d), illustrated in Figure 5, are essential factors affecting the energy efficiency of a towing vehicle. Lower values for both parameters are ideal, as they help minimise energy consumption and operational costs (Singh *et al.*, 2022). Conversely, high drag coefficients and drag force lead to slower speeds, reducing efficiency in underwater survey operations (Jagadeesh *et al.*, 2009; Shirazi *et al.*, 2019; Yang *et al.*, 2021; Singh *et al.*, 2022).

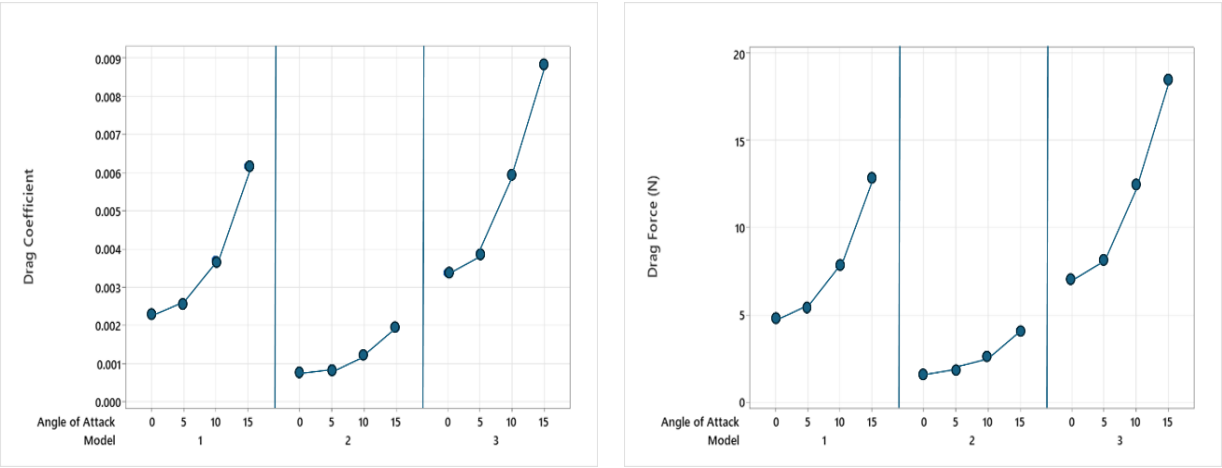

(a) **(b)**

Figure 5: Comparison of (a) drag coefficient and (b) drag force.

It was found that the drag force increased with the angle of attack for all three models, as noted by Panda *et al*. (2020), though the rate of increase varied between the designs. Model 1 showed a steady increase in drag force from 4.83 N at 0° to 12.93 N at 15°. Model 2 showed a more moderate rise, from 1.65 N at 0° to 4.08 N at 15°. In contrast, Model 3 showed the highest drag forces, with values starting at 7.08 N at 0° and increasing to 18.50 N at 15°. This indicates that Model 3 is extremely sensitive to changes in the angle of attack, leading to a significant increase in drag at steeper angles, which may adversely affect operational efficiency at higher towing angles if not balanced with lift force.

Corresponding to the drag force data, the drag coefficient also increased with the angle of attack for all models. Model 1 showed a gradual rise in drag coefficient from 0.0023 at 0° to 0.0062 at 15°, reflecting a steady increase in hydrodynamic resistance. Model 2 kept a relatively low drag coefficient, starting at 0.0008 at 0° and increasing to 0.0019 at 15°. This suggests a more streamlined design that experiences minimal drag even at higher angles. Model 3, on the other hand, displayed a more substantial increase, from 0.0034 at 0° to 0.0088 at 15°.

3.2 Lift Coefficient & Lift Force

Lift coefficient (C_L) and lift force (F_L), presented in Figure 6, play a crucial role in supporting the stability and buoyancy of the vehicle. Achieving an optimal balance between lift and drag is essential to ensure the vehicle stays in its desired position and orientation during towing (Graver, 2005). Insufficient lift can lead to instability, while excessive lift may compromise the vehicle's hydrodynamic performance (Yang *et al*., 2021).

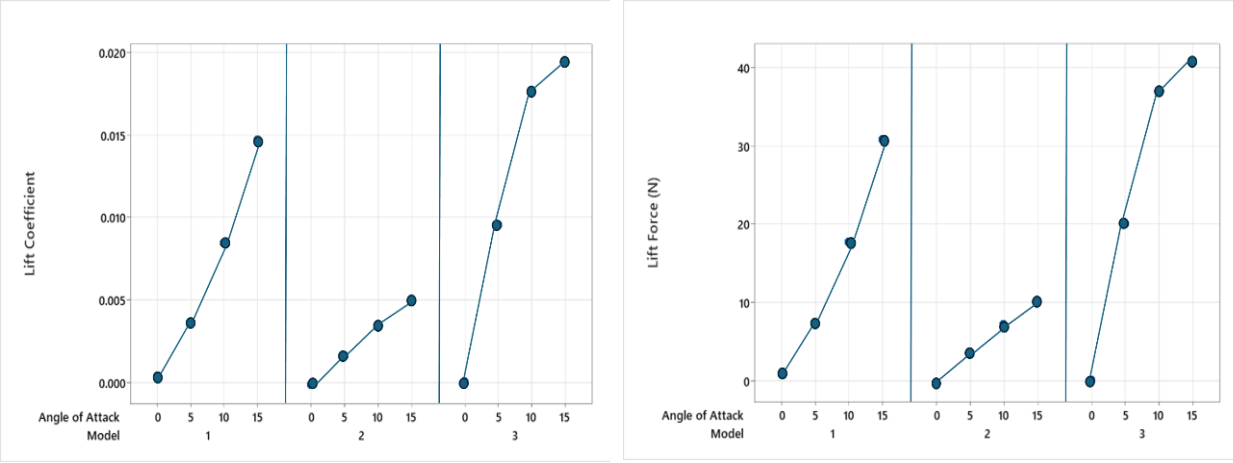

(a) **(b)**

Figure 6: Comparison of (a) lift coefficient and (b) lift force.

The lift force and lift coefficient for all three models increased with the angle of attack, as stated by Panda *et al*. (2020), although the rate of increase varied between the designs. Model 1 showed a steady rise in lift force from 0.8414 N at 0° to 30.81 N at 15°, with a similar increase in lift coefficient from 0.0004 to 0.0147. This shows a consistent ability to generate lift, making Model 1 suitable for applications requiring moderate lift at higher towing angles.

Model 2, starting with a negative lift force at 0° (-0.2185 N), showed improvement at higher angles, reaching 10.22 N at 15° with the lift coefficient rising from 0.0001 to 0.0049. Despite the negative lift at 0°, Model 2 showed a more stable lift generation as the angle of attack increased.

Model 3 displayed the highest lift forces, with values rising from 0.1421 N at 0° to 40.53 N at 15°, and the lift coefficient increasing from 0.00007 to 0.0193. This significant lift generation makes Model 3 highly effective at higher angles, ideal for applications requiring high lift, such as deep-water surveys. Model 3 consistently showed the greatest lift potential, improving stability and manoeuvrability during towing operations, as also highlighted by Vijayakumar & Rayaprolu (2020), who reported similar findings in their study on hydrodynamic performance.

3.3 L/D Ratio

The lift-to-drag (L/D) ratio, shown in Figure 7, is a key indicator of a vehicle's hydrodynamic performance, reflecting its ability to generate significant lift with minimal drag for efficient and stable towing operations. A higher L/D ratio indicates better energy efficiency and stability, making it essential in selecting optimal vehicle designs (Jagadeesh *et al*., 2009; Nordin *et al*., 2017; Tian *et al*., 2021).

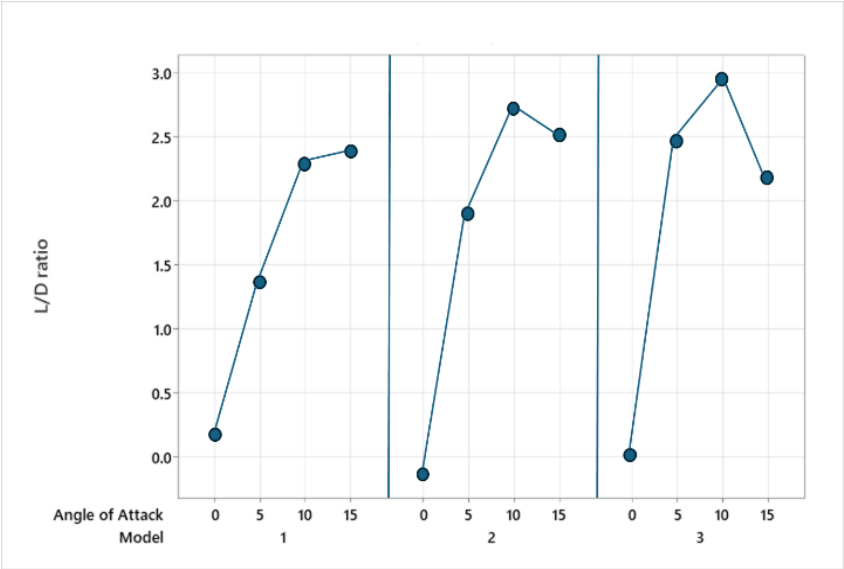

Figure 7: Comparison of L/D ratio.

At 0° angle of attack, Model 1 showed the highest L/D ratio of 0.1743, showing a more favourable balance of lift and drag as compared to the other two models. In contrast, Model 2 showed a negative L/D ratio (-0.1324), which suggests that this model generates insufficient lift relative to its drag, making it the least efficient at this angle. Model 3 had a modest L/D ratio of 0.0201, reflecting a poor lift-to-drag performance at 0° as compared to Model 1.

As the angle of attack increased, the L/D ratios for all the models increased significantly, particularly at 5°, 10° and 15°. Model 1's L/D ratio rose to 1.369 at 5° and peaked at 2.384 at 15°. This trend reflects a more favourable balance between lift and drag as the angle of attack increases, showing enhanced aerodynamic performance at higher angles of attack. Similarly, Model 2 showed a sharp improvement in efficiency, with its L/D ratio increasing from -0.1324 at 0° to 2.508 at 15°, the second highest among the three models at this angle. Model 3 showed the most significant improvement in L/D ratio, increasing from 0.0201 at 0° to 2.9467 at 10°, before slightly decreasing to 2.191 at 15°. This shows that Model 3 achieves the highest L/D ratio across all angles of attack, reflecting its superior lift-to-drag efficiency.

On the whole, Model 3 shows the most favourable lift-to-drag performance across all the angles of attack, suggesting a highly efficient design in terms of balancing lift and drag forces, and therefore the most efficient aerodynamic performance. Model 1 shows gradual improvement in L/D ratio with increasing angle of attack, while Model 2 starts with a negative L/D ratio at 0° but improves significantly at higher angles, achieving a positive and efficient lift-to-drag performance at 15°.

3.4 Qualitative Results

The static pressure contours from the CFD analysis across the angles of attack provide critical insights into the hydrodynamic performance of the three models. The distribution of static pressure along the models' surfaces shows how efficiently each design interacts with the surrounding fluid and its potential impact on overall performance.

Figures 8 and 9 show the comparison of static pressure contours around Models 1, 2 and 3 when each model moves through the fluid at lower angles of attack of 0° and 5° respectively at a speed of 2.05 m/s. The pressure is concentrated around the frontal surface for all underwater towing models at lower angle of attack, creating a high-pressure zone at an angle of attack of 0°.

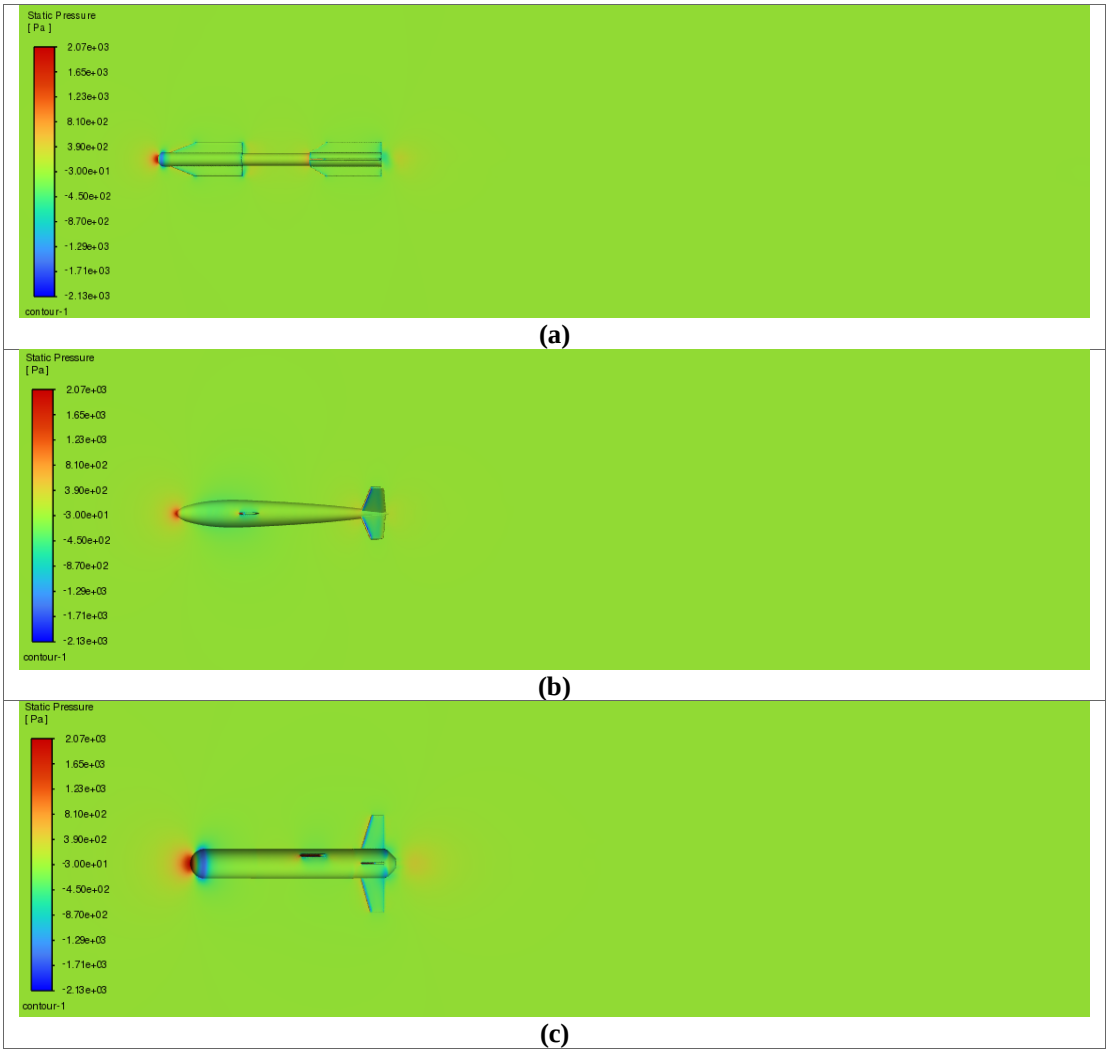

Figure 8: Static pressure distributions for (a) Model 1, (b) Model 2 and (c) Model 3 with angle of attack = 0°.

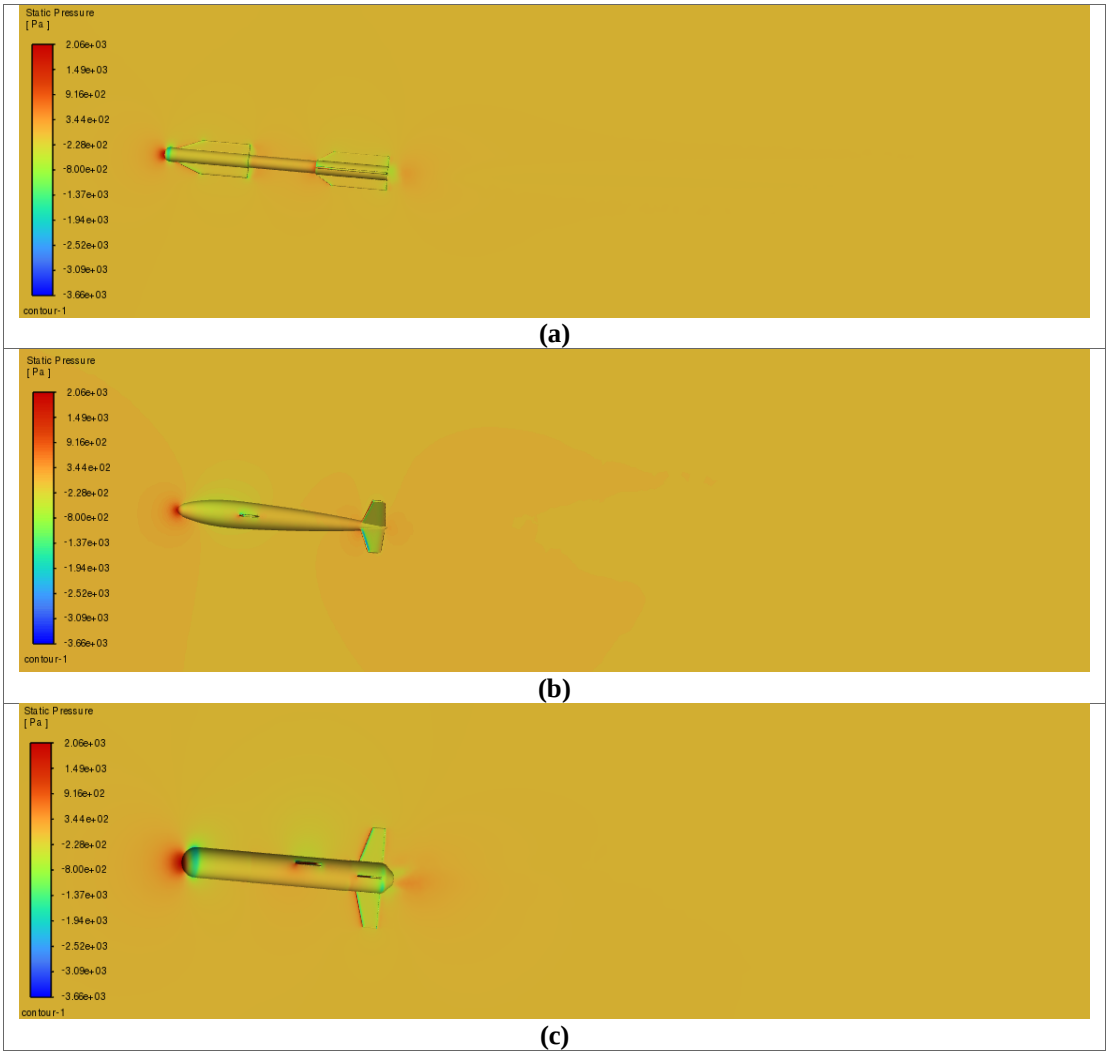

Figure 9: Static pressure distributions for (a) Model 1, (b) Model 2 and (c) Model 3 with angle of attack = 5°.

At an angle of attack of 5°, Model 1 displays a high-pressure concentration on the windward side at the leading edge, coupled with a low-pressure zone on the leeward side. Model 2 shows a more uniform pressure distribution than Model 1, with reduced high-pressure zones at the leading edge and a better-defined low-pressure region on the leeward side. Model 3 exhibits high-pressure zones at the leading edge and efficient pressure recovery at the rear section, with the presence of fins stabilising the flow to reduce pressure fluctuations at lower angles of attack. The gradient diminishes smoothly along the body, indicative of streamlined flow separation and the stabilising fins enhance pressure recovery, minimising turbulence.

Figures 10 and 11 show the comparison of static pressure contours around Models 1,2 and 3 when each model moves through the fluid at higher angles of attack of 10 and 15°, respectively, at a speed of 2.05 m/s. It is found that Model 1 shows a high-pressure region concentrated on the windward side at the leading edge, coupled with a low-pressure zone on the leeward side. However, the rear of the model shows poor flow recovery, which leads to turbulence and energy losses. Model 2 shows a more balanced pressure distribution with reduced high-pressure regions on the windward side and better-defined low-pressure zones on the leeward side. The pressure recovery at the rear is smoother, reducing turbulence. High pressure distribution is observed below the wing area as compared to the upper wing area, indicating generation of lift. Model 3 is found to have the most optimised pressure distribution at these

angles of attack. High-pressure zones on the windward side are minimised, and the low-pressure region on the leeward side is well-controlled. The stabilising fins ensure efficient flow recovery and reduce pressure fluctuations. Higher pressure distribution observed below the wing area compared to the upper wing area indicates generation of higher lift due to pressure difference as the angle of attack increases. Model 3 generates the highest stabilising lift due to its optimised geometry and fins, which enhance control and stability.

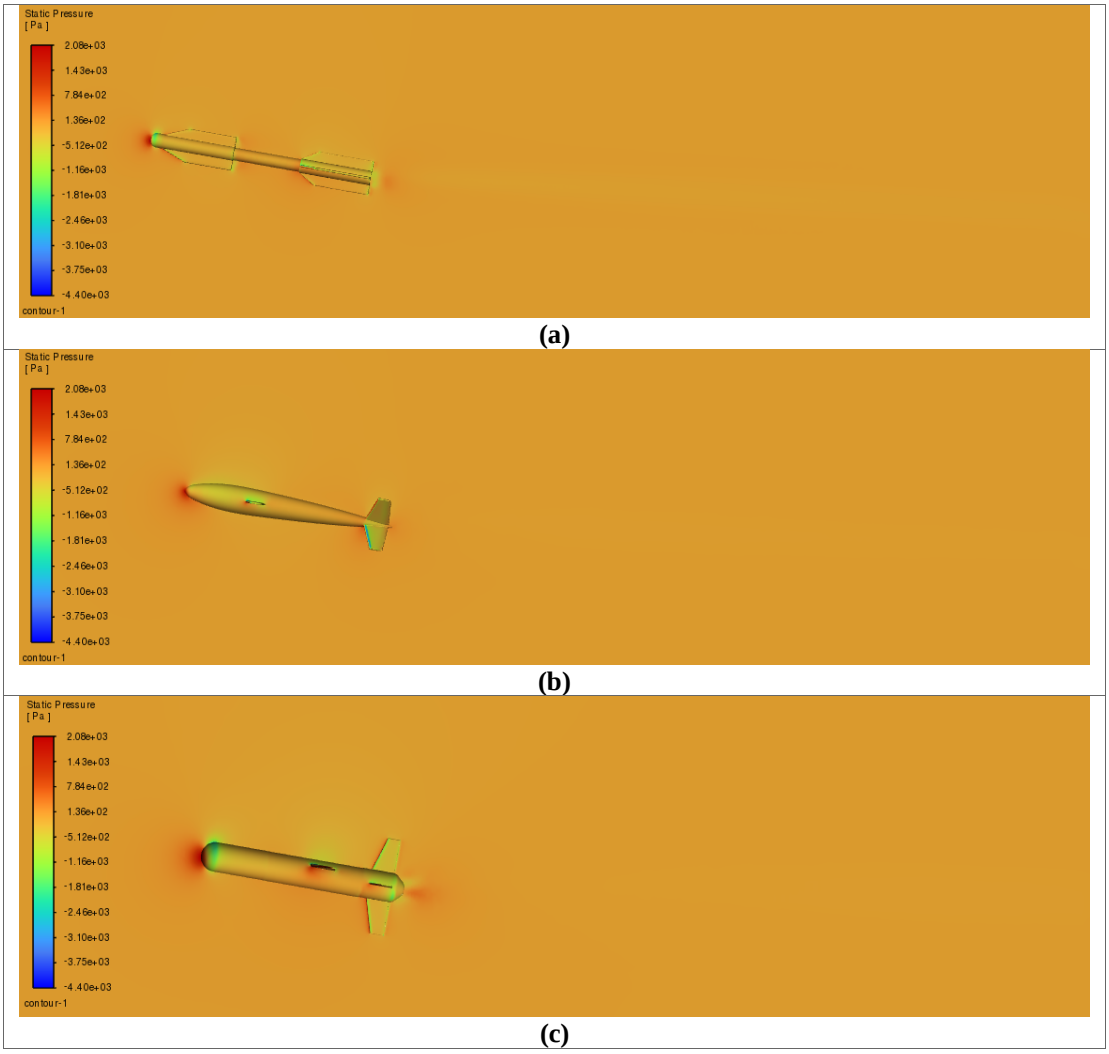

Figure 10: Static pressure distributions for (a) Model 1, (b) Model 2 and (c) Model 3 with angle of attack = 10°.

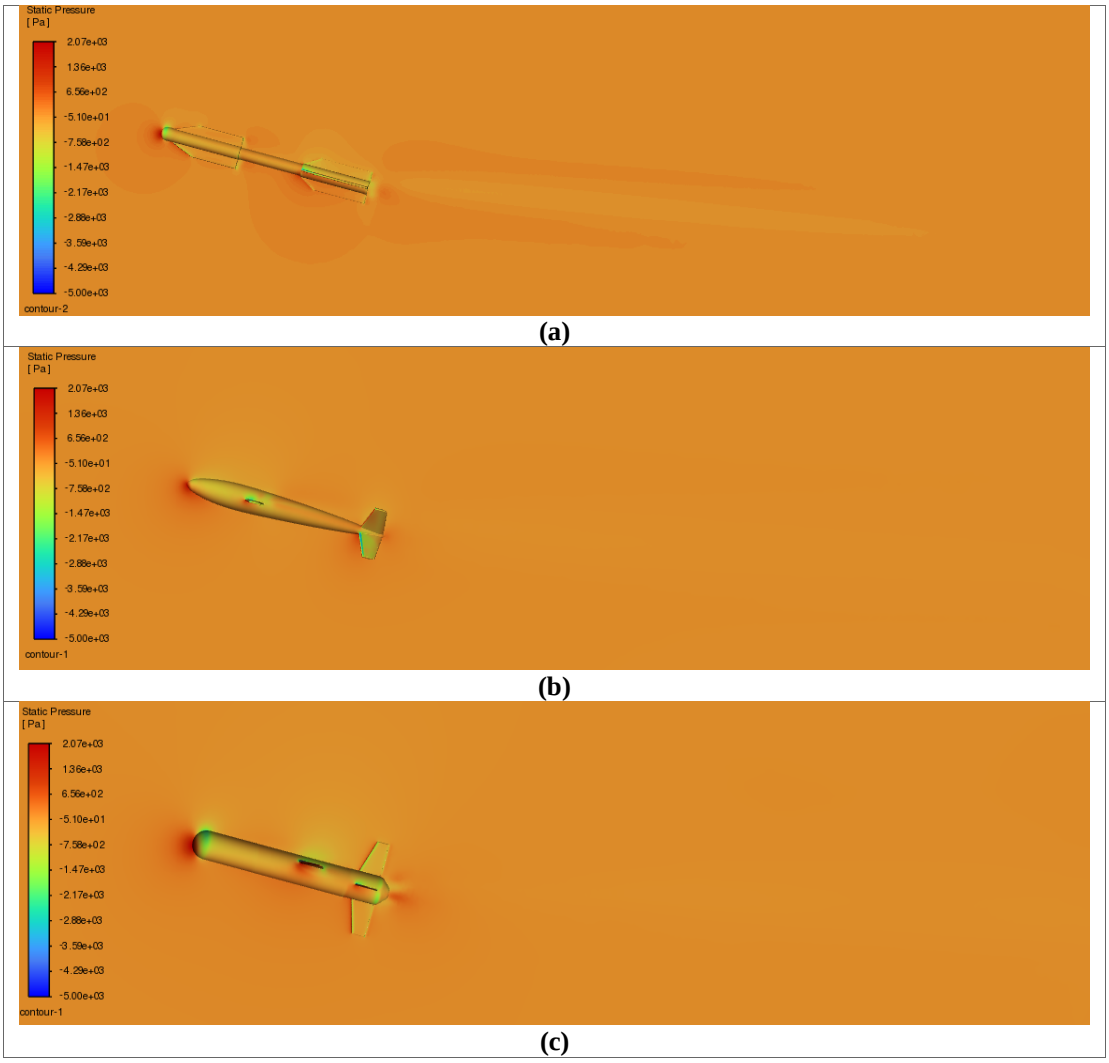

Figure 11: Static pressure distributions for (a) Model 1, (b) Model 2 and (c) Model 3 with angle of attack = 15°.

3.5 Comparative Performance Across All Angles of Attack

Table 3 summarises the performance of the three underwater towing vehicle designs based on drag performance, lift performance, lift-to-drag (L/D) ratio, stability and manoeuvrability at varying angles of attack. It is found that Model 3 outperforms the other models, showing the highest L/D ratio and efficient performance at higher angles (10 and 15°), making it ideal for operations where stability and manoeuvrability are crucial. Its superior stability at steeper angles makes it optimal for towing. Model 1 performs well at low angles (0 and 5°), with moderate lift and drag resistance, and a steady increase in L/D ratio, making it suitable for specific applications. However, its manoeuvrability at higher angles is limited. Model 2 shows improvements at higher angles but is inefficient at 0° and requires design optimisation. Its low L/D ratios suggest limited overall performance, though it could be used for specialised tasks. In conclusion, Model 3 recorded better performance for lift force and L/D ratio compared to other models across all angles of attack.

Table 3: Hydrodynamic performance comparison of underwater towing models.

Model	Drag Performance	Lift Performance	Lift-to-Drag (L/D) Ratio	Stability	Manoeuvrability
Model 1	Moderate drag force, low drag coefficient at low angles (0° and 5°)	Moderate lift force, steady increase in lift coefficient	Moderate L/D ratio (highest at 15°)	High stability at lower angles; stable	Moderate manoeuvrability; limited at higher angles due to increased drag.
Model 2	Poor drag performance at 0° (negative L/D ratio), but improved at higher angles	Low lift force at 0°, but increased lift at higher angles (10° - 15°)	Improved L/D ratio at higher angles, but lower overall efficiency	Moderate stability at higher angles; prone to instability at low angles	Moderate manoeuvrability at higher angles; less agile at lower angles due to drag inefficiencies
Model 3	High drag force but efficiently balances with high lift force at higher angles	High lift force at all angles, with substantial increase at higher angles	Excellent L/D ratio (highest at 10° and 15°)	High stability at higher angles	High manoeuvrability at moderate to high angles

4. CONCLUSION

This study investigated the hydrodynamic performance of three underwater towing vehicle designs at varying angles of attack (0, 5, 10 and 15°), with particular attention to drag force, lift force, lift-to-drag (L/D) ratio, stability and manoeuvrability. The findings revealed that Model 3 consistently outperformed the other configurations at higher angles of attack, demonstrating an optimal balance between lift and drag forces, as well as enhanced stability and manoeuvrability. These characteristics suggest its suitability for demanding underwater operations. Model 1 exhibited better performance at lower angles, indicating its potential for missions requiring low-resistance towing with minimal directional variation. In contrast, Model 2 showed limited hydrodynamic efficiency and requires further design refinement for broader applicability. These findings emphasise the importance of selecting the appropriate model based on angle of attack, stability and manoeuvrability in underwater towing operations. In future studies, the simulation results will be validated through actual experimental activities.

ACKNOWLEDGMENT

The authors would like to express their sincere appreciation to Dr. Ahmad Syahid A. Fawzal for his technical guidance and methodological support, particularly in the area of Computational Fluid Dynamics (CFD).

Gratitude is also extended to Ir. Dr. Mior Azman Meor Said and Mr. Mohd Syaifuddin Mohd from the Department of Mechanical Engineering, Center of Sustainable Resources for Intelligent and Efficient Mobility (CSRIEM), Universiti Teknologi PETRONAS (UTP), as well as to Dr. Ahmad Faisal Mohamad Ayob from the Faculty of Ocean Engineering Technology, Universiti Malaysia Terengganu (UMT), for their valuable consultancy and technical expertise, which significantly enhanced the accuracy and reliability of the computational setup and analysis.

The authors also wish to express their heartfelt appreciation to Mr. Hazuan Hasnie Hashim, Mr. Khairul Anuar Ahmad, Mr. Ahmad Subardi Mohd Wazir, Mr. Mohd Ridzuan Mohd Rashid, and Mdm. Nur Adina Azizi from STRIDE for their dedicated efforts in fabricating the Underwater Towing Vehicle prototype. Their commitment and technical expertise were instrumental in the success of the real-world testing and innovation competition participation.

REFERENCES

Dantas, J.L.D. & de Barros, E.A. (2013). Numerical analysis of control surface effects on AUV manoeuvrability. *Appl. Ocean Res.*, **42**: 168–181.

Divsalar, K., Shafaghat, R., Farhadi, M. & Alamian, R. (2020). Numerical simulation of hydrodynamic properties of Alex type gliders. *Int. J. Eng.*, **33**: 324–333.

Ferziger, J.H., & Perić, M. (2002). *Computational methods for fluid dynamics* (3rd ed.). Springer.

Graver, J.G. (2005). *Underwater gliders: Dynamics, control and design* (Doctoral dissertation, Princeton University). Princeton University.

Hong, L., Zhang, D., Xu, H., Wang, X. & Zhao, M. (2023). Numerical investigation on hydrodynamic characteristics and drag influence of an open-frame remotely operated underwater vehicle. *J. Mar. Sci. Eng.*, **11**: 2143.

Jagadeesh, P., Muralib, K. & Idichandy, V.G. (2009). Experimental investigation of hydrodynamic force coefficients over AUV hull form. *Ocean Eng.*, **36**: 113–118.

Knupp, P.M. (2001). Algebraic mesh quality metrics. *SIAM J. Sci. Comput.*, **23**: 193-218.

Li, X., Zhang, D., Zhao, M., Wang, X. & Shen, Y., 2024. Hydrodynamic analysis and drag-reduction design of an unmanned underwater vehicle based on computational fluid dynamics. *J. Mar. Sci. Eng.*, **12**: 1388.

Liu, Y., Yang, Y., Zhang, H. & Zhang, L. (2020). Computational fluid dynamics prediction of the dynamic behavior of autonomous underwater vehicles. *IEEE J. Oceanic Eng.*, **45**: 724–734.

Liu, X., Liu, C., Chen, C. & Kui, H., (2023). Longitudinal stability analysis of underwater towed body based on CFD. *J. Phys.: Conf. Ser.*, **2441**: 012041.

Myring, D. F. (1976). A theoretical study of body drag in subcritical axisymmetric flow. *Aeronaut. Q.*, **27**: 186–194.

Nordin, K. H., Ovinis, M. & Javaid, M.Y. (2017). Study on the effect of wing geometry on underwater glider hydrodynamics. *ARPN J. Eng. Appl. Sci.*, **12**: 3101–3104.

Panda, J.P., Mitra, A. & Warrior, H.V. (2020). A review on the hydrodynamic characteristics of autonomous underwater vehicles. *Proc. Inst. Mech. Eng., Part M: J. Eng. Marit. Environ.*, **235**: 15–29.

Park, J., Rhee, S.H., Im, J.B., Ji, B.H. & Lee, S.J. (2023) . Experimental study on the towing stability of a towed underwater object. *Int. J. Naval Architect. Ocean Eng.*, **15:** 100539.

Phillips, A. B., Turnock, S.R. & Furlong, M. (2010). The use of computational fluid dynamics to aid cost-effective hydrodynamic design of autonomous underwater vehicles. *Proc. Inst. Mech. Eng. Part M J. Eng. Marit. Environ.*, **224**: 239–254.

Sakaki, A. & Sadeghian Kerdabadi, M. (2020). Experimental and numerical determination of the hydrodynamic coefficients of an autonomous underwater vehicle. *Sci. J. Marit. Univ. Szczecin.*, **6**: 124–135.

Shirazi, A.T., Nazari, M.R. & Manshadi, M. D. (2019). Numerical and experimental investigation of the fluid flow on a full-scale pump jet thruster. *Ocean Eng.*, **182**: 527–539.

Singh, R., Sarkar, P., Goswami, V. & Yadav, R. (2022). Review of low-cost micro remotely operated underwater vehicle. *Ocean Eng.*, **266**: 108795.

Stryczniewicz, K. & Drężek, P. (2019). CFD approach to modelling hydrodynamic characteristics of underwater glider. *Trans. Aerosp. Res.*, **4**: 32–45.

Tian, X., Zhang, L.H., Zhang, H., Wang, Y., Liu, Y., Yang, Y. & Song, L. (2021). The optimal lift–drag ratio of underwater glider for improving sailing efficiency. *IEEE J. Oceanic Eng.*, **46**: 808–816.

Vijayakumar, R. & Rayaprolu, V. S. (2022). Towing tank experiments on underwater gliders for varying angles of attack. *OCEANS 2022*, 21-24 February 2022, Chennai, India

Yang, X., Wu, J., Li, Q. & Lv, H. (2021). Numerical simulation of depth tracking control of an underwater towed system coupled with wave–ship interference. *J. Mar. Sci. Eng.*, **9**: 874.

Yildiz, A. (2023). Investigation of mesh independence in numerical modeling of sharp-crested weirs at different heights. 26th Int. Symp. Environ. Ind. (SIMI 2023), Bucharest, Romania.

Zhou, G., Xiang, X., Liu, C. & Yang, S. (2020). Design and simulation of open frame underwater towing vehicle. *2020 Int. Conf. Syst. Sci. Eng. (ICSSE)*, 31 August - 3 September 2020, Kagawa, Japan.

Zhou, J., Si, Y. & Chen, Y. (2023). A review of subsea AUV technology. *J. Mar. Sci. Eng.*, **11**: 1119.

METALLURGICAL FAILURE ANALYSIS OF A TOWING DAMPER FOR A LIGHTWEIGHT BOAT TRAILER

Muhammad Azrain Mohammad[1], Nor Azlan Sarjo[1], Mohd Azim Md. Burhanuddin[1], Ezza Nur Adzlilliya Azali[1], Mohd Moesli Muhammad[2], Mohammad Syafiq Mohammad Rafi[3], Fadzli Ibrahim[1] & Wan Fadilah Wan Abdullah[1]

[1]Automotive & Mechanical Technology Division
[2]Maritime Technology Division
[3]Robotics & Artificial Intelligence Technology Division

Science & Technology Research Institute for Defence (STRIDE), Malaysia

[*]Corresponding author: azrain.mohammad@stride.gov.my

ABSTRACT

This study presents a comprehensive metallurgical failure analysis of a fractured towing damper for a lightweight single deck boat 1.5 tonne trailer. The component reportedly fractured during operational deployment, prompting a detailed forensic investigation to determine the underlying causes of failure. The failure was characterised through an integrated methodology comprising of macroscopic and microscopic examinations, metallographic assessments, hardness measurement, and chemical composition analysis. The findings revealed that the failure mechanism was predominantly due to tensile overload, as evidenced by dimple rupture features on the fracture surface. Additionally, comparative analysis indicated that the failed component exhibited lower manganese (Mn) content and lower hardness values than its predecessor, adversely impacting its mechanical strength. The study provides critical insights into failure prevention strategies and outlines recommendations to enhance the durability and reliability of towing dampers, thereby enhancing their performance in demanding operational environments.

Keywords: *Failure analysis; towing damper; fracture mechanics; metallurgical evaluation; structural reliability.*

1. INTRODUCTION

Towing dampers are critical components engineered to attenuate dynamic loads and dissipate vibrational energy encountered during towing operations in land or / and maritime applications (Gharib & Karkoub, 2018; Ferhath, & Kasi, 2024). These devices function by absorbing mechanical shocks generated by road-induced oscillations or hydrodynamic forces in marine environments, mitigating excessive sway, instability and abrupt changes in speed or direction (Li *et al*., 2012, Li & Zuo, 2017; Liang *et al*., 2023). The functionality of towing dampers, particularly their role in reducing vibrations and shocks, is crucial for maintaining stability during towing operations (Lee *et al*., 2022). By effectively managing transient loads, towing dampers enhance towing stability and minimise structural stresses on towing assemblies, thereby prolonging component lifespan and optimising vehicle control (Sorge, 2016; Foti *et al*., 2020; Wang *et al*., 2023). The strategic implementation of such dampers significantly stabilises towing systems, promoting longevity and operational efficiency. This aligns with recent studies that discuss advancements in damping technologies, specifically focusing on the optimisation of towing systems (Isahak *et al*., 2020).

In defence-related applications, the structural reliability of towing dampers is paramount, as even minor failures can compromise mission readiness and safety. Structural defects in towing assemblies have been linked to equipment damage, operational delays and increased failure rates, particularly when

transporting heavy payloads over rugged terrains or at high speeds (Banerjee *et al*., 2019; Gurmai & Kiss, 2019; Wang *et al*., 2019). Previous studies have underscored the consequences of inadequate damping, indicating that failures in towing assemblies can lead to high maintenance costs and affect mission-critical operations, although specific studies evaluating towing systems may vary in focus across the literature (Zhang *et al*., 2022).

The implications extend beyond safety concerns, whereby such failures impose significant logistical and financial burdens, contributing to elevated maintenance costs and prolonged equipment downtime (Ziezulewicz, 2023). It has been reported that maintenance-related expenses account for a substantial portion of total operating costs in various operational contexts (Ghorbanhosseini, 2020; Pahl, 2022). Given that mechanical failures can significantly impact vessel availability and operational efficiency, ensuring the reliability of critical components, including those used in towing systems, is essential for sustaining components operability and mission effectiveness. Failure modes in towing dampers are frequently attributed to material fatigue, suboptimal alloy composition and exposure to extreme loading conditions (Zhang *et al*., 2020; Wang *et al*., 2022; Azrain *et al*., 2024).

Thus, systematic failure analysis is crucial for optimising towing damper design, improving material properties and enhancing structural resilience. Exploring the mechanisms leading to damper failures can guide the engineering of materials with improved resistance to factors that contribute to failure. Innovations in material sciences and structural engineering are being presented in ongoing studies, focusing on enhancing the performance and longevity of towing dampers through advanced design and material selection (Shareef, 2023; Yang *et al*., 2023; Shen, 2024; Qiu *et al*., 2024).

This study presents a comprehensive metallurgical failure analysis of a fractured towing damper from a lightweight single deck boat 1.5 tonne trailer. The component, sourced locally, was manufactured from high-strength alloy steel. It reportedly fractured during operational deployment, prompting a detailed forensic investigation to determine the underlying causes of failure. The primary objectives of this study are to identify the failure mechanism of the towing damper and assess the material properties that contributed to its failure. The scope of the work includes a series of macroscopic and microscopic examinations, metallographic assessments, hardness measurement, and chemical composition analysis, aimed at understanding the material's integrity and failure mode.

2. METHODOLOGY

2.1 Sample Collection and Preparation

Upon retrieval, the fractured component underwent initial documentation through high-resolution imaging to capture the fracture characteristics (Figure 1). The sample was stored under controlled ambient conditions to prevent further degradation prior to testing. In order to facilitate the analysis, the sample was sectioned by using a high precision cooling cutter to preserve the microstructural integrity and fracture surface morphology. The identified area of interest was then cleaned with an industrial solvent to eliminate contaminants that could interfere with subsequent microscopic and spectroscopic analyses.

2.2 Material Inspection

2.2.1 Visual and Macroscopic Examination

A comprehensive visual and macroscopic examination of the fractured towing damper was conducted to characterise and evaluate the fracture mode, surface irregularities and deformation mechanisms. As depicted in Figure 2, the piston rod of the towing damper exhibited a complete fracture. Notably, a segment of the piston rod remained lodged within the lug / hook eye (a ring-shaped component) as highlighted by the red arrow. This observation suggests that the fracture mechanism did not result in an instantaneous separation but rather a progressive failure mechanism.

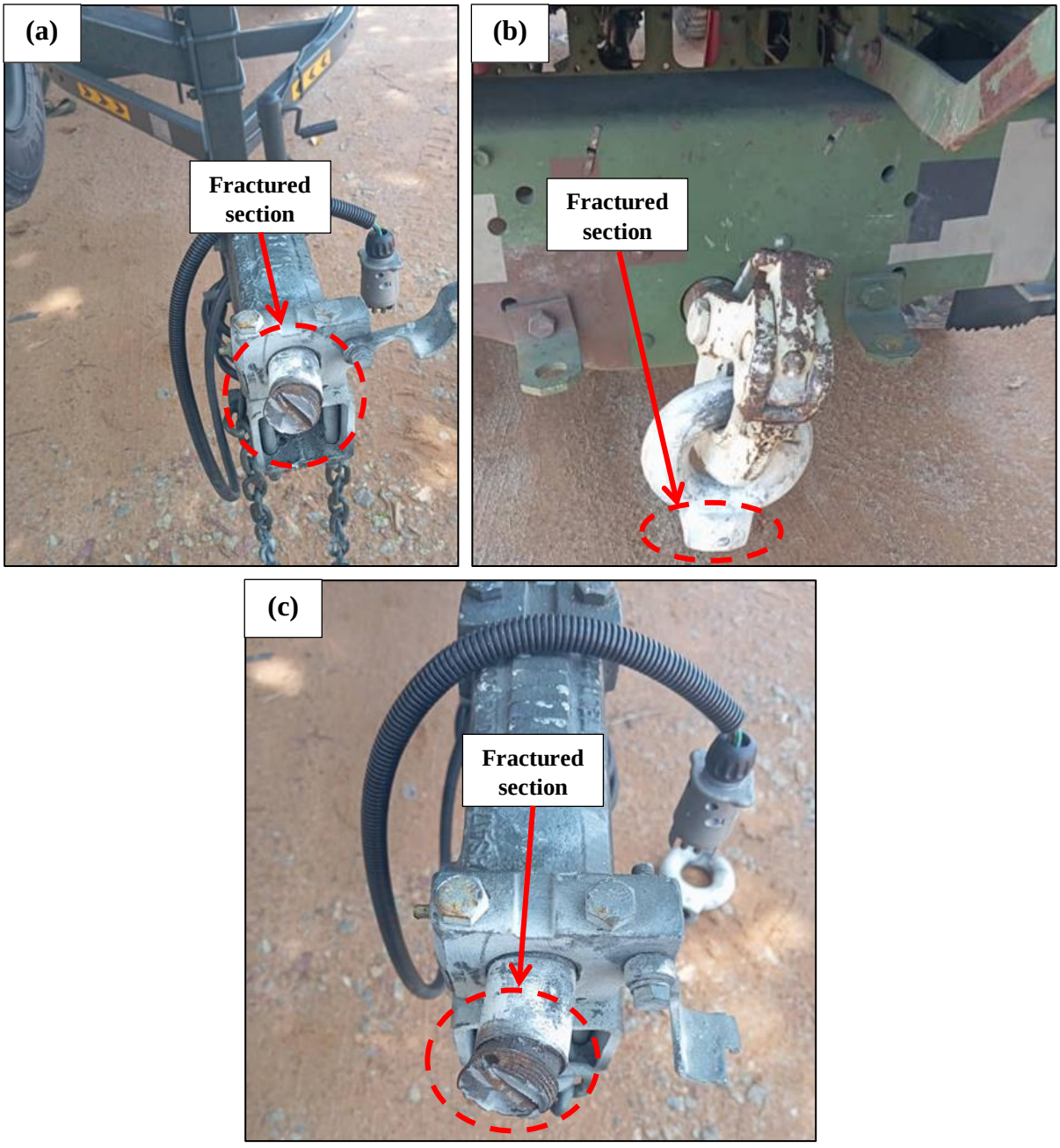

Figure 1: Towing damper for a single-deck assault boat 1.5-tonne trailer. (a) and (b) Overall view of the fractured towing damper. (c) Zoomed image of the fracture section.

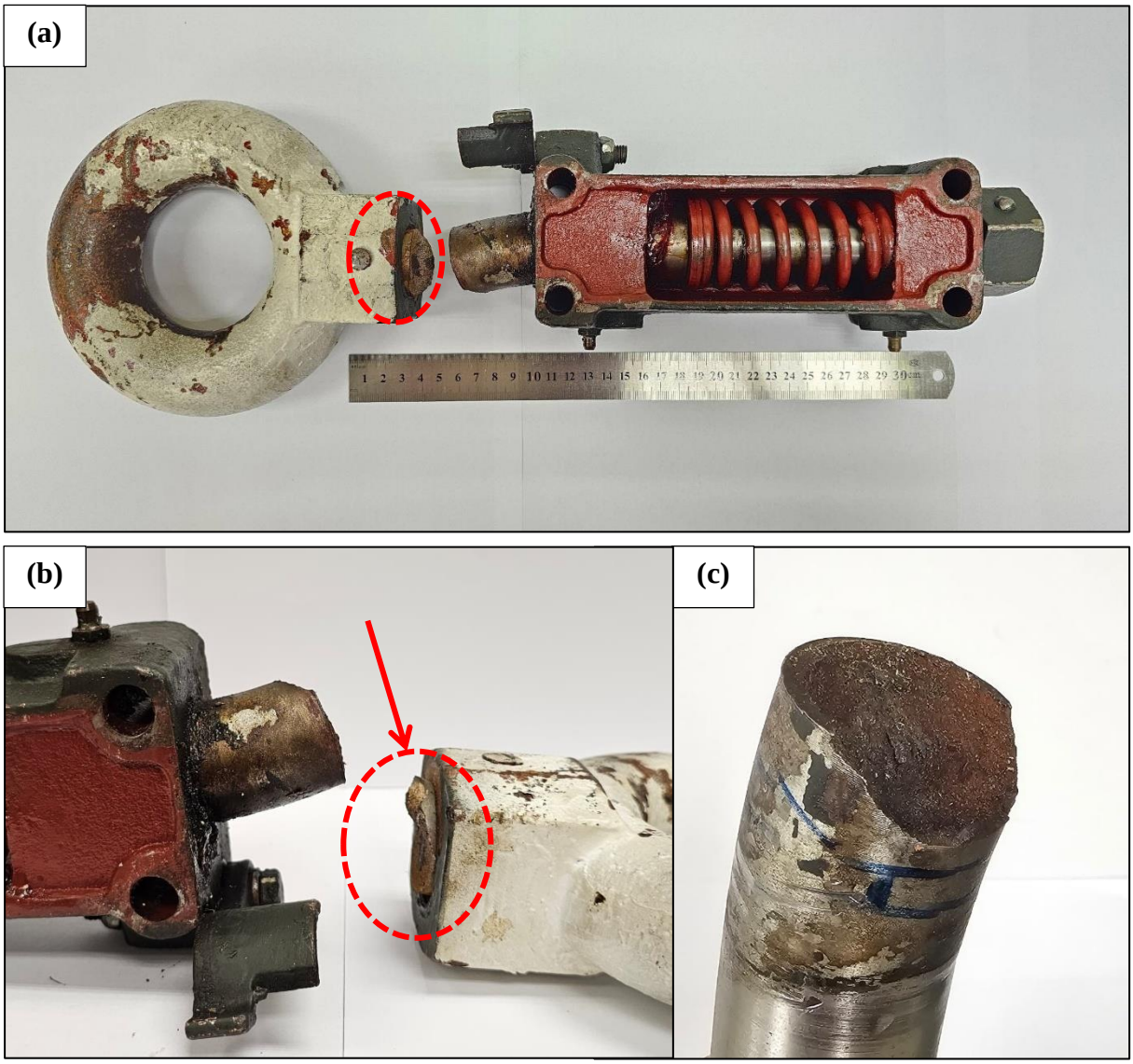

Figure 2: Fractured piston rod of the towing damper. (a) Overall view of the as-received sample. (b) Close-up image showing the piston rod fracture with a segment lodged within the lug / hook eye (indicated by the red arrow). (c) Detailed view of the fracture surface, highlighting deformation features and irregularities.

The fracture surface was meticulously analysed for indicative features of plastic deformation, including necking and shear lip formation, which are hallmarks of ductile overload failure. Additionally, the surface was scrutinised for irregularities such as fatigue striation marks, secondary cracking, discolouration and material discontinuities, as these features may suggest underlying material defects or environmental influences that contributed to failure initiation. In order to facilitate a more in-depth analysis, high-resolution optical imaging was utilised to document critical failure regions, providing essential visual evidence to support further fractographic and microstructural evaluations.

2.2.2 Microscopic Examination

An Apreo FEI field emission scanning electron microscope (FESEM) was employed to examine the fracture surface morphology at various ranges of magnifications. The primary objective of this microscopic examination was to identify fractographic features indicative of the failure mechanism, particularly dimple formations, cleavage facets and intergranular characteristics. Special attention was given to detecting microstructural anomalies such as voids, inclusions and secondary cracks which

could provide critical insights into the underlying factors that contributed to failure initiation and propagation. The selected regions of interest were further analysed to establish a correlation between fractographic observations and the material's failure response.

2.2.3 Metallographic Examination

A cross-sectional sample of the towing bar damper was prepared for metallographic examination to evaluate the microstructural characteristics of the fractured towing damper. The preparation process involved progressive polishing using finer abrasives, followed by chemical etching with a suitable reagent to reveal the material's grain structure and internal features. Subsequent examination under optical microscopy enabled a detailed assessment of the grain morphology, material homogeneity and possible evidence of degradation, including inclusions, phase transformations or corrosion-induced microstructural changes. This evaluation was crucial in determining whether intrinsic material defects or service-induced degradation played a role in the failure mechanism.

2.2.4 Hardness Test

The mechanical integrity of the fractured towing damper was assessed through Vickers hardness (HV) testing using a Tinius Olsen hardness tester. Hardness measurements were recorded at multiple locations across the plastically deformed fracture region and the outer surfaces to identify variations in material strength. The obtained values were compared against a reference towing damper sample, and the correlation between hardness and tensile strength was used to estimate mechanical property deviations, in line with standard practices in hardness-based strength approximations. This approach provides a practical and cost-effective method for inferring tensile strength from indentation hardness values, although such correlations are inherently approximate and should be interpreted with caution (Pavlina & Van Tyne, 2008; Genculu, 2024). The results were subsequently averaged and analysed to evaluate material property variations that could have contributed to the observed failure behaviour.

2.2.5 Chemical Composition Analysis

A Shimadzu EDX 720 energy dispersive X-ray fluorescence (EDXRF) spectrometer was used to determine the elemental composition of the failed towing damper. The analysis focused on identifying key alloying elements that influence mechanical properties, wear resistance and corrosion behaviour. Specifically, the investigation examined manganese (Mn), which affects hardenability; chromium (Cr), nickel (Ni) and molybdenum (Mo), which contribute to strength and corrosion resistance; and copper (Cu) and silicon (Si), which impact toughness and machinability. The composition of the failed towing damper was systematically compared with a previously tested model, allowing for the identification of any significant deviations that could have contributed to the observed mechanical deficiencies and failure mode.

3. RESULTS AND DISCUSSION

3.1 Visual and Macroscopic Examination

The initial visual examination of the fracture surface of the towing damper revealed distinct characteristics typical of ductile failure modes. As detailed in Figure 3(a), the cup-and-cone morphology observed on the fracture surface strongly indicates a significant deformational response prior to fracture, which is characteristic of ductile materials undergoing tensile stress (Craig, 2005). The identification of a shear lip around the fracture edges, as shown in Figures 3(b) and 3(c), further substantiates the ductile nature of the failure, indicating that substantial plastic deformation occurred before the final rupture, confirming findings consistent across various studies (DeVries *et al*., 2010; Ruckert *et al*., 2011). The presence of necking, as illustrated in Figure 3(d), indicates that the material surpassed its yield strength

under elevated tensile loading, corroborating observations made by Murakami and Ritchie (2012) regarding the mechanisms of material failure in similar studies.

A thorough assessment was conducted to investigate any potential signs of cyclic loading or brittle fracture, typically associated with fatigue failures. The absence of fatigue striations on the fracture surface, a hallmark of cyclic loading, as well as the lack of fast fracture features, strongly confirm that these failure mechanisms were not involved in the damper's failure process (Ruckert *et al*., 2006; Kondo *et al*., 2008). Murakami & Ritchie (2012) reiterated that ductile failures often show distinct morphologies that differ from those seen in fatigue-induced fractures, further validating the absence of fatigue characteristics in this case. Therefore, the findings suggest that the load applied to the towing damper exceeded its material capacity, ultimately leading to an overload ductile failure, consistent with the descriptions found in comprehensive analyses of material fractures in engineering contexts (DeVries *et al*., 2010).

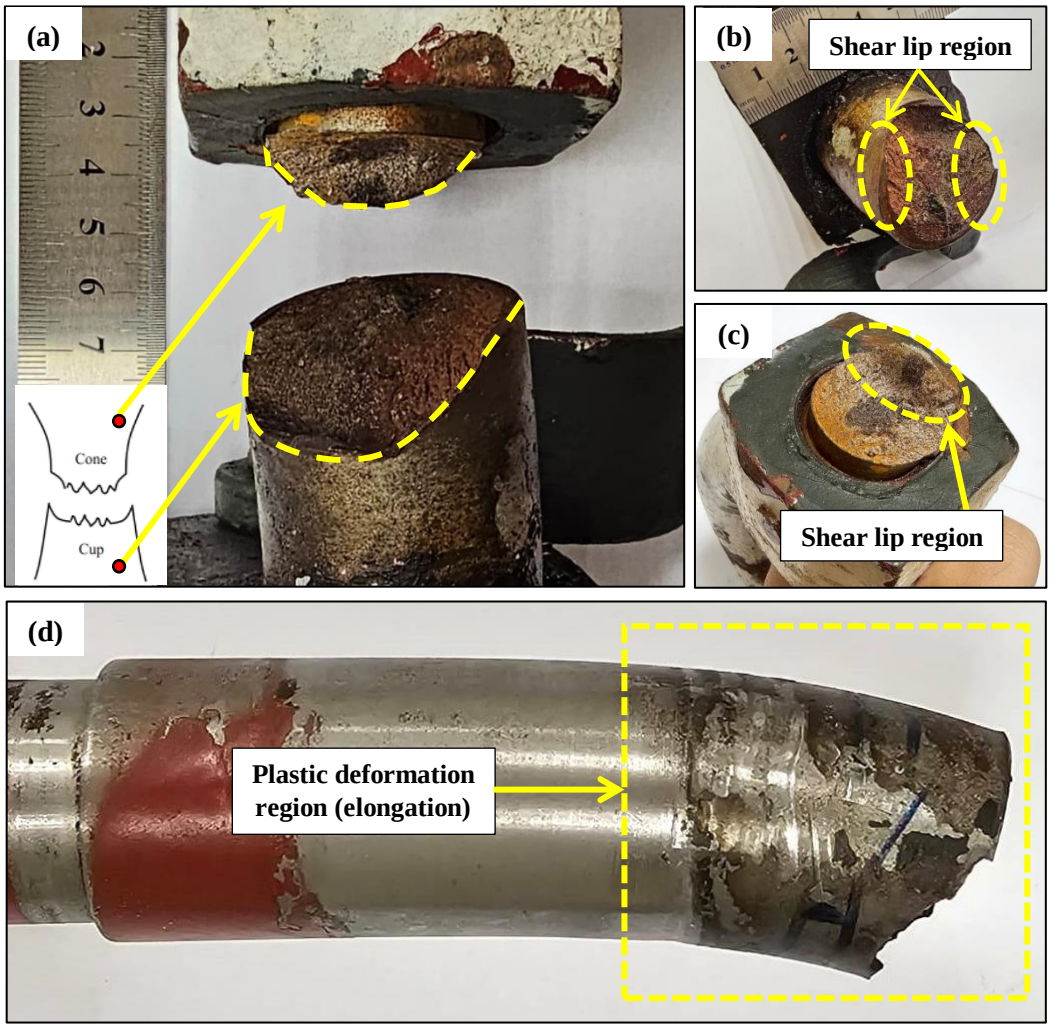

Figure 3: Fractured piston rod of the towing damper. (a) A cup-and-cone morphology. (b) and (c) Shear lip formation indicative of tensile overload (indicated by the yellow arrows). (d) Plastic deformation region.

3.2 Microscopic Examination

In order to elucidate the fracture mechanism further, fractography was conducted using FESEM. The analysis at varying magnifications, as presented in Figure 4 reveal a rough and fibrous surface, consistent with ductile fracture characteristics, reinforcing the conclusions drawn from the macroscopic

examinations. The presence of extensive plastic deformation markings supports the hypothesis of overload failure.

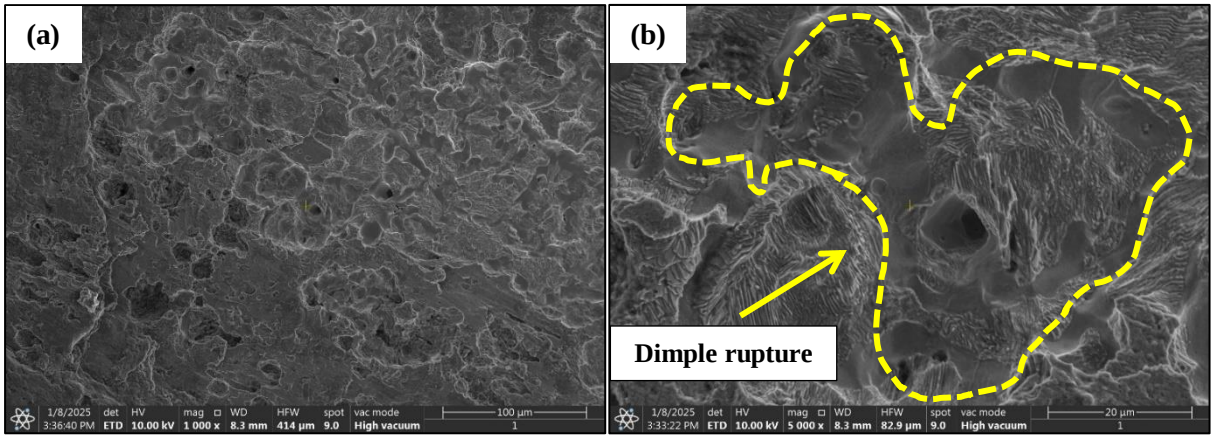

Figure 4: Dimple rupture at the fracture surface. (a) 1,000× magnification and (b) 5,000× magnification.

At lower magnification (1,000×), as shown in Figure 4(a), the fracture surface displays a heterogeneous, rough topology with large and uneven depressions resulting from dimple rupture. This observation is characteristic of microvoid coalescence, a key feature of ductile fracture. The formation of these dimples within the sample begins with localised stress concentration at inclusions, second-phase particles or microstructural discontinuities. Under continued tensile loading, these voids grow, elongate and coalesce, ultimately resulting in the rupture of the material (Dhaher, 2017; Jaber *et al.*, 2019).

At higher magnification (5,000×), as depicted in Figure 4(b), the fracture surface reveals deep, well-defined dimples, confirming that plastic deformation played a dominant role in the final failure. These dimples appear equiaxed, indicating that the tensile stress was applied in a uniform direction, resulting in a common cup-and-cone type fracture. The presence of coarse and deep dimples suggests that the material sustained a significant plastic strain before rupture, a defining feature of ductile overload failure. The fracture surface of the towing damper showed no periodic fatigue striations, crack arrest marks, or ratchet lines, confirming that the failure did not occur through progressive crack propagation typical of fatigue failures. Additionally, the absence of intergranular features, such as brittle cleavage facets and grain boundary separations rules out grain boundary embrittlement and stress corrosion cracking (SCC) as potential failure mechanisms for the towing damper. A similar failure mechanism was reported by Sujata *et al*. (2013) in their study on the fatigue failure of an aeroengine compressor disc. Their investigation revealed that while fatigue striations were observed in the early propagation phase, the final failure region exhibited dimple rupture due to overload failure. This similarity reinforces the notion that the towing damper fracture resulted from excessive tensile stress leading to ductile overload, rather than from progressive fatigue crack growth (Dhaher, 2017).

3.3 Metallographic Examination

Subsequently, metallographic analysis was conducted to evaluate the internal structure of the towing damper. The polished and etched cross-section samples, as displayed in Figure 5, exhibited a uniform microstructure without visible defects such as inclusions, voids and intergranular cracking. Keehan *et al*. (2006) emphasised that a well-executed metallographic analysis can assess the quality of the internal structure, indicating that failure may not be attributable to poor manufacturing quality when no significant defects are found. Henceforth, the absence of defects further supports the assertion regarding the integrity of the material.

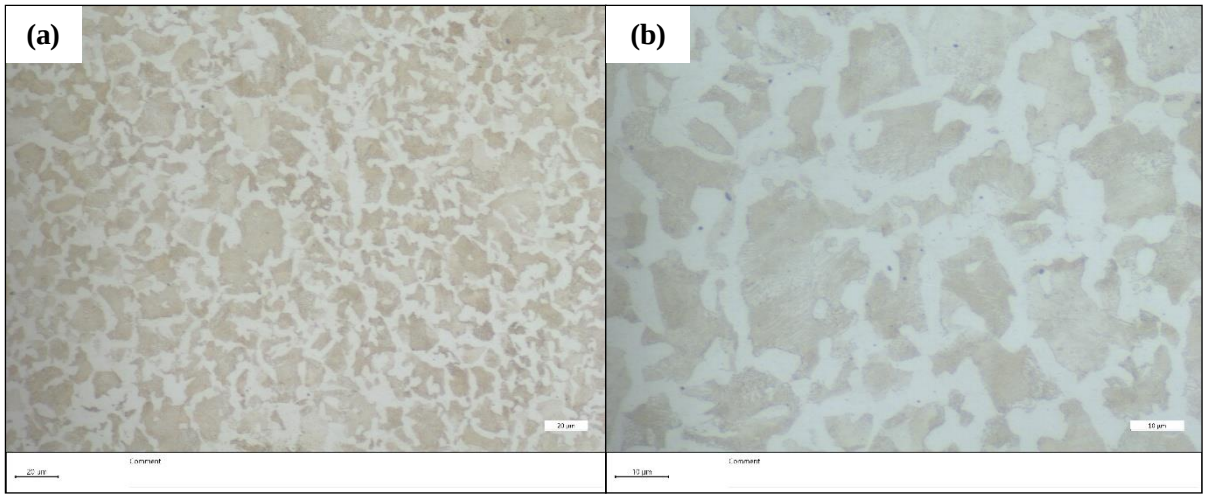

Figure 5: Microstructure image of the towing damper. (a) 200× magnification and (b) 500× magnification.

Moreover, the lack of carbide precipitation or segregation suggests there were no thermal processing issues that could have weakened the component. Sun *et al*. (2024) reported that variations in the thermal treatment of high-manganese alloys can lead to significant changes in microstructure, emphasising that carbide formation detrimentally affects mechanical properties. Thus, the current observations align with established knowledge on the microstructural integrity of high-performance steels.

3.4 Hardness Test

On the other hand, hardness testing was performed to assess the mechanical properties of the failed component. The results revealed that the hardness of the fractured towing damper was significantly lower than that of the reference sample (188.58 HV vs. 206.60 HV), indicating inferior mechanical properties. This finding parallel with the results established by Keehan *et al*. (2006) in their study on the effect of carbon additions towards the microstructure and mechanical properties of steel weld metals. They demonstrated a strong correlation between hardness and tensile strength in steel weld metals, reinforcing the observed relationship between hardness values and tensile performance of the two towing damper models. Furthermore, lower hardness values imply reduced work-hardening capacity in the material as discussed by Ran *et al*. (2023), which diminishes its ability to withstand tensile stress before critical deformation occurs.

3.5 Chemical Composition Analysis

Concurrently, elemental composition analysis showed that the manganese (Mn) content in the failed towing damper was substantially lower than that of the reference sample. Studies indicate that manganese significantly enhances the hardening characteristics and resistance to deformation in steel (Hájek *et al*., 2022). Reduced manganese content likely contributed to the lower tensile strength observed in the failed sample. Additionally, the absence of chromium (Cr) and molybdenum (Mo) in the failed towing damper as compared to the reference sample is critical, as these elements enhance wear resistance and toughness. Their absence fundamentally impacts mechanical performance (Liu *et al*., 2021; Yan *et al*., 2023).

The comparative elemental analysis shown in Table 1 highlights significant compositional discrepancies between the failed and reference towing dampers. Most notably, the Mn content in the failed sample was markedly lower (0.64%) as compared to the reference (1.51%). Given Mn's role in enhancing hardenability and tensile strength, this reduction likely impaired the alloy's capacity to resist deformation under load. Additionally, the failed damper lacked critical alloying elements, such as Cr, Mo, and Ni, all of which were present in the reference sample. Cr and Mo are known to improve wear resistance and toughness, while Ni contributes to overall strength and ductility.

Table 1: Chemical composition result of the towing damper.

No.	Elements	Failed towing damper (%)	Reference towing damper (%)
1.	Nickel (Ni)	Not detected	0.14
2.	Copper (Cu)	0.02	0.33
3.	Manganese (Mn)	0.64	1.51
4.	Silicon (Si)	0.31	0.28
5.	Chromium (Cr)	Not detected	0.25
6.	Molybdenum (Mo)	Not detected	0.26
7.	Iron (Fe)	Balance	Balance

The absence of these elements suggests a significant downgrade in the alloy grade used for the failed part, potentially due to material substitution or inadequate quality control during manufacturing. Even minor shifts in these alloying elements can significantly affect the steel's mechanical response, especially under high tensile stress, which is consistent with the overload fracture mechanism identified earlier. These results emphasise the importance of strict material specifications in the production of critical structural components such as towing dampers.

Overall, the metallographic analysis, hardness testing and elemental composition analysis collectively reinforced the understanding that the premature failure of the towing damper resulted from inadequate mechanical properties linked to its material composition and processing history.

4. CONCLUSION

In summary, this study has systematically analysed the failure mechanism of the towing damper for a lightweight single deck boat 1.5 tonne trailer. The findings indicated that the primary cause of failure was ductile overload, as evidenced by fractographic analysis that revealed microvoid coalescence and deep dimple rupture, eliminating the possibility of fatigue or environmentally assisted cracking as the contributing factors. Hardness testing further demonstrated that the failed damper exhibited lower mechanical strength as compared to the reference sample, which when correlated with tensile strength using established hardness-to-strength conversion principles, suggests underlying deficiencies in material processing, heat treatment or microstructural uniformity. This is further supported by elemental analysis which revealed a noticeably lower Mn content in the failed specimen, which is an alloying element known to influence hardenability and mechanical performance in steels.

The discrepancies in hardness and mechanical performance suggest that variations in manufacturing conditions played a significant role in the premature failure. Potential contributing factors include inadequate heat treatment, material inhomogeneity and manufacturing defects, such as porosity and inclusions, all of which could have reduced the component's ability to withstand operational stresses.

The study highlights the importance of stringent material selection, quality control and processing optimisation in ensuring the reliability of towing dampers under service conditions. Future works should focus on detailed microstructural evaluation, residual stress analysis and real-world load simulations to further refine failure prevention strategies.

ACKNOWLEDGEMENT

The authors would like to thank the officers and staff from the various laboratories at the Science & Technology Research Institute for Defence (STRIDE), Ministry of Defence, Malaysia for their technical support during the investigation.

REFERENCES

Azrain, M.M., Mohd Moesli, M., Mohd Subhi, D.Y., Abdul Rauf, A.M., Azmahani, A., Nik Hassanuddin, N.Y., Muhammad Izzamir, F.I, Mohammad Syafiq, M.R. & Mahdi, C.I. (2024). Failure analysis on lugless joining shackles of a naval ship. *Defence S&T Tech. Bul.*, **17**: 126–133.

Banerjee, S., Deokar, A.K., Srirama, R.K. & Joshua, S.D. (2019). Dynamic analysis of towing operation with military tracked recovery vehicle. *Vibroeng. Procedia*, **29**: 94–99.

Craig, B.D. (2005). Material failure modes, Part I: A brief tutorial on fracture, ductile failure, elastic deformation, creep and fatigue. *J. Fail. Anal. Prev.*, **5**: 13–14.

DeVries, P.H., Ruth, K.T. & Dennies, D.P. (2010). Counting on fatigue: Striations and their measure. *J. Fail. Anal. Prev.*, **10**: 120–137.

Dhaher, N.H. (2017). *Materials Science and Engineering*. CreateSpace Independent Publishing Platform, California.

Ferhath, A.A. & Kasi, K. (2024). The evolution of damper technology for enhanced ride comfort and vehicle handling in vehicle suspension system. *Int. J. Dynam. Control*, **12**: 3908–3946.

Foti, F., Denoël, V., Martinelli, L. & Perotti, F. (2020). A stochastic and continuous model of aeolian vibrations of conductors equipped with stockbridge dampers. *In* Papadrakakis, M., Fragiadakis, M. & Plevris, V. (Eds.). *Proceedings of the EURODYN 2020 Conference*. EURODYN 2020, Greece, pp. 1234–1240.

Genculu, S. (2024). Correlation of hardness values to tensile strength. *CAB Worldwide*, Buford, Georgia, US.

Gharib, M. & Karkoub, M. (2018). Design and experimental analysis of new industrial vibration dampers. *J. Mech. Sci. Tech.* **32**: 3523–3535.

Ghorbanhosseini, S. (2020). A Review of the failure and damage forms of metals under cyclic loading. *Int. J. Curr. Sci. Res. Rev.*, **3**: 178–184.

Gurmai, L. & Kiss, P. (2019). A comparative study of destructive effects resulting from road profile acting on off-road towed vehicles. *J. Terramech.*, **81**: 57–65.

Hájek, J., Nový, Z., Kučerová, L., Jirková, H., Salvetr, P., Motyčka, P., Hajšman, J. & Bystřická, T. (2022). A new alloying concept for low-density steels. *Materials*, **15**: 2539.

Isahak, A.H., Abdullah, M.F., Faidzi, M.K., Ali, A. & Mubasyir, M.M. (2020). Fatigue crack growth behaviour of sandwiched metal panel of aluminium and mild steel under constant amplitude loading. *Int. J. Integr. Eng.*, **12**: 81–90.

Jaber, H., Kovacs, T. & Tóth, L. (2019). Effects of water/TiO_2 nano-fluid quenching media on microstructure and properties of CK35 steel. *Eur. J. Mater. Sci. Eng.*, **4**: 92–100.

Keehan, E., Karlsson, L., Andrén, H.O. & Bhadeshia, H.K.D.H. (2006). Influence of carbon, manganese and nickel on microstructure and properties of strong steel weld metals: Part 3–Increased strength resulting from carbon additions. *Sci. Tech. Weld. Join.*, **11**: 19–24.

Kondo, Y., Ogawa, T. & Kubota, M. (2008). Study on the parameters applicable to the stress estimation of fatigue fracture surface without striations. *J. Solid Mech. Mater. Eng.*, **2**: 537–548.

Lee, D.H., Huynh, T., Kim, Y.B. & Park, J.S. (2022). Motion control system design for barge-type surface ships using tugboats. *J. Mar. Sci. Eng.*, **10**: 1413.

Li, P. & Zuo, L. (2017). Influences of the electromagnetic regenerative dampers on the vehicle suspension performance. *Proc. Inst. Mech. Eng. D J. Automob. Eng.*, **231**: 383–394.

Li, Z., Zuo, L., Luhrs, G., Lin, L. & Qin, Y.X. (2012). Electromagnetic energy-harvesting shock absorbers: design, modeling, and road tests. *IEEE Trans. Veh. Technol.*, **62**: 1065–1074.

Liang, H., Fu, J., Li, W., Wang, Y., Luo, L., Qi, S. & Yu, M. (2023). Theoretical switch model of novel asymmetric magnetorheological damper for shock and vibration application. *Smart Mater. Struct.*, **33**: 015008.

Liu, Z., Gao, X., Xiong, M., Li, P., Rao, D. & Misra, R.D.K. (2021). Recrystallization behavior and microstructure evolution in high-manganese austenitic steel. *Steel Res. Int.*, **92**: 2100029.

Murakami, Y. & Ritchie, R.O. (2012). Effects of hydrogen on fatigue-crack propagation in steels. *In* Gangloff, R.P. & Somerday, B.P. (Eds.). *Gaseous Hydrogen Embrittlement of Materials in Energy Technologies*. Woodhead Publishing Ltd, UK, pp. 379–417.

Pahl, J. (2022). Maritime spare parts management: Current state-of-the-art. In *55th Annual Hawaii Int. Conf. Sys. Sci.: HICSS 2022*. IEEE Computer Society Press, US, pp. 1676–1685.

Pavlina, E. J. & Van Tyne, C.J. (2008). Correlation of yield strength and tensile strength with hardness for steels. *J. Mater. Eng. Perform.*, **17**: 888–893.

Qiu, Z., Chen, R., Wu, C., Liu, D. & Gan, X. (2024). Optimized design of silicone oil torsional damper for diesel generator. *J. Phys.: Conf. Ser*., **2790**: 012007.

Ran, J.M., Hu, X.Y., Zhu, B. & Zhang, Y.S. (2023). Realistic microstructural RVE-based simulations of stress-strain behavior of a medium-manganese steels. *In* Zhang, Y. & Ma, M. (Eds.). *Proc. 6th Int. Conf. Adv. High Strength Steel Press Hardening (ICHSU 2022)*. Atlantis Press, Netherlands, pp. 370.

Ruckert, C.O.F.T., Messias Filho, A.A., Bose Filho, W.W., Spinelli, D. & Tarpani, J.R. (2011). Load ratio estimation through striation height and spacing analysis of an aerospace Al alloy 7475-T7351. *J. Mater. Eng. Perform.*, **20**: 382–389.

Ruckert, C.O.F.T., Tarpani, J.R., Filho, W.B. & Spinelli, D. (2006). On the relation between micro-and macroscopic fatigue crack growth rates in aluminum alloy AMS 7475-T7351. *Int. J. Fract.*, **142**: 233–240.

Shareef, S.S. (2023). Earthquake consideration in architectural design: Guidelines for architects. *Sustainability*, **15**: 13760.

Shen, S. (2024). Resilience and sustainability: Engineering solutions in disaster-affected real estate markets. *Sustain. Dev*., **32**: 6748–6762.

Sorge, F. (2016). Optimization of vehicle-trailer connection systems. *J. Phys.: Conf. Ser.*, **744**: 012209.

Sujata, M., Jagannathan, N., Raghavendra, K., Manjunatha, C.M. & Bhaumik, S. K. (2013). Fatigue fracture of a compressor disc of an aeroengine. *J. Fail. Anal. Prev.*, **13**: 437–444.

Sun, J., Jiang, M., Dong, L., Ding, Z., Bao, Y. & Luo, S. (2024). Effect of aging temperature on the microstructure and properties of alloyed high-manganese steel. *Mater.wiss. Werkstofftech.*, **55**: 1045–1051.

Wang J., Li, J. & Shi, Z. (2022). Crack evolution law and failure mode of red sandstone under fatigue–creep interaction. *Fatigue Fract. Eng. Mater. Struct.*, **45**: 270–284.

Wang, W.L., Huang, B., Du, J.M. & Iwnicki, S. (2019). Fatigue analysis of a railway hydraulic damper with welding imperfections under actual in-service load conditions. *In* Luo, X., Akram A., Steven Guan, S. & Pamucar, D. (Eds.). *2019 Int. Conf. Model. Anal. Simul. Technol. Appl. (MASTA 2019)*. Atlantis Press, Netherlands, pp. 371–375.

Wang, Z., Zhang, N., Zhang, Q. & Jiang, S. (2023). Effect of trailer suspension damping tuning on rearward amplification of car-trailer combinations. In *2023 7th CAA Int. Conf. Veh. Control Intel. (CVCI)*. IEEE, China, pp. 1–6

Yan, J., Zhou, M., Wu, H., Liang, X., Xing, Z., Li, H., Zhao, L., Jiao, S. & Jiang, Z. (2023). A review of key factors affecting the wear performance of medium manganese steels. *Metals*, **13**: 1152.

Yang, X., Zhu, J., Song, Y. & Li, Y. (2023). Design and experimental research of stepped bypass magnetorheological damper. *J. Intell. Mater. Syst. Struct.*, **34**: 1527–1547.

Zhang, L., Niu, F., Liu, M., Luo, J. & Ju, X. (2022). Mechanical behavior of cracked rock in cold region subjected to step cyclic loading. *Geofluids*, **2022**: 6220549.

Zhang, Q., Wei, S. & Chen, Y. (2020). Failure analysis of the fifth wheel couplings utilized in heavy semi-trailer tractors. *Eng. Fail. Anal.*, **109**: 104352.

Ziezulewicz, G. (2023). *Report: Navy Ships Face Growing Maintenance Delays, Costs*. Available online at: https://www.navytimes.com/news/your-navy/2023/02/04/report-navy-ships-face-growing-maintenance-delays-costs/ (Last access date: 5 March 2025).

PERFORMANCE OF BULLET RESISTANT GLASS CLAD POLYCARBONATE WITH RESIN AS AN INTERLAYER

Lee Wei Szer, Mohammed Alias Yusof*, Fakroul Ridzuan Hashim, Muhamad Azani Yahya, Ariffin Ismail, Mohd Fauzy Mohd Nor, Osmera Ismail & Ameen Topa

National Defence University of Malaysia (UPNM), Malaysia

*Email: alias@upnm.edu.my

ABSTRACT

Laminated glass is a type of safety glass that is commonly used in bullet resistant windows and bulletproof glazing. However, it often fails under ballistic impact due to full penetration and splintering. This research aims to investigate the performance of bullet resistant glass clad polycarbonate with resin as an interlayer. A total of twelve laminated samples, each measuring 500 mm × 500 mm with an overall thickness of 21 mm, were prepared and tested, comprising three samples for each configuration. The configurations were: triple laminated glass (control), triple laminated polycarbonate, double laminated glass clad with 6 mm polycarbonate at the centre, and double laminated glass clad with 6 mm polycarbonate at the back. The experimental work was carried out in accordance with EN 1063: Glass in Building - Security Glazing - Testing and Classification of Resistance Against Bullet Attack. Ballistic testing was conducted at the Science and Technology Research Institute for Defence (STRIDE), using 9 mm soft core bullets as the projectile. In the experimental setup, the firing distance between the firearm and glass sample was fixed at 5 m. The velocity of the bullet was recorded at approximately ±400 m/s. Each of the sample was individually tested under the same ballistic conditions to evaluate their resistance performance and failure behaviour when subjected to ballistic loading. The test results showed that both the triple laminated glass and triple laminated polycarbonate experienced complete penetration, while the double laminated glass clad with 6 mm polycarbonate at the centre achieved only partial penetration with rear splintering. In contrast, the double laminated glass clad with 6 mm polycarbonate at the back successfully withstood the ballistic loading from the 9 mm projectile with no penetration and no rear splinter damage. These results demonstrate that placing the polycarbonate layer at the rear significantly enhances ballistic protection, and that double laminated glass clad with 6 mm polycarbonate at the back with the thickness of 21 mm can be used as bullet resistant glass to stop 9 mm bullets for applications in buildings.

Keywords: *Laminated glass; polycarbonate; ballistic; bullet resistance; penetration.*

1. INTRODUCTION

Glass is a fragile material that exhibits inadequate resistance to impact loading and lacks post-fracture loading capacity. For example, in the Malaysian context, most buildings are not equipped with bullet resistant glass. Instead, they typically use tempered glass, which is vulnerable to severe damage and fragmentation when subjected to high impact force. This can cause serious safety risks in violent or shooting scenarios (Dahshaini, 2020; Farik, 2023). This shortcoming can be prevented by pairing glass with polymer interlayers to form laminated elements. These laminated elements then offer ductile behaviour after cracking, as the interlayer is firmly bonded to the glass layer even when cracked or shattered (Elkilani et al., 2024). During loading, the glass layers do not suddenly fail but gradually, which contributes to the overall ductile behaviour (Konrád *et al*., 2022).

Laminated glass has been widely used in the construction industry (El-Sisi *et al*., 2024) for both non-structural decoration applications and structural load-bearing components. However, the brittle

characteristic of the glass layers remains a concern especially when considering the relatively unlikely, yet high-risk, loading scenarios such as projectile impacts and blast-accelerated debris impacts. This vulnerability has emphasised the critical importance of ballistic glazing in applications(Ahani & Ahani, 2023). Laminated glass is increasingly applied in high-security buildings, including military facilities (Jibrin, 2024), where protection against blast loads, forced entry and ballistic threats is essential. For example, laminated glass is commonly used in guard posts, control centres and entry checkpoints within military compounds to provide visibility while ensuring safety from potential attacks. The use of laminated glass in such buildings helps to reduce the risk of injury from shattered glass and enhances the overall resilience of the structure against security threats (AIS, 2020).

Nevertheless, laminated glass still has several key weaknesses, especially when exposed to high-velocity ballistic impact. Although the interlayer improves post-fracture integrity, the glass layers themselves remain brittle and may experience full penetration when struck by a bullet (Ahani & Ahani, 2023). In many cases, the interlayer is not sufficient to absorb or dissipate the energy from ballistic impact, which can lead to splintering, spalling or even injury from glass fragments at the back surface (Dahshaini, 2020). Over time, exposure to environmental factors such as moisture, UV rays and temperature changes may also cause delamination, which reduces the long-term performance of the laminated glass (Farik, 2023; El-Sisi *et al*., 2024). These limitations highlight the importance of exploring improved glazing systems, such as combining laminated glass with polycarbonate and resin interlayers, which this study focuses on to achieve improved ballistic resistance for use in buildings.

In a recent study by Osnes *et al*. (2021), the ballistic performance of double-laminated glass plates was assessed through both experimental testing and finite element simulations. The research compared a single double-laminated glass plate with a dual-layer setup separated by an air gap. The laminated glass was made up of annealed soda-lime silica float glass and a PVB interlayer, which functions to retain glass fragments upon impact. Using 7.62 mm armour-piercing bullets, the study recorded the residual velocities to evaluate ballistic resistance, and found that the dual-layer configuration significantly increased the ballistic limit. Finite element simulations, which applied 3D node splitting and simplified material models, were able to closely replicate the global response of the glass under high-velocity impact. In another study, Biolzi (2022) investigated the post-failure behaviour of two-ply laminated glass under quasi-static loading, comparing the performance of various interlayer materials, namely polyvinyl butyral (PVB), SentryGlas (SG) and Saflex DG41 (DG41), bonded between tempered or toughened glass layers. Tests on both undamaged and partially damaged laminated glass showed that interlayer stiffness and glass fragment size significantly influenced post-breakage behaviour. SG and DG41 provided higher residual stiffness and better load-carrying capacity, acting more like monolithic glass, while PVB-based specimens demonstrated limited structural performance after failure. Similarly, Konrád *et al*. (2022) conducted a study on the ballistic resistance and post-impact behaviour of laminated glass subjected to high-velocity projectile impacts through experimental and numerical approaches. The research showed that the number of glass layers, interlayer thickness, and impact velocity played key roles in determining performance. The laminated glass was observed to fail through radial and circumferential cracking, but the interlayer was effective in holding the broken fragments together, thus preserving residual integrity. Numerical simulations further provided insight into stress distribution and crack propagation patterns, complementing the experimental findings.

This study proposes the use of polycarbonate and polyurethane (PU) resin as an alternative interlayer material in laminated glass to enhance ballistic resistance performance. Polycarbonate is a thermoplastic material that has excellent energy absorption and impact resistance, which helps to slow down or stop projectiles by spreading the impact energy across its surface (Zhang *et al*., 2023). Unlike laminated glass, polycarbonate can deform plastically under high-impact conditions, making it more resistant to penetration (Rodrigues Dias & Miranda Pereira, 2023). Meanwhile, PU resin provides strong bonding between the layers and can potentially offer better energy dissipation and glass fragment retention compared to conventional PVB interlayers (Nurul *et al*., 2022). Its flexible and adhesive characteristics also help maintain the structural connection between the layers after impact. Therefore, by combining

polycarbonate with PU resin, this study aims to investigate the performance of bullet resistant glass clad polycarbonate with resin as an interlayer, based on full penetration or non-penetration after the bullet impact.

2. METHODOLOGY

A total of twelve laminated samples, each measuring of 500 mm × 500 mm with thickness of 21 mm, were prepared and tested. The samples were categorised into four configurations, each consisting of three samples as shown below:

a. Triple laminated glass (Control sample)
b. Triple laminated polycarbonate
c. Double laminated glass clad with 6 mm polycarbonate at the centre
d. Double laminated glass clad with 6 mm polycarbonate at the back

All the samples were subjected to ballistic impact tests. The experimental work was carried out in accordance with EN 1063: *Glass in Building - Security Glazing - Testing and Classification of Resistance Against Bullet Attack* (CEN, 1999), which specifies the classification of bullet-resistant glass into seven levels (BR1 to BR7), based on the type of firearm, bullet calibre, mass and velocity. Each class represents increasing levels of ballistic protection, from low-calibre handguns to high-powered rifles. Testing was conducted at fixed range of 5 m, with three shots fired per sample at specific velocities and distances. In this study, class BR2 (Table 1) was selected as the reference ballistic threat level. This class involves testing with a 9 mm soft core bullets fired at impact velocity of 400 m/s. It represents a realistic threat scenario for civilian and commercial buildings, where protection against handgun threats is required (Architectural Armour, 2023).

Table 1: Test requirements for testing the bullet resistance of glazing using class BR2 (CEN, 1999).

Class	Type of weapon	Calibre	Type	Mass (g)	Test condition			
					Test range (m)	Bullet velocity (m/s)	No. of strikes	Striking distance (mm)
BR2	Hand gun	9 mm Luger	Soft core	8.0 ±0.5	5.0 ±0.5	400 ±10	3	120 ±10

The glass material is annealed soda lime silica float glass with a flexural strength of 70 MPa and the polymer is PU resin, while the polycarbonate used in this experiment is unfilled polycarbonate with flexural strength of 100 MPa. The configuration of the laminated glass with polycarbonate, as shown in Figure 1, consists of double layer of 6 mm thick glass and a layer of 6 mm thick polycarbonate, with 1.5 mm of PU resin applied at each interlayer. This results in total thickness of 21 mm.

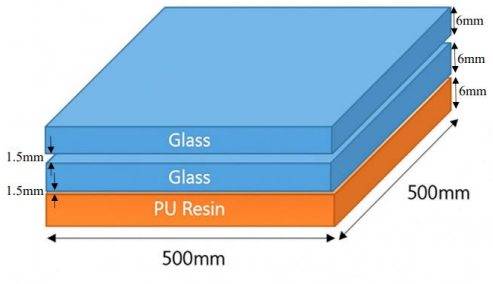

Figure 1: The configuration of the laminated glass with polycarbonate.

In this experimental study, 9 mm soft core bullets impacted the laminated glass panels. The bullet consists of a hardened lead core, a lead cap, a brass jacket and an end cap (Figure 2). The total mass of the bullet is 8g ± 0.2g.

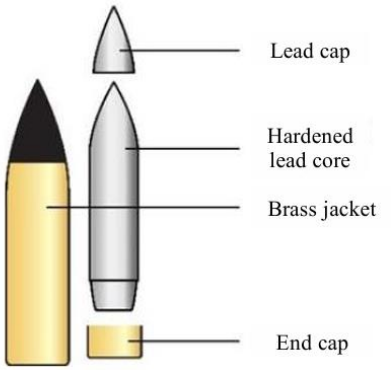

Figure 2: 9 mm soft core bullets.
(Source: Barrett *et al.*, 2016)

The ballistic impact tests were conducted using a universal test gun in a ballistic range. The bullets were fired from a test barrel with striking velocities of 400 ± 10 m/s. The distance between the muzzle and target glass sample was approximately 5 m, and there were three fixed striking points at distance of 120 mm (CEN, 1999) as shown in Figure 3.

Figure 3: A sample measuring 500 mm × 500 mm with fixed striking points at distance of 120 mm.

The projectile velocity was measured using a portable projectile velocity measurement system. In order to assess ballistic resistance, the ballistic limit velocity was measured as the velocity at which 50% of the projectiles penetrated the material ($\boldsymbol{V_{50}}$) and comparing it to the velocity corresponding to 0% penetration ($\boldsymbol{V_0}$) (Alia, 2014). The energy absorption of bulletproof materials as a function of a real density was calculated using the following equation (Alia, 2014):

$$E = \frac{1}{2}\, m \left(V_i^2 - V_r^2\right) = \frac{1}{2}\, m\, V_{50} \qquad (1)$$

where:

E is the energy absorption
m the mass of the projectile
V_i the initial impact velocity
V_r the projectile residual velocity
V_{50} the ballistic limit velocity.

3. RESULTS & DISCUSSION

The ballistic resistance of different configurations of laminated glass samples was assessed based on average impact velocity and energy absorption, as recorded in Table 2. The control sample, comprising triple laminated glass, recorded energy absorption of 603 J, which reflects its high stiffness but brittle fracture behaviour that limits post-impact energy dissipation. In comparison, the triple laminated polycarbonate configuration absorbed slightly higher energy of 637 J, consistent with its lower stiffness but greater ductility. For the hybrid configurations, the resistance performance varied with polycarbonate placement. When positioned at the centre, polycarbonate facilitated energy dissipation but slightly reduced stiffness, resulting in energy absorption of 654 J. Conversely, placing polycarbonate at the back yielded the highest energy absorption of 668 J, as the fractured glass layers dispersed the initial impact energy while the rear polycarbonate acted as a final barrier, preventing penetration and minimising spall risk.

Table 2: The result of the experiment.

Configuration	Average Velocity (m/s)	Energy Absorption (J)
Triple laminated glass (control sample)	409	603
Triple laminated polycarbonate	409	637
Double laminated glass clad with 6 mm polycarbonate at the centre	404	654
Double laminated glass clad with 6 mm polycarbonate at the back	409	668

Figure 4 shows the failure of the triple laminated glass with PU resin interlayer. The bullet completely penetrated the laminate and the aluminium foil at the back was torn, confirming that both the projectile and splinters passed through the sample. The glass surface displayed extensive radial cracks, forming a cone-shaped fracture zone that represents the brittle failure. PU resin alone was unable to absorb or dissipate the kinetic energy of the projectile, leading to full perforation. This configuration offers minimal ballistic protection, as it lacks any form of energy-dissipating or splinter-containment layers.

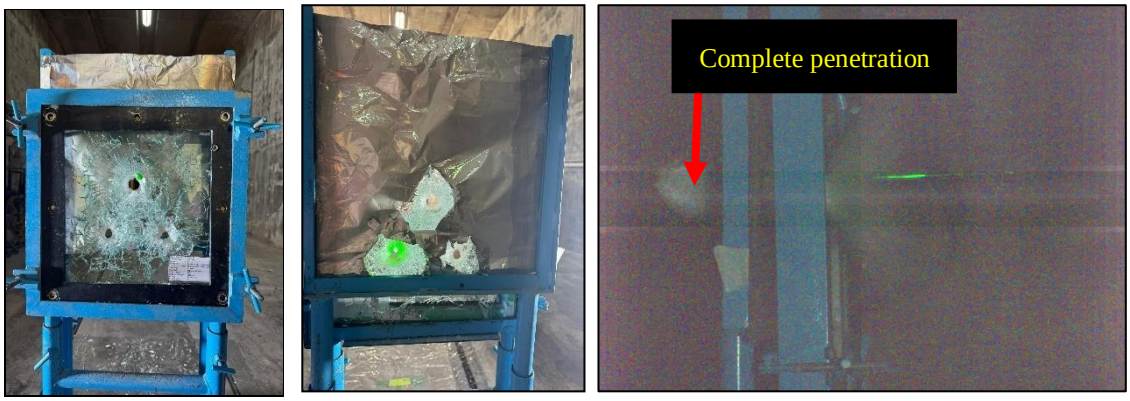

Figure 4: Triple laminated glass.

Figure 5 shows that the triple laminated polycarbonate also suffered complete penetration. However, unlike glass, the polycarbonate panel did not shatter. Instead, the impact area showed plastic deformation with some cracking and tearing around the entry and exit points. The projectile managed to pass through and the aluminium foil was visibly damaged. Although polycarbonate is known for its ductile and energy-absorbing properties, when used alone without glass reinforcement, it lacks the stiffness needed to stop high-velocity projectiles. While this configuration showed better splinter control than glass, it failed to prevent penetration due to insufficient stopping power.

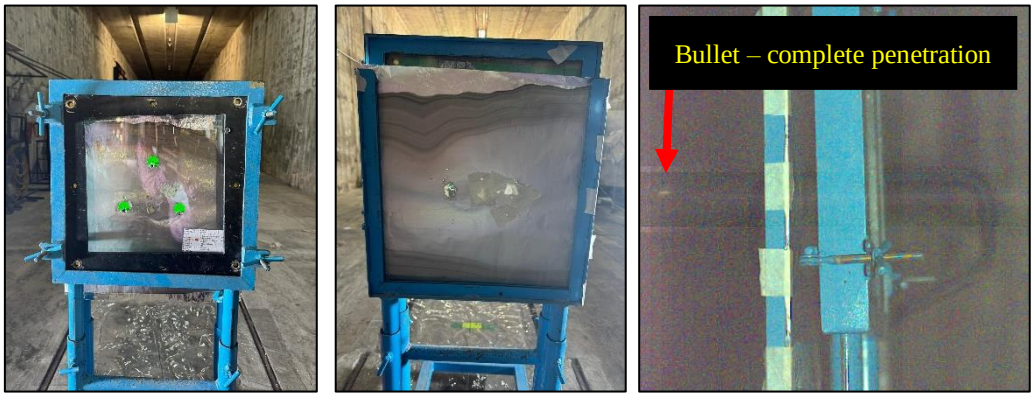

Figure 5: Triple laminated polycarbonate.

Figure 6 shows that for the double laminated glass clad with 6 mm polycarbonate at the centre, the bullets caused partial penetration, where the projectile did not penetrate for the first and second shot, and glass splinters reached and tore the aluminium foil**.** However, on the third shot, the bullet successfully penetrated the laminated glass sample. The damage suggests that although the polycarbonate at the centre helped slow down the bullet, it was not as effective in containing splinters or preventing back layer damage. The crack pattern revealed a wide fractured area in the front glass layer and signs of internal delamination between the layers. This configuration showed a moderate level of ballistic resistance that was able to reduce penetration depth, but still allowed dangerous rear-side splintering. The polycarbonate layer at the centre was unable to fully capture or dissipate the residual kinetic energy before it reached the back surface.

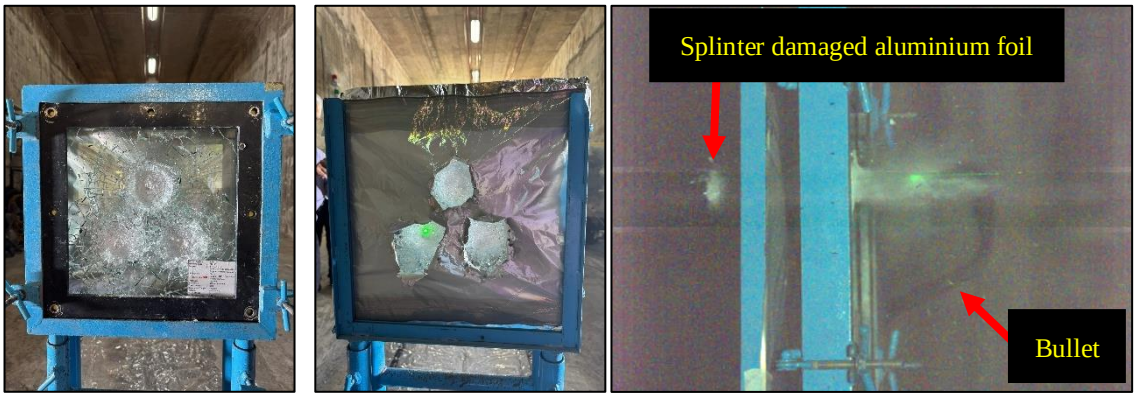

Figure 6: Double laminated glass clad with 6 mm polycarbonate at the centre.

Figure 7 shows that the double laminated glass clad with 6 mm polycarbonate at the back is the best performing sample among all the configurations tested. The laminated glass with PU resin interlayer and polycarbonate layer positioned at the back successfully prevented full penetration. The aluminium foil at the rear remained undamaged, and all glass splinters were found at the front of the sample. The crack pattern with smaller radial cracks were confined to the impact zone, suggesting better energy absorption. The back polycarbonate layer effectively functioned as a catchment barrier, absorbing the residual energy and preventing both projectile breakthrough and splintering. This result confirms that back-positioned polycarbonate plays a critical role in splinter containment, which is essential for ballistic protection.

Figure 7: Double laminated glass clad with 6 mm polycarbonate at the back.

4. CONCLUSION

Based on the ballistic impact test results, it can be concluded that the laminate configuration significantly affects the bullet resistance performance. Among the four types of samples tested, only the double laminated glass clad with 6 mm polycarbonate at the back successfully prevented complete penetration and rear splinter damage. The presence of the polycarbonate layer at the back effectively absorbed the residual impact energy and acted as a barrier to restrain crack propagation and splinter projection. On the other hand, the triple laminated glass with PU resin interlayer and triple laminated polycarbonate both experienced complete penetration and showed extensive damage, indicating insufficient energy absorption capacity. The double laminated glass clad with 6 mm polycarbonate at the centre was able to reduce the projectile velocity, but still allowed splintering and damage to the rear foil, showing moderate resistance. Therefore, the placement of polycarbonate at the back of the laminate provided the best ballistic protection, proving to be the most effective in absorbing energy, containing splinters, and maintaining the integrity of the laminate structure under high-velocity impact.

REFERENCES

Ahani, A. & Ahani, E. (2023). An overview for materials and design methods used for enhancement of laminated glass. *Hybrid Adv.*, **3**: 100063.

AIS (2020). *Applications of Laminated Glass in High-Security Areas*. Available online at: https://www.aisglass.com/blog/applications-of-laminated-glass-in-high-security-areas (Last access date: 21 July 2025).

Alia, R.A., Cantwell, W.J., Langdon, G.S., Yuen, S.C.K. & Nurick, G.N. (2014). The energy absorbing characteristics of composite tube-reinforced foam structures. *Compos. Part B Eng.*, **61**: 127-135.

Architectural Armour (2023). *Security Glass*. Available online at: https://www.architecturalarmour.com/security-products/security-glass (Last access date: 11 August 2025).

Bandaru, A.K., Chavan, V.V., Ahmad, S., Alagirusamy, R. & Bhatnagar, N. (2016) Ballistic impact response of Kevlar® reinforced thermoplastic composite armours. *Int. J. Impact Eng.*, **89**: 1-13.

Barrett, S., Rasmus, V. & Ahmad, O. (2016). *Ballistic Properties of Projectile Material.* Student Report, Department of Mechanicall and Manufacturing Engineering, Aalborg University, Denmark.

Biolzi, L., Cattaneo, S. & Simoncelli, M. (2022). Post-failure behaviour of 2-ply laminated glass plates with different interlayers. *Eng. Fract. Mech.*, **268**: 108496.

Castori, G. & Speranzini, E. (2017) Structural analysis of failure behavior of laminated glass. *Compos. Part B Eng.*, **125**:89–99.

CEN (European Committee for Standardization) (1999). *EN 1063: Glass in Building – Security Glazing – Testing and Classification of Resistance Against Bullet Attack*. European Committee for Standardization (CEN), Brussels, Belgium.

Dahshaini, N., Sharifah Mastura, S.M.D, Nadiah & Syariani, M.S. (2020). Analysis of glass fracture pattern on soda lime and tempered glass caused by shotgun bullet impact. *Malays. J. Med. Health Sci.*, **16**: 131-135.

Elkilani, A., Salim, H., Elemam, H., Elsisi, A., Bowman, A., Johnson, C. & Elbelbisi, A. (2024). Numerical and experimental blast response of multilayer laminated glass panels. *Constr. Build Mater.*, **449**: 138520.

El-Sisi, A., Elsawi, M., M., El-Emam, H., Elbelbisi, A. & Salim, H. (2024). Environmental bond degradation of different laminated glass panels. *Polymers*, **16**: 2040.

Farik, Z. (2023). *Guard accidentally fires gun, shatters bank door*. Available online at: https://www.thestar.com.my/news/nation/2023/12/27/guard-accidentally-fires-gun-shatters-bank-door (Last access date: 21 July 2025).

Jena, P.K., Ramanjeneyulu, K., Kumar, K.S. & Bhat, T.B. (2019). Ballistic studies on layered structures. *Mater. Des.*, **30**: 1922–1929.

Jibrin, M.Y. (2024). Crystalline and polymeric interactions in multi- layered bulletproof glass: A study of ballistic resistance and structural integrity. *Int. J. Cryst. Mater.*, **1**: 10–17.

Konrád, P., Hála, P., Schmidt, J., Zemanová, A. & Sovják, R. (2022). Laminated glass plates subjected to high-velocity projectile impact and their residual post-impact performance. *Materials*, **15**: 8342.

Martín, M., Centelles, X., Sole, A., Barreneche, C., Fernandez, A.I. & Cabeza, L.F. (2020). Polymeric interlayer materials for laminated glass: A review. *Constr. Build Mater.*, **230**:116897.

Nurul, N.M., Salleh, N. & Faiz, R. (2022). Enhancement of glass fracture resistance using polyurethane resin interlayer. *Malays. Constr. Res. J.*, **34**: 77–85.

Osnes, K., Holmen, J. K., Grue, T. & Børvik, T. (2021). Experimental tests and numerical simulations of ballistic impact on laminated glass. *EPJ Web Conf.*, **250**: 02022.

Rodrigues Dias, R. & Miranda Pereira, I. (2023). High strain rate compressive behavior of ballistic polycarbonate: Experimental and numerical modelling. 29 October - 2 November 2023, *17th Braz. Polym. Conf.*, Joinville, Santa Catarina, Brazil.

Zhang, Y., Chen, L. & Wu, Q. (2023). Ballistic performance of transparent polycarbonate-glass laminates. *Int. J. Impact Eng.*, **178**: 104504.

ASSESSMENT OF OIL SPILL AND MICROPLASTIC REMOVAL FROM SEAWATER USING NEWLY SYNTHESISED FERROFLUID: A LABORATORY SCALE STUDY

Suganeeswaran Mohanakrishanan[1], Nik Harnida Suhainai[1], Nor Aliya Hamizi[2], Mohd Rafie Johan[2], Irwan Nurdin[3], Syazwan Hanani Meriam Suhaimy[4], Nik Hassanuddin Nik Yusoff [5] & Asmalina Mohamed Saat[1*]

[1]Universiti Kuala Lumpur, Malaysian Institute of Marine Engineering Technology (UniKL-MIMET), Malaysia
[2]Nanotechology and Catalysis Research Centre, University Malaya, Malaysia
[3]Chemical Engineering Department, Politeknik Negeri Lhokseumawe, Indonesia
[4]Department of Physics and Chemistry, Faculty of Applied Sciences and Technology, Universiti Tun Hussein Onn (UTHM), Malaysia
[5]Science & Technology Research Institute for Defence (STRIDE), Ministry of Defence, Malaysia

[*]Email: asmalina@unikl.edu.my

ABSTRACT

In recent times, oil spills and microplastic pollution have become major environmental concerns due to their significant impact on ecosystems. Therefore, appropriate measures should be implemented to prevent or minimise such pollution in the future. In this study, the functionalised nanoparticles (FNPs), synthesised using phenyl phosphonic acid (PAPh), were employed to remove oil and microplastic from seawater in laboratory scale. This technique is cost-effective and facilitates the easy recovery of oil spills without causing additional pollution. The development of hydrophobic materials with magnetic properties, capable of serving as adsorbents for both oil spills and microplastics, presents an intriguing challenge. Iron oxide was functionalised with phenyl phosphonic acid (an organic acid) to produce a hydrophobic and oleophilic sorbent material for oil extraction. The performance of the functionalised iron oxide nanoparticles (FNPs) demonstrated superior extraction efficiency for engine oil compared to mineral oil. The oil extraction rate remained consistent over seven consecutive extraction cycles. Extraction efficiencies for engine oil and microfibres from seawater were recorded at 74.2 and 95.5%, respectively. These findings confirm that FNPs enhance oil absorption capacity and reusability. Moreover, they demonstrate that FNPs can be effectively utilised to clean and collect both oil spills and microplastics from marine environments, thereby contributing to the sustainability of the ocean ecosystem.

Keywords: *Microplastics; oil spills; magnetic adsorbent; ferrofluid; iron oxide nanoparticles (NPs).*

1. INTRODUCTION

Oil spills and microplastics are among the most harmful pollutants in the marine environment, posing significant threats to marine ecosystems. Prevention may not be easily achievable in the future, thus necessitating measures to remove oil spills and microplastics from seawater (Choudhury *et al*., 2018; Che Ishak *et al*., 2020;). An oil spill is a form of pollution resulting from human activities that release liquid petroleum hydrocarbons into the environment, particularly affecting marine ecosystems. The term typically refers to marine oil spills, where oil is discharged into water bodies. Oil spills are most frequently caused by the discharge of crude oil from tankers, offshore platforms, drilling rigs, pipelines, refineries and storage facilities. Meanwhile, microplastics are minute plastic particles, defined by Horton & Dixon (2018) as plastics with a diameter of less than 5 mm (approximately 0.2 in). These particles pose significant harm to marine and aquatic life (Frias & Nash, 2019). Microplastics are divided into two categories; primary and secondary. Primary microplastics are intentionally manufactured small plastic pieces, such as microbeads found in personal care products, plastic pellets (nurdles) used in industrial processes, and plastic fibres used in synthetic textiles such as nylon.

Secondary microplastics result from the breakdown of larger plastic products into smaller particles due to weathering processes such as exposure to sunlight, wind abrasion, and wave action. They contribute significantly to the presence of microplastics in the environment, persisting and accumulating due to their non-biodegradable nature (Mathew *et al*., 2024).

Both oil spills and microplastics have catastrophic economic and environmental impacts on society, resulting in numerous consequences. Removing oil spills and microplastics from seawater is a challenging task requiring effective methods. Common methods for removing oil spills from the sea surface include in situ burning, biodegradation, oil skimmers, and oil dispersants (Yang *et al*., 2022). For microplastics, researchers have explored various methods such as biodegradation, incineration, landfilling, recycling, and the use of innovative technologies such as ferrofluids and magnetic extraction systems (Anand *et al*., 2023). In most cases, sorbents can be employed for hydrocarbon recovery, providing a long-term alternative. Several key parameters must be considered when classifying sorbent materials, including affordability, availability and accessibility. In addition, the material should exhibit high sorption capacity. It should also be non-toxic and easily recoverable. Low oil absorption capacity and limited reusability are common challenges in oil spill remediation. It is crucial to produce sorbent materials with high surface area to increase absorption capacity and enable reusability over multiple extraction cycles (Kamar *et al*., 2024). To date, sorbent materials have only been tested and studied under controlled laboratory temperatures. Limited data exist regarding their performance in real-world field conditions or on a large scale to fully understand their potential and viability (Saper *et al*., 2024).

Many techniques using magnetic nanoparticles (NPs) as sorbents for oil removal have been studied (Tuan Hoang *et al*., 2018). However, problems may arise due to factors such as sorbent reusability and efficiency. No sorbent material has yet been established at a commercially viable level for large-scale oil recovery. Challenges in developing magnetic nanoparticles include creating efficient processes for removing oil and microplastics from seawater. Poor porosity is one problem in removing oil from seawater using magnetic nanoparticles due to slow diffusion, resulting in a slow oil recovery process. The development of highly hydrophobic and oleophilic magnetic nanoparticles with improved porosity (allowing faster oil diffusion) that can adsorb oil and microplastics from seawater has been reported (Singh *et al*., 2020). The paper discusses how encapsulation with various materials nanoparticles, polymers, and biosorbents affects oil recovery efficiency, selectivity and durability. Effectiveness also varies depending on oil types, water salinity, and temperature. Developing sorbent materials that can be reused after several extraction cycles remains a challenge. Magnetic separation can effectively concentrate microplastics for removal, minimising the energy and time required as compared to traditional methods such as filtration (Bakhteeva *et al*., 2023).

Ferrofluid is a non-toxic magnetic liquid composed of oil and magnetite (iron oxide powder), and has been proposed as a method for removing oil spills and microplastics from seawater (Pan *et al*., 2023). It possesses notable magnetic, oleophilic and hydrophobic properties. The ferrofluid is designed to attract and capture oil spills and microplastics, facilitating their removal from water. It has been demonstrated that nanoparticles can be rendered oleophilic by functionalising their surfaces. Ferrofluid disperses onto the oil spill on the water surface and interacts with the oil due to its oleophilic properties. The dispersed ferrofluid then strongly responds to an external magnetic field (such as a neodymium magnet) during the removal of oil spills from the water surface (Zahn *et al*., 2012). It can be magnetically recovered, regenerated and reused multiple times without significant loss of oil removal efficiency, thereby reducing costs and environmental impact. Regarding microplastic removal, ferrofluids are widely discussed as binding with microplastics via hydrophobic and oleophilic interactions similar to those involved in oil spill removal. Many techniques using magnetic nanoparticles as sorbents for oil removal have been studied (Tuan Hoang *et al*., 2018).

However, problems may arise due to factors such as sorbent reusability and efficiency. No sorbent material has yet been established at a commercially viable level for large-scale oil recovery. Challenges in developing magnetic nanoparticles include creating efficient processes for removing oil and microplastics from seawater. Poor porosity is one problem in removing oil from seawater using magnetic nanoparticles due to slow diffusion, resulting in a slow oil recovery process. The development

of highly hydrophobic and oleophilic magnetic nanoparticles with improved porosity (allowing faster oil diffusion) that can adsorb oil and microplastics from seawater has been reported (Singh *et al*., 2020).

Microplastic removal using ferrofluids has shown variable efficiencies under laboratory conditions: 98% in wastewater (Ibrahim, 2024) and 91% in freshwater (Nizam *et al*., 2023). Meanwhile, for oil spills, mineral oil removal from freshwater has recorded efficiencies up to 90%, decreased efficiency in seawater due to reduced magnetism. Vegetable and motor oils show lower efficiencies due to interactions between the ferrofluid and the oil types (Beer, 2015). One study reported oil removal efficiencies of approximately 66% for sunflower and olive oils using ferrofluids and magnets in a home-based experiment (Akbal, 2021). This indicates that oil removal efficiency depends on oil type, environmental conditions, and the surfactant or encapsulation type of the ferrofluid. Additionally, optimisation of variables such as oil volume, magnetite nanoparticle concentration, stirring rate and contact time are important factors influencing high removal efficiency (Beer, 2015; Nizam *et al*., 2023).

The synthesis of ferrofluids without the addition of stabilising agents or surfactants represents a promising innovation that may enhance microplastic removal performance (Hamzah *et al*., 2021). Ferrofluids can be formulated by mixing vegetable oil with iron oxide powder to produce a magnetic liquid capable of capturing microplastics from water (Pan *et al*., 2023). However, current research highlights the need for improvements in both efficiency and reusability. A further limitation is the lack of data reflecting real-world conditions, particularly in seawater environments. Most existing studies focus on freshwater, especially wastewater treatment (Honarmandrad *et al*., 2023). Furthermore, the available literature typically addresses either oil removal or microplastic removal in isolation. Few, if any, studies have investigated the use of ferrofluids for the simultaneous removal of oil and microplastics. While ferrofluids are effective in magnetising and removing oil, their application to microplastics removal is less straightforward. As plastics are not inherently magnetic, ferrofluids must be engineered or combined with magnetic particles that can bind to plastics, a technically complex process that remains under development(Bui & Tran, 2025).

Despite these challenges, the use of ferrofluids for oil spill and microplastic remediation remains in the early stages of development and shows considerable potential as a solution to the growing problem of marine pollution. Given the limitations discussed, there is a clear need to develop novel stabilised ferrofluids with improved efficiency in seawater for the dual removal of oil spills and microplastics. It is also essential to address challenges related to sorbent absorption capacity and reusability.

Accordingly, this research focuses on synthesising novel stabilised ferrofluids using phenyl phosphonic acid (PAPh), designed for the removal of both oil spills and microplastic pollutants in marine environments. The functionalised nanoparticles (FNPs) were evaluated based on the influence of PAPh ratios, their effectiveness in extracting oil and microplastics, the impact of repeated oil extraction cycles, as well as their effect on seawater uptake.

2. METHODOLOGY

The new ferrofluid was synthesised by functionalising iron oxide (Fe_2O_3) FNPs with PAPh. The materials used to functionalise the nanoparticles (NPs) were iron oxide (50 mg), isopropanol (20 mL) and phenyl phosphonic acid, employing an ultrasonic cleaner. Five samples of NPs were prepared. The initial mass of NPs in each sample was identical, at 50 mg. For the first sample, the NPs were not functionalised with PAPh and were designated as untreated NPs.

50 mg of iron oxide NPs with an average particle size ranging from 20 to 40 nm were initially dispersed in isopropanol (IPA) (20 mL) and stirred using a magnetic stirrer. Various ratios of PAPh were added to the mixture and stirred thoroughly to ensure homogeneity. The mixture was then subjected to ultrasonic treatment in a bath for approximately 30 min. The FNPs were collected using a neodymium magnet. Subsequently, the NPs were washed and stored in a desiccator after drying at 60°C. The reagents used in the experiments included PAPh, n-hexane and isopropanol (IPA), all obtained from

Sigma Aldrich. The oil extraction performance was evaluated using three types of dispersion media: seawater, distilled water and ethanol. Two types of oils were selected for analysis: engine and mineral oils. Table 1 summarises the FNPs, while Table 2 presents the properties of the oils used in the experiments.

Table 1: Summary of FNPs.

Sample	NP (mg)	PAPh (mL)	Ratio (NPs: PAPh)
A	50	0	Untreated
B	50	2.5	20: 1
C	50	5	10: 1
D	50	10	5: 1
E	50	15	3.33: 1

Table 2: Properties of engine and mineral oils.

Types of oil	Properties	Value
Engine oil	Density @ 27°C	0.889 g/cm^3
	Viscosity	161 cSt
Mineral oil	Density @ 27°C	0.838 g/cm^3
	Viscosity	14.2 cSt

Oil extraction experiments were conducted at room temperature. Engine oil was mixed with seawater as the dispersion medium, after which the FNPs were dispersed into the mixture to interact with the oil. The FNPs were then extracted from the mixture using a neodymium magnet. This procedure was repeated using distilled water and ethanol as dispersion media. The same process was applied to mineral oil. The collected FNPs were washed with n-hexane and recollected using a magnet. The FNPs could be reused for subsequent extractions after drying at 60 °C for 15 min. The performance of the FNPs in oil extraction for both oil types and dispersion media were recorded and calculated using the following equations for absorption efficiency and volume of oil absorbed:

$$\text{Efficiency} = 1 - \frac{\text{volume of absorbed oil (mL)}}{\text{volume of oil used in the experiment}} \quad (1)$$

$$\text{Volume of absorbed oil} = \text{Initial volume of oil} - \text{Volume of remained oil} \quad (2)$$

The adsorption rate for each oil was determined by dispersing 10 mg of FNPs into a beaker containing 0.5 mL of oil at room temperature. The FNPs were extracted from the beaker repeatedly until all suspended NPs were removed. The following equation was used to calculate the adsorption rate:

$$q = \frac{(m_2 - m_1)}{m_1} \quad (3)$$

where q is the adsorption rate (g/g); m_2 is the weight of NPs after removal and m_1 is the initial weight of the NPs before the oil extraction experiment.

3. RESULTS & DISCUSSION

3.1 Effect of PAPh Ratio on FNP Weight Change

Figure 1 illustrates the FNPs that were prepared prior to the oil extraction experiments. The addition of PAPh leads to a decrease in weight change. Higher ratios of PAPh exhibit a smaller decrease in weight change. The quantity of PAPh at 10 mL, with NP to PAPh ratios of 5:1, demonstrates the highest weight of NPs. This finding almost similar with previous researcher that found rati 4:1 is the optimal ratio(Lei *et al*., 2022). Increasing the amount of PAPh results in an increase in NP weight. Additionally, 15 mL of PAPh with a ratio of 3.33:1 shows lowest values for NP weight. The results indicate that the optimum reaction between NP and PAPh occurs in the samples with a ratio of 5:1, owing to the maximum weight increase observed. The linear regression shows lower R^2 is 0.6904 with equation of y = -0.0468x + 0.0147 for the FNPs weight change as the ratios decreased from 20 to 3.33.

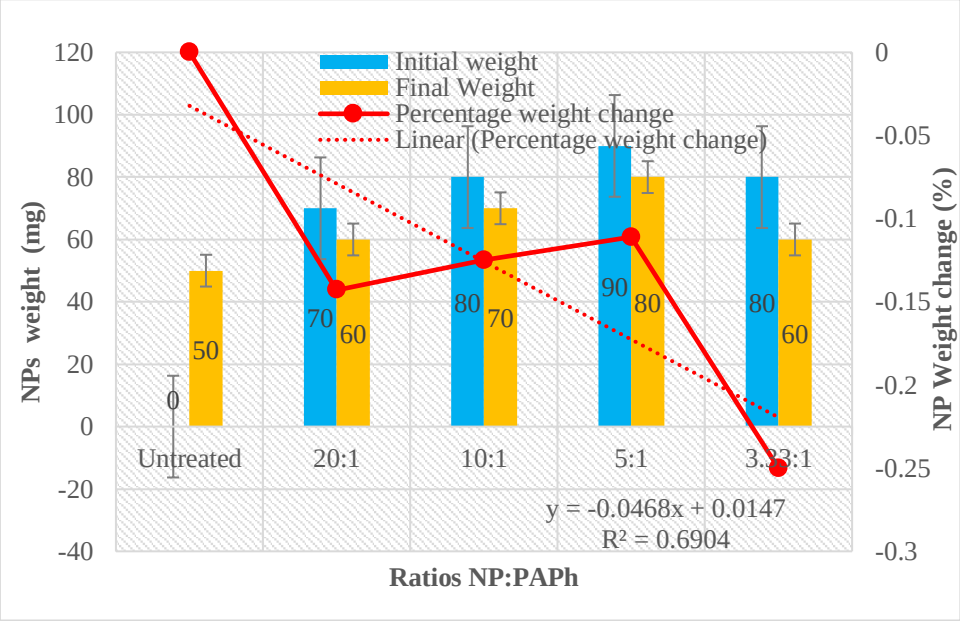

Figure 1: The FNPs' weight changes.

3.2 Effect of FNPs on Oil Extraction in Various Medium Dispersion

The oil extraction experiment utilised 10 mg of FNPs (Fe_3O_4-PAPH), 15 mL of dispersing agents (seawater, distilled water and ethanol) and 0.5 mL of oil (engine and mineral oils). 10 ml of phenyl phosphonic acid and 50 mg of Fe_3O_4-PAPH were used to prepare the FNPs for this experiment due to the maximum weight change observed in the FNPs. Tables 3 and 4 present the visual observations of engine and mineral oil in various dispersion media. All the images demonstrate that both engine and mineral oil were successfully extracted from all dispersion media: seawater, distilled water, and ethanol.

Figure 2 displays the oil extraction ratios from seawater, distilled water and ethanol for engine and mineral oils. The oil extraction ratio was measured over two cycles. Engine oil was found to have higher efficiency in seawater and distilled water as compared to mineral oil. A similar finding was reported earlier by Beer (2015), whereby the efficiency of engine oil removal was much higher as compared to mineral oil. Higher oil extraction was observed in ethanol, followed by seawater and distilled water. The efficiency of oil extraction in ethanol is attributed to its solvent properties. Ethanol has a high affinity for oil molecules, resulting in improved oil extraction performance (Ferreira-Dias *et al*., 2003). Seawater contains salts and minerals that interfere with the extraction process. Meanwhile, distilled

water lacks the necessary properties to effectively extract oil molecules. Seawater and distilled water showed no significant impact on the oil recovery process (Kara *et al.*, 2017). These findings indicate that ethanol can be employed to enhance oil recovery.

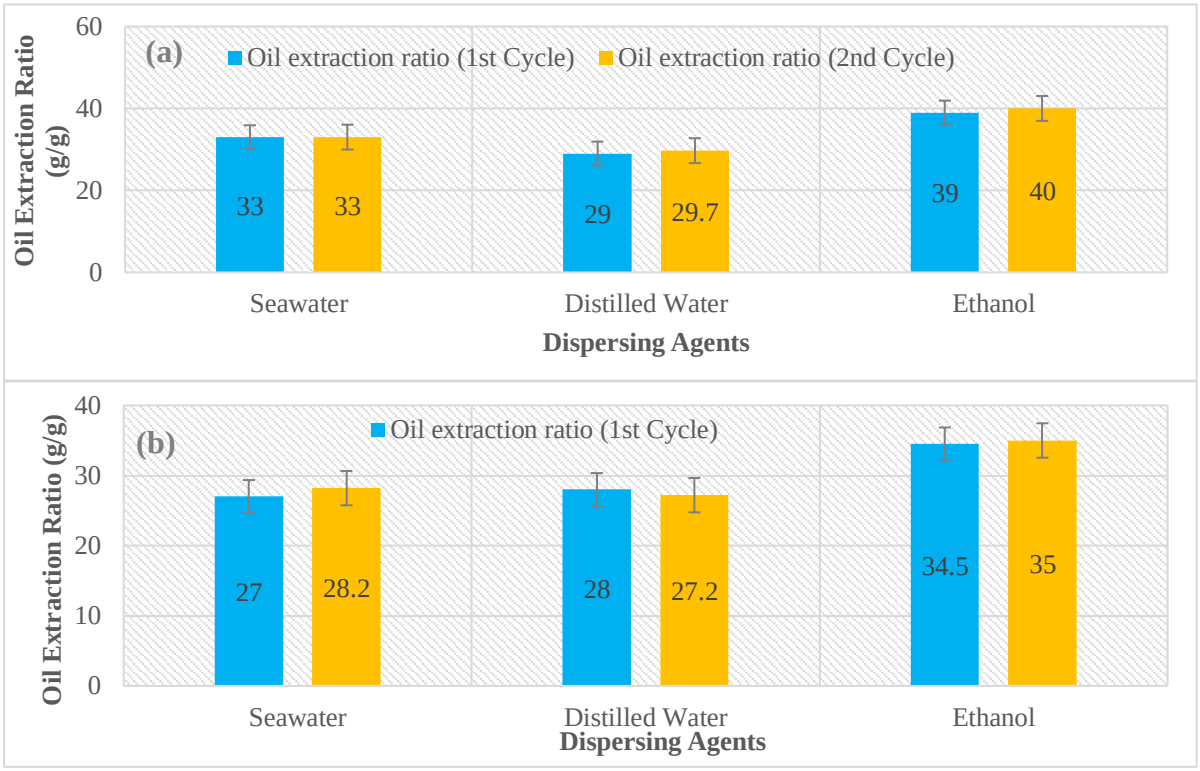

Figure 2: The performance of oil extraction in seawater, distilled water and ethanol using FNPs: (a) Engine oil (b) Mineral oil.

Table 3: Visual observation of engine oil extraction in (a) seawater (b) distilled water and (c) ethanol.

	Solution	Solution after addition of FNPs	FNP removal
(a) Seawater	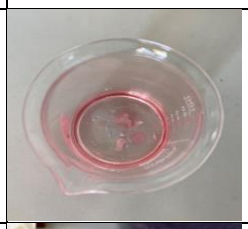		
(b) Distilled water			
(c) Ethanol	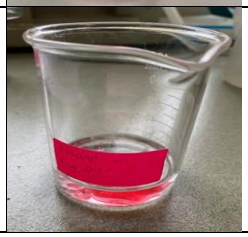		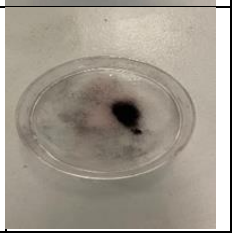

Table 4: Visual observation of mineral oil extraction in (a) seawater (b) distilled water (c) ethanol.

	Solution	Solution after addition of FNPs	FNP removal
(a) Seawater			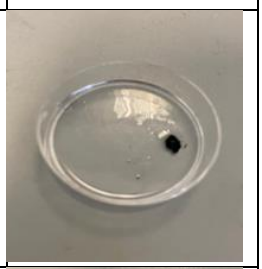
(b) Distilled water	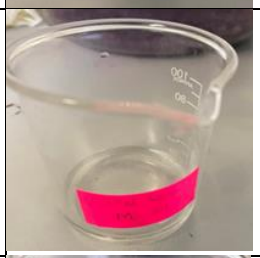	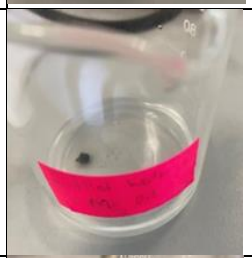	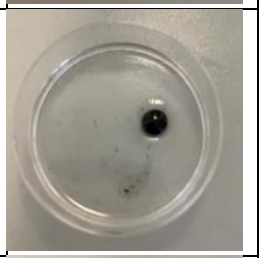
(c) Ethanol			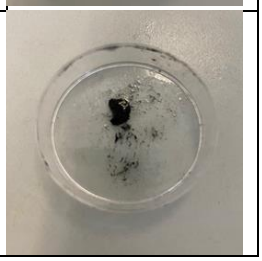

Figure 3 illustrates the oil extraction efficiency over two cycles for engine and mineral oils in seawater, distilled water and ethanol with FNPs. The efficiency exhibits a trend similar to the oil extraction ratios presented in Figure 2. Maximum efficiency was observed in ethanol, followed by seawater and distilled water for both engine and mineral oils. The efficiency of engine oil is better as compared to mineral oil in the dispersion medium seawater. The efficiency observed in the second cycle generally increased for both oils, demonstrating that the ferrofluid can be reused without compromising its oil collection performance. The iron oxide surface functionalised with PAPh exhibits superhydrophobic and lipophilic characteristics, making it suitable as a magnetic carrier. The findings confirm that oil recovery is achievable in seawater. Various methods have been employed to synthesise NPs, including co-precipitation, hydrothermal synthesis, ultrasonic bath, sol-gel and thermal techniques. In this study, the surface of the sorbent material was functionalised by treatment with PAPh, which facilitates the formation of a self-assembled monolayer (SAM) with ease. Core–shell NPs possess a large surface area and inherently exhibit superhydrophobic and lipophilic properties, rendering them excellent magnetic carriers. It has been established that phenyl phosphonic acid binds strongly to Fe_3O_4 nanoparticles, enabling high hydrocarbon extraction rates and reusability across multiple extraction cycles. This binding enhances the dispersibility of the nanoparticles in crude oil, facilitating their effective recovery from water.

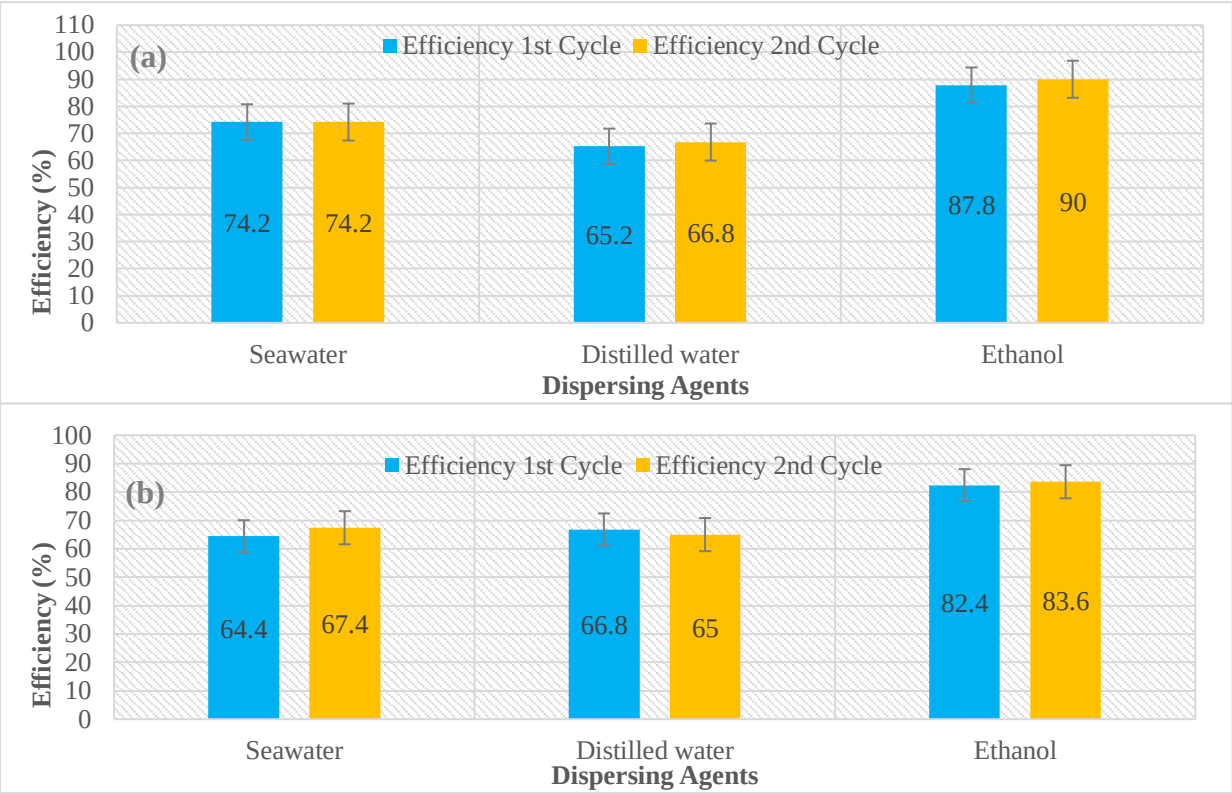

Figure 3: The efficiency of FNPs for oil extraction in seawater, distilled water and ethanol using FNPs. (a) Engine oil; (b) Mineral oil.

3.4 Effect of Oil Extraction Cycle of FNPs from Seawater

The oil extraction ratios for two successive cycles of engine and mineral oils are presented in Figure 4. The FNPs were extracted multiple times, confirming the formation of hydrocarbons around the oleophilic PAPh. The extraction efficiency for engine oil is greater than that for mineral oil. The increased extraction ratio is attributed to the significantly higher viscosity of the engine oil. Fe_3O_4-PAPh has been demonstrated to be an efficient sorbent material through extraction of more than two cycles. However, although various sorbent materials based on magnetic nanoparticles have been studied (Singh *et al*., 2020), data on the reusability of these sorbents, also referred to as cyclic use, have not been provided. Therefore, it can be inferred that the stability of such materials decreases over multiple extraction cycles. In the oil recovery process, it is essential to develop a sorbent with excellent reusability to enhance the efficiency of oil recovery from seawater. Figure 5 shows the corresponding oil extraction ratio over seven consecutive cycles, revealing that the ratio remains nearly constant throughout, ranging from 33 to 31.5 g/g. Only engine oil was selected for seven consecutive number of cycle due to finding in earlier part that engine oil performance is better than mineral oil. Eco-friendly magnetic ferrofluids synthesised using natural extracts of orange peel extract have shown the ability to be reused for at least five cycles in oil spill cleanup without significant loss in oil removal capacity, outperforming some commercial sorbents such as polypropylene (Ong *et al*., 2021). This observation indicates that the FNPs functionalised with PAPh can be utilised over multiple cycles without significant deterioration in oil extraction performance.

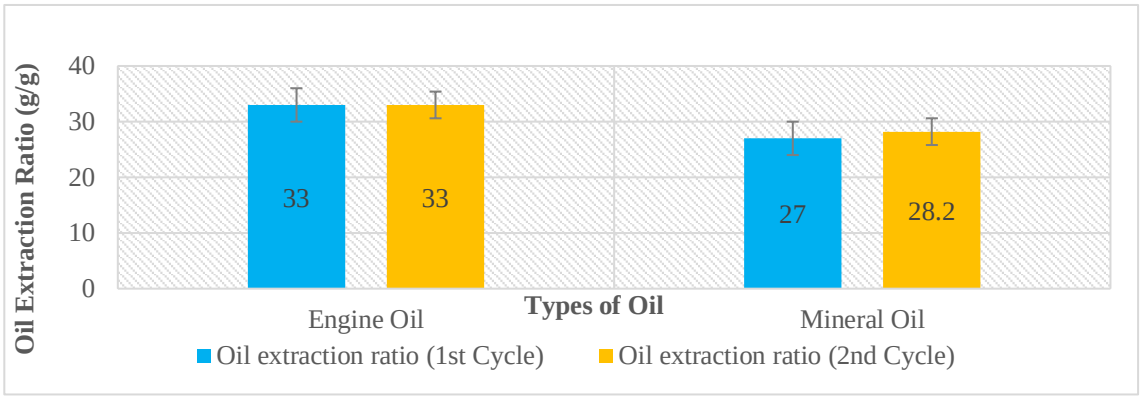

Figure 4: Oil extraction performance for engine oil and mineral oil from seawater.

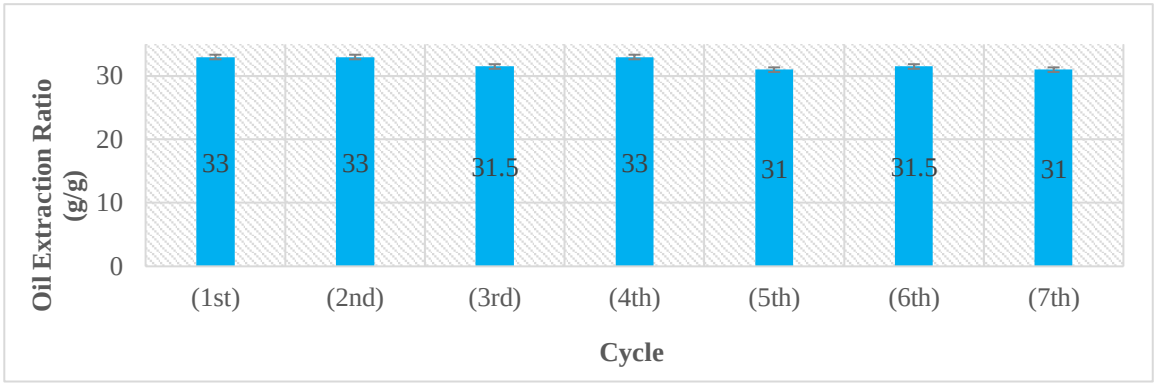

Figure 5: The performance of oil extraction cycles for engine oil.

3.5 Effect of FNP Mass on Seawater Uptake

The prepared FNPs were evaluated for hydrophobic behaviour by conducting water uptake experiments. The FNPs were added to a beaker containing seawater and subsequently extracted using a neodymium magnet. The experiment was performed with four different masses of FNPs: 10, 20, 30 and 40 mg. All the experiments were conducted at room temperature. Figure 6 illustrates the seawater extraction mass and ratio corresponding to the different FNP masses. The amount of seawater extracted was calculated relative to the mass of FNPs. It was recorded that 2 mg of seawater was extracted by 10 mg of NPs, whereas 2.1 mg of seawater was extracted by 30 mg of NPs. The seawater extraction ratios for 10 and 40 mg of NPs were 0.20 and 0.05 respectively, as shown in Figure 6. The extraction ratio of seawater decreases as the mass of NPs increases. The water extraction is attributed to the aperture effect, which clearly indicates a very low mass loss of water. Hence, the FNPs demonstrated their superhydrophobic nature in this observation. The linear regression analysis yielded a highly significant R^2 value of 0.9096, with the equation $y = -0.0041x + 0.2238$, indicating a decrease in seawater extraction ratio as the mass of FNPs increased.

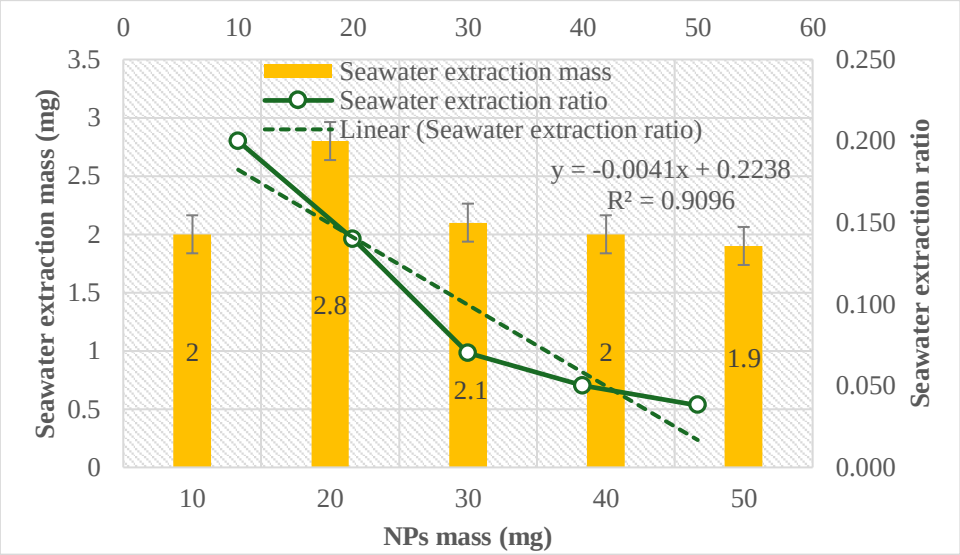

Figure 6: Seawater extraction mass and ratio.

3.6 Effect of FNPs on Microplastic Extraction

Table 5 presents the visual observations of various microplastic extractions using FNPs. The extraction of microplastics dispersed in seawater using FNPs without an oil base was conducted at room temperature. Various microplastics were selected, including polyphenylene ether (PPE), polyethylene terephthalate (PET), microfibres, and microbeads. FNPs containing 20 mg of Fe_3O_4 and Fe_3O_4-PAPh were dispersed in seawater and subsequently collected using a neodymium magnet. The seawater dispersed with various types of plastic became clear after extraction. The plastics were clearly attracted to the FNPs and were easily collected using the neodymium magnet. The amount of plastic extracted is shown in Figure 7. Both Fe_3O_4 and Fe_3O_4-PAPh FNPs exhibited strong affinity towards the microplastics, with microfibres demonstrating the highest extraction efficiency at 95.5%. This was followed by microbeads, PPE and PET, with efficiencies of 93.5, 89.3, and 78.3% respectively. The microplastic removal shows high efficiencies due to its stable properties of complete mixture of hydrocarbons (Hamzah *et al.*, 2021). A similar observation was reported earlier by Bui & Tran (2025), who also highlighted the role of ferrofluid stability in enhancing microplastic removal.

The FNPs functionalised with PAPh improved the colloidal stability and control the interparticle interaction. The phosphonic group (–PO(OH)2) strongly chemisorb onto metal oxide surface of FNPs. The phosphonic acid also suppresses agglomeration and enhance colloidal stability that essential in the synthesis of ferrofluid. The hybridisation of FNPs and phosphonic acid improved the responsiveness and performance of the ferrofluid in magnetic applications (Tufani *et al.*, 2025). The combination of phosphonic acid to FNPs form a stable ferrofluid that is suitable for other applications such as sensors, heat transfer and magnetic separation (Oehlsen *et al.*, 2022).

Table 5: Visual observation of various microplastic extraction using FNPs.

Types of microplastic	Solution before NPs addition	Solution after NPs addition	Solution after NPs extraction	Extracted NPs and microplastic
Extraction of polyphenylene ether (PPE)	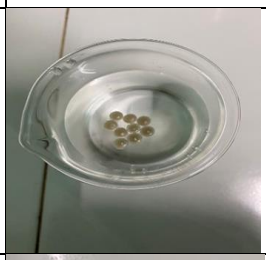			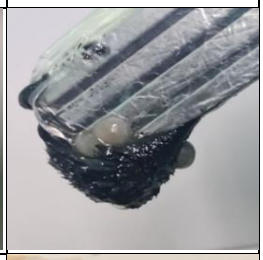
Extraction of Polyethylene Terephthalate (PET)				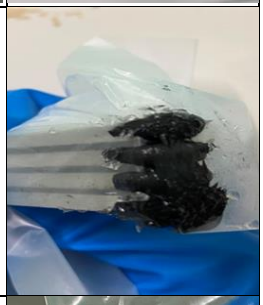
Extraction of microfibres				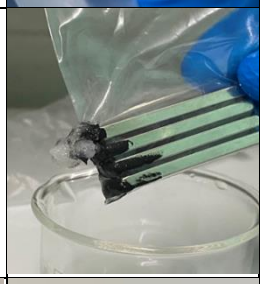
Extraction of macrobeads				

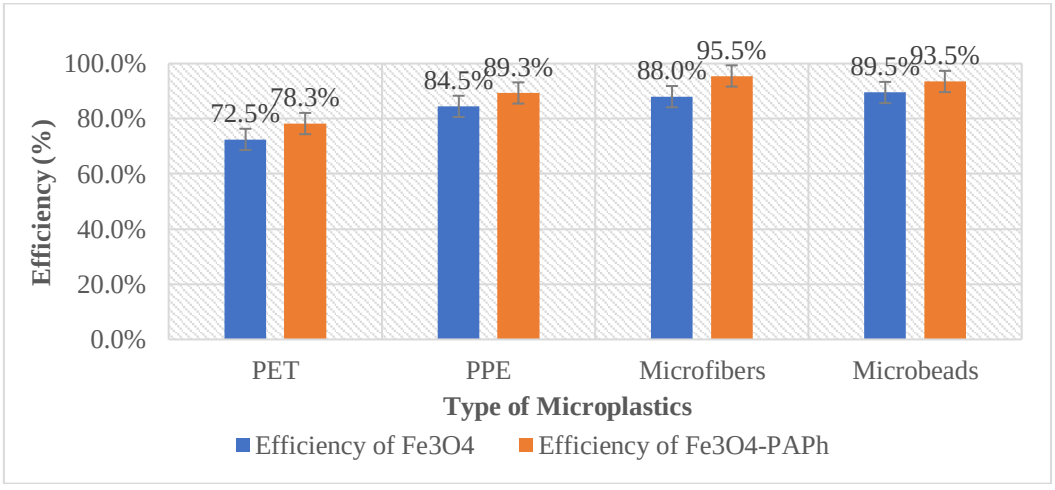

Figure 7: Microplastic extraction efficiency.

4. CONCLUSION

This paper presented the performance of newly prepared FNPs synthesised using PAPh. The surface of the sorbent material is functionalised with PAPh, which facilitates the formation of a SAM with ease. It was found that PAPh binds strongly to Fe_3O_4 nanoparticles, enabling high hydrocarbon extraction rates as well as reusability over multiple extraction cycles. The oil extraction experiments were conducted using different aqueous media, revealing that the type of dispersion medium can significantly impact oil extraction efficiency. Prior to the extraction experiments, it was essential to identify the optimum FNP, Fe_3O_4-PAPh. The ratio of NPs to PAPh of 5:1 was determined to be most suitable for oil extraction purposes. The presence of PAPh enhanced the removal efficiency of oil from seawater. Seawater as a dispersion medium exhibited superior sorption capacity compared to distilled water, demonstrating that the FNPs are effective for extracting and remediating oil spills in marine environments. This study successfully achieved oil extraction efficiencies of up to 90% in ethanol and 74.2% in seawater for mineral oil. The sorbent material maintained performance over six consecutive extraction cycles, with no significant decline in oil extraction efficiency observed after the seventh cycle. However, extraction efficiency varied notably between different oil types, with engine oil exhibiting better performance than mineral oil. Furthermore, the FNPs demonstrated effective microplastic extraction from seawater, achieving an efficiency of 95.5% for microfibres following functionalisation with PAPh.

These findings confirm that the FNPs address common challenges in oil spill remediation, namely low oil absorption capacity and limited reusability. Thus, this study has demonstrated that FNPs functionalised with PAPh produced stable ferrofluid with improved magnetic properties for oil spill and microplastic removal.

REFERENCES

Akbal, C. (2021). Removing oil spill from water by ferrofluid. *Open Sch. J. Open Sci.*, **4**:2.

Anand, U., Dey, S., Bontempi, E., Ducoli, S., Vethaak, A.D., Dey, A. & Federici, S. (2023). Biotechnological methods to remove microplastics: a review. *Environ. Chem. Lett.*, **21**: 1787–1810.

Bakhteeva, I.A., Medvedeva, I.V., Filinkova, M.S., Byzov, I.V., Minin, A.S., Zhakov, S.V., Uimin, M.A., Patrakov, E.I., Novikov, S.I., Suntsov, A.Y. & Demin, A.M. (2023). Removal of microplastics from water by using magnetic sedimentation. *Int. J. Environ. Sci. Technol.*, **20**: 11837–11850.

Bui, N.T. & Tran, T.D. (2025). Microplastic removal using CoFe2O4/SDS ferrofluid: Efficiency, reusability, and environmental impact. *Watershed Ecol. Environ.*, In press.

Che Ishak, I., Arof, A. & Zoolfakar, R. (2020). The Causes of the oil spill incidents: A review paper. *Int. J. Mech. Prod. Eng.*, **8**: 56-61.

Choudhury, A., Sarmah, R., Bhagabati, S.K., Dutta, R., Baishya, S., Borah, S., Pokhrel, H., Mudoi, L.P., Sainary, B. & Borah, K. (2018). Microplastic pollution: An emerging environmental issue. *J. Entomol. Zool. Stud.*, **6**: 340-344.

Ferreira-Dias, S., Valente, D.G. & Abreu, J.M.F. (2003). Comparison between ethanol and hexane for oil extraction from Quercus suber L. fruits. *Grasas y Aceites*, **54**: 378–383.

Hamzah, S., Ying, L.Y., Azmi, A.A.A.R., Razali, N.A., Hairom, N.H.H., Mohamad, N.A. & Harun, M.H.C. (2021). Synthesis, characterisation and evaluation on the performance of ferrofluid for microplastic removal from synthetic and actual wastewater. *J. Environ. Chem. Eng*, **9**: 1-8.

Ibrahim, G. (2024). Synthesis and evaluation on the performance of ferrofluid in wastewater treatment. *American Acad. Sci. Research J. Eng., Technol. Sci.*, **97**: 216–231.

Kamar, M.H., Ishak, I., Hassan, F., Yusoff, N.S., Idrus, M.A.M.M., Hamizi, N.A. & Saat, A.M. (2024). Evaluation of new green kapok and cogon fibre composite sorbent material for oil spill cleaning and recovery. *Adv. Struct. Mater.*, **215:** 271–281.

Kara, N., Erbaş, S. & Baydar, H. (2017). The effect of seawater used for hydrodistillation on essential oil yield and composition of oil-bearing Rose (Rosa damascena Mill.). *Int. J. Sec. Metabolite*, **4:** 482-487 .

Lei, J., Luo, Z., Qing, S., Huang, X. & Li, F. (2022). Effect of surfactants on the stability, rheological properties, and thermal conductivity of Fe3O4 nanofluids. *Powder Technol.*, **399**: 117197.

Mathew, J.T., Inobeme, A., Adetuyi, B.O., Adetunji, C.O., Popoola, O.A., Olaitan, F.Y., Akinbo, O., Shahnawaz, M., Oyewole, O.A., Eniola, K.I.T. & Yerima, M.B. (2024). General introduction of microplastic: Uses, types, and generation. In Mohd., S., Adetunji, C.O., Ahmad Dar, M. & Zhu, D. (Eds.), *Microplastic Pollution.* Springer Nature, Singapore, pp. 3–21.

Nizam, N., Mohanasunthar, S., Azmi, A.A., Anuar, S.T., Ibrahim, Y.S. & Khalik, W.M.A.W.M. (2023). Removal efficiency for micro-polystyrene in water by the oil-based ferrofluid employ response surface methodology. *Sains Malays*, **52**: 2191–2207.

Oehlsen, O., Cervantes-Ramírez, S. I., Cervantes-Avilés, P. & Medina-Velo, I. A. (2022). Approaches on ferrofluid synthesis and applications: Current status and future perspectives. *ACS Omega*, **7**: 3134–3150.

Ong, K., Yao, X., Yeap, P. & Song, Y. (2021). Synthesis of an Eco-friendly and Reusable Magnetic Ferrofluid using Orange Peel Extract for Oil Spill Cleanup. *The Stockholm Junior Water Prize 2021,* Stockholm, Sweden.

Pan, Y., Gao, S.-H., Ge, C., Gao, Q., Huang, S., Kang, Y., Luo, G., Zhang, Z., Fan, L., Zhu, Y., & Wang, A.-J. (2023). Removing microplastics from aquatic environments: A critical review. *Environ. Sci. Ecotech.* , **13**: 100222.

Beer, P.B (2015). The efficiency of using ferrofluid and magnets to remove oil spills from water. *California State Science Fair*, California, US.

Saper, A.A.M., Munaim, M.A., Azaim, F.Z.Z., Nasir, N.A., Zamanhuri, P.Z.N.M., Alaauldin, S., Mat, N.C., Ishak, I., Kamil, M.S., Ghazali, N., Hamizi, N. & Saat, A.M. (2024). Sea trial evaluation of kapok-sawdust as new green oil adsorbent in portable oil spill collectors. In Ismail, A., Zulkipli, F.N., Mohd Daril, M.A. & Ochsner, A. (Eds.), *Engineering Frontiers: A Multidisciplinary Odyssey.* Springer Nature Switzerland. pp 289–297.

Singh, B., Kumar, S., Kishore, B. & Narayanan, T. N. (2020). Magnetic scaffolds in oil spill applications. *Environ. Sci.: Water Res. Technol.*, **6**: 436–463.

Tuan Hoang, A., Viet Pham, V. & Nam Nguyen, D. (2018). A Report of Oil Spill Recovery Technologies. *Int. J. Appl. Eng. Res.* **13**: 4915-4928.

Tufani, A., Popov, N., Kovač, J., Čampelj, S., Mavrič, A., Landovský, T., Cigl, M., Vaňkátová, P., Loula, M., Novotná, V., Poberžnik, M., Herrero-Saboya, G., Martin-Samos, L., Mertelj, A. & Lisjak, D. (2025). Nonconductive ferrofluids from permanently magnetic nanoplatelets hybridized with polar phosphonic ligands. *Dalton Trans.*, **54**: 7906–7922.

Yang, M., Zhang, B., Xin, X., Liu, B., Zhu, Z., Dong, G., Zhao, Y., Lee, K. & Chen, B. (2022). Microplastic-oil-dispersant agglomerates in the marine environment: Formation mechanism and impact on oil dispersion. *J. Hazard. Mater.*, **426**: 127825.

Zahn, M., Hatton, T.A. & Khrushrushahi, S.R. (2012). Magnetic Colloid Petroleum Oil Spill Clean-Up of Ocean Surface, Depth and Shore Region. *U.S. Patent Application:* US 2012/0211428 A1.

SMART CHOICE APPLICATION: A DECISION SUPPORT APPLICATION FOR OPTIMIZING HANDHELD CHEMICAL DETECTOR SELECTION IN EMERGENCY SCENARIOS

Patrick Wengler[1*] & Andrea Malizia[2]

[1]Department of Industrial Engineering
[2]Department of Biomedicine and Prevention, University of Rome Tor Vergata, Italy

[*]Email: patrick.wengler@vo.lu

ABSTRACT

The urgent need to improve decision-making capabilities in the selection of chemical detection devices is driven by the necessity to mitigate the malicious use of chemical agents. In response, the Smart Choice application was developed to optimize the selection of handheld chemical detectors. The primary motivation for this application stems from the critical requirement for rapid and accurate chemical detection in scenarios involving chemical terrorism or accidental releases during natural hazard-triggered technological disasters (NATECH). Such situations necessitate swift and reliable detection technologies to safeguard human life and protect the environment. The Smart Choice application utilizes data on observed signs, odors and chemical identifiers to streamline the identification process, ensuring an efficient response to chemical incidents while enhancing safety measures. By integrating a comprehensive database with a user-friendly interface, this application represents a significant advancement in chemical incident management, addressing the challenges faced by first responders in hazardous environments.

Keywords: *Smart Choice application; handheld chemical detectors; chemical agent database; first responders; emergency response.*

1. INTRODUCTION

According to Gaulton *et al*. (2023), who surveyed chemical incidents from November 2014 to June 2020 via the global evidence-based surveillance (EBS) strategy, a total of 1,592 recorded chemical incidents occurred in 121 countries, involving 252 unique chemicals. Of these incidents, 97 were attributed to malicious or deliberate use, indicating criminal intent, while the majority of 479 incidents were linked to industrial accidents and the release of chemical agents at production facilities. Their analysis identified the most common chemicals involved in these incidents: (i) chlorine, which was present in 105 incidents, (ii) ammonia in 89 incidents, (iii) methanol in 86 incidents, and (iv) carbon monoxide in 47 incidents. For 525 incidents, the chemicals remained unidentified. Chlorine, ammonia and methanol are widely used in industry but are also associated with numerous major incidents involving chemical agents.

A chemical is deemed hazardous if it possesses high levels of toxicity, flammability and reactivity, leading to reactions that can harm organs and tissues. According to Guidotti *et al*. (2020), exposure to these hazardous substances can occur through inhalation, skin contact, ingestion or injection. Hazardous chemicals, such as toxic industrial chemicals (TICs), can be unintentionally released into the environment. Examples include petroleum products (such as gasoline and natural gas) and industrial substances (such as pesticides and chlorine). Chemical weapons, which are intentionally released, are often classified based on their effects on the human body. Nerve agents (such as SARIN, VX and VR) can enter the body through skin contact or inhalation, directly attacking the nervous

system. Lung irritants (such as chlorine and phosgene) are harmful when inhaled, causing significant damage to the respiratory system. Vesicants (such as mustard gas) damage the skin and can also affect internal organs if absorbed. The effects of exposure to hazardous chemicals can range from temporary illness or injury to permanent health issues or even death, depending on the severity and duration of the exposure (Hayoun *et al*., 2024). Therefore, early detection of these substances is critical for mitigating their harmful effects.

The evolving threat of chemical incidents, as highlighted by research from the University of Maryland's VNSA CBRN database (Sim & Binder, 2022), underscores the importance of providing first responders with basic information about the chemicals that they may encounter. This knowledge is crucial not only for selecting the correct decontamination procedures and personal protective equipment (PPE), but also for accurately assessing the scene, preventing cross-contamination, and avoiding incorrect chemical identification, which are errors that could have significant consequences. These outcomes can be mitigated through the use of appropriate detection technologies. First responders with even basic knowledge of CBRN / HAZMAT protocols can quickly and effectively communicate vital information, even with minimal training, ensuring that the correct action plans and detection devices are chosen. The integration of a smart application for handheld chemical detectors would enhance this process. Such an application could suggest suitable detection equipment and provide a list of potential chemicals based on initial data inputs. This information could later serve as evidence, with screenshots added to the chain of custody to support the investigation.

Chemical agents, if weaponized for terrorist purposes, can cause extensive harm to populations and infrastructure. These materials can be used to create conventional weapons, enhance explosives or develop advanced munitions. Keeping detailed records during an incident is essential, whether the event is an accident, a natural hazard triggering technological disasters (NATECH) or a terrorist attack. Early access to accurate information can greatly assist in building a legal case and determining the appropriate protective measures for first responders (Santella & Steinberg, 2023).

The early detection of chemical agents is critical in preventing further incidents. One historical example is World War I, often referred to as the "chemical war," where chemical agents were used but modern detection and protection equipment were unavailable (Gaulton & Cole, 2011). Early detection systems had to be developed to mitigate the damage. Today’s technologies cover a wider spectrum, including toxic industrial chemicals, thanks to advancements in detection capabilities. Despite the evolution of detection tools, lessons from World War I remain relevant. For instance, early methods involved identifying chemical agents such as sarin, sulphur mustard, and chlorine through smell or taste (Garcia *et al*., 2011). Though the extent of detection technology during the war was not well documented, some argue that these sensory-based methods marked the beginnings of portable detection systems. The "Geruchsproben Test" (odor test) developed by Switzerland is a potential example of one of the earliest field detection tools (Figure 1).

Personal observations during the research revealed that even specialized units occasionally selected incorrect detection equipment, complicating chemical identification. In order to address this, a survey was conducted among first responders to assess their interest in a mobile application that could guide the selection of appropriate detection tools. As shown in Figure 2, the respondents overwhelmingly supported the idea, recognizing its potential to enhance operational effectiveness. These insights have driven further development of the Smart Choice Application to help first responders make informed decisions during chemical incidents. This application is designed to function independently of specific computer systems, making it versatile and dependable in a range of situations.

2. CHEMICAL AGENT DETECTION

The threat posed by chemical agents remains a significant concern due to their continued use in industry and the potential for misuse, even in today's world (Binder & Ackerman, 2023). Despite global regulations and efforts to eliminate chemical weapons, these substances remain accessible, posing risks

to both human health and the environment. This ongoing threat underscores the critical need to equip first responders, such as firefighters, law enforcement, military personnel and healthcare workers, with the necessary tools and knowledge to effectively detect and monitor chemical agents.

Figure 1: "Geruchsproben Test" developed by Switzerland during World War I (Courtesy of the author).

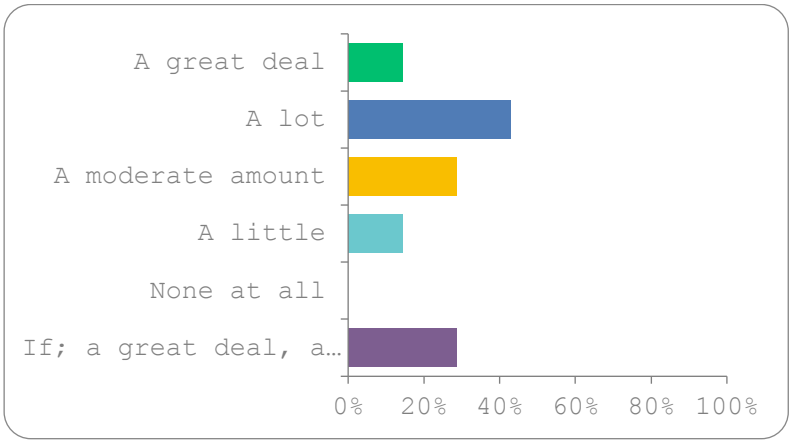

Figure 2: Survey results on the usefulness of an application for selecting detection tools during chemical incidents.

Detection capabilities are essential for identifying hazardous substances, assessing contamination levels, understanding exposure risks, and ensuring proper decontamination and personal protection. While a variety of detection systems are available, ranging from cost-effective to advanced technologies, it is crucial to select the right equipment based on the specific risks and responsibilities of responders (Fish *et al*., 2011). Factors such as weather conditions, and the chemical properties of the agents should also be considered when choosing detection technologies. Ultimately, the goal is to safeguard lives by efficiently detecting, decontaminating and investigating incidents involving chemical agents. This necessitates not only the right equipment but also the expertise and experience to utilize these tools effectively, allowing responders to operate safely in contaminated environments.

The Smart Choice application for chemical handheld detectors will rely on the effectiveness of its database, which significantly influences the selection of detection technology. Initially, the database focused on chemical warfare agents, with plans to expand to include other chemical agents and detectors

in the future. The first prototype of the database was developed based on identified threats from incidents, terrorism and NATECH events. It was constructed using various sources, including NIOSH (2005), DOT (2024), FEMA (2024) and NRT (2024). While the database currently lacks some toxic industrial chemicals, there are plans for future additions.

The parameters included in the database were meticulously reviewed and benchmarked against literature, scientific papers and other relevant documents. This selection process aims to ensure that the database supports the optimal choice of handheld chemical detectors for various situations and locations, enhancing the software's search and prediction capabilities. One of the major outcomes of the research was the recommendation to consider three different technologies to avoid false positives, as illustrated in Figure 3.

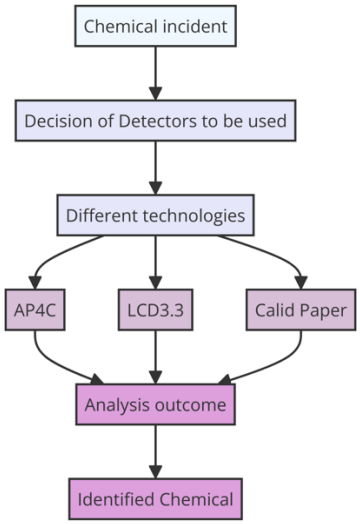

Figure 3: Detection principles for identifying chemical agents using three different technologies as an example.

In the field of chemical warfare, the detection of chemical agents is crucial for ensuring the safety and security of populations. While technological methods for detection are commonly utilized, the sense of smell can also be important in identifying the presence of chemical agents. However, since no technology exists that detects chemical agents based solely on smell, this factor cannot be incorporated into benchmarking processes. In order to enhance detection capabilities, certain detectors combine vapor and aerosol detection methods. Multi-sensor detectors equipped with various sensors, such as ion mobility spectrometry (IMS), photoionization detectors (PID) and flame ionization detectors (FID), provide comprehensive coverage for identifying chemical threats in diverse scenarios. These detectors are illustrated in Figure 4, which highlights their functionality and emphasizes the use of three different detection technologies, as shown in Figure 3.

Table 1 summarizes the numerical data obtained from the theoretical benchmarking of the detectors based on available information. It is essential to note that these results may vary depending on the detector's library and intended application. Additionally, discrepancies may arise due to the limited information available regarding the detection capabilities of many chemicals as compared to those of the detectors.

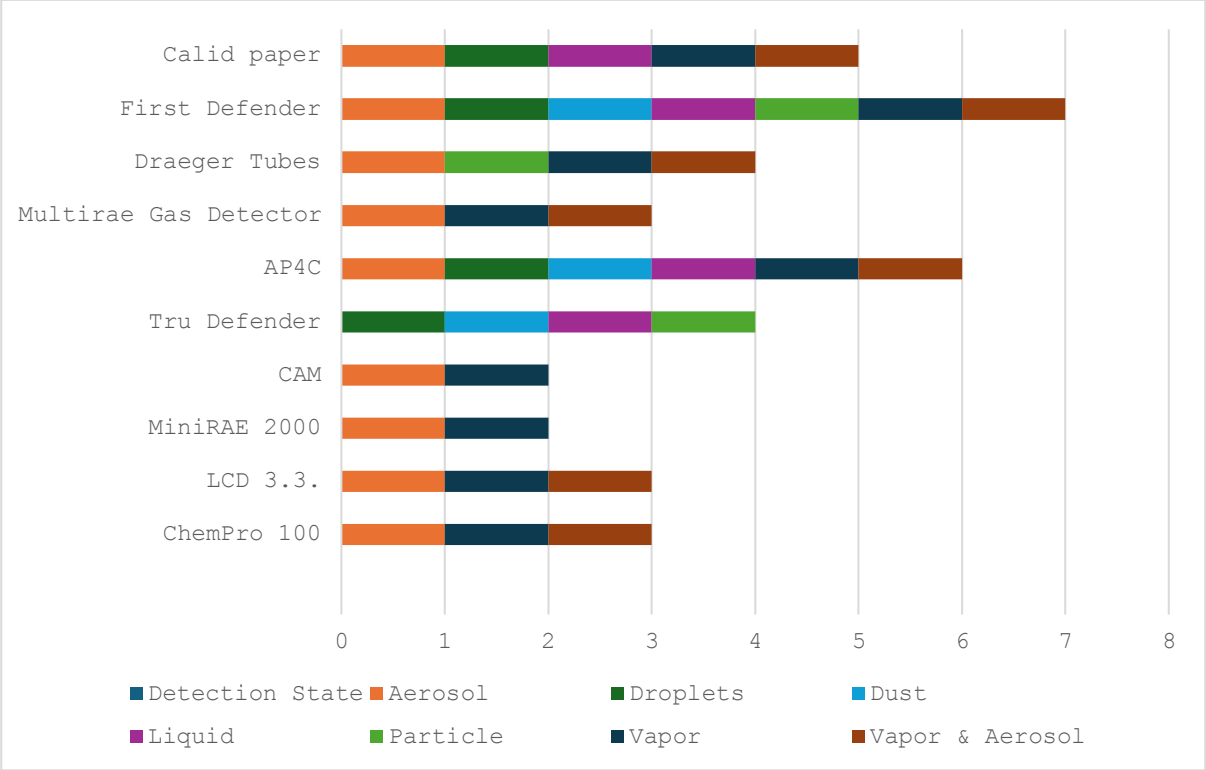

Figure 4: Detection functionalities of various detectors after benchmarking.

Table 1: Results from Figure 4 detailing the number of different chemicals each specific detector can identify based on the conducted benchmarking.

Handheld Detector	Number of Chemicals Measured
ChemPro 100	22
LCD 3.3	10
MiniRAE 2000	14
CAM	8
Tru Defender	62
AP4C	17
Multirae Gas Detector	9
Draeger Tubes	11
First Defender	8
Calid paper	6

3. SMART CHOICE APPLICATION: A DECISION SUPPORT APPLICATION FOR HANDHELD CHEMICAL DETECTOR SELECTION

Stage 1: In the aftermath of a chemical incident, the initial response is crucial in determining the severity of the situation and the appropriate course of action. Stage 1 of the response process involves the operator, if available, using the application to select observed signs and symptoms on the scene. This step is essential for narrowing down potential chemical agents and guiding the choice of detection equipment. The application's ability to quickly and accurately process this information can significantly enhance the effectiveness of the response via its main interface, as shown in Figure 5.

Stage 2: In this stage of the response process, the operator selects any odors detected at the scene, which can provide vital clues about the presence and type of chemical agents involved. The application allows the operator to input specific smells, such as a scent resembling almonds, garlic, rotten eggs or other distinct odors. By documenting these olfactory cues, the operator can further narrow down the possible chemical agents, assisting in the selection of appropriate detection tools and safety measures. This step is crucial for confirming initial assessments and ensuring a more targeted response to the incident.

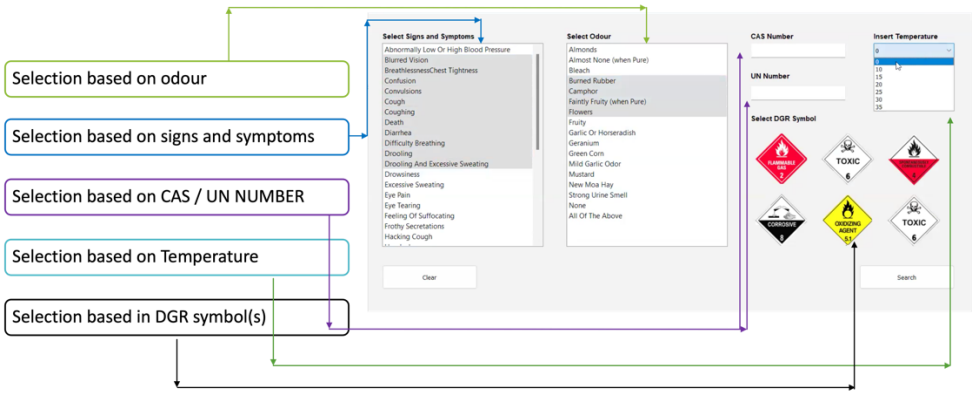

Figure 5: Main interface for the selection of chemical handheld detectors.

Stage 3: If no other clues are present, the operator has the option to enter the Chemical Abstracts Service (CAS) number if it is available. The CAS number serves as a unique identifier for specific chemical substances, providing a precise way to identify the chemical agent involved in the incident. By entering this number into the application, the operator can quickly access information about the substance. This step allows for a more accurate and efficient response, enabling the first responders to tailor their actions to the specific chemical present, thereby enhancing safety and effectiveness during the incident.

Stage 4: The operator may input the United Nations (UN) number if it is available. The UN number is a four-digit code used to identify hazardous materials during transportation, providing crucial information about the chemical or substance involved. By entering this number into the application, the operator can instantly access information on the substance present. This step enhances the precision of the incident assessment, allowing first responders to make well-informed decisions regarding containment, decontamination and safety measures tailored to the identified chemical.

Stages 3 and 4 can be entered without having to select Stages 1 and 2.

Stage 5: The operator selects the appropriate dangerous goods (DGR) symbol that corresponds to the chemical or substance involved in the incident. These symbols provide visual warnings of the specific hazards associated with the material, such as flammability, toxicity, corrosiveness or environmental dangers. If only the DGR symbol is selected, the application will provide a complete listing of all the chemicals in the database sharing this specific property, as can be seen in Figure 6 when selecting only flammable agents.

Figure 6: Outcome of the research criteria, displaying the DGR symbol for flammable chemicals present in the application.

Stage 6: The operator selects the current temperature at the scene, a crucial factor that influences the behavior of chemicals. Temperature can significantly impact the physical state and volatility of a chemical, determining whether it remains stable, vaporizes or undergoes other changes. By inputting the temperature into the application, the operator can account for these effects, which are vital for choosing the most effective detection equipment. Understanding how temperature affects a chemical's consistency and vapor production allows the response team to make more accurate decisions, ensuring that the selected detection methods are suited to the conditions and reducing the risk of exposure to hazardous vapors.

4. APPLICATION RESULTS

Upon completing the input stages, the application processes the collected data to generate tailored recommendations on which detectors are most suitable for identifying the specific chemical agents involved in the incident. The results presented by the application are designed to guide first responders in selecting the optimal detection equipment, ensuring a more accurate and effective response. As shown in Figure 7, the application identifies detectors that are well-suited for the chemical properties and conditions provided, while also indicating which detectors might be less effective or unsuitable for the task.

Figure 7: Results of the application's recommendation process.

Despite the thoroughness of the process, the application is designed to provide a broad range of possible chemicals, especially in situations where the input data from the first responders is limited or incomplete. This feature is crucial for ensuring that all potential threats are considered, even when specific details are unclear. As illustrated in Figures 6 and 7, the application's ability to generate a wide range of possible chemical matches ensures that first responders are prepared for various scenarios, reducing the risk of overlooking a hazardous substance and choosing the right handheld detector.

5. CONCLUSION

The Smart Choice application enhances the precision of detector selection by utilizing a robust database of chemical agents. When specific data, such as a CAS or UN number, is entered, the application accurately identifies the corresponding chemical and supplies comprehensive details, such as the appropriate detectors to use and the chemical's parts per million (ppm) levels at varying temperatures.

The results serve as a critical tool for first responders, offering informed recommendations on which detection equipment to use based on the chemical and environmental data provided. By allowing for ongoing updates to the database and providing a comprehensive range of possible chemical agents, the application ensures that responders are equipped with the best possible guidance in real-time. This capability not only enhances the safety and effectiveness of their response but also ensures that they can adapt to the ever-changing landscape of chemical threats.

Moreover, the Smart Choice application is designed to operate independently on any computer with the necessary software installed, all of which is freely available. This functionality means that the application can be used without an internet connection, increasing its versatility and practicality in field operations. The application runs through a Python script that can be executed via the terminal, as long as the main program is installed on the device. This offline capability, combined with the use of readily available software, makes the Smart Choice application a practical and effective tool for first responders in various emergency situations.

In summary, the Smart Choice application, with its extensive chemical database, potential Globally Harmonized System of Classification and Labelling of Chemicals (GHS) symbol integration, and offline operability, provides a powerful resource for first responders. It supports quick, informed decision-making, ensuring safety and efficiency in handling chemical incidents.

REFERENCES

Binder, M. & Ackerman, G. (2023). *CBRN Terrorism.* Available online at: https://oxfordre.com/internationalstudies/view/10.1093/acrefore/9780190846626.001.0001/acrefore-9780190846626-e-706 (Last access date: 9 October 2024).

DOT (US Department of Transportation) (2024). *Emergency Response Guidebook*. US Department of Transportation (DOT), Washington DC, US.

FEMA (Federal Emergency Management Agency) (2024). *Chemical Warfare Agents*. Available online at: https://www.fema.gov/oet-tools/chemical-incident-consequence-management/3/2 (Last access date: 16 June 2024)

Fish J., Stout R. & Wallace E. (2011) *Practical Crime Scene Investigation for Hot Zones: The Equipment*. CRC Press, Florida, US.

Garcia, A.F., Rand, D. & Rinard, J. (2011). *IHS Jane's CBRN Response Handbook*. IHS Global, Limited, London, UK.

Gaulton, T., Hague, C., Cole, D., Thomas, E. & Duarte-Davidson, R. (2023). Global event-based surveillance of chemical incidents. *J. Expos. Sci. Environ. Epidemiol.*, **33**: 111–117.

Guidotti, M., Ranghieri, M. & Econdi, S. (2020). Detection, identification and monitoring of chemical warfare agents: A comparison between on-field and in-field lab approach. *In:* Sindona, G.,

Banboub, J.H. & Di Gioia, M.L. *(Eds.) Toxic Chemical and Biological Agents, Detection, Diagnosis and Health Concerns*. Springer, Moordrecht, Netherlands, pp. 235-238.

Hayoun M.A., Ausman C., Yarrarapu S.N.S & Swoboda, H. (2024). *Toxicology, V-Series Nerve Agents*. StatPearls Publishing, Treasure Island, Florida, US.

Melnikova, N., Wu, J., Yang, A. & Orr, M. (2018). Acute chemical incidents with injured first responders, 2002-2012. *Disaster Med Public Health Prep.*, **12**:211-221.

NRT (National Response Team) (2024). *Guidance, Technical Assistance and Planning; Hazards (Oil, Chemical, Radiological, etc. Chemical*. Available online at: https://www.nrt.org/Main/Resources.aspx?ResourceType=Hazards%20(Oil,%20Chemical,%20Radiological,%20etc)&&ResourceSection=2&Category=Chemical (Last access date: 9 July 2024).

NIOSH (National Institute for Occupational Safety and Health) (2005). *Pocket Guide to Chemical Hazards*. NIOSH Publications, Cincinnati, US.

Santella, N., Steinberg, L. J. (2011). *Accidental releases of hazardous materials and relevance to terrorist threats at industrial facilities. Emergency*, **8***: 53.*

Sim, S. S. & Binder, M. K. (2022). *Violent Non-State Actor Chemical, Biological, Radiological, and Nuclear (VNSA CBRN) Event Database, Version 1.0, Unconventional Weapons & Technology Division (UWT), Maryland: National Consortium for the Study of Terrorism and Responses to Terrorism (START). Asymmetric Threats Analysis Center (ATAC)*. University of Maryland. College Park, Maryland, US.

UNICRI (United Nations Interregional Crime and Justice Research Institute) (2023). *A Prosecutor's Guide to Chemical and Biological Crimes, 201-208*, United Nations Interregional Crime and Justice Research Institute (UNICRI), Turin, Italy.

PHYSIOLOGICAL ISSUES IN MILITARY UNIFORMS

Nik Nur Ilyani Mohamed Nazri*, Nur Shairah Zolhani & Nur Aisyah Aziz

BTWC and Antidote Unit, Chemical and Biological Defence Technology Division, Science and Technology Research Institute for Defence (STRIDE), Ministry of Defence, Malaysia

*Email: nikilyani.nazri@stride.gov.my

ABSTRACT

Military uniforms face several complicated physiological challenges that necessitate innovative solutions to increase troop comfort, health and operational performance. One of these challenges is heat stress and cooling, where troops may encounter dehydration, decreased mental and physical performance, potentially lethal heat-related diseases, all of which are made worse by the protective equipment they wear. Another crucial issue is moisture management, as improper sweat management can cause pain, skin rashes and other heat-related illnesses that can interfere with a soldier's ability to perform his or her tasks. In order to ensure that soldiers are not hindered by physical discomfort during their duties, these issues need to be resolved. The optimal management of weight and mobility in uniforms and equipment also presents a significant challenge. Maintaining military mobility, avoiding strain, tiredness and impaired endurance depends on determining the delicate balance between safety, functionality and equipment weight. To lessen the overall burden carried by soldiers, significant expenditures have been made in research and development projects utilising lightweight materials and ground-breaking design ideas. Another complex issue with military clothes is physical defence against illnesses. Soldiers are routinely deployed to areas where there are serious disease dangers, necessitating detailed plans that consider uniform design components. Other than the uniform itself, developing good hygiene habits and instructional programmes have become crucial parts of this effort to support troop health in general. Innovative solutions have emerged in response to these numerous obstacles. Thermal-regulated materials have been carefully designed to maximise body temperature and moisture management, ensuring soldier comfort under a variety of environmental demands. Another significant development is water-repellent coatings, which improve military performance and safety in adverse weather. On the other hand, the introduction of ergonomic design signals a paradigm shift by prioritising the soldiers' comfort and mobility, while maintaining their level of protection. In order to continuously inhibit the transmission of hazardous microorganisms, antimicrobial textiles have ushered in a new era of ensuring troop health. In conclusion, these innovative solutions collectively reflect a revolutionary evolution in the modern world military uniform.

Keywords: *Military uniforms; heat stress and cooling; moisture management; military mobility; advanced textile technology.*

1. INTRODUCTION

Military uniforms are subjected to numerous physiological challenges during routine operations. Physiology refers to the processes and functions of the human body and its various systems (Lemoine & Pradeu, 2018). It involves studying bodily functions, considering components such as cellular processes, organ function and the regulation of physical activities (Amiri *et al.*, 2022). In the context of military service, physiological challenges refer to issues affecting the physical well-being and performance of personnel. Military personnel are often described as “tactical athletes” due to the requirement to perform a wide range of demanding physical and mental tasks under pressure, including maintaining physical fitness, managing fatigue and coping with the physiological effects of strenuous activity (Flood & Keegan, 2022).

However, these physiological issues are linked to human factors that should be taken into account while creating military clothes. Optimising the performance, safety and well-being of military personnel in various operating and training environments requires the study and implementation of ideas from various sources, including engineering, psychology and others. This is to guarantee that military uniforms are standardised, with unique styles of clothing that set them apart from civilians (Krueger, 2014). One of the examples of human factors that needs to be considered is body armour. Body armour, such as protective vest, needs to be designed so as not to burden the users. This is because some of these vests have heavy ceramic protection plate inserts, which not only significantly increase the load each soldier carries but also tend to limit mobility and impair vital biological functions (Basak *et al*., 2020). Thus, these human factors should be considered to ensure that military personnel can perform their duties effectively. The human body must regulate its temperature, prompting various researchers to suggest using wearable technology and artificial intelligence to measure human comfort in real-time. This is because insufficient thermal comfort can lead to health issues and reduced workplace productivity (Farooq & Zhang, 2021).

Though the human body can regulate its temperature through thermoregulatory processes such as muscular contraction, sweat glands functioning, blood vessel constriction and dilatation (Zhang, 2001), heatstroke, hypothermia and pain can occur from sudden temperature fluctuations brought on by strong sunshine, rain or storms, since the skin is susceptible to these extreme conditions (Yeo, 2004). Multiple methods may be used to fabricate enhanced personal thermal garments based on the heat transmission mechanism. For instance, in colder areas, heat transmission from people to their surroundings can be minimised through thermal conduction and convection. Additionally, wearers can benefit from the creation of innovative materials that reflect thermal radiation to them. On the other hand, novel materials may also be produced to improve the body's natural ability to transmit heat and convection to the surrounding air (Farooq & Zhang, 2021).

This is necessary to ensure that their cognitive function is excellent because military personnel face unique cognitive challenges, such as tasks that require intense physical and mental tiredness, high levels of worry and stress, as well as highly unpredictable environments (Campbell & Nobel, 2009). These tasks demand sustained attention and rapid information processing, requiring high levels of cognitive ability (Amiri *et al.,* 2022). One of the physiological factors that influences cognitive performance is aerobic, hence the physiological issues regarding the military uniform need to be addressed as there is a relation to their cognitive performance (Martin *et al.,* 2020).

It is essential to fully recognise and understand the unique physiological challenges faced by military personnel when wearing uniforms. A thorough assessment of these issues serves as the foundation for developing effective, specialised solutions that address and resolve uniform-related concerns. By examining the intricate aspects of these physiological factors, more sophisticated and efficient responses can be formulated to optimise comfort, functionality and overall health of military personnel in uniform.

2. TYPE OF PHYSIOLOGICAL ISSUES

2.1 Heat and Stress Cooling

Military personnel face numerous challenges and unpredictable conditions in the course of their duties, many of which pose significant threats to their well-being and even their lives (Alele *et al.,* 2020). One particularly daunting challenge arises when personnel are exposed to elevated temperatures, a scenario exacerbated by the necessity of wearing bulky protective gear and uniforms during training exercises or operational missions (Parsons *et al.,* 2019). This exposure increases the risk of developing exertional heat stroke (EHS), a condition characterised by the body's core temperature rising to dangerous levels due to an inability to effectively dissipate heat (Hunt *et al.,* 2016). Exertional heat stroke occurs when the body's mechanisms for regulating temperature become overwhelmed, leading to an imbalance between the heat generated during physical exertion and the body's capacity to cool itself down (Jardine,

2007). The progression of this condition can manifest in various stages, starting with mild symptoms such as muscle cramps and advancing to heat exhaustion, ultimately culminating in the potentially fatal state of heat stroke (Périard *et al.*, 2022).

In a normal homeothermic organism like humans, the body maintains a tightly regulated internal temperature, typically around 37 °C when at rest in moderate conditions (Cramer & Jay, 2016). When exposed to heat, the body employs various physiological mechanisms, including dilating blood vessels in the skin and sweating, to dissipate heat and prevent overheating (Leon & Helwig, 2010). However, these thermoregulatory processes can become overwhelmed, especially in the context of strenuous physical activity and heavy clothing or gear combined with environmental factors can impede the body's ability to lose heat efficiently; hence, the core body temperature will soar uncontrollably (Chen, 2023). While a moderate increase in core temperature (1 to 2 °C) is usually manageable, a more substantial rise (4 to 5 °C) can have severe health consequences (Leon & Bouchama, 2015).

The physiological challenges associated with heat exposure significantly impact the ability of military personnel to perform their duties comfortably and effectively (Buller *et al*., 2021) This issue is particularly pertinent in military operations that require deployment to hot environments for missions such as disaster relief, often with minimal notice, sometimes as little as 12 h (Knapik *et al.*, 2012). Exertional heat stroke is one such heat-related condition that can develop in these contexts, and it poses a serious threat as it is a life-threatening emergency characterised by a dangerous elevation in the body's core temperature that overwhelms the normal thermoregulatory mechanisms (Donham *et al*., 2020). In such scenarios, there is limited opportunity for adequate heat preparation, heightening the importance of implementing strategies to mitigate the adverse effects of heat at both the environmental and individual levels (Ashworth *et al.*, 2020). Moreover, the combination of the physical demands of military duties, heavy protective equipment and extreme environmental conditions can create a situation rife with risk for the development of exertional heat stroke among military personnel (DeGroot *et al.*, 2022).

Addressing these challenges necessitates a multifaceted approach that encompasses environmental modifications, such as providing adequate shade and hydration stations, as well as individual interventions, including pre-mission acclimatisation protocols and specialised gear designed to enhance heat dissipation (Lucas *et al.*, 2014). Moreover, comprehensive training programmes can educate military personnel on recognising the signs of heat-related illnesses and implementing appropriate preventive measures (Moore *et al.*, 2015). By proactively addressing the risks associated with heat exposure, military organisations can safeguard the health and performance of their personnel, ensuring they remain resilient and capable of fulfilling their duties even in the most demanding environmental conditions (Ashworth *et al.*, 2020).

2.2 Moisture Management

Moisture management is one of the physiological issues in military uniforms (Yunusxodjaeva *et al.*, 2024). Poor moisture control can make it difficult for soldiers to perform their duties effectively and, in certain situations, even jeopardise their health. In military clothing, managing moisture involves addressing both internal liquids such as perspiration and external ones such as rain (Gibson *et al*., 2013). Consequently, these textiles may encounter difficulties as it can become heavy, clingy and unbreathable. This can lead to a significant decline in the wearer's comfort and performance (Basuk *et al*., 2018). Furthermore, maintaining effective moisture management in military uniforms is essential because soldiers' tasks often entail high levels of physical exertion in challenging environments (Revaiah *et al*., 2020).

In view of this, military uniforms should be breathable in hot environments since sweat can trap heat near the body and cause overheating if it is not adequately drained away from the skin. This is due to the fact that effective moisture management, in this case, sweating, helps to control body temperature

(Ogden *et al.*, 2022). However, moisture management is also important in cold environments as it can reduce hypothermia incidences. Hypothermia is a medical condition characterised by dangerously low body temperature, typically below 35 °C. It occurs when the body loses heat more rapidly than it can produce, causing the core temperature to drop to a level where normal bodily functions become compromised (Duong & Patel, 2022). It is necessary to address the issue of moisture management in military uniforms to ensure that military personnel are appropriately attired for ease and safety while performing their demanding and vital responsibilities. According to Santee *et al.* (2020), it may be hypothesised that only evaporative loss is thermo-physiologically significant, as only evaporated sweat modifies heat exchange with the environment, even if sweat retained in clothing may increase skin moisture and affect comfort perception.

In low heat flux situations, internal moisture retards heat penetration and vaporisation occurs, allowing water vapour to enter the clothing and its air spaces. In high external radiant heat flux situations, moisture within these air layers facilitates heat penetration, with vapour tending to condense on the skin surface (Taylor & Patterson, 2016). These factors have given rise to several active and passive moisture management techniques that may aid in limiting heat storage to physiologically compensable levels. However, the majority of military soldiers have no choice but to rely on certain textiles' ability to absorb perspiration from the skin's surface so that evaporation may take place elsewhere (Yunusxodjaeva *et al.*, 2024).

2.3 Weight and Mobility

The challenges faced by military personnel extend beyond the realm of heat exposure to encompass issues related to mobility and operational efficacy, often exacerbated by the weight and design of their equipment and uniforms. Heavy equipment, coupled with uniforms made of dense materials, can impose significant physical strain, leading to fatigue, reduced endurance and limitations in mobility (Joseph *et al.*, 2018).

It is a well-known fact that increased weight has a significant impact on the mobility of military personnel. While traversing difficult terrains such as rocky mountains, high-altitude regions, arid deserts and dense jungle landscapes, these soldiers are required to carry substantial burdens over considerable distances (Bhattacharyya *et al*., 2024). For instance, during military operations, U.S. Army infantrymen and U.S. Marines routinely carry combat loads that range from 36 to 54 kg (Krueger, 2014). These soldiers operate in environments that are diverse and demanding. As a result, soldiers face significant physical demands during their missions, which can have far-reaching consequences (Halvarsson *et al*., 2019).

This hypothesis is supported by the high occurrence of fractures from overuse injuries, ligamentous damage, skin blisters and associated neurological impairments due to load carriage in military uniforms (Orr *et al.*, 2021). One common sequel of long-term load carriage is the stress or fatigue fracture, occurring when normal bone remodelling balance between osteoclastic removal and growth of new secondary tissue metabolically outstrips available calcium supply to compensate (Knapik *et al.*, 2012). Stress fractures, in military contexts, in areas such as the pelvis, tibia, calcaneus and metatarsals, cause serious impediments to operational readiness of military units (Walsh *et al.*, 2021).

The rate of uniform-related load carriage injuries highlights the critical nature that maintaining mobility must take as a priority for military forces (Carlton & Orr, 2014). This means that uniforms and equipment will be continuously improved to ensure they allow for fluid movement, which can quickly adapt to the rapid transformations of the battlefield in a moment. Developing adequate levels of protection, functionality and mobility continues to be a challenge to optimise the operational effectiveness whilst maintaining the physiological health of military personnel on deployment (Amiri *et al.*, 2022).

In addressing these challenges, military organisations employ a multifaceted approach that encompasses the development of innovative gear and uniform designs, the implementation of training programmes focused on injury prevention and physical conditioning, as well as the adoption of operational strategies aimed at optimising load distribution and management. By prioritising the well-being and mobility of their personnel, military forces can enhance their overall readiness and effectiveness in fulfilling their mission objectives, even in the most demanding and challenging operational environments (Halvarsson *et al*., 2019).

2.4 Body Protection gainst Diseases

The significance of military uniforms extends beyond their traditional role of safeguarding against physical threats. While historically designed to shield soldiers from ballistic projectiles, extreme weather conditions and environmental hazards, contemporary challenges faced by military personnel have expanded to include risks associated with diseases and biological threats (Sinclair *et al.*, 2008). As underscored by Murray *et al.* (2007), the diverse deployment scenarios encountered by military personnel often entail exposure to disease-prone environments, necessitating comprehensive risk-reduction strategies.

Addressing health risks in military service has become increasingly critical as the nature of warfare evolves. Beyond traditional physical threats, modern military operations now face complex hazards such as chemical, biological, radiological and nuclear (CBRN) exposures, as well as the heightened risk of infectious disease transmission (Sammito *et al*., 2021; Ayemoba *et al*., 2022). As a result, the role of military uniforms must expand beyond basic physical protection to incorporate advanced technologies designed to mitigate these multifaceted threats. Continued research and innovation are essential to ensure that protective gear meets the demands of both current and emerging challenges (Wolf *et al*., 2020).

Moreover, beyond the mere physical attributes of the uniform, the role of education and hygiene practices is pivotal. Providing soldiers with comprehensive knowledge about disease recognition, preventive measures, and the importance of personal hygiene constitutes a crucial aspect of modern military training (Martini *et al.*, 2021). Empowering soldiers with this information equips them to identify potential disease indicators promptly and maintain optimal hygiene standards, reducing the risk of transmission within military settings (Odonkor *et al.*, 2019). Therefore, the evolution of military uniforms must transcend their traditional focus on physical protection, incorporating strategies to mitigate the risks posed by diseases and biological threats.

Furthermore, the ever-evolving nature of modern warfare necessitates a proactive approach to protective gear development. Innovation in material science, nanotechnology and biomedical research opens avenues for the creation of uniforms that offer not only enhance physical protection but also incorporate features such as self-cleaning fabrics, pathogen-resistant coatings and adaptive technologies capable of responding to dynamic environmental conditions (Kok *et al.*, 2024).

In summary, while traditional military uniforms were designed primarily for physical protection, the contemporary landscape calls for a paradigm shift. Advanced military attire must be equipped with cutting-edge technologies to address the multifaceted challenges faced by soldiers, encompassing defence against physical, chemical, biological and infectious threats (Bhushan *et al.*, 2022). The integration of education on disease recognition and hygiene practices supplements these advancements, reinforcing the comprehensive approach needed to ensure the well-being and safety of military personnel in diverse operational environments (Owens, 2011).

3. INNOVATIVE SOLUTIONS

Producing protective textiles that exhibit excellent air permeability, are lightweight, comfortable, durable, and cost-effective is essential (Rinaldho *et al*., 2020). Nonetheless, it is challenging to fulfil all these attributes in protective clothing simultaneously, as certain characteristics are inherently contradictory. Innovative technologies are being implemented in the textile manufacturing sector to create more sustainable fabrics with enhanced protective capabilities. Advanced protective textiles are produced through coating, finishing, laminating or the application of nanoparticles (Amiri *et al*., 2022). Advanced protective textiles should possess the following characteristics, as shown in Figure 1, to ensure comfort within the military setting.

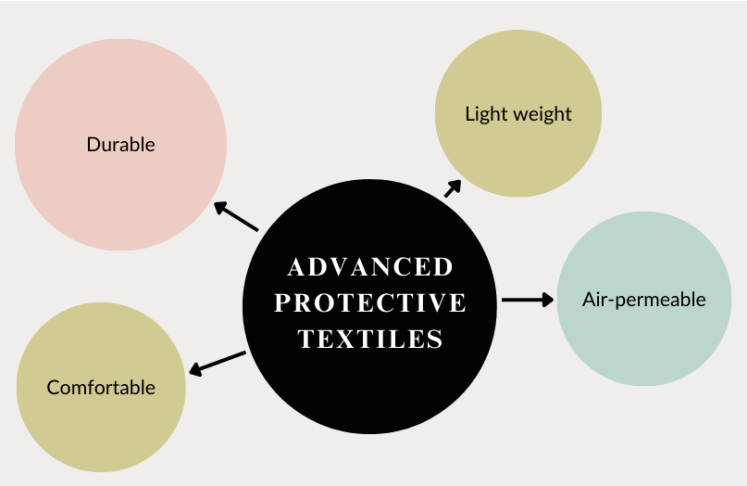

Figure 1: Characteristics of advanced protective textiles. (Source: Amiri *et al*., 2022).

3.1 Thermal Regulated Fabric

Ensuring optimal thermal comfort within military settings is crucial for enhancing the operational capabilities of personnel during training exercises and warfare. This emphasis on thermal comfort aligns with the understanding that maintaining an ideal thermal environment plays a pivotal role in managing human energy and overall performance (Peng & Cui, 2020). The human body operates within a delicate balance, constantly generating heat through metabolic processes and regulating its dissipation into the surrounding environment to maintain homeostasis (Charkoudian, 2016). Therefore, the maintenance of an appropriate thermal environment becomes paramount, particularly when wearing military uniforms, to support the physiological needs of soldiers in varying operational conditions.

The advancement of technology in fabric development for military uniforms has seen a significant surge, particularly in the realm of thermal regulation. Innovative textiles are being explored extensively, not only within industrial sectors but also through cutting-edge academic research (Peng & Cui, 2020). Among the most notable advancements in this domain are materials utilising phase change material (PCM) technology. PCM serves as a heat storage material that can be manipulated to provide either heating or cooling effects, making it a prominent choice in the development of thermal-regulated clothing (Babu & Arunraj, 2018). Furthermore, other intelligent features could also be integrated into military attire, such as sensor-equipped gear that monitors vital signs and physiological parameters (Parsons *et al*., 2019).

These thermal-regulated materials serve a dual purpose: in hot climates, they aid in dissipating excess heat by facilitating airflow and enhancing heat disposal, while in colder environments, they offer insulation by trapping warm air close to the body (Farooq & Zhang, 2021). The utilisation of such

uniforms can significantly contribute to enhancing the comfort and performance of soldiers across diverse environmental conditions (Steffens *et al.*, 2019). Figure 2 shows the comprehensive development of thermally regulated fabrics, showcasing various pathways aimed at improving thermal comfort for the human body. This includes innovations in material science, intricate fibre engineering, state-of-the-art finishing techniques, novel structural designs and advancements in garment shapes (Rezić & Kiš, 2020). For instance, technologies such as Omni-Heat by Columbia utilise reflective silver dots within textiles to effectively retain body heat, exemplifying the potential integration of such features into military uniform development (Peng & Cui, 2020). Furthermore, beyond PCM technology, ongoing research explores multifaceted approaches to optimise thermal comfort. These include advancements in moisture-wicking fabrics, breathable materials that regulate humidity and intelligent textiles capable of dynamically adapting to temperature fluctuations (Lei *et al*., 2023).

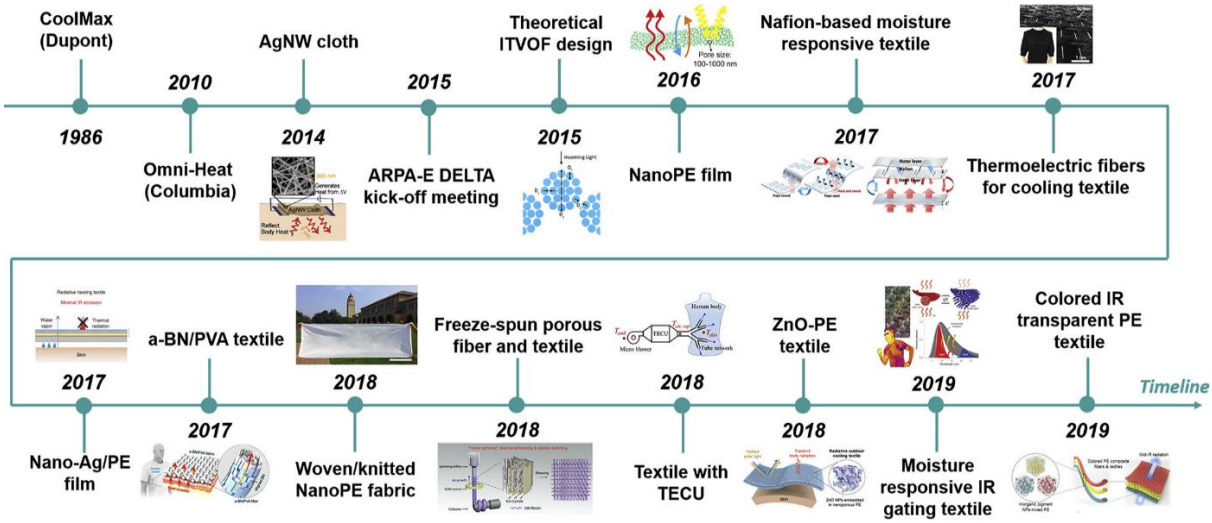

Figure 2: Roadmap of advanced textiles for personal thermal management and energy. (Source: Peng & Cui, 2020)

The integration of advanced fabric technologies into military uniforms offers promising improvements in comfort, endurance and operational effectiveness. Innovations in thermal regulation can help mitigate the adverse effects of extreme temperatures, enhancing the well-being and performance of personnel in the field. Moisture, alongside temperature, is a key factor in maintaining human comfort (Rinaldho *et al*., 2020). Polymeric materials, such as polylactic acid, Nafion and polyvinyl acetate, have been used to develop moisture-responsive clothing due to their ability to absorb moisture through hydroxyl groups. Hydrogels, composed of hydrophilic and hydrophobic copolymers, exhibit sharp volume changes around a critical temperature: swelling below it and shrinking above it. As a result, thermally responsive hydrogels have been explored for personal thermal management, especially in humid environments (Farooq & Zhang, 2021).

3.2 Water Repellent Treatment

Advancements in water-repellent treatments for military uniforms stand as pivotal strides toward enhancing performance, comfort, and safety, particularly in wet and windy conditions. Water-repellent fabrics are designed to shed water rather than absorb it, maintaining a level of breathability that waterproof fabrics often lack, which is essential for prolonged wear and high mobility. While dedicated rain gear is available for soldiers, water-repellent coatings offer distinct advantages in certain operational scenarios where waterproof textiles may cause overheating or restrict movement due to their impermeability (Brown & Kent, 2020). The coating ensures that uniforms remain lightweight and

comfortable while providing adequate protection against environmental hazards such as rain and wind (Basuk *et al*., 2018). Moreover, it reduces the likelihood of fabric degradation and mould growth in humid conditions, further extending the lifespan of military uniforms (Zhou *et al.*, 2021).

However, it is crucial to strike a balance between repellent properties and fabric breathability. Excessive focus on repelling water could compromise the uniform's ability to regulate temperature, leading to thermal discomfort in hot environments (Ashworth *et al.,* 2020). Innovations such as nano-coating technologies are being explored to enhance both water resistance and breathability, allowing soldiers to remain comfortable in diverse environmental conditions (Brown & Kent, 2020). As the demand for multi-functional textiles grows, continued research will be needed to ensure that these materials provide maximum protection without compromising mobility or comfort, addressing the unique requirements of soldiers in the field.

Understanding the nuances between waterproof and water-repellent fabrics is essential. Waterproof textiles are characterised by their filled pores and sealed spaces between yarns and fibres, resulting in a continuous surface that exhibits minimal air permeability. Conversely, water-repellent fabrics involve fibres coated with hydrophobic compounds, leaving the pores unfilled. This distinction allows water-repellent fabrics to remain permeable to both air and water vapour, unlike the airtight and impermeable nature of waterproof fabrics (Sheraz *et al.*,2023). The significance of water-repellent treatments lies in their ability to mitigate a soldier's exposure to cold water, thereby reducing overall clothing saturation and minimising the risk of hypothermia in wet and cold environments (Kwon *et al.,* 2021). Typically, these treatments are applied as coatings or laminates on fabrics, imbuing them with hydrophobic properties (Kim, 2021).

Recent studies, such as the groundbreaking research conducted by Kim *et al.* (2020), have significantly expanded the understanding of the effectiveness of various methods for testing water repellence in textiles, which has become crucial in military and outdoor applications. The study examined twelve distinct types of laminated and coated woven fabrics commonly used in outdoor apparel, with a particular focus on military uniforms (Gupta & Khare, 2021). The spray method, which is widely regarded as a reliable means of evaluating water repellence, was employed as the primary testing technique. This method is commonly recommended by industry standards for assessing a fabric's ability to repel water under simulated rain conditions (Wang *et al.*, 2021).

Furthermore, the laminating method has demonstrated superiority in producing fabrics with both excellent waterproofing and breathability, which are two key factors influencing performance and comfort, particularly for military personnel operating in diverse environmental conditions (Júnior *et al.,* 2022). The significance of breathability is further emphasised by research indicating that inadequate airflow in garments can lead to moisture accumulation and heat retention, which may severely compromise a soldier's effectiveness in the field (Bashari *et al.,* 2020). In addition, growing concerns over the environmental impact of water-repellent treatments have drawn attention to the urgent need for sustainable alternatives to conventional methods, which often rely on hazardous substances such as perfluorinated compounds (PFCs) (Gupta & Khare, 2021).

The selection of military uniform water-repellent treatment methods is a significant operational performance issue that has serious environmental consequences. In light of the endeavour to identify sustainable and practical methods for military organisations, treatments such as lamination have emerged as viable alternatives to conventional chemically intensive processes (Kim *et al.,* 2020). Laminating, which is a process that bonds different fabric layers and thereby creates waterproofing barriers without the need for additional chemical treatments (Wang *et al.,* 2021), seems to be one of the most promising solutions as it not only stops polluting but also extends life-time by maintaining water repellence throughout numerous washing processes (Sheraz *et al.*, 2023).
As well as aligning their procurement with broader environmental conservation goals by favouring sustainable practices, military organisations can help reduce water pollution and chemical runoff, often associated with some traditional water repellent treatments such as fluorocarbons, which have been

increasingly scrutinised due to persistent toxicity in the natural environment (Sfameni *et al*., 2022). In addition, the environmental stewardship that goes hand-in-hand with using environmentally friendly water-repellent treatments helps to reduce its overall carbon footprint within the armed forces itself and further demonstrates concern for service personnel of next-generation chemicals. Traditional water-repellent coatings often contain harmful chemicals that can leach from the products and be absorbed into human tissues over time, leading to endocrine disruption or carcinogenic outcomes (Kucukali-Ozturk *et al.,* 2017). Consequently, by utilising the bamboo laminating process or bio-based alternatives for military clothing production, it is possible to considerably reduce the risks of adverse effects on both environmental and human health according to the modern principles of sustainability (Hasan *et al.,* 2023).

Moreover, the overall durability of water-repellent textiles was identified as an important parameter with implications for maintenance and life span. Hot-water-extractable (HWE) and total water-repellent content in the textile increased more for durables than nondurables textiles even after repeated dry cleaning or laundering; however, the reduction rate of laboratory detergency procedures was greater for durable finishing treatment (Pervez *et al.,* 2022). However, it should be noted, that the demarcation line of durable versus non-durable textiles is somewhat a relative distinction here, emphasising the degree of water repellence rather than an absolute classification related to specific treatments (Rungruangkitkrai *et al.,* 2024). This emphasises that strategies used to water-repellent treat military uniforms should be performant, with a low impact on the environment (Chieng *et al.,* 2019). Methods such as lamination help military organisations improve fabric performance, as they look for more ecologically sensitive ways to generate these fabrics. As a result, durability aids the all-weather capability and water repellence of treatment in military textile items for various operational excursions and leads to an increase in sustainability (Amiri *et al*., 2022).

Further research and development in this field are investigating new methods to increase the durability of water-repellent treatments. These efforts can include looking into other options for environmentally friendly materials to use as coatings, methods to prevent these same applications from breaking down or wearing out over time, and even considering a composite coating that would offer enhancements such as sturdier stain protection or UV shielding (Suhardi *et al.,* 2022). Incorporation of these advanced water-repellent treatments in military uniforms increases the durability and serviceability of soldiers under extreme weather scenarios. These innovations manage water exposure effectively, all the while maintaining breathability and contributing greatly to comfort, safety on soldiers' bodies, and support in performing missions (Adams, 2019). Consequently, it is vital to keep exploring and applying new waterproof methods helpful for improve military uniforms. Although the core will be to analyse the continuing utility of these materials, user feedback on practical efficacy is the future of adaptive and smart fabrics for a whole new domain in military gear technology (Mantravadi *et al.,* 2019).

3.3 Ergonomic Design

Advancements in ergonomic design within military uniforms mark a pivotal leap forward in augmenting the comfort, manoeuvrability and operational efficacy of soldiers. These innovations are rooted in a profound comprehension of the physical demands encountered by military personnel during diverse missions and operational scenarios. The imperative for ergonomic design stems from the recognition that poorly designed gear can lead to a myriad of health issues, notably musculoskeletal disorders (MSDs), which have become prevalent among soldiers worldwide and are a leading cause of military personnel departing from service (Halvarsson *et al.,* 2019).

A significant contributing factor to these musculoskeletal issues is the gradual increase in the weight of soldiers' equipment over time. This escalation is attributed to the inclusion of new combat gear, heavy weaponry and other essential equipment, exacerbating the physical burden on soldiers. An essential aspect of crafting ergonomic military uniform designs involves considering various parts of the body

and their interactions with the equipment. For instance, research conducted by Melia *et al.* (2021) emphasises the importance of insole materials used in military personnel's backpacks. Their findings suggest that incorporating multiple insoles can significantly alleviate back foot pain and reduce forefoot plantar pressure. This underscores the criticality of prioritising ergonomics and comfort in the design and implementation of military equipment.

Understanding and accommodating human characteristics, limitations and capabilities form the cornerstone of effective design practices. A holistic comprehension of human physiology, biomechanics and ergonomics is indispensable in formulating designs that align with specific requirements. This knowledge is pivotal, as humans are integral to every aspect of the work system to achieve optimal outcomes, be it planning, designing, implementation or evaluation (Suhardi *et al.*, 2022).

Certainly, the contemporary evolution of ergonomic advancements within military uniform design signifies a comprehensive approach aimed not only at addressing immediate physical discomfort but also at integrating a spectrum of considerations to optimise soldier comfort and functionality in diverse operational settings (Suhardi *et al.*, 2022). These advancements encompass a wide array of factors, extending beyond mere alleviation of physical strain to ensuring holistic well-being and enhanced operational effectiveness (Adams, 2019). Additionally, the strategic distribution of weight across the body has emerged as a critical focus. Efforts are directed towards reducing strain by effectively distributing the load of equipment and gear, thereby mitigating potential musculoskeletal issues arising from prolonged use (Orr *et al.*, 2021).

An adaptive design approach has become essential in military uniforms, with adjustable components tailored to accommodate varying body shapes and sizes. This inclusivity enhances comfort and mobility across diverse operational scenarios (Knapik *et al.*, 2010). Current research continues to explore innovative solutions to improve ergonomic performance, focusing on advanced materials that provide enhanced durability, flexibility and weight management. Emerging design principles also aim to optimise uniform functionality in complex and demanding environments (Rinaldho *et al.*, 2020).

The design of military uniforms, informed by ergonomic principles, is crucial as it minimises physical strain and enhances both comfort and performance in collaboration with military personnel. The equipment is designed to enhance comfort and protection while improving performance and overall survivability of soldiers in extreme environments, thereby contributing to operational efficiency. Ergonomic design mitigates issues such as musculoskeletal disorders and fatigue by addressing health risk factors, including load distribution, material flexibility and movement efficiency, which can adversely affect sustainable soldier performance (Teyeme *et al.*, 2021).

Recent advancements underscore the diversity of tailored ergonomic solutions across various military settings. An Indonesian-specific design for a field shoe effectively integrates ergonomic principles and demonstrates adaptability to the diverse terrains found throughout the country. This perspective illustrates how local topographies can enhance military gear, thereby improving functionality and user comfort (Bhattacharyya *et al.*, 2024). The study by Hunt *et al.* (2016) found that the design of military footwear significantly contributes to stability and balance during physically challenging activities. The author concludes that traditional military boots restrict lateral foot movement and provide ankle protection, but post-exercise assessments indicated a diminished return to pre-exercise conditions. The findings suggest the need for further advancements in modern boot design to maintain stability during high-intensity activities and minimise injury risk (Kodithuwakku *et al.*, 2020).

Furthermore, the findings indicate that ergonomic military clothing serves as a health standard and plays a crucial role in enhancing mission effectiveness, as it promotes soldiers' safety, mobility and overall endurance across various operational environments (Burch *et al.*, 2020). Research progress indicates that further advancements in ergonomic design are essential for enhancing and optimising military uniforms, thereby supporting soldier performance during missions (Birrell *et al.*, 2010). In a separate

study conducted by Lindner *et al.* (2012), researchers focused on evaluating the impact of two types of military boots, standard and minimalist, on slip events experienced before and after executing military style tasks. Their investigation highlighted the crucial role played by both internal and external factors, such as footwear design and muscle fatigue, in assessing the likelihood of slipping and falling during military operations.

The study underscored the multifaceted nature of slip and fall incidents, emphasising the need to consider various contributing elements comprehensively. Understanding how footwear design interacts with physiological factors, such as muscle fatigue, emerged as pivotal in ensuring the safety of military personnel during task performance (Owens, 2011). By discerning the nuanced interplay between intrinsic and extrinsic factors, military units can better equip themselves to mitigate the risks associated with potential accidents and enhance operational safety (Kim *et al.*, 2020). The integration of biomechanical insights, ergonomic considerations and an in-depth understanding of environmental factors remains essential in refining footwear designs tailored for specific operational contexts (Nagano & Begg, 2018). This holistic approach not only ensures enhanced performance and adaptability but also serves as a crucial element in safeguarding personnel welfare and operational efficiency within diverse and challenging environments.

3.4 Antimicrobial Textile

The first textiles to incorporate antimicrobials were developed in 1867 as a response to the proliferation of skin infections and the contamination that was occurring at the time. Due to this, the textile industry became interested in the topic, which led to an increase in the production of materials that possess antimicrobial properties and their incorporation into the industry (Lopes *et al*., 2022). Hence, in modern military uniforms, innovations such as antimicrobial fabrics are a powerful tool for improving soldier health and operational preparedness. These fabrics offer a wide range of advantages and are designed to stop the spread of hazardous germs. Usually, these antimicrobial textiles are invented to prevent the growth or kill bacteria, viruses and fungi (Gulati *et al.*, 2022).

Antimicrobial textiles represent a significant advancement in material science, where fibres are impregnated with compounds to suppress microbial growth, offering protection against a range of pathogens. These antimicrobial compounds fall into three main categories, which are chemical, natural and nano agents, each with distinct mechanisms of action (Ibrahim *et al.*, 2021). As depicted in Figure 3, various antimicrobial agents, including chemical compounds and nanoparticles, work synergistically to inhibit the proliferation of bacteria, fungi and viruses, thus enhancing the hygienic properties of the textiles (Aguda & Lateef, 2022).

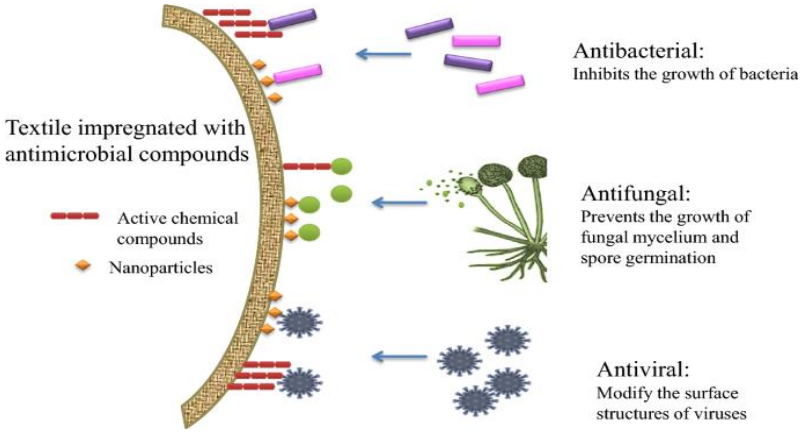

Figure 3: Textile embedded with antimicrobial agents inhibiting bacteria, fungi and viruses through chemical and nanoparticle action.
(Source: Gulati *et al.*, 2022)

Quaternary ammonium compounds, also known as QACs, are a type of chemical agent that is widely utilised because of their ability to effectively disrupt the cell membranes of microorganisms. It has been demonstrated that QACs, which are cationic surfactants, are effective against a wide variety of pathogens. These pathogens include Gram-positive bacteria such as *Staphylococcus aureus* and *Streptococcus pneumoniae*, as well as Gram-negative bacteria such as *Escherichia coli* and *Pseudomonas aeruginosa* (Morais *et al*., 2016). They are a dependable solution for applications where rapid antimicrobial activity is required, such as in healthcare and military settings, as their action is immediate (Ibrahim *et al*., 2021).

On the other hand, natural agents, derived from plants, animals and microorganisms, are gaining more and more recognition for their sustainability and biocompatibility. A notable example is chitosan, which is a biopolymer that is derived from chitin. Due to its positive charge, it is effective against microorganisms because it interacts with the negatively charged membranes of microbial cells, resulting in cell leakage and death (Roy *et al*., 2017). Chitosan's potential as an environmentally friendly solution for textile applications is highlighted by the fact that it is effective against a wide range of microorganisms, including bacteria, fungi, and even viruses (Ye *et al*., 2006). In addition, because it is biodegradable, it is an appealing alternative to synthetic antimicrobial agents, which is in line with the objectives of global sustainability (Massella *et al*., 2019).

Meanwhile, nano agents, particularly nanoparticles, exhibit distinctive properties attributable to their diminutive size (1-100 nm), which enhances their interaction with microbial cells. Silver nanoparticles are among the most extensively researched nano agents, widely recognised for their potent antimicrobial properties (Gulati *et al*., 2022). These nanoparticles release silver ions that permeate microbial cells, functioning as biocides by compromising the cell membrane and disrupting cytoplasmic metabolism. This process is facilitated by augmented free radical production and interactions with biomolecules (Giannossa *et al*., 2013). The commonly accepted mechanism is depicted in Figure 4. The sustained antimicrobial action provided by nanoparticles, along with their effectiveness against resistant strains, positions them as vital components in the development of durable antimicrobial textiles (Morais *et al*., 2016). Furthermore, ongoing research has illustrated that nano agents can be engineered to enhance both antimicrobial efficacy and fabric durability, rendering them applicable for a variety of uses, including medical textiles, sportswear and military uniforms (Vojnits *et al*., 2024). The increasing focus on incorporating eco-friendly nano agents, such as copper and zinc oxide (ZnO) nanoparticles, underscores a trend towards sustainable innovation in textile manufacturing (Ibrahim *et al*., 2021).

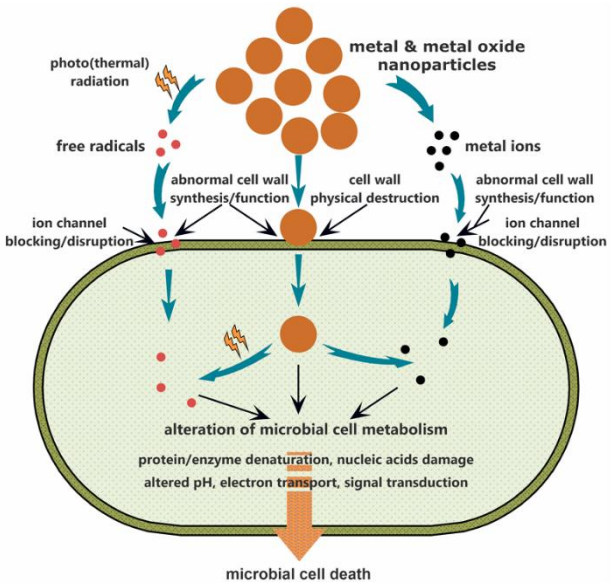

Figure 4: The primary antimicrobial mechanisms of metal and metal oxide nanoparticles. (Tanasa *et al*., 2023)

The dynamic landscape of antimicrobial textiles involves ongoing research and exploration to harness the potential of various antimicrobial agents. Researchers continually investigate both synthetic and natural compounds to improve their compatibility with textile materials and optimise their performance. For instance, Morais *et al.* (2016) explored a range of antimicrobial agents, highlighting the importance of balancing efficacy with safety and sustainability in textile applications. Meanwhile, Bibi *et al.* (2024) emphasised the comparative benefits of natural agents, which tend to be more environmentally friendly and less toxic compared to synthetic alternatives. Recent advances also focus on novel applications and the evaluation of antimicrobial textiles' environmental impacts (Gao & Cranston, 2008). Furthermore, methods used to assess antimicrobial efficacy are constantly refined to ensure that treated textiles meet safety and performance standards (Morais *et al.*, 2016).

Moreover, integrating antimicrobial agents into textiles not only protects against microbial threats but also opens up promising applications, from medical textiles to everyday apparel, promoting hygiene and reducing the risk of infections (Periolatto *et al.*, 2017). As research and technology continue to advance, innovations in antimicrobial textiles are expected to offer enhanced protection, contributing to safer and healthier environments across multiple sectors (Jagadeesan, 2018; Zhao *et al.*, 2021).

One such development is the emergence of bio-functional textiles that merge traditional fabrics with pharmaceutical nanocarriers, offering exciting prospects for wearable medication delivery systems. These fabrics, designed to improve skin penetration while minimising toxicity risks, represent a significant advancement in the medical field (Jagadeesan, 2018). Textile materials with antimicrobial properties can also serve as carriers for the gradual release of active ingredients, enabling new treatments for conditions such as hormone imbalances, melanoma, psoriasis and atopic dermatitis, or even acting as carriers for opioids or aromatherapy treatments (Hossain *et al.*, 2024; Bibi *et al.*, 2024).

In the case of fungi, growth is greatly reduced on antimicrobial fibres synthesised with modified silica containing silver and carbon. This reinforces the efficacy of fabric embedding with metal ions, such as in experiments showing broad-spectrum antifungal activity against *Fusarium chlamydosporum*, *Penicillium sp.* and *Aspergillus niger* using cotton treated with silver and zinc ion-containing azole complexes (Nabipour *et al*., 2020). Moreover, these guanazole-treated textiles also displayed flame-retardant characteristics, making them even more attractive to applications in health care, among other fields, as protective clothing. Although such treated textiles show significant antimicrobial properties, one cannot ignore the apprehensions over their durability in terms of multiple washes and related leachability issues, especially from metal ions used for these purposes (Jin *et al*., 2023).

Cellulose fibres with ZnO nanoparticles synthesised on their surfaces through a fungal process using *Phanerochaete chrysosporium* have exhibited antimicrobial activity. In addition, these fibres also showed antifungal activity against the cellulolytic fungus *Phanerochaete chrysosporium* (Shah *et al.*, 2021), yeast *Geotrichum candidum* and opportunistic pathogenic fungi *Aspergillus niger*. However, while fungal-mediated synthesis of ZnO nanoparticles serves as a green alternative to legacy-based syntheses, its scalability and economic feasibility remain an active area for future investigation. Furthermore, though the antimicrobial and antifungal activities are promising, long-term studies of the potential implications of nanoparticle exposure on health, particularly when used in clothes for consumers, need to be conducted.

The application of antimicrobial clothing extends beyond sportswear, offering multifaceted utility across diverse fields. Notably, its potential in long-duration space missions has garnered attention, given the unique challenges posed by the space environment (Jagadeesan, 2018; Hossain *et al.*, 2024). Although microbial presence in space systems is generally low and the risk of microbial growth within spacesuits remains limited, maintaining hygiene remains a critical concern. One of the primary issues is the absence of laundry facilities, which necessitates wearing garments for extended periods. These clothes are infrequently laundered and only sporadically replenished, increasing the risk of microbial contamination through skin contact. This prolonged usage amplifies hygiene challenges and highlights

the need for innovative strategies to mitigate microbial risks. Consequently, antimicrobial textiles emerge as a vital solution for maintaining hygiene during extended space missions, particularly in the absence of conventional laundering methods (Gulati *et al*., 2022).

Therefore, the evolving landscape of antimicrobial textiles presents a promising avenue for addressing hygiene concerns across various domains, from sportswear applications to space exploration (Vojnits *et al.,* 2024). As research advances, innovative solutions that prioritise hygiene, comfort, and functionality continue to redefine the boundaries of antimicrobial textile applications, offering multifaceted benefits in diverse settings (Mamillapalli, 2016). Efforts toward advancing these technologies remain pivotal in ensuring hygiene and well-being in both terrestrial and extraterrestrial environments (Pinho *et al*., 2011).

Despite that, it is important to critically assess the balance between efficacy and safety. For instance, antimicrobial agents, particularly nanoparticles, are integrated into textiles; there remains a need for further research into their long-term health effects and environmental impact. For instance, while zinc oxide nanoparticles show antimicrobial efficacy, their potential toxicity and bioaccumulation warrant caution (Saleem & Zaidi, 2020). Nevertheless, as this field expands, ongoing evaluations of consumer perceptions, alongside rigorous safety assessments, will be essential to maintain a balance between innovation and health considerations.

4. CONCLUSION

In conclusion, the role of military uniforms transcends mere attire, serving as integral components in safeguarding the comfort, safety, and performance of military personnel. However, alongside their benefits, military uniforms present a host of unique physiological challenges that necessitate scientific scrutiny and innovative solutions. These challenges span a spectrum, including but not limited to heat stress, moisture management, weight and mobility constraints, and protection against diseases and environmental hazards. Addressing these challenges requires a concerted effort, drawing upon interdisciplinary research and leveraging advancements in various scientific domains. For instance, the development of thermal-regulated fabrics has revolutionised uniform design, enabling the effective regulation of body temperature and mitigation of heat stress in extreme environments. Similarly, advancements in water-repellent treatments have enhanced moisture management capabilities, ensuring the wearer remains dry and comfortable even in humid or wet conditions. Moreover, the integration of ergonomic principles into uniform design has yielded significant improvements in mobility and comfort, reducing the physical strain experienced by soldiers during prolonged missions or strenuous activities. Furthermore, the adoption of antimicrobial textiles has emerged as a crucial measure to safeguard against infectious diseases and maintain hygiene standards in military settings. Looking ahead, the pursuit of excellence in military uniform design demands a continued commitment to interdisciplinary collaboration and scientific innovation. Prioritising sustainability in material sourcing and manufacturing processes is paramount to minimise environmental impact and ensure the long-term viability of uniform solutions. Exploring cutting-edge materials, such as nanotechnology-based fabrics or smart textiles embedded with sensors and adaptive capabilities, holds immense promise for enhancing the comfort, safety, and performance of military personnel in diverse operational contexts. By embracing a forward-thinking approach and harnessing the power of scientific inquiry, the evolution of military uniforms can continue to support and enhance the physical and cognitive capabilities of military personnel. Ultimately, this ongoing endeavour will contribute to their overall well-being and operational effectiveness across a spectrum of challenging and dynamic environments, ensuring they remain agile, resilient, and mission-ready in the face of evolving threats and demands.

5. REFERENCES

Adams, J.M. (2019). The value of worker well-being. *Pub. Health Rep.*, **6**: 583-586.

Aguda, O.N. & Lateef, A. (2022). Recent advances in functionalization of nanotextiles: a strategy to combat harmful microorganisms and emerging pathogens in the 21st century. *Heliyon*, **8**.

Alele, F., Malau-Aduli, B.S., Malau-Aduli, A. & Crowe, M. (2020). Epidemiology of exertional heat illness in the military: a systematic review of observational studies. *Multidiscip. Digital Publish. Inst.*, **17**: 7037-7037.

Amiri, S., Moghanjougi, Z.M., Nezamdoost-Sani, N. & Rezazadeh-Bari, M. (2022). Safety, health, and environmental aspects of protective textiles. *In* Mondal, M. I. H. (Ed.), *Protective Textiles from Natural Resources*. Woodhead Publishing, Cambridge, pp. 839-879.

Ashworth, E.T., Cotter, J.D. & Kilding, A.E. (2020). Methods for improving thermal tolerance in military personnel before deployment. *Mil. Med. Res.,* **7***:* 58.

Ayemoba, O., Adekanye, U., Iroezindu, M., Onoh, I., Lawal, I., Suleiman, A. & Okeji, N. (2022). The Nigerian military public health response to COVID-19: a 14-month appraisal. *Health secur*., **20**: 203-211.

Babu, V.R. & Arunraj, A. (2018). Thermo regulated clothing with phase change materials. *J. Text. Eng. Fash. Technol.*, **4**: 344-347.

Basak, S., Senthilkumar, T., Krishnaprasad, G. & Jagajanantha, P. (2020). Sustainable development in textile processing. *In* Sharma, A. K. & Singh, R. (Eds.), *Sustainable Green Chemical Processes and their Allied Applications*. Springer, Singapore, pp. 559-573.

Bashari, A., Koohestani, A.H.S. & Salamatipour, N. (2020). Eco-friendly dual-functional textiles: green water-repellent & anti-bacterial. *Fib. Polym.*, **21**: 317-323.

Basuk, M., Choudhari, M., Maiti, S. & Adivarekar, R.V. (2018). Moisture management properties of textiles and its evaluation. *Curr. Tren. Fash. Technol. & Text. Eng.*, **3**: 50-55.

Bhattacharyya, D., Pal, M., Chatterjee, T. & Varshney, R. (2024). Extreme interaction among human environment–equipment: a pilot study on the ergonomic design of military snow boots. *Ergo. Des.*, **32**: 19-25.

Bhushan, B., Gupta, N., Mittal, S., Tomar, R., Verma, P. & Kaur, G. (2022). Antimicrobial textiles: recent developments and functional perspectives. *Polym. Bull.*, **79**: 5747-5771.

Bibi, A., Afza, G., Afzal, Z., Farid, M., Sumrra, S.H., Hanif, M.A. & Zubair, M. (2024). Synthetic vs. natural antimicrobial agents for safer textiles: a comparative review. *RSC. Advan.*, **14:** 30688-30706.

Birrell, S.A. & Haslam, R.A. (2010). The effect of load distribution within military load carriage systems on the kinetics of human gait. *Appl. Ergo.*, **41**: 585-590.

Brown, T. & Kent, M. (2020). Water-repellent coatings for military textiles: enhancing performance and comfort. *Journ. Milit. Text. Res.*, **14**: 101-115.

Buller, M.J., Delves, S.K., Fogarty, A.L. & Veenstra, B. (2021). On the real-time prevention and monitoring of exertional heat illness in military personnel. *Elsevier BV.*, **24**: 975-981.

Burch, R.F., Wade, C., Garner, J.W. & Carruth, D.W. (2020). Muscle activity during postural stability tasks: role of military footwear and load carriage. *Multidis. Digital Publish. Inst.*, **6**: 35-35.

Campbell, D.J. & Nobel, O.B.Y. (2009). Occupational stressors in military service: a review and framework. *Mil. Psychol.*, **21**: S47-S67.

Carlton, S.D., & Orr, R.M. (2014). The impact of occupational load carriage on carrier mobility: a critical review of the literature. *Taylor & Francis*, **20**: 33-41.

Charkoudian, N. (2016). Human thermoregulation from the autonomic perspective. *Auton. Neurosci.*, **196**: 1-2.

Chen, D. (2023). Temperature regulation during exercise and the individual differences. *SHS. Web Confer.*, **174**: 0301.

Chieng, B.W., Ibrahim, N.A., Daud, N.A. & Talib, Z.A. (2019). Functionalization of graphene oxide via gamma-ray irradiation for hydrophobic materials. *In* Thomas, S., Pasquini, A., & Syed Shakoor, S.A. (Eds.), *Radiation Technology for Advanced Materials: Applications in Nanoscience and Biomedicine*. Elsevier, Amsterdam, Netherlands, pp. 177-203.

Cramer, M.N. & Jay, O. (2016). Biophysical aspects of human thermoregulation during heat stress. *Auton. Neurosci.*, **196**: 3-13.

DeGroot, D., Henderson, K. & O'Connor, F. (2022). Exertional heat illness at Fort Benning, GA: unique insights from the army heat center. *MSMR.*, **29**: 2-7.

Donham, B., Frankfurt, S., Cartier, R.A., Ohara, S. & Sieg, V. (2020). Low incidence of death and renal failure in United States military service members hospitalized with exertional heat stroke: a retrospective cohort study. *Oxford Univ. Press.*, **185**: 362-367.

Duong, H. & Patel, G. (2022). *Hypothermia*. Available online at: https://www.ncbi.nlm.nih.gov/books/NBK545239/ (Last access date: 8 October 2024).

Farooq, A.S. & Zhang, P. (2021). Fundamentals, materials and strategies for personal thermal management by next-generation textiles. *Compos-A: Appl. Sci.*, **142**: 106249.

Flood, A. & Keegan, R.J. (2022). Cognitive resilience to psychological stress in military personnel. *Front. Psychol.*, **13**: 809003.

Gao, Y. & Cranston, R. (2008). Recent advances in antimicrobial treatments of textiles. *Text. Res. Journ.*, **78**: 60-72.

Giannossa, L.C., Longano, D., Ditaranto, N., Nitti, M.A., Paladini, F., Pollini, M. & Cioffi, N. (2013). Metal nanoantimicrobials for textile applications. *Nanotechnol. Rev.*, **2**: 307-331.

Gibson, P., Schreuder-Gibson, H., Yip, P W., Denker, B., Benaddi, H., Wang, S., Bromberg, L. & Hatton, T.A. (2013). Moisture transport for reaction enhancement in fabrics. *In* Smith, J. & Brown, L. (Eds.), *Journal of Textiles*. Hindawi Publishing Corporation, Cairo, Egypt, pp. 1-8.

Gulati, R., Sharma, S. & Sharma, R. (2022). Antimicrobial textile: recent developments and functional perspective. *Polym. Bull.*, **79**: 5747-5771.

Gupta, V. & Khare, P. (2021). Advances in laminated textiles for military applications: performance and environmental considerations. *Text. Res. Journ.*, **91**: 1452-1468.

Halvarsson, A., Seth, M., Tegern, M., Broman, L. & Larsson, H. (2019). Remarkable increase of musculoskeletal disorders among soldiers preparing for international missions-comparison between 2002 and 2012. *BMC. Musculoskelet. Disord.*, **20**: 1-7.

Hasan, K.M.F., Hasan, K.M.N.A., Ahmed, T., Szili-Török, G., Pervez, M.N., Bejó, L., Sándor, B. & Alpár, T. (2023). Sustainable bamboo fiber reinforced polymeric composites for structural applications: A mini review of recent advances and future prospects. *Case Stud. Chem. Environ. Eng.*, 8

Hossain, M.M., Islam, T., Jalil, M.A., Rakibuzzaman, S.M., Surid, S.M., Zabed, M.R.I. & Hossain, S. (2024). Advancements of eco-friendly natural antimicrobial agents and their transformative role in sustainable textiles. *SPE. Polym.*, **5**: 241-276.

Hunt, A., Billing, D.C., Patterson, M.J. & Caldwell, J.N. (2016). Heat strain during military training activities: the dilemma of balancing force protection and operational capability. *Taylor & Francis*, **3**: 307-317.

Ibrahim, A., Laquerre, J.É., Forcier, P., Deregnaucourt, V., Decaens, J. & Vermeersch, O. (2021). Antimicrobial agents for textiles: types, mechanisms and analysis standards. *Text. Funct. Appl.*, **13**: 261-293.

Jagadeesan, K. (2018). *Antimicrobial Textiles for Long Duration Space Flight.* Majors Papers, Department of Textiles, Fashion Merchandising, and Design, University of Rhode Island, Rhode Island.

Jardine, D.S. (2007). Heat illness and heat stroke. *A. Acad. Ped.*, **28**: 249-258.

Jin, L., Ji, C., Chen, S., Song, Z., Zhou, J., Qian, K. & Guo, W. (2023). Multifunctional Textiles with Flame Retardant and Antibacterial Properties: A Review. *Molecules*, **28**

Joseph, A., Wiley, A., Orr, R., Schram, B. & Dawes, J.J. (2018). The impact of load carriage on measures of power and agility in tactical occupations: a critical review. *Inter. Journ. Environ. Res. & Pub. Health*, **15**: 88.

Júnior, H.L.O., Neves, R.M., Monticeli, F.M. & Dall Agnol, L. (2022). Smart fabric textiles: recent advances and challenges. *Text.*, **2**: 582-605.

Kim, H.J., Oh, S., Kim, K., Won, S.Y., Kim, H.J., Ko, S.C., Woo, S.Y. & Park, E. (2020). Accident prevention activity and accident experience in the Republic of Korea military. *BMJ.*, **167**: 187-191.

Kim, H.A. (2021). Water repellency/proof/vapor permeability characteristics of coated and laminated breathable fabrics for outdoor clothing. *Coatings*, **12**: 12.

Knapik, J., Montain, S.J., McGraw, S., Grier, T., Ely, M. & Jones, B.H. (2012). Stress fracture risk factors in basic combat training. *Int. J. Sports Med*., **33**: 940-946.

Knapik, J., Reynolds, K., Santee, W.R. & Friedl, K.E. (2010). Load carriage in military operations: a review of historical, physiological, biomechanical, and medical aspects. *In* Friedl, K.E. (Ed.), *Military Medicine and Performance*, Borden Institute, Fort Detrick, Maryland, pp. 1-250.

Kodithuwakku, A.S.N., Chander, H., Turner, A.J., Wilson, S.J., Simpson, J.D., Knight, C. & Carruth, D. (2020). Muscle activity during postural stability tasks: role of military footwear and load carriage. *Safety*, **6**: 35.

Kok, C.R., Bram, Z., Thissen, J.B., Horseman, T.S., Fong, K.S., Reichert-Scrivner, S.A. & Be, N.A. (2024). The military gear microbiome: risk factors surrounding the warfighter. *Appl. Environ. Microbiol*., **90**.

Krueger, G.P. (2014). Psychological issues in military uniform design. *In* Sparks, E. (Ed.), *Advances in Military Textiles and Personal Equipment*, Woodhead Publishing, Cambridge, pp. 64-78.

Kucukali-Ozturk, M., Berkalp, Ö.B. & Nergis, B. (2017). Design of a light weight fabric from natural cellulosic fibers with improved moisture related properties. *IOP. Publish*, **254**: 182005.

Kwon, J., Kim, K., Ju, J. & Lee, J.Y. (2021). Performance evaluation of water-repellent combat uniforms using a static manikin and human subjects under a rainfall tower system. *Fash. Text.*, **8**: 1-16.

Lei, L., Shi, S., Wang, D., Meng, S., Dai, J.G., Fu, S. & Hu, J. (2023). Recent advances in thermoregulatory clothing: materials, mechanisms, and perspectives. *ACS. Nano*., **17**: 1803-1830.

Lemoine, M. & Pradeu, T. (2018). Dissecting the meanings of "physiology" to assess the vitality of the discipline. *Physiol.*, **33**: 236-245.

Leon, L.R. & Helwig, B.G. (2010). Heat stroke: role of the systemic inflammatory response. *A. Physiol. Soc.*, **109**: 1980-1988.

Leon, L.R. & Bouchama, A. (2015). Heat stroke. *Compr. Physiol*., **5**: 611-647.

Lindner, T., Schulze, C., Woitge, S., Finze, S., Mittelmeier, W. & Bader, R. (2012). The effect of the weight of equipment on muscle activity of the lower extremity in soldiers. *J. Strength Cond. Res*., **26**.

Lopes, T.J., Rosa, G.R., Fernandes, G.A., Scheeren, C.W., Da Silva Júnior, A.H. & Martins, M.L. (2022). Chemical and biological protective textiles. *In* Mondal, M. I. H. (Ed.), *Protective Textiles from Natural Resources*. Woodhead Publishing, Cambridge, pp. 649-687.

Lucas, R.A.I., Epstein, Y. & Kjellström, T. (2014). Excessive occupational heat exposure: significant ergonomic challenge and health risk for current and future workers. *Bio. Med. Central*, **3**.

Mamillapalli, V. (2016). Nanoparticles for herbal extracts. *AJP.*, **10**.

Mantravadi, P.K., Kalesh, K.A., Dobson, R.C.J., Hudson, A.O. & Parthasarathy, A. (2019). The quest for novel antimicrobial compounds: emerging trends in research, development, and technologies. *Antibiotics*, **8**.

Martin, K., Périard, J., Rattray, B. & Pyne, D.B. (2020). Physiological factors which influence cognitive performance in military personnel. *Hum. Fact.*, **62**: 93-123.

Martini, M., Simonetti, O., Orsini, D., Armocida, E. & Zimmermann, A.P. (2021). The avid eaters of lives. new and old infectious diseases in Italy at the time of world war I: a historical overview of military medicine and public health. *Journ. Prevent. Medic. Hyg.*, **62**. E972.

Massella, D., Argenziano, M., Ferri, A., Guan, J., Giraud, S., Cavalli, R. & Salaün, F. (2019). Bio-functional textiles: combining pharmaceutical nanocarriers with fibrous materials for innovative dermatological therapies. *Pharmaceutic.*, **11**: 403.

Melia, G., Siegkas, P., Levick, J. & Apps, C. (2021). Insoles of uniform softer material reduced plantar pressure compared to dual-material insoles during regular and loaded gait. *Appl. Ergon.*, **91**: 103298.

Moore, A., Stacey, M., Bailey, K., Bunn, R.J., Woods, D.R., Haworth, K.J., Brett, S. & Folkes, S.E.F. (2015). Risk factors for heat illness among British soldiers in the hot collective training environment. *BMJ.*, **162**: 434-439.

Morais, D.S., Guedes, R.M. & Lopes, M.A. (2016). Antimicrobial approaches for textiles: from research to market. *Materials*, **9**.

Murray, C.K., Horvath, L.L., Ericsson, C.D. & Hatz, C. (2007). An approach to prevention of infectious diseases during military deployments. *Clin. Infect. Dis*., **44**: 424-430.

Nabipour, H., Wang, X., Rahman, M.Z., Song, L. & Hu, Y. (2020). An environmentally friendly approach to fabricating flame retardant, antibacterial and antifungal cotton fabrics via self-assembly of guanazole-metal complex. *Journ. Clean. Product.*, **273**.

Nagano, H. & Begg, R. (2018). Shoe-insole technology for injury prevention in walking. *Multidis. Digital Publish. Inst.*, **18**: 1468-1468.

Odonkor, S.T., Kitcher, J., Okyere, M. & Mahami, T. (2019). Self-assessment of hygiene practices towards predictive and preventive medicine intervention: A case study of university students in Ghana. *Int. J. Environ. Res. Public Health*, **16**.

Ogden, H.B., Rawcliffe, A.J., Delves, S.K. & Roberts, A. (2022). Are young military personnel at a disproportional risk of heat illness?. *BMJ. Mil. Health.*, **10**: 1-6.

Orr, R., Pope, R., Lopes, T.J.A., Leyk, D., Blacker, S., Bustillo-Aguirre, B. S. & Knapik, J.J. (2021). Soldier load carriage, injuries, rehabilitation and physical conditioning: an international approach. *Int. J. Environ. Res. Pub. Health.*, **18**: 4010.

Owens, J.R. (2011). Key elements of protection for military textiles. *In* Pan, N. & Sun, G. (Eds.), *Functional Textiles for Improved Performance, Protection and Health.*, Woodhead Publishing, pp. 249-268.

Parsons, I., Stacey, M. & Woods, D.R. (2019). Heat adaptation in military personnel: mitigating risk, maximizing performance. *Front. Med.*, **10**.

Peng, Y. & Cui, Y. (2020). Advanced textiles for personal thermal management and energy energy. *Joule.*, **4**: 724-742.

Périard, J.D., DeGroot, D. & Jay, O. (2022). Exertional heat stroke in sport and the military: epidemiology and mitigation. *Exp. Physiol.*, **107**: 1111-1121.

Periolatto, M., Ferrero, F., Vineis, C., Varesano, A. & Gozzelino, G. (2017). Novel antimicrobial agents and processes for textile applications. *In* Periolatto, M., Ferrero, F., Vineis, C., Varesano, A., & Gozzelino, G. (Eds.), *Novel Antimicrobial Agents and Processes for Textile Applications*. IntechOpen, London, pp. 1-11.

Pervez, M.N., Hossain, M.Y., Talukder, M.E., Faisal, A.M., Hasan, K. F., Islam, M., Ahmed, F., Cai, Y., Stylios, G. K., Naddeo, V. & Mondal, M.I.H. (2022). Nanomaterial-based smart and sustainable protective textiles. *In* Mondal, M.I.H. (Ed.), *Protective Textiles from Natural Resources*., Woodhead Publishing, Cambridge, pp. 75-111.

Pinho, E., Magalhães, L., Henriques, M. & Oliveira, R. (2011). Antimicrobial activity assessment of textiles: standard methods comparison. *Annals Microbiol.*, **61**: 493-498.

Revaiah, R.G., Kotresh, T.M. & Kandasubramanian, B. (2020). Technical textiles for military applications. *Journ. Text. Inst.*, **111:** 273-308.

Rezić, I. & Kiš, A. (2020). Design of experiment approach to optimize hydrophobic fabric treatments. *Polym.*, **12**: 2131.

Rinaldho, A.R., Gani, E.A. & Bagdja, A. (2020). Ergonomics in military platform design: a review. *Inter. Journ. Edu. Social Sci. Res.*, **5**: 362-372.

Rowen, J.W. & Gagliardi, D. (1947). Properties of water-repellent fabrics. *J. Res. Natl. Bur. Stand.*, **38**, 103-117.

Roy, J., Salaün, F., Giraud, S., Ferri, A. & Guan, J. (2017). Chitosan-based sustainable textile technology: process, mechanism, innovation, and safety. *In* Roy, J., Salaün, F., Giraud, S., Ferri, A., & Guan, J. (Eds.), *Chitosan-based Sustainable Textile Technology*. IntechOpen, London, pp. 1-10.

Rungruangkitkrai, N., Phromphen, P., Chartvivatpornchai, N., Srisa, A., Laorenza, Y., Wongphan, P. & Harnkarnsujarit, N. (2024). Water repellent coating in textile, paper and bioplastic polymers: A comprehensive review. *Polymers*, **16**.

Saleem, H. & Zaidi, S.J. (2020). Sustainable use of nanomaterials in textiles and their environmental impact. *Materials*, **13**: 134.

Sammito, S., Hadzic, V., Karakolis, T., Kelly, K.R., Proctor, S.P., Stepens, A. & Zimmermann, W.O. (2021). Risk factors for musculoskeletal injuries in the military: a qualitative systematic review of the literature from the past two decades and a new prioritizing injury model. *Milit. Medic. Res.*, **8**: 1-40.

Santee, W.R., Berglund, L.G., Cardello, A.V., Winterhalter, C.A., Looney, D.P., González, J. & Potter, A.W. (2020). Physiological assessment of soldiers wearing military uniforms of different fabrics during intermittent exercise. *J. Sport. Hum. Perform.*, **8**.

Sfameni, S., Lawnick, T., Rando, G., Visco, A., Textor, T. & Plutino, M.R. (2022). Functional silane-based nanohybrid materials for the development of hydrophobic and water-based stain resistant cotton fabrics coatings. *Nanomat.*, **12**: 3404

Shah, N., Kumar, P., Gupta, S. & Chandel, A. (2021). White-rot fungus mediated green synthesis of zinc oxide nanoparticles and their impregnation on cellulose to develop environmentally friendly antimicrobial fibers. *Biotech.*, **11**: 1-10.

Sheraz, M., Choi, B., & Kim, J. (2023). Enhancing Textile Water Repellency with Octadecyltrichlorosilane (OTS) and Hollow Silica Nanoparticles. *Polymers*, **15**

Sinclair, R., Boone, S.A., Greenberg, D., Keim, P. & Gerba, C.P. (2008). Persistence of category A select agents in the environment. *Appl. Environ. Microbiol.*, **74**: 555-563.

Steffens, F., Gralha, S.E., Ferreira, I.L.S. & Oliveira, F.R. (2019). Military textiles - an overview of new developments. *Key Engin. Materials*, **812**: 120-126.

Suhardi, B., Manaruzzaki, A., Hanif, F.S., Hestyrosari, M.F. & Farikha, N.A.N. (2022). Analysis of the military attribute's selection based on ergonomic aspects in the Indonesian national armed forces. *Asian J. Soc. Sci*., **4**: 35-42.

Tanasa, F., Teaca, C.A., Nechifor, M., Ignat, M., Duceac, I.A. & Ignat, L. (2023). Highly specialized textiles with antimicrobial functionality - advances and challenges. *Text.*, **3**: 219-245.

Taylor, N.A.S. & Patterson, M.J. (2016). Military clothing and protective material: protection at the limits of physiological regulation. *Stud. Mechanobiol. Tis. Eng. Biomater.*, **19**: 303-332.

Teyeme, Y., Malengier, B., Tesfaye, T., Ciesielska-Wrobel, I., Haji Musa, A.B. & Van Langenhove, L. (2021). A review of contemporary techniques for measuring ergonomic wear comfort of protective and sport clothing. *Autex Res. Journ.*, **21**: 32-44.

Vojnits, K., Mohseni, M., Parvinzadeh Gashti, M., Nadaraja, A.V., Karimianghadim, R., Crowther, B. & Pakpour, S. (2024). Advancing antimicrobial textiles: a comprehensive study on combating escape pathogens and ensuring user safety. *Materials*, **17**: 383.

Walsh, G.S. & Low, D.C. (2021). Military load carriage effects on the gait of military personnel: a systematic review. *Appl. Ergo.*, **93**: 103376.

Wang, L., Zhang, J. & Chen, Y. (2021). Innovative sustainable water-repellent treatments for textiles: assessing the lamination process in military applications. *Journ. Text. Sci & Engin.*, **67**: 315-325.

Wolf, S.T., Kenney, L.E. & Kenney, W.L. (2020). Ultraviolet radiation exposure, risk, and protection in military and outdoor athletes. *Curr. Sports Medic. Rep.*, **19**: 137-141.

Ye, W., Xin, J.H., Li, P., Lee, K.L.D. & Kwong, T.L. (2006). Durable antibacterial finish on cotton fabric by using chitosan-based polymeric core-shell particles. *J. Appl. Polym. Sci.*, **102**: 1787-1793.

Yeo, P.T. (2004). Heat stroke: a comprehensive review. *AACN. Clin. Issues.*, **15**: 93-280.

Yunusxodjaeva, K., Vakhidova, U. & Yunusxodjaeva, N. (2024). Research of improving the method of designing ergonomic clothing for special purpose, taken into account of the construction of the "armholesleeve" unit. *E3S. Web Confer*., **538**: 04004.

Zhang, X. (2001). Heat-storage and thermo-regulated textiles and clothing. *In* Tao, X. (Ed.), *Smart Fibres, Fabrics and Clothing*, Woodhead Publishing, Cambridge, pp. 34-57.

Zhao, Y., Zhang, J. & Liu, W. (2021). The environmental impact of antimicrobial textiles: a comprehensive review. *Sustain.*, **13**: 2667-2679.

Zhou, Z., Sun, K. & Yang, Y. (2021). Natural and synthetic superhydrophobic surfaces. *Inter. Core Journ. Engin.*, **7**: 241-261.